Identifying Combinatorial Drug Targets for Ras Pathway-Driven Melanomas

Identifying combinatorial drug targets for Ras pathway-driven melanomas

A dissertation presented

by

Haley Ellen Manchester

to

The Division of Medical Sciences

in partial fulfillment of the requirements

for the degree of

Doctor of Philosophy

in the subject of

Biological and Biomedical Sciences

Harvard University

Cambridge, Massachusetts

May 2020

Dissertation Advisor: Karen Cichowski Haley Ellen Manchester

Identifying combinatorial drug targets for Ras pathway-driven melanomas

Abstract

Cutaneous melanoma is a highly metastatic skin cancer, with ~100,000 new cases estimated to occur in 2020 in the US. Melanomas are defined by oncogenic "driver" mutations that constitutively activate the Ras/Raf/MEK/ERK signaling (henceforth called Ras/ERK) pathway. Clinical agents that target various components of this pathway have been developed, although they are not typically curative. For *BRAF*-mutant melanomas, combined BRAF and MEK inhibitors prolong survival, although patients still relapse within ~11 months. Unfortunately, Ras/ERK pathway inhibitors are even less effective in *NRAS*-mutant tumors, with MEK inhibitors stimulating only partial responses in 15-20% of patients. Thus, *NRAS* mutations are associated with poor overall survival, and there is a great need for improved therapies. The goal of my thesis has been to identify agents that potentiate the effects of Ras/ERK pathway inhibitors as a means of developing more effective therapies for *NRAS* and other Ras pathway-driven melanomas.

This dissertation describes three promising therapeutic combinations. In one approach, we discovered a new combinatorial therapy for *NRAS*-mutant melanomas by performing an unbiased negative selection CRISPR-Cas9 screen. Specifically, we identified the de-ubiquitinase USP7 as a target that when suppressed, sensitizes *NRAS*-mutant melanomas to MEK inhibitors. Further genetic and mechanistic analysis revealed USP7 interacts with two other hits from our screen and together form a complex that regulates H2B ubiquitination, a marker of transcriptional elongation. Through epigenetic and transcriptional studies, we found that this complex regulates the expression of CABLES1, which is required for triggering cell death and tumor regression.

Using candidate-based approaches, we also identified two additional combination therapies that target *BRAF*-, *NRAS*-, and *NF1*-mutant melanomas. Specifically, we discovered that histone de-acetylase (HDAC) inhibitors potentiate responses to Ras/ERK signaling pathway inhibitors in *BRAF-, NRAS-,* and *NF1*-mutant melanomas by suppressing DNA repair pathways (Maertens et al. 2019). Additionally, we demonstrated that the combination of Ras/ERK signaling pathway and bromodomain and extraterminal domain (BET) inhibitors represents a promising new therapeutic approach to reduce acquired and intrinsic resistance in *BRAF*-mutant melanomas (Katherine R. Singleton 2017). In summary, this dissertation details three promising combination therapies for Ras/ERK pathway-driven melanomas and describes the distinct mechanisms by which they function.

Table of Contents

List of Figures

Chapter 1: Introduction

Chapter 2: Co-suppression of MEK and USP7 triggers a synthetic lethal response in NRAS-mutant melanomas

Chapter 3: MAPK Pathway Suppression Unmasks Latent DNA Repair Defects and Confers a Chemical Synthetic Vulnerability in BRAF, NRAS, and NF1-Mutant Melanomas

Chapter 4: Melanoma Therapeutic Strategies That Select Against Resistance by Exploiting MYC-Driven Evolutionary Convergence

Chapter 5: Conclusions and Future Directions

Appendices

List of Tables

Acknowledgements

First, I want to thank my mentor, Dr. Karen Cichowski, for her help and support during my time in graduate school. Whenever I had questions, she was always willing to meet or talk over the phone. Without her guidance and sense of humor, I would not have gotten through the ups and downs of my research.

Secondly, I am incredibly appreciative of all the support various members of the Cichowski lab have given me ever since I joined in 2015. Some members in particular that I would like to thank are: Amy, for her support and kindness; Nelly, for her laughter and aid during the long days in the mouse house; Naomi, for checking in on me when I struggled through my first project; Ophelia, for teaching me about the importance of standing up for myself; Steph, for her kindness, enthusiasm, and help, especially as I started looking for careers outside of research; Abby, for her loyalty, support, and amazing desserts; Patrick, for his enthusiasm, patience, and planning abilities; Naiara, for her contagious laughter, Spanish lessons, and patience with both my scientific and lingual abilities; Rachel, for her support throughout my project, even when she was hobbling with a torn ACL; Ryan, for his humor, incredible kindness, selflessness, and funny t-shirts; Caroline, for all of the hard work she put towards this project; Lisa, for her gentleness, laughter, support; Masha, for being a goofball and never shutting up; and last but certainly not least, my dearest Marina, for loving me even though she constantly had to pick up after me. Marina, I am so glad you joined the Cichowski lab, and if I could, I would give you millions of embossed napkins. I would also like to thank Bill Hahn and members of his lab for their help and feedback during our joint lab meetings, and I would like to thank Steve Elledge and Tim Martin, who aided me in the CRISPR screen. I want to thank members of my PQE and DAC committees (Andi, Kevin, Jean, Nelly, Myles, Len, and Steve) and the BBS office (Kate, Anne, Maria, and Danny) for always believing in me. I also want to thank Biorender for letting me create great figures, which were created with biorender.com. Lastly, I would like to

re-thank Ryan, Elaine, Amy, Jeff, and Marina, who remotely helped me figure out how to save my thesis figures into high quality images. I am really lucky to have so many incredible friends.

I would also like to thank the amazing people I met through my graduate school program. Marina, of course, but also Rachel, Max, Carmen, Sisi, John, Pierce, Kaia, Rachel, Lara, Kayla, Renee, Maurizio, just to name a few. Every time I hung out with you, I always had so much fun. John, during my first rotation, you made sure that I never sat alone during lunch. You are very much missed.

Thank you to past and present members of the Roberts lab. You taught me how to be a better scientist and person, and I never would have gotten into Harvard without your support. Especially to: Charlie Roberts, for your mentorship; Katherine, for your optimism, support, love, and countless giggles; Xiaofeng, for always answering my questions quickly; Elaine, for being the best rock climbing buddy; and of course, Jeff, who followed me to BBS and is such a supportive friend.

I am thankful for the amazing people I met during my time at Bates College – especially my roommates Jocelyn and Jess, Jocelyn's sage wife Flora, my close friend Somi, and Dr. Paula Schlax, whose class made me realize that I loved science despite my initial dream of being an English major. Paula, you are such an incredible teacher, and I am so thankful that I decided to take that Chem 101 class my first year.

I am thankful for my Boston friends – Catherine, Drew, Jen, Matt M, Liz, Adam, Angela, Dave, Matt S, Yukang, Billy, Ben, Becky, Brandon, Alex, and so many more – thank you for providing some normalcy to my crazy life and for teaching me that it is OK to relax and have passions other than work.

I would like to thank my forever friends, who I met when I moved to my hometown in first grade. You are always there for me, from supporting me in high school plays to traveling to New

York for my bachelorette party, and for that I am so so grateful. First shout out to Meghan – thank you for keeping me sane! Second shout out to The Thread – Steph, Katie S, Sam, Shannon, Caitlin, and Katie F – my second family – I am so thankful that I stayed friends with you all, even when Steph kept stealing my sandwiches in the sixth grade. Thank you for your support during my time at Harvard. “When you find people who not only tolerate your quirks but celebrate them with glad cries of ‘Me, too!’ be sure to cherish them. Because those weirdos are your tribe.”

Thank you to my new family – Kim, Ray, Alex, Jackie – for your support during my time in graduate school as well. Alex, I would especially like to thank you for your patience during all those times I came home grumpy after a long day in lab. You are the kindest person and a wonderful roommate.

Thank you to my family. My cousins, aunts, uncles – you helped me out during all the rough times. My grandparents – you supported me throughout college and taught me to work hard. My parents – you taught me that I can do anything I set my mind to. My brother Gunnar – you always make me smile. My sister Merry – you are my best friend, I could not have survived this without your laughter. My pet siblings Ellie, Tang, and Waffles – thanks for the unconditional love!

Lastly, I would like to thank my little Boston family – my husband Brendan and my pets Featherduster and Popover. Duster, thank you for staying up all those late nights and cuddling with me as I studied. Poppy, thank you for providing humor to every situation and for forcing me to go on long walks. Brendan, my love, when I first met you at a college party in 2009, you had on a top hat, a dinosaur sweatshirt, and an eyebrow ring, and I remember thinking, “Here is someone who will never bore me.” Thank you for being my therapist, my exercise buddy, my fellow pet wrangler, and my life coach and partner. I could not imagine getting through any of this without you. I love you and I like you.

Chapter 1 : Introduction

This dissertation focuses on the development of three novel and promising therapeutic combinations for patients with Ras/Raf/MEK/ERK (henceforth called Ras/ERK) pathway-driven melanomas. Melanomas, like many cancers, depend on the Ras/ERK signaling pathway for cell survival and growth, and this has led to the development of several pathway-specific inhibitors. For *BRAF*-mutant melanomas, the combination of MEK and BRAF-mutant-specific inhibitors have improved overall survival of these patients; however, relapse does occur within ~11 months (Chapman et al. 2011; Robert, Karaszewska, et al. 2015; Dummer et al. 2017). For *NRAS*-mutant melanomas, MEK inhibitors are even less effective, stimulating only partial responses in patients, with a dismal progression free survival of 2-3 months. Therefore, there is an unmet need to develop improved therapies for these individuals. We approached this problem using two strategies, which I will describe in this dissertation. First, we took an unbiased approach to identify targets that when suppressed cause potent cell death in combination with MEK inhibitors in *NRAS*-mutant melanomas. Specifically, we performed a negative selection genome-scale CRISPR-Cas9 screen and focused on hits with existing inhibitors in preclinical or clinical studies. Using this approach, we identified the de-ubiquitinase USP7 as a new therapeutic target in melanoma. Second, in collaboration with members of my laboratory and the Wood laboratory at Duke University, we also took a candidate-based approach, and through these efforts we identified two additional promising therapeutic combinations, Ras/ERK pathway inhibitors combined with either HDAC or BET inhibitors (Maertens et al. 2019; Katherine R. Singleton 2017).

Overall, this introduction sets the stage for my work by summarizing background about melanoma, including key signaling nodes and epigenetic dependencies that are present in these malignancies. I will also review how genome-scale CRISPR screens have been used to identify therapeutic targets in cancer, and I will specifically describe the target of interest

identified through our screen in Chapter 2, USP7. Lastly, I will briefly introduce two epigenetic regulators BET and HDAC proteins, which are the subjects of Chapters 3 and 4.

MELANOMA

Clinical outcomes

Cutaneous melanoma is a highly metastatic and treatment refractory skin cancer that originates from the malignant transformation of pigment-producing cells called melanocytes. In the US, it is the fifth most common cancer, with approximately 100,350 new cases expected to appear in 2020, leading to 6,850 deaths (ACS 2020; Howlader N 2019; Siegel, Miller, and Jemal 2019). Most melanomas are detected early through skin examinations; however, if they are not diagnosed or removed early enough, melanomas can spread to lymph nodes and other parts of the body, resulting in a poor prognosis. Early stage melanomas that are localized to the epidermis can be surgically resected, with a five-year survival rate of ~99%. If the melanoma spreads regionally to the lymph nodes, the 5-year survival rate is 65%, and if it metastasizes, the 5-year survival rate is only 25% (Figure 1-1). Despite several recent advances, most treatments for metastatic melanoma are still not curative. Therefore, there is a need for more effective therapies for individuals with advanced disease.

The strongest risk factors for developing melanoma are family history, fair skin, multiple moles, immunosuppression, and a history of UV radiation exposure through outdoor or indoor means, such as tanning beds. About 90% of melanomas are attributed to UV sun damage and arise sporadically, with the majority occurring in older (>55 years) patients on sun exposed areas such as the head and neck (Schadendorf et al. 2015). Populations with a red-hair/ fair-skin phenotype are more susceptible to developing melanoma because of intrinsic carcinogenic effects from inactivating variants of the highly polymorphic melanocortin 1 receptor gene *MC1R* as well as

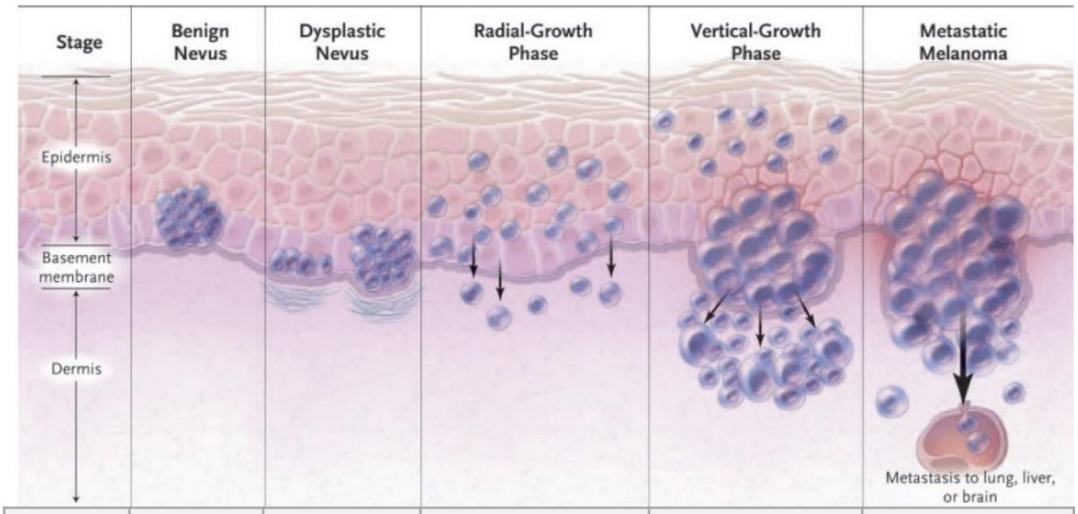

	Benign Nevus	Dysplastic Nevus	Radial-Growth Phase	Vertical-Growth Phase	Metastatic Melanoma
Clinical stage	0	0, I	0, I	I, II	III, IV
5-year survival (%)	100%	~99%	~99%	~99%	Stage III: 65% Stage IV: 25%
Biologic events	• Benign • Limited growth	• Premalignant • Lesions may regress • Random atypia	• Decreased differentiation • Unlimited hyperplasia • Cannot grow on soft agar • Clonal proliferation	• Decreased differentiation • Crosses basement membrane • Grows in soft agar • Forms tumor	• Decreased differentiation • Dissociates from primary tumor • Grows at distant sites, starting with lymph nodes, then lung, liver, or brain
Examples of molecular lesions that may occur	*BRAF* mutation	CDKN2A loss PTEN loss *TP53* inactivation	Increased CD1	E-cadherin loss N-cadherin expression MMP-2 expression Survivin Reduced TRPM1	E-cadherin loss N-cadherin expression MMP-2 expression Survivin Absent TRPM1

Adapted from Miller and Mihm, 2006

Figure 1-1. Clinical stages and examples of biologic events that may occur during the progression of melanoma

reduced UV radiation protection (Raimondi et al. 2008). Overall, the risk of melanoma is 20 times more common in non-Hispanic whites than in other populations, with an annual global rate as high as 28 cases per 100,000 people. A familial predisposition underlies ~8-12% of melanomas, and ~40% of these patients carry mutations in cyclin-dependent kinase inhibitor 2A (*CDKN2A*), a gene that encodes the two tumor suppressive proteins $p16^{INK4a}$ and $p14^{ARF}$ (FitzGerald et al. 1996).

Oncogenic drivers of melanoma

Studies investigating the molecular basis of melanoma genesis and progression have revealed key “driver” mutations (*i.e.* mutations that confer a fitness advantage to a tumor cell) and “passenger” mutations (*i.e.* mutations that do not confer a fitness advantage); however the precise steps that underlie melanoma pathogenesis remain poorly defined. Melanomas have the highest mutational load of human tumors due to increased DNA damage from UV rays, with a large number of genes containing common UV-associated signatures such as C>T or G>T transitions (Schadendorf et al. 2015; Berger et al. 2012; Pleasance et al. 2010). For example, *TP53*, a prominent tumor suppressor, is mutated in ~15% of cutaneous melanoma samples and usually contains putative UV-related mutations ('Genomic Classification of Cutaneous Melanoma' 2015). However, there is evidence that not all driver mutations stem from UV damage. As mentioned earlier, there are patients with family history of the disease who develop melanoma independent of UV damage. Additionally, some melanomas develop in non-sun-exposed skin or on internal organs. Finally, the majority of cutaneous melanomas contain mutations in the Ras/ERK signaling pathway, which controls fundamental cellular processes including cell growth, differentiation, and apoptosis; however, most of these mutations are not attributable to direct UV damage ('Genomic Classification of Cutaneous Melanoma' 2015; Hodis et al. 2012) (Figure 1-2). For example, mutations in codon V600 of the serine/threonine kinase BRAF are not caused directly by UV damage, and yet they occur in 50-60% of all cutaneous melanoma tumor cases. One hypothesis put forth to explain this observation is that UV rays may indirectly cause genetic aberrations by releasing free radicals.

Interestingly, mutations in the Ras/ERK pathway have been observed in benign melanocytic neoplasms, or skin moles, suggesting that mutations in the Ras/ERK pathway represent early steps that prime melanocytes to eventual transformation. Studies using *BRAF*-mutant mouse models have shown that mutations in the Ras/ERK pathway are not sufficient to

transform melanocytes and instead lead to oncogene-induced senescence (Gray-Schopfer et al. 2006; Michaloglou et al. 2005; Dankort et al. 2009; Dhomen et al. 2009; Pollock et al. 2003; Vredeveld et al. 2012). However, UV exposure or stochastic acquisition of additional genetic alterations, such as the mutational inactivation of *TP53,* leads to malignant growth (Dhomen et al. 2009).

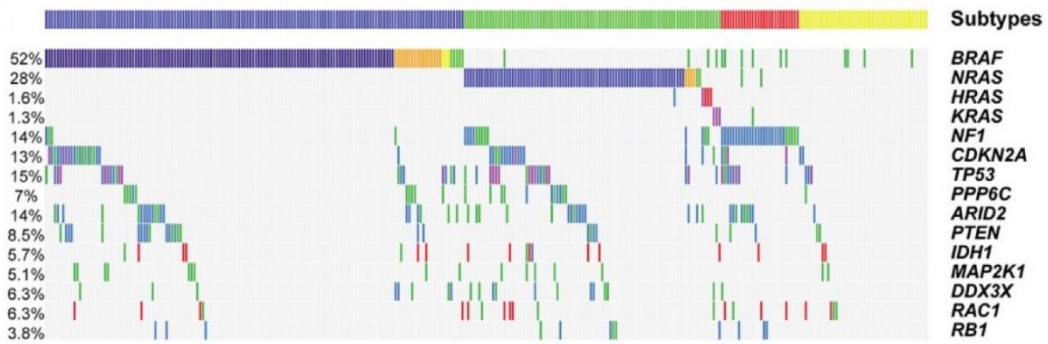

Figure 1-2. Driver mutations in melanoma

Common mutations in patients with melanoma, grouped by *BRAF* (blue subtype), *NRAS* (green subtype), *NF1* (red subtype), and wild-type (yellow subtype). COSMIC (Catalogue of Somatic Mutations in Cancer); LOF (loss of function). Figure adapted from Genomic Classifications of Melanoma, 2015.

Examples of common secondary mutations are those that inactivate tumor suppressors such as *CDK2NA*, *TP53*, and *PTEN* or activate oncogenic genes such as *RAC1* and *TERT*. Genetic amplification of some genes is also linked to tumorigenesis. One transcription factor amplified in 8-20% of sporadic melanomas is *MITF*, a master regulator of melanocyte development and a lineage survival oncogene in melanoma. MITF is also downstream of the Ras/ERK pathway and has been found to stimulate cell cycle progression, motility, and evasion of apoptosis (Levy, Khaled, and Fisher 2006).

Because the Ras/ERK pathway is commonly affected in melanoma growth and progression, melanomas are often defined by mutations in genes that function in this pathway. Fortunately, two members of the Ras/ERK pathway, BRAF and MEK, have proven to be targetable, resulting in the development of several small molecule inhibitors (Chapman et al.

2011; Robert, Karaszewska, et al. 2015). Although generally not curative, MEK and BRAF-mutant-specific inhibitors cause profound tumor regression in *BRAF*-mutant melanomas, highlighting the importance of the Ras/ERK pathway to melanoma survival and growth. Therefore, Ras/ERK pathway inhibitors have become standard of care for many advanced melanoma patients.

THE RAS SIGNALING PATHWAY

Because of the importance of the Ras/ERK pathway in melanoma biology, this section will focus on our current understanding of Ras signaling and how it is deregulated in cancer. After providing a brief overview of pathways that stem from Ras, I will then summarize current research investigating Ras/ERK signaling in melanoma.

Overview of Ras and Ras effector pathways

The initiation of Ras signaling typically begins with the activation of a receptor tyrosine kinase (RTK) (examples: HER2/ERBB2 or EGFR) on the cell surface through growth factors, cytokines, and/or extracellular mitogens (Lemmon and Schlessinger 2010). Once activated, RTKs auto-phosphorylate, generating binding sites for adaptor molecules which in turn recruit cytoplasmic Ras GTPase Exchange Factors, or RasGEFs, to the plasma membrane. Ras family proteins – HRAS, KRAS, and NRAS – are independently recruited to the plasma membrane. There they constantly cycle between active (GTP-bound) and inactive (GDP-bound) states that are catalyzed by RasGEFs and Ras GTPase Activating Proteins (RasGAPs) respectively (Simanshu, Nissley, and McCormick 2017; Bourne, Sanders, and McCormick 1990). Because the GTP hydrolysis activity of Ras proteins is inherently slow, RasGAPs are essential for ensuring that Ras activity is turned off. The rate of activation or inactivation by RasGEFs and RasGAPs depends on the proximity of these proteins to Ras in the plasma membrane.

Active Ras (Ras-GTP) controls cell proliferation, survival, and transformation through several signaling cascades, including but not limited to the 1) Raf/MEK/ERK, 2) PI3K/AKT, and 3) RAL-GDS signaling pathways (Figure 1-3). Though other Ras effector pathways have been identified, these three pathways in particular are important for cell growth and survival, and therefore are the best studied. Because melanomas commonly harbor mutations in genes that function within the Raf/MEK/ERK and PI3K/AKT pathways, I will briefly summarize these pathways.

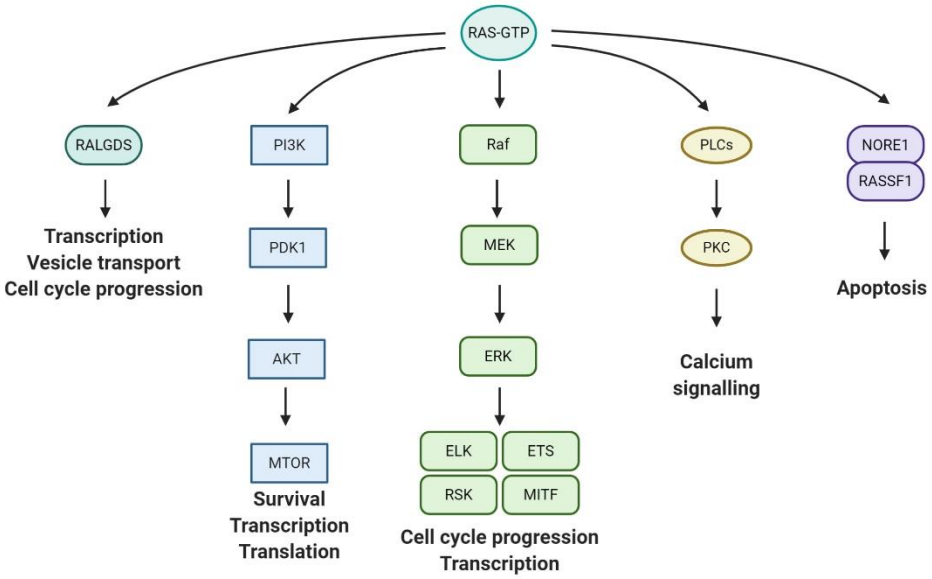

Figure 1-3. Simplified schematic of Ras effector pathways

Schematic illustrating how active Ras-GTP can regulate cell cycle progression, transcription, translation, and apoptosis. ELK, ETS, RSK, and MITF are a few of many effector proteins activated by ERK. Figure adapted from Downward, 2003.

To activate the Raf/MEK/ERK arm of the pathway, Ras binds to and activates three closely related Raf proteins, RAF1, BRAF, and ARAF, which are recruited to the plasma membrane by adaptor proteins and RasGEFs. In turn, Raf proteins phosphorylate and activate mitogen-activated protein kinases (MAPKs) MEK1 and MEK2, which then activate ERK1 and ERK2 through activation loop phosphorylation (Leevers, Paterson, and Marshall 1994; Leevers and Marshall 1992; Wood et al. 1992; Marais et al. 1995). ERK proteins phosphorylate and

activate many cytosolic and nuclear substrates, such as ETS transcription factors, which enhance cell proliferation and survival signals, and cyclin D1, which regulates cell-cycle progression. ERK proteins also ultimately negatively regulate the Ras/ERK pathway through negative feedback effects on RasGEFs, RasGAPs, and other proteins.

In addition to the canonical Ras/ERK pathway, Ras activates the PI3K/AKT pathway by first directly interacting with type I phosphatidylinositol 3-kinase (PI3Ks). PI3Ks phosphorylate phosphatidylinositol, bringing AKT serine/threonine kinase to the plasma membrane and causing its activation. Activated AKT in turn transmits downstream signals that regulate cell survival, protein synthesis, and metabolism (Engelman, Luo, and Cantley 2006). PI3Ks can also stimulate RAC, a RHO family protein important for regulation of the actin cytoskeleton.

The Ras pathway in cancer

Because pathways downstream of Ras signaling are important for cell survival and growth, Ras and its downstream effectors are often hijacked and overactivated by cancer cells, leading to malignant transformation (Downward 2003). About 20-25% of all human cancers harbor activating missense mutations in *RAS*. Of these cancers, the majority possess activating mutations in *KRAS* (85%), followed by activating mutations in *NRAS* (~15%) and *HRAS* (<1%). About 98% of mutations are found at one of three mutational hotspots: G12, G13, and Q61. Mutations in G12 and G13 impair the ability of RasGAPs to bind and change active Ras (Ras-GTP) to an inactive state (Ras-GDP), while mutations in Q61 impair the Ras catalytic site by decreasing intrinsic GTP hydrolysis through stabilization of the transition state, resulting in a protein with low hydrolysis rates and high signaling output (Bos 1989; Der, Finkel, and Cooper 1986; Ahmadian et al. 1999). Though *KRAS*, *NRAS*, and *HRAS* are highly similar in their primary sequences, there is a striking difference in the mutational profiles of *RAS* gene isoforms in cancer, suggesting tissue-distinct roles for Ras in driving oncogenesis. For example, *KRAS* is

commonly mutated in pancreatic, lung, and colorectal carcinoma, whereas *NRAS* is predominantly mutated in cutaneous melanoma ('Genomic Classification of Cutaneous Melanoma' 2015). Work thus far suggests that specific cancers select for certain mutations due to differential tissue expression patterns and the unique functional activities of each *RAS* family member. These features may include different effectors or subcellular localizations, but more work is needed to fully understand these differences (Lau and Haigis 2009; Haigis et al. 2008).

Upstream of Ras proteins, cancers can constitutively activate Ras signaling by inactivating RasGAPs, with the most well-studied example being through loss of neurofibromin 1 (*NF1*). *NF1* is mutated in a familial cancer syndrome called neurofibromatosis type I and has also been found to be mutated or suppressed in cancers such as cutaneous melanoma, glioblastoma, lung cancer, and neuroblastoma (2008; Ding et al. 2008; McGillicuddy et al. 2009; Parsons et al. 2008; Holzel et al. 2010). Additionally, over-expression of other upstream factors, such as RTKs EGFR and HER2/ERBB2, have both been found to be key drivers in many cancers, including breast cancer and melanoma (Lemmon and Schlessinger 2010).

Downstream components that are often mutated or amplified in cancers include Raf and MEK proteins as well as PI3K and AKT within the PI3K/AKT pathway. Loss of function defects in PTEN, a negative regulator of the PI3K/AKT pathway, can also occur and are relatively common in melanoma. In conclusion, genetic alterations in many upstream and downstream components of the Ras pathway contribute to its activation in cancer.

Ras signaling pathways in melanoma

Melanomas are classified into four genomic subtypes based on the presence or absence of mutations in the Ras pathway: *BRAF, NRAS, NF1,* and triple wild-type (WT) ('Genomic Classification of Cutaneous Melanoma' 2015). Overall, about 50-60% of melanoma patients having activating mutations in *BRAF*, with 89% of these mutations occurring within the kinase

activation loop domain (V600E/K/G/R) which increase overall activity (Davies et al. 2002). Though there are three main isoforms of *RAF* (*ARAF*, *BRAF*, and *RAF1*), *BRAF* is the only *RAF* isoform that is mutated in melanoma. One potential explanation for the differential mutation frequency of these genes is that activating mutations of *BRAF* require only one genetic mutation compared to two genetic events that must occur to activate *ARAF* or *RAF1* (McCubrey et al. 2007).

NRAS mutations occur in 15-30% of all melanomas and are found to be mutually exclusive with *BRAF* mutations (Ellerhorst et al. 2011). Though mutations in other *RAS* isoforms have been detected in melanomas, they occur at a much lesser frequency than *NRAS* mutations, with less than 2% of all melanomas harboring activating mutations in *KRAS* or *HRAS*. About 80% of *NRAS*-mutant melanomas exhibit mutations in codon 61, resulting in permanent activation by locking *NRAS* in its GTP bound state (Der, Finkel, and Cooper 1986; Ahmadian et al. 1999). Interestingly, mutant *NRAS* has been found to activate the Raf/MEK/ERK pathway through RAF1, mainly because activation of ERK induces persistent phosphorylation of BRAF, which prevents BRAF from binding to NRAS and, in turn, inhibits BRAF activity (Dumaz 2011; Ji, Flaherty, and Tsao 2010; Dumaz et al. 2006; Heidorn et al. 2010). Therefore, *NRAS*-mutant melanomas are normally not sensitive to BRAF inhibition alone (Kaplan et al. 2012).

Melanomas without recurrent mutations in either *BRAF* or *NRAS* exhibit significant enrichment of *NF1* alterations (Hodis et al. 2012). About 10-12% of melanomas have inactivating mutations in the RasGAP *NF1*, and this is associated with elevated activation of H/KRAS-GTP and resistance to BRAF inhibitors through RAF1/MEK/ERK and PI3K/AKT signaling (Nissan et al. 2014; Maertens et al. 2013; Whittaker et al. 2013). Additionally, there is a so-called “triple wild-type” subset, in that they do not have any clear mutations in *NRAS*, *BRAF*, or *NF1*. However, many of these “wild-type” melanomas still contain constitutive

activation of the Ras/ERK pathway, further highlighting the importance of the pathway to melanoma malignant growth. For example, activating mutations and amplification of upstream RTKs *KIT* and *EGFR* are observed in this subset.

The incidence of *NRAS* and *BRAF* mutations vary between patients, and the reasons for this variability is currently under investigation (Curtin et al. 2005; Lee, Choi, and Kim 2011). *NRAS*-mutant melanomas occur in all sites of cutaneous melanoma, including sun-exposed and sun-unexposed skin, and typical *NRAS*-mutant melanoma patients tend to be older (>55 years) and contain a pattern of UV exposure and lesions. Additionally, *NRAS* mutations are rarely present in benign melanocytic nevi. In contrast, *BRAF* mutations are more common in intermittently sun-exposed skin, in younger patients without a pattern of UV exposure, and in benign melanocytic nevi. Histologically, mutant *NRAS* tumors have thicker lesions and are more aggressive than other subtypes, with elevated mitotic activity and higher rates of lymph node metastasis (Devitt et al. 2011). Because *NRAS* mutations are associated with a more aggressive disease, *NRAS* mutation status is a predictor of poorer outcomes in patients, with a lower median overall survival (OS) compared to non-*NRAS*-mutant melanomas (Muñoz-Couselo et al. 2017). This is compounded by the limited activity of current therapies in these tumors, which will be discussed below. Therefore, there is an urgent need for new therapies for these patients.

TARGETING RAS-DRIVEN MELANOMAS

In this section, I will highlight the standard of care for individuals with advanced stage melanoma. I will also summarize treatments that are in clinical trials and identify areas of unmet need for these patients.

Targeting the Ras pathway

The discovery of the dependence of melanomas on the Ras/ERK pathway led to the

development of several pathway-specific inhibitors and revolutionized the standard of care for many advanced stage melanoma patients (Davies et al. 2002; Chapman et al. 2011). Before 2011, patients were treated with either the chemotherapy dacarbazine or the immunomodulating drug cytokine IL-2, with a median overall survival of ~9 months. (Luke and Schwartz 2013). The first small molecule Ras/ERK pathway inhibitor to enter the clinic was the selective V600-mutant BRAF inhibitor vemurafenib. Excitingly, clinical trials found that vemurafenib increased the overall response rate (ORR) in *BRAF*-mutant patients to 48% compared to just 5% for dacarbazine (Chapman et al. 2011). However, resistance to BRAF inhibition eventually occurred, and subsequent studies identified that resistance was mainly through enhanced activation of the Ras/ERK signaling pathway (Solit and Rosen 2011). To combat this, the selective BRAF inhibitor dabrafenib was combined with the MEK inhibitor trametinib, and this combination therapy increased the overall response rate of patients to 64% compared to vemurafenib, with a median progression free survival (PFS) of 11.4 months versus 7.4 months and a median overall survival (OS) of 25.1 months compared to 18.7 months (Robert, Karaszewska, et al. 2015). Similar results were observed with the combination of BRAF inhibitor vemurafenib and MEK inhibitor cobimetinib (Ribas et al. 2014). Therefore, the combination of BRAF and MEK inhibitors were approved for *BRAF*-mutant melanoma patients and have since become the standard of care. Immunotherapies in the context of the standard of care will also be discussed below.

Unfortunately, Ras/ERK pathway targeted therapies have not been as successful in non-*BRAF*-mutant melanomas. With the exception of one specific mutant *KRAS* allele, Ras proteins have been difficult to target, and while *in vitro* MEK inhibitor data appeared promising for *NRAS*-mutant tumors, Phase II and III trials of the MEK inhibitor binimetinib in *NRAS*-mutant melanoma patients had an ORR of 15-20%, median PFS of only 2.8 months, and OS of 11 months (Dummer et al. 2017; Singh, Longo, and Chabner 2015; Solit et al. 2006). The potential efficacy of MEK inhibitors in *NF1*-mutant tumor is not yet known. Regardless, there is an urgent

need for improved therapies for non-*BRAF*-mutant melanoma patients. One approach in *NRAS*- and *NF1*-mutant tumors would be to develop combination therapies that might increase the efficacy of MEK inhibitors.

Mechanisms of resistance to Ras pathway inhibitors in melanoma

Despite initial responses to BRAF/MEK inhibitors, most *BRAF*-mutant tumors develop resistance to Ras/ERK pathway inhibitors, either through *de novo* or acquired mutations. Pre-existing, *de novo* resistance mechanisms are attributed to the complex heterogeneity seen in melanoma tumors due to repeated DNA damage from UV exposure. Additionally, epigenetic alterations or genomic mutations in intrinsic bypass survival pathways, such as the PI3K/AKT pathway, may promote resistance. For example, a common mutation found in melanoma leads to loss of PTEN, which is a negative regulator of the PI3K/AKT pathway, and this has been shown to cause resistance in patient tumors (Paraiso et al. 2011).

Acquired resistance has mainly been associated with mutations in *NRAS* or the downstream kinase *MEK1*, *BRAF* amplification or splicing, overexpression of *COT*, and activation of RTKs (Wagle et al. 2014; Shi et al. 2012; Corcoran et al. 2010; Poulikakos et al. 2011; Wagle et al. 2011; Johannessen et al. 2010; Nazarian et al. 2010; Van Allen et al. 2014).. Resistance to MEK inhibitors may also occur through impaired activation of the transcription factor FOXO3a, leading to a reduction in *BCL2L11* expression and suppression of apoptosis (Yang, Chang, et al. 2010). In conclusion, though targeting the Ras/ERK pathway with BRAF and MEK specific inhibitors does initially lead to a response, eventually cancer cells can acquire multiple compensatory defects to evade cell death; thus, there is an urgent need for additional therapies that can target these diverse mechanisms of resistance.

Additional therapies for advanced stage melanoma

In addition to targeted small molecule therapies, immune checkpoint inhibitors are also used in the clinic to treat advanced stage melanomas. The clinical development of CTLA-4 and PD-1/PD-L1-blocking antibodies has had a profound impact on the treatment of melanoma, with a PFS of 16.8 months and 5-year OS of 60% with the anti-CTLA-4 therapy ipilimumab plus anti-PD-1 therapy nivolumab in treatment-naïve patients harboring a *BRAF* mutation (Larkin et al. 2019). Non-*BRAF*-mutant melanomas, such as *NRAS*-mutant, have a lower response rate to immune checkpoint inhibitors ipilimumab and nivolumab, with a 5-year a PFS of 11.2 months and OS rate at 46% (Dummer et al. 2017; Sarkisian and Davar 2018). Because not all patients respond successfully to these therapies, considerable effort is being invested in the identification of predictive biomarkers. One promising biomarker is serum lactate dehydrogenase (LDH), with high baseline levels associated to a less favorable outcome in terms of response rate to BRAF and MEK inhibitors and anti-PD-1 immunotherapy (Hodi et al. 2018). Other studies hint that tumor mutational burden and the presence of tumor-infiltrating lymphocytes, PD-L1 expression, and intestinal microbiota are all linked to better responses as well (Garrett 2015; Cristescu et al. 2018). Resistance does eventually occur with immune checkpoint inhibitors, and mechanisms include T cell dysfunction, melanoma cell dedifferentiation, and upregulation of compensatory immune checkpoint proteins (Jenkins, Barbie, and Flaherty 2018).

Studies are also ongoing about whether patients should be treated with BRAF and MEK inhibitors before immune checkpoint inhibitors, or vice versa. Most evidence supports a positive effect of Ras/ERK pathway inhibitors on immune recognition, meaning that BRAF and MEK inhibitors may lead to a better response when given to patients before immunotherapies (Hu-Lieskovan et al. 2015). However, one major gap in knowledge pertains to the optimal scheduling and sequencing of targeted agents and immunotherapies. Studies thus far have generally been

performed at very early time points in the course of therapy, and later analyses have found that the effects of Ras/ERK therapy on melanoma antigen expression and T-cell infiltration may dissipate over time (Cooper et al. 2016). Therefore, more studies are needed to determine the appropriate combination and sequence of inhibitors to treat melanoma patients.

Combination targeted therapies

Combining Ras/ERK pathway inhibitors with other small molecule inhibitors or immune checkpoint inhibitors is currently being evaluated in clinical trials based on promising preclinical studies. One example is the combination of MEK and CDK4/6 inhibitors in patients with *NRAS*-mutant melanoma, and early results have shown partial responses in 33% and stable disease in 52% of patients (Sosman et al. 2014). Other combinations currently in clinical trials are Ras/ERK pathway inhibitors with PI3K or MET inhibitors in *BRAF*-mutant and non-*BRAF*-mutant melanomas (Table 1-1). However, to date, no clinical combinations have been found to be effective in a majority of patients, especially in patients with non-*BRAF*-mutant melanomas.

Table 1-1. A selection of current clinical trials of combination therapies with Ras/ERK pathway inhibitors in *BRAF* or *NRAS* mutant melanomas

Completed, recruiting, active not recruiting, and not yet recruiting clinical trials that involve combination therapies with Ras/ERK pathway inhibitors in melanoma.

Melanoma type	Drugs	Last posted date	Phase	Target(s)	Status	NCT
NRAS mutant	Binimetinib (MEK162) + ribociclib (LEE001)	2018	I/II	MEK + CDK4/6	Completed	NCT01781572
	Binimetinib (MEK162) + palbociclib	2019	III	MEK	Completed	NCT01763164
	Trametinib (MEKINISTR) + Hydroxycholorquine (PLAQUENILR)	2019	I	MEK + autophagy	Not yet recruiting	NCT03979651
	Cobimetinib + IN10018	2020	I	MEK + FAK	Recruiting	NCT04109456
	Trametinib + LXH254	2020	I	MEK + pan-RAF	Recruiting	NCT02974725
	LXH254 + LTT462	2020	I	Pan-RAF+ ERK	Recruiting	NCT02974725
	LXH254 + Ribociclib	2020	I	Pan-RAF + CDK4/6	Recruiting	NCT02974725
BRAF mutant	Pimasertib + SAR245209	2017	I	MEK + PI3K/mTOR	Completed	NCT01390818
	LGX818 + MEK162 + nivolumab + ipilimumab	2019	II	BRAF + MEK + anti-CTLA4 + anti-PD-1	Active, not recruiting	NCT02631447
	LGX818 + MEK 162 + BKM120/LEE011/BGJ398/INC280	2020	II	BRAF + MEK + PI3K or CDK4/6 or FGFR or c-MET	Active, not recruiting	NCT02159066

Therefore, additional approaches are needed to identify rational combination treatments that may produce a more robust and durable response. One promising strategy that we have successfully explored in other cancers is to target both oncogenic kinases and epigenetic regulatory proteins in cancer (De Raedt et al. 2014; Malone et al. 2017; Guerra et al. 2020; Maertens et al. 2019). Additionally, another promising strategy is to take an unbiased approach through functional genomic screens, which I have employed in my research.

GENETIC SCREENS TO IDENTIFY NEW DRUG TARGETS

One approach that can be used to identify potential therapeutic targets of interest is functional genomic screening. Though mutational analyses of tumors have identified many targetable proteins, such as members of the Ras/ERK pathway in melanoma, “driver” mutations identified in tumors only represent a small number of proteins that are druggable. Some cancer targets may not be genetically activated through mutation, amplification, or translocation, but are still important oncogenic drivers in specific genetic contexts, such as epigenetic regulators. In addition, tumors may harbor unique cancer specific vulnerabilities, which could be exploited by targeting critical “protective” pathways (Luo, Solimini, and Elledge 2009). To identify these alternative types of targets, functional genomic screening platforms, such as loss-of-function genome-wide CRISPR-Cas9 screens, are powerful tools. They can be used to provide an unbiased genome scale identification of other genes that, when suppressed, kill specific cancers or cooperate/ enhance the effects of other targeted agents.

CRISPR, which stands for bacterial type II clustered regularly interspaced short palindrome repeats, and its associated Cas9 protein system have been adapted into mammalian cells to generate a simple and efficient means of generating targeted mutations (Cong et al. 2013). Short 20-nucleotide guide RNAs (sgRNAs) guide Cas9 proteins to target loci, and Cas9 then generates precise double strand breaks which are repaired by error-prone non-homologous end-joining (NHEJ), leading to a production of indels and frame-shifts and thus

“knock-out” alleles. Because of the simplicity of the CRISPR-Cas9 system, it can easily be scaled up through pooled microarray synthesis of sgRNAs, generating CRISPR-Cas9 libraries with multiple sgRNAs targeting most, if not all, known genes in the human genome. This then enables the use of pooled genome-scale loss-of-function CRISPR screens to systematically interrogate gene function in different biologic processes. Since the first development of a genome-scale CRISPR library, many laboratories have used these screens to identify genes essential in different genetic contexts and genes involved in drug or toxin resistance (Wang, Birsoy, et al. 2015; Hart et al. 2015; Shalem et al. 2014).

In a pooled screening format, the complete sgRNA library is synthesized, cloned, and transfected into a pool of cells, and the cells are then separated based on an observed phenotype related to cell morphology, chemistry, or cell viability (Figure 1-4) (Xue et al. 2016; Dhanjal, Radhakrishnan, and Sundar 2017). Viable cells can then be used for a positive selection and/or a negative selection assessment. In a positive selection screen, genetic manipulation (such as through CRISPR-Cas9 mediated gene knock out) will favor cell proliferation and/ or survival under the created selective pressure. Conversely, negative selection screens identify cells (and thus guides) that have been depleted from the pool of cells over the treatment period. The depletion of cells is then attributed to the specific genetic perturbations that affect cell survival and/or proliferation.

Synthetic lethality is when an individual defect in one of two distinct genes does not elicit a lethal effect on cells, but simultaneous defects together lead to cell death. In the context of cancer, synthetic lethality is also used to identify drugs or drug combinations that will elicit cell death only in cancer cells but not in normal tissues. For example, cancers with loss-of-function mutations in BRCA2, which is important for DNA double-strand break repair by homologous recombination (HR), are specifically sensitive to inhibition of the protein PARP, which is involved in base excision repair (Farmer et al. 2005; Bryant et al. 2005). Therefore, PARP and BRCA2

are synthetic lethal partners. Recently, large-scale gene-knockout studies have become the standard to map synthetic lethal interactions in cancer cells. Additionally, the concept of synthetic lethality can be applied to identify drug targets that synergize to cause potent cell death with other drugs that, on their own, do not.

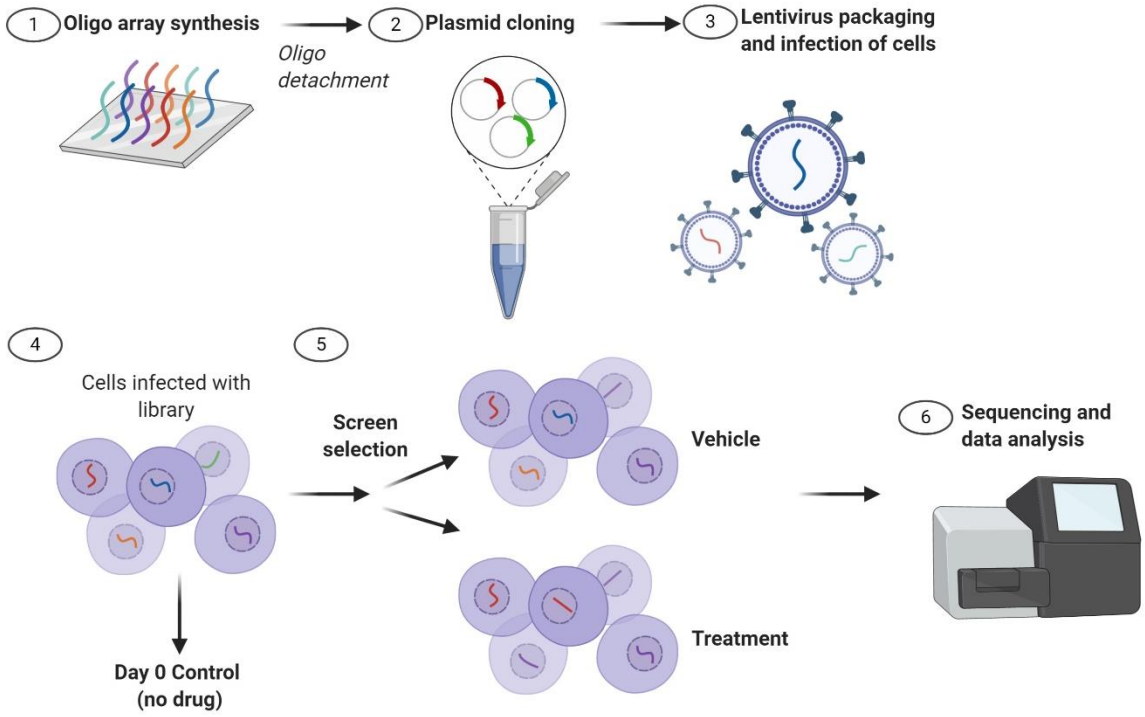

Figure 1-4: Schematic example for a negative-selection CRISPR-Cas9 screen

(1) sgRNAs are synthesized using pooled microarray (2) before being cloned into a plasmid backbone that contains the Cas9 protein sequence as well. (3) Lentivirus is packaged and (4) cells are infected with library. A day 0 is collected as a control before (5) drugs are added for a select amount of time. (6) Genomic DNA is then extracted, sequenced, and analyzed.

In Ras-driven malignancies, large-scale gene-knockout or knockdown studies have been used to identify pathways of resistance as well as synthetic lethal partners to BRAF and/or MEK inhibitors (Table 1-2). However, in many cases, identified targets are part of Ras signaling, either within the Raf/MEK/ERK pathway or PI3K/AKT pathway. We hypothesized that there might be several reasons why identified targets are primarily components of the Ras pathway. First, often the dose of MEK or BRAF inhibitors used is equivalent to the IC50 dose, which

Table 1-2: Negative selection gene knockout or knockdown studies to identify synthetic lethal partners to BRAF and/or MEK inhibitors in Ras-driven malignancies.

Type of screen	Screen schematic	Length of treatment time before sequencing	Cancer type	Ras/ ERK pathway mutational status	Drug treatment	Top hits	Citation
Negative selection, CRISPR-Cas9	Custom screen targeting kinases, phosphatases, druggable genes (2194 genes)	21 days	Lung	*KRAS* mutant	MEK inhibitor cobimetinib or ERK inhibitor GDC-0994	MAPK7, RAF1, MAPK1, KRAS	Dompe et al., 2018
Negative selection, CRISPR-Cas9	Whole genome	14 days	Pancreatic and lung	*KRAS* mutant	MEK inhibitor trametinib (dose varied depending on cell line)	SHOC2, MAPK1, RAF1, BRAF	Sulahian et al., 2019
Negative selection, CRISPR-Cas9	Druggable genes and survival pathways screen (378 genes)	21-28 days	Lung, colon, pancreatic, ovarian	*KRAS* mutant	MEK inhibitor AZD6244, GDC-0623, ERK inhibitor SCH772984, pan-PI3K inhibitor BKM120. At doses yielding on-target inhibition and 25% growth inhibition.	AKT1, RAF1, BRAF, IGF1R, AKT2, RICTOR, MTOR, SRC	Anderson et al., 2017
Negative selection, CRISPR-Cas9	6K cancer library (6000 cancer-related genes)	14 days	Melanoma	*BRAF* mutant, *BRAF* inhibitor resistant	RAF inhibitor PLX4720 (1uM)	SOS1, PURA, HRAS, SAFB, CRKL, ETV5, CDK6, DYNCH1, H2AFX, MAZ, SRC, EFGR, RAF1	Li et al., 2019
Negative selection, shRNA	Whole genome	6 days	Lung	*KRAS* mutant	MEK inhibitor trametinib (dose that elicits 40% reduction in viability)	MTOR, RRAGC, RAF1, ERBB3	Molina-Arcas, et al., 2019
Negative selection, shRNA	Kinase and kinase-related genes (535 genes)	14 days	Lung and colon	*KRAS* mutant	MEK inhibitor AZD6244	RAF1, BRAF	Lamba et al., 2014
Negative selection, shRNA	Kinome (526 genes)	10 population doublings	Lung and pancreatic	*KRAS* mutant	MEK inhibitor trametinib (25nM – inhibits ERK signaling without affecting proliferation)	BRAF, RAF1, ERK2, FGFR1	Manchado et al., 2016
Negative selection, shRNA	Druggable (1,200 genes)	7 days	Lung, colorectal, pancreatic	*KRAS* mutant	MEK inhibitor AZD6244 (1uM)	BCL-XL, RAF1	Corcoran et al., 2013
Negative selection, shRNA	Phosphatome (298 genes)	18 days	Colon	*BRAF* mutant	BRAF inhibitor vemurafenib (2uM)	PTPN11, CLEC1B, PPFIA1	Prahallad et al., 2015
Negative selection, shRNA	Kinome (518 genes)	21 days	Lung, colon	*KRAS* mutant	MEK inhibitor AZD6244 (IC50)	ERBB3, RAF1	Sun et al., 2014
Negative selection, shRNA	"Signaling components" (5,046 genes)	10 days	Lung	*BRAF* mutant	BRAF inhibitor vemurafenib (IC50)	YAP, PCK1, UPB1, SUZ12, MAP3K3, PARP1	Lin et al., 2015
Negative selection, shRNA	Whole genome	16 population doublings (~14-16 days)	Colorectal	*BRAF* mutant, *BRAF* inhibitor resistant	RAF inhibitor PLX4720 (3uM)	MET, MLL, PTPN11, ERBB3, SHOC2, RAF1, MAP2K2	Whittaker et al., 2015

results in incomplete inhibition of the pathway. Therefore, genes that enhance the cytostatic effects of BRAF or MEK inhibitors are often “on target” and affect direct components of this pathway. Secondly, screens usually are terminated after 10-20 population doublings and this selects for hits that can be either cytostatic or cytotoxic. Therefore, in Chapter 2 of my thesis, we describe a different experimental design for our loss-of-function, genome-scale CRISPR-Cas9 screen to identify targets that, when suppressed, actively kill *NRAS*-mutant melanomas when combined with MEK inhibitors.

TARGETING DE-UBIQUITINASES

Using a negative selection genome-scale CRISPR-Cas9 screen approach, which will be discussed in Chapter 2, I have shown that loss of the de-ubiquitinase USP7 potently sensitizes *NRAS*- and *BRAF*-mutant melanomas to Ras/ERK pathway inhibitors. In this section, I provide background about de-ubiquitinases and their role in cancer.

Regulation of ubiquitin

Ubiquitin (Ub) is a 76-amino acid protein that can be conjugated onto a substrate protein, “tagging” the substrate protein for trafficking or degradation within the cell (Nalepa, Rolfe, and Harper 2006; Bedford et al. 2011; Komander, Clague, and Urbe 2009). The process of “tagging” a protein with ubiquitin is executed by several enzymes and enzyme complexes, including E1, E2, and E3 Ub ligases and deubiquitinase enzymes (DUBs). In summary, E1 enzymes activate Ub and transfer it to E2 enzymes; E2 enzymes transfer Ub to E3 ligases; and E3 ligase complexes transfer Ub to the lysine residues of proteins (Figure 1-5). In the case of protein degradation, polyubiquitin chains are built up on the targeted protein, leading to recognition by the ubiquitin-proteasome system (UPS) and degradation of the polyubiquitin labeled protein. Conjugation of a single Ub molecule (monoubiquitination), by contrast, has been shown to regulate target activity instead of causing degradation. For example,

monoubiquitinated histone H2B has been shown to regulate transcriptional elongation, and monoubiquitination of PCNA leads to error-free DNA replication. DUBs remove monoubiquitin or polyubiquitin chains from the lysine residues of proteins, reversing the function of E2 ubiquitin conjugating enzymes and E3 ligases. The dynamic balance between ligase and DUB activity within a cell regulates cellular activities such as apoptosis, cell division, and cell signaling.

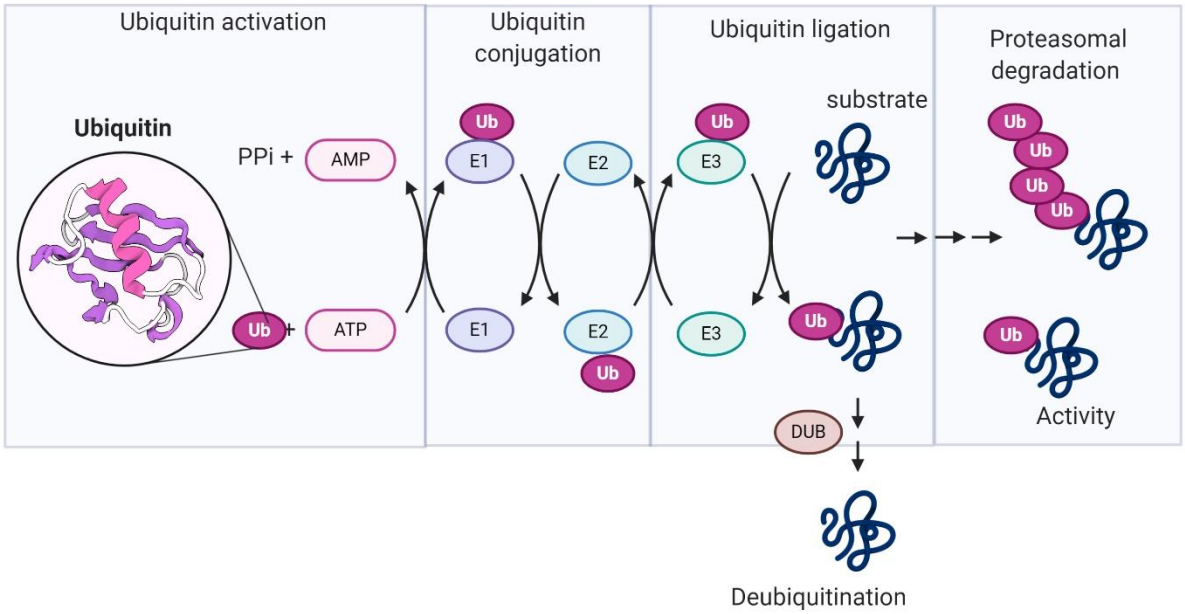

Figure 1-5. Simplified schematic of ubiquitin regulation in the cell

Ubiquitin is first activated by E1 proteins, which then conjugate ubiquitin to E2 proteins. E3 ligase complexes then transfer ubiquitin from E2 proteins to a substrate protein. Polyubiquitination marks the substrate for proteasomal degradation, while monoubiquitination may affect the protein's activity in the cell. Deubiquitinases (DUB) remove poly or mono ubiquitin from substrates. Figured adapted from Wertz and Murray, 2019.

De-ubiquitinases in cancer

In total, there are approximately 98 DUBs encoded in the human genome, and they are categorized into 6 subfamilies: USPs (ubiquitin-specific proteases), UCHs (ubiquitin carboxyl-terminal hydrolases), OTUs (ovarian-tumor proteases), MJDs (Machado-Joseph disease protein domain proteases), JAMMs (JAMM/MPN domain-associated metallopeptidases) and MCPIPs (monocyte chemotactic protein-induced proteases) (Reyes-Turcu, Ventii, and Wilkinson 2009).

USP DUBs are the largest family, with approximately 60 members. DUBs vary in their targets, with some DUBs preventing degradation of proteins through the proteasome, while others altering signals mediated by non-degradation ubiquitin. By removing ubiquitin, DUBs also generate free ubiquitin, releasing it into the ubiquitin pool where it can then be bound and activated by E1 enzymes.

Irregular DUB expression is commonly associated with increased migration, invasion and carcinogenesis in cancers. For example, the DUB A20/TNFAIP3 is a negative regulator of the NF-kB pathway, and several studies have identified deletions or mutations of A20/TNFAIP3 in Non-Hodgkin's Lymphoma (Honma et al. 2009). Within melanoma, the DUB USP13 has been shown to stabilize and upregulate MITF through deubiquitination (Zhao et al. 2011). Because many DUBs contain catalytic domains that are easy to target, a number of inhibitors are currently in development (Table 1-3). Additionally, the approval of Bortezomib (Velcade), a pan-DUB inhibitor, as therapy for multiple myeloma and mantle cell lymphoma has led to increased interest in developing more specific DUB inhibitors for cancer (Lim and Baek 2013).

USP7 function

Ubiquitin-specific peptidase or protease 7 (USP7), which is also known as herpesvirus-associated ubiquitin-specific protease (HAUSP), is a USP family DUB that can remove polyubiquitin chains and monoubiquitin from substrates (Cheon and Baek 2006). Found initially in the nucleus, it has subsequently been show to exhibit a dynamic overall cellular distribution under different pathological conditions and genetic perturbations (Everett et al. 1997). For example, it has been found in both the cytoplasm and the mitochondria. Overall, it is widely expressed in all tissue types. The structure of USP7 contains four domains: an N-terminal tumor necrosis factor-receptor associated factor (TRAF) domain, a catalytic domain, a 5-ubiquitin-like domain, and a C-terminal regulatory domain (Holowaty et al. 2003). The catalytic domain

recognizes and cleaves ubiquitin from the substrate, while the C-terminal regulatory domain recognizes and binds to the substrates.

Table 1-3: Selected preclinical inhibitors targeting members of the USP family of DUB proteins

Table adapted from (Harrigan et al. 2018).

USP	Inhibitors	Disease indication	Company/ Institution	Stage of Development
USP1	ML323	Oncology	University of Delaware and National Institutes of Health	Preclinical
USP2	ML364	Inflammation	National Institutes of Health	Preclinical
USP4	Vialinin A	Inflammation and oncology	Tokyo University of Agriculture and Shanghai Institutes for Biological Sciences	Preclinical
USP7	ADC-01, ADC-03	Oncology, immuno-oncology	Almac Discovery	Preclinical
	P5091, P22077	Oncology, immuno-oncology	Progenra	Preclinical
	XL188, XL177A	Oncology, immuno-oncology	Buhrlage Lab, Dana-Farber Cancer Institute	Preclinical
	HBX41108, HBX19818	Oncology, immuno-oncology	Hybrigenics	Preclinical
	GNE6640	Oncology, immuno-oncology	Genentech	Preclinical
	FT671	Oncology, immuno-oncology	Forma Therapeutics	Preclinical
	ALM2	Oncology, immuno-oncology	Almac Discovery	Preclinical
USP9X	WP1130	Oncology	University of Michigan	Preclinical
USP10 and USP13	Spautin 1	Inflammation	Shanghai Institute of Organic Chemistry and Harvard Medical School	Preclinical
USP11	Mitoxantrone	Oncology	Thomas Jefferson University	Preclinical
USP20	GSK2643943A	Oncology	GSK	Preclinical

Functionally, USP7 is involved in a diverse array of cellular processes (Bhattacharya et al. 2018; Li et al. 2002). USP7 was first identified as a stabilizer of the herpesvirus E3 ligase ICP0, and since then, it has been reported to interact with and regulate numerous mammalian E3 ligases, epigenetic modifiers, and transcription factors, among other targets (Everett et al. 1997; Kim and Sixma 2017). Of its targets, the role of USP7 in stabilizing MDM2, an E3 ubiquitin ligase that targets p53 for proteasomal degradation, has garnered the most interest because *TP53*, the gene for p53, is often lowly expressed in cancers (Prives 1998; Cummins et al. 2004b). As mentioned earlier, p53 is an important tumor suppressor that exerts antiproliferative effects, including growth arrest, apoptosis, and cellular senescence in response to various types of stresses, and therefore cancer cells often lowly express *TP53* or have loss-

of-function mutations in this gene (Vogelstein, Lane, and Levine 2000). Under normal circumstances, USP7 has been found to associate with MDM2 to protect the E3 ubiqutin ligase from auto-ubiquitination, allowing MDM2 to continue to reduce p53 protein levels by ubiquitinating it for proteasomal degradation. In addition to its interaction with MDM2 and p53, USP7 has been found to control the stability of many different proteins involved in important pathways within the cell, such as DNA replication, DNA damage, DNA repair, and epigenetics. For example, during DNA damage, USP7 has been found to stabilize Chk1, a checkpoint kinase, as well as its activator Claspin and checkpoint with forkhead and RING finger domain protein (Chfr) (Alonso-de Vega, Martin, and Smits 2014; Faustrup et al. 2009; Oh, Yoo, and Seol 2007).

USP7 has also been found to regulate monoubiquitination of different proteins, thus regulating their activity (van der Horst et al. 2006; Song et al. 2008). For example, USP7 has been found to regulate the localization of PTEN, a tumor suppressor, and control the activity of FOXO4, an important transcription factor that is downstream of the PI3K/AKT pathway. Finally, and most relevant for this dissertation, USP7 also has been found to contribute to epigenetic regulation by de-ubiquitinating histone H2B, an important regulator of transcriptional elongation.

Increased expression levels of USP7 have been detected in breast cancers (Luise et al. 2011), prostate cancer (Song et al. 2008), multiple myeloma (Chauhan et al. 2012), ovarian cancer (Ma and Yu 2016; Wang, Mazurkiewicz, et al. 2016), glioma (Cheng et al. 2013), and hepatocellular carcinoma (Zhang et al. 2020). Additionally, several studies have argued that USP7 can contribute to drug resistance in leukemia, multiple myeloma, and colon cancer through stabilization of DNA methyltransferase 1 (DNMT1), histone deacetylase 1 (HDAC1) and Beclin-1 (Du et al. 2010; Meyer et al. 2013; Xia et al. 2020). Therefore, a potential role for USP7 in cancer has been suggested in many contexts, although the mechanisms by which it functions in each of these cancers are largely unknown.

Clinical development of USP7 inhibitors

Because inhibition of USP7 increases the amount of ubiquitinated MDM2, thus indirectly increasing p53 protein stability, USP7 has been the focus of academic and industrial efforts to develop inhibitors in order to assess its effects in cancers where *TP53* is intact but lowly expressed (Li and Liu 2020). These efforts have led to the development of several small molecule inhibitors that target the catalytic domain either by forming covalent bonds to block ubiquitin or by binding to an allosteric site near the catalytic center (Srivastava, Suri, and Asthana 2019; Zhang and Sidhu 2018). In total, 19 covalent or non-covalent USP7 inhibitors have been described, with Genentech, Forma Therapeutics, and Progenra, Inc. as the three major biotechnology companies that currently are working to develop clinical USP7 inhibitors.

So far, the preclinical effect of USP7 inhibitors as a single agent has been investigated in chronic lymphocytic leukemia (CLL), multiple myeloma (He et al. 2020), colorectal cancer (Li et al. 2020), and hepatocellular carcinoma (Zhang et al. 2020) primarily because USP7 is frequently over-expressed in these cancers. In these experiments, USP7 inhibitors were found to slow cell growth both *in vitro* and *in vivo*, but not cause significant cell death or complete tumor regression. Therefore, these inhibitors might benefit from being combined with an already established inhibitor, such as BRAF/MEK inhibitors. Additionally, the role of USP7 in melanoma has not been well-studied. Therefore, after identifying it in our negative selection CRISPR-Cas9 screen, we decided to further investigate USP7 as a target that, when suppressed, would cooperate with MEK inhibition in melanoma.

THE EPIGENETIC LANDSCAPE OF CANCER

Coincidentally, all three of the new therapeutic targets that we have identified in melanoma regulate histone modifications on chromatin. Therefore, I briefly summarize the field of epigenetics below.

Epigenetics is the study of heritable phenotype changes that do not involve variations within the DNA sequence (Allis and Jenuwein 2016). The human genome is comprised of genomic loci that contain genes as well as promoters and enhancers, which are proximal and distal regulatory elements that control gene expression in specific cell types. Within the nucleus, the genome is packaged into ~30 million nucleosomes, forming massive complexes termed chromatin. The activity of a gene or locus is tied to its chromatin organization and how accessible it is to regulatory factors and transcriptional machinery. Repressive states can be propagated through specific histone modifications, DNA methylation, regulatory proteins, and noncoding RNAs, whereas active states can be sustained by transcription factors, other histone modifications, and chromatin modifying cofactors that bind to promoters and enhancers, engage RNA polymerase, and stimulate transcriptional activity.

One key epigenetic mechanism of gene regulation is through post-translational modifications of histones. Histones are proteins that package and compact DNA into the structures called nucleosomes. The level of compaction directly correlates with how physically available a gene is for transcription, and often the level of compaction is associated with a specific post-translational modification that occurs on the nearby histone. Each histone is comprised of four core proteins – histones H2A, H2B, H3, and H4 – with histones H3 and H4 commonly modified because they possess a long tail at the N-terminal end of their structure that is amenable to covalent modifications. Examples of common histone modifications include histone 3 lysine 27 trimethylation (H3K27Me3), which is associated with transcriptional repression, and histone H2B ubiquitination (H2Bub), which is associated with transcriptional elongation. As will be discussed in Chapter 2, we believe that USP7 inhibition mediates its therapeutic response in melanoma through its effects on H2Bub.

Histone post-translational modifications are regulated by specific classes of epigenetic regulator proteins: writers, erasers, and readers (Figure 1-6). Writers and erasers catalyze the placement and removal of epigenetic marks on histones and DNA, whereas readers activate gene expression by recognizing a specific modification and recruiting transcription and elongating factors to its site. Examples of histone writers include lysine acetyltransferases (KATs) which catalyze the addition of an acetyl mark to lysine residues, causing chromatin to "open" by neutralizing the lysine charge (Dawson and Kouzarides 2012). Histone deacetylases (HDACs) work antagonistically to KATs by removing or "erasing" acetyl marks and closing chromatin to transcription; therefore HDACs are known as histone erasers. Finally, examples of histone readers are bromodomain and extra-terminal domain (BET) proteins, which recruit transcription and elongation factors after interacting with acetylated lysine residues on histones.

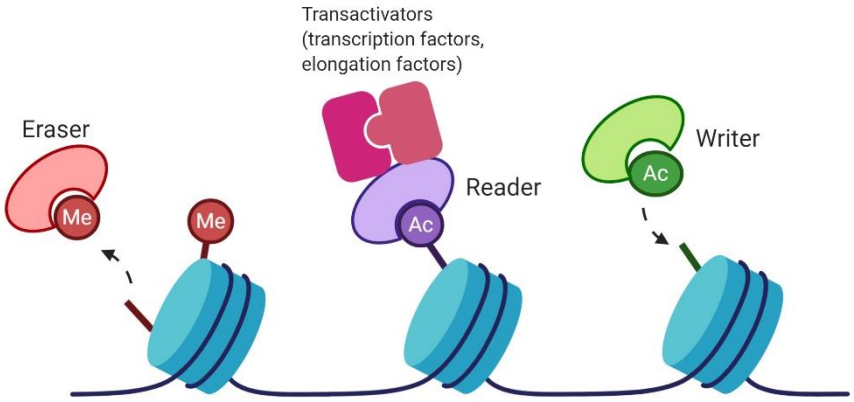

Figure 1-6. Epigenetic proteins that regulate histone modifications

Histone erasers remove modifications, such as methylation, from histone tails. Histone readers recognize histone marks and recruit transcription factors and elongation factors, leading to transcriptional activation of a nearby gene. Histone writers add histone modifications, such as acetylation.

The epigenetic landscape of melanoma

In addition to numerous genetic alterations, cancer cells have been found to harbor global epigenetic abnormalities (Jones and Baylin 2002). Studies suggest that epigenetic alterations may serve as key initiating events in some forms of cancer. The fact that epigenetic

aberrations can often be reversed or suppressed by targeted agents highlights the therapeutic promise of inhibitors that target these proteins. Like many cancers, melanomas also harbor epigenetic abnormalities that contribute to its pathogenesis. For example, aberrant promoter methylation is one epigenetic hallmark of melanoma, which leads to the transcriptional silencing of several tumor suppressors, such as *PTEN* and *RASSF1A* (Lahtz et al. 2010; Mirmohammadsadegh et al. 2006; Spugnardi et al. 2003). Additionally, melanomas can switch from a proliferative to a metastatic phenotype through epigenetic regulation of SOX10, a transcription factor that promotes *MITF* expression (Verfaillie et al. 2015). Somatic mutations within genes that encode different epigenetic regulators, such as mutations within components of the chromatin remodeling BAF complex, are also found at relatively high frequency in melanoma. Finally, gain of function alterations in *EZH2*, the catalytic component of the polycomb repressive complex group 2 (PRC2), occur in 2-4% of melanomas, increasing the abundance of the repressive histone mark H3K27Me3 (Souroullas et al. 2016; Zingg et al. 2015; Gao et al. 2013). Therefore, because epigenetic alterations are important for melanoma progression, the field has been investigating whether targeting epigenetic regulators might also prevent therapeutic resistance. Two epigenetic regulators that I have investigated in the course of my dissertation are discussed below: BET and HDAC proteins.

Bromodomain and extra-terminal domain family proteins

Bromodomain and extra-terminal domain (BET) family proteins are histone readers that recognize activating histone acetylation marks and recruit transcription and elongation factors to activate transcription. There are four proteins within this family in humans - BRDT, BRD2, BRD3, and BRD4 - all of which contain two amino-terminal bromodomains that bind acetylated chromatin and extra-terminal domains which interact with specific binding partners (Zeng and Zhou 2002). In addition to these two domains, BRD4 contains a carboxyl-terminal domain (CTD), which stimulates the transcription of growth-promoting genes by recruiting the elongation

complex p-TEFb (Wu and Chiang 2007). BRD4 in particular is also a cofactor of the Mediator complex, which transduces signals from transcription factors and activators at enhancers to promoters and initiates transcription.

Table 1-4. Current BET inhibitors in clinical trials

Drug	Company	Phase	Target(s)	Cancer	Status	NCT	Combinations?
OTX015/ Birabresib	Merck	I	BRD2/3/4	Leukemia, glioblastoma, NUT midline carcinoma, breast cancer, non-small cell lung cancer, castration-resistant prostate cancer	Completed	NCT02698189 NCT02698176 NCT01713582 NCT02259114	No
TEN-010	Hoffman-La Roche	I	BRD2/3/4	AML, advanced solid tumors	Completed	NCT02308761 NCT01987362	No
GSK525762/ I-BET762	GlaxoSmithKline	I	BRD2/3/4	NUT midline carcinoma, breast cancer, solid tumors, hematologic malignancies	Some completed, some recruiting	NCT02964507 NCT03266159 NCT01943851 NCT03150056 NCT01587703 NCT02706535 NCT03925428 NCT03702036 NCT04116359	Yes – trametinib (MEKi), entinostat (HDACi), chemotherapy, androgen deprivation therapy, fulvestrant (endocrine therapy)
CPI-0610	Constellation Pharmaceuticals	I/II	BRD2/3/4	MPNST, MM, lymphoma, mylofibrosis	MPNST withdrawn due to lack of enrollment; rest are completed/ recrutiing	NCT02986919 NCT02157636 NCT01949883 NCT02158858	Yes – Ruxolitinib (JAK inhibitor)
PLX51107	Plexxikon	I	BRD2/3/4	AML, solid tumors	Recruiting/ completed	NCT04022785 NCT02683395	Yes – azacytidine (DNMT inhibitor)
ABBV-075	AbbVie	I	BRD2/3/4	Advanced malignancies	Completed	NCT02391480	Yes – venetoclax (BH3 mimetic)
BI 894999	Boehringer Ingelheim	I	BRD2/3/4	Advanced malignancies	Recruiting	NCT02516553	No
BMS 986158	Bristol-Myers Squibb	I/IIa	BRD2/3/4	Advanced cancers, pediatric brain cancer	Recruiting	NCT02419417 NCT03936465	Yes – nivolumab (anti-PD-1)
AZD5153	AstraZeneca	I	BRD2/3/4	Relapsed or refractory solid tumors, lymphomas, NHL	Recruiting	NCT03205176 NCT03527147	Yes – olaparib (PARPi), acalabrutinib (BTKi), AZD6738 (ATRi), Hu5F9-G4 (anti-CD47), rituximab (anti-CD20)

Interestingly, inhibition of BRD4 has been found to suppress the expression of several oncogenes, including *MYC, TMPRSS2-ETS* fusion genes, *FOSI1, CDK6*, and *TERT*, as well as others (Delmore et al. 2011; Dawson et al. 2011; Segura et al. 2013; Zuber et al. 2011). Accordingly, numerous BET and BRD4 specific inhibitors are currently in early stage clinical trials for treating solid and hematological malignancies (Table 1-4). BET inhibitors are small molecules that interact with the acetylated lysine-binding pocket of the BET family proteins, triggering displacement of BET proteins at enhancers and promoters genome-wide. In melanoma, BRD4 is significantly upregulated in primary and metastatic tissues compared to melanocytes and nevi, and therefore represents a promising target (Segura et al. 2013). Interestingly, in Chapter 4, we found that the combination of BET and Ras/ERK pathway inhibitors causes cell death and tumor regression in *BRAF*-mutant melanomas.

Histone de-acetylase proteins

Histone de-acetylase (HDAC) proteins are another important class of epigenetic regulators relevant to cancer (Li and Seto 2016). HDACs are a diverse family of proteins that deacetylate protein substrates, including histone tails, and are therefore considered to be histone erasers. They are ubiquitously expressed and play key roles in a variety of cellular processes, including gene transcription, DNA repair, cell metabolism, response to cell stress, and organismal development. There are four phylogenetic classes of HDAC family proteins based on their similarity to yeast proteins. Class I HDACs (HDAC 1, 2, 3, and 8) show homology to yeast Rpd3, Class II HDACs (HDAC4, 5, 6, 7, 8, 10) show homology to yeast protein Hda1, Class III HDACs show homology to yeast Sir2, and Class IV HDACs show homology to both Rpd3 and Hda1.

Increased expression of one or more HDACs has been found in melanoma, prostate, breast, colon, gastric, and liver cancers. Additionally, decreased histone acetylation is also described as a hallmark of cancer cells. A number of HDAC inhibitors have been developed, many with clear anti-cancer effects, and four have received FDA approval for treating cancer: vorinostat (cutaneous T-cell lymphoma [CTCL]), pomidepsin (peripheral T-cell lymphoma [PTCL], CTCL), belinostat (PTCL), and panobinostat (multiple myeloma). However, though HDAC inhibitors are effective in hematological malignancies, they are not effective in solid tumors as monotherapies. This has led to investigations in combining HDAC inhibitors with other anti-tumor drugs, such as PARP inhibitors, proteasome inhibitors, immune checkpoint inhibitors, and mTOR inhibitors, among others (Min et al. 2015; Laporte et al. 2017; Kim et al. 2014; Malone et al. 2017; Booth et al. 2017). In melanoma, HDAC inhibition has been shown to suppress *MITF* expression. This served as one rationale for assessing the effects of HDAC inhibitors with BRAF and/or MEK inhibitors, which will be discussed in Chapter 3 (Yokoyama et al. 2008).

OVERVIEW OF DISSERTATION

Advanced-stage, unresectable cutaneous melanoma is a lethal disease. While there have been some advances in identifying treatments for these patients, there still is an unmet need for additional therapies, especially in non-*BRAF*-mutant melanomas. This thesis describes three promising therapeutic combinations that target oncogenic Ras/ERK pathway signaling and epigenetic regulators.

In Chapter 2, I focus on the combination of Ras/ERK pathway and USP7 inhibitors, which I identified through an unbiased negative selection genome-scale CRISPR-Cas9 screen. In this screen, we employed two single vector CRISPR lentiviral libraries – one library that targets 7,564 “druggable” genes and a library that targets 11,347 “undruggable” genes – and performed the screen in the *NRAS*-mutant melanoma cell line SKMEL2. After identifying and validating hits, we then further investigated one hit in particular, USP7, for two reasons: 1) it currently has inhibitors in preclinical studies and 2) two other hits in our screen, EPOP and ELOB, have been shown to form a complex with USP7 regulating H2B ubiquitination (H2Bub). We found that genetic and chemical perturbation of USP7 sensitized a panel of *NRAS*-mutant melanoma cell lines to MEK inhibitors *in vitro* and that the combination of USP7 and MEK inhibition causes profound tumor regression in two *NRAS*-mutant xenografts. Additionally, we observed that *BRAF*-mutant melanomas were also sensitive *in vitro* and *in vivo* to USP7, BRAF, and MEK inhibition, demonstrating that the therapeutic effects of this combination are not restricted to *NRAS*-mutant melanomas. Finally, we deconstructed the mechanism of action of this combination by evaluating the effect of USP7-EPOP-ELOB/C complex inhibition on transcription. We found that inhibition of this complex increases RNA and protein expression of the tumor suppressor CABLES1, which stabilizes p53 family members p63 and p73 in response to MEK inhibition.

In Chapter 3, I present work that I contributed to on targeting *NRAS*-, *BRAF*-, and *NF1*-mutant melanomas with combined Ras/ERK pathway and HDAC inhibitors. For this paper, I conducted a number of *in vitro* and *in vivo* experiments, including examining the effects of these agents in xenografts as well as investigating the role of MGMT as a therapeutic biomarker. Importantly, in this study we determined that combined HDAC and Ras/ERK pathway inhibition causes dual suppression of homologous repair (HR) and non-homologous end-joining (NHEJ) DNA repair pathways, leading to irreversible DNA damage and cell death. Additionally, we identified *MGMT* expression as a biomarker the predicts sensitivity to these agents, and we provide a tractable strategy to identify patients who are most likely to respond to this therapeutic combination.

In Chapter 4, I present a collaborative paper on targeting *BRAF*-mutant melanoma with Ras/ERK pathway and BET inhibitors, in which I performed all of the *in vivo* xenograft therapeutic experiments. In this study, we determined that resistance to BRAF and MEK inhibitors in *BRAF*-mutant melanomas ultimately occurs through the downstream activation/ induction of the transcription factor *c-MYC* (*MYC*). Initially, *MYC* expression is suppressed during BRAF and MEK inhibition, but once resistance occurs, *MYC* expression is re-activated, stimulating cell growth. BET inhibitors inhibit BRD4, which has been shown to transcriptionally regulate *MYC*. By treating *BRAF*-mutant melanomas both *in vitro* and *in vivo* with Ras/ERK and BET inhibitors, we found that together these agents induce more potent tumor regression and prevent resistance.

Finally, in Chapter 5, I discuss my conclusions as well as the future implications of these studies. I review the current efforts to treat non-*BRAF*-mutant melanomas with targeted therapies and summarize future research avenues to pursue based on results from my thesis work. I also discuss the final studies that will be required to dissect the role of CABLES1 in

cancer and provide a working model that synthesizes my research in the context of developing treatments for melanoma.

Chapter 2 : Co-suppression of MEK and USP7 triggers a synthetic lethal response in *NRAS*-mutant melanomas

Co-suppression of MEK and USP7 triggers a synthetic lethal response in *NRAS*-mutant melanomas

Haley E. Manchester[1,2], Timothy D. Martin[1,2,4], Caroline J. Guild[1,2], Lisa Situ[1,2], Rachel Davis[1,2], Ryan Kuzmickas[1,2], Joon Yoon[5], Marina Watanabe[1,2], Ophelia Maertens[1,2,3,6], Shannan Ho Sui[5], Stephen J. Elledge[1,2,4], Karen Cichowski[1,2,3]

[1]Genetics Division, Department of Medicine, Brigham and Women's Hospital, [2]Harvard Medical School, [3]Ludwig Center for Dana-Farber/Harvard Cancer Center, [4]Department of Genetics, Howard Hughes Medical Institute, [5]Harvard Chan Bioinformatics Core, Harvard T.H. Chan School of Public Health [6]Novartis Institutes for BioMedical Research

Author Attributions:

Conception and design: H.E. Manchester, S.J. Elledge, K. Cichowski

Development of methodology: H.E. Manchester, T.D. Martin, O. Maertens

Acquisition of data (provided animals, acquired and managed patients, provided facilities, etc.): H.E. Manchester, T.D. Martin, C.J. Guild, L. Situ, R. Davis, M. Watanabe, S.J. Elledge, K. Cichowski

Analysis and interpretation of data (e.g. statistical analysis, biostatistics, computational analysis): H.E. Manchester, T.D. Martin, C.J. Guild, L. Situ, R. Davis, R. Kuzmickas, J. Yoon, O. Maertens, S.H. Sui, S.J. Elledge, K. Cichowski

Administrative, technical, or material support (i.e., reporting or organizing data, constructing database): H.E. Manchester, C.J. Guild, L. Situ, R. Davis

Study supervision: S.H. Sui, S.J. Elledge, K. Cichowski

Note: Work from this chapter is in preparation for publication.

ABSTRACT

While combined BRAF/MEK inhibitors are initially effective in *BRAF*-mutant melanomas, the majority of patients ultimately relapse. MEK inhibitors are even less effective in *NRAS*-mutant melanomas, eliciting only partial responses in a subset of individuals. Therefore, there is an urgent need to develop improved therapies, especially for *NRAS*-mutant tumors. Using a genome-scale negative selection CRISPR-Cas9 screen we identified the de-ubiquitinase USP7 as a promising therapeutic target that when suppressed sensitizes *NRAS*-mutant melanomas to MEK inhibitors. Specifically, genetic and chemical suppression of USP7 synergizes with MEK inhibitors *in vitro* and together these agents cause potent tumor regression *in vivo*. However, USP7 inhibitors also potentiate the effects of BRAF/MEK inhibitors in *BRAF*-mutant tumors, demonstrating a broader cooperativity with Ras pathway inhibitors in melanoma. We further show that USP7 inhibitors function by inhibiting USP7-EPOP-ELOB/C complexes, which regulate histone H2B ubiquitination and the transcriptional elongation of a subset of genes. Specifically, suppression of this complex induces the expression of the tumor suppressor CABLES1, which subsequently stabilizes p63 and p73 proteins in the presence of MEK inhibitors. Together these observations suggest that USP7 normally protects melanomas from the lethal effects of MEK inhibitors by restraining the expression of CABLES1 and p53 family members. Additionally, these observations also reveal a promising therapeutic strategy for *NRAS*-mutant and possibly *BRAF*-mutant melanomas.

INTRODUCTION

Cutaneous melanoma is a highly metastatic and treatment refractory skin cancer, with ~100,000 new cases estimated to occur in 2020 in the US alone (ACS 2020). More than three-fourths of melanomas are defined by oncogenic “driver” mutations that constitutively activate the Ras/Raf/MEK/ERK pathway (henceforth referred to as the Ras/ERK pathway), which regulates cell proliferation, differentiation, and apoptosis ('Genomic Classification of Cutaneous Melanoma'

2015). About 50-60% of melanomas harbor gain-of-function mutations in *BRAF*; ~20% are driven by activating mutations in *NRAS*; and 10-12% contain loss-of-function mutations in the Ras GTPase activating protein (Ras GAP) neurofibromin 1 (*NF1*).

The discovery of critical oncogenic mutations in Ras pathway components led to the development of highly selective kinase inhibitors that target the mutant form of BRAF and the downstream effector MEK (Luke et al. 2017). In *BRAF*-mutant melanomas, the combination of MEK inhibitors (MEKi) and BRAF inhibitors (BRAFi) induces a response in 76-90% of patients, resulting in improved overall survival (Flaherty et al. 2012; Robert et al. 2019; Long et al. 2015; Robert, Karaszewska, et al. 2015). Nevertheless, the majority of individuals relapse, and do so on average in 11 months (Long et al. 2015; Robert, Karaszewska, et al. 2015). Unfortunately, MEK inhibitors are even less effective in *NRAS*-mutant melanomas, with only 15-20% exhibiting partial responses to MEK inhibitors, which delay progression by ~4 months (Dummer et al. 2017; Sarkisian and Davar 2018). Together, these observations suggest that while Ras/ERK pathway inhibition will remain an important cornerstone of melanoma treatment, we must identify more effective therapeutic drug combinations, in particular for *NRAS*-mutant tumors. According, additional therapeutic targets must be identified.

One means of identifying new, and potentially druggable, dependencies is through functional genomic screens. The CRISPR-Cas9 (clustered regularly interspaced short palindromic repeats- CRISPR-associated protein 9) screening approach has been shown to be a powerful tool for high-throughput discovery of genetic dependencies in mammalian systems (Wang et al. 2014; Shalem et al. 2014). In particular, negative selection CRISPR-Cas9 screens are useful for identifying new therapeutic targets that may impair tumor cell survival alone when suppressed or sensitize cancers to other therapeutic targets (Huang et al. 2020). In this study, we performed a CRISPR-Cas9 negative selection screen to identify genes that when suppressed might sensitize *NRAS*-mutant melanomas to MEK inhibitors. Importantly, we

modified this screen to enrich for targets that were likely to induce cytotoxic responses, rather than cytostatic responses.

Here we demonstrated that the deubiquitinase USP7 (also known as HAUSP) is an important therapeutic target in both *NRAS*- and *BRAF*-mutant melanomas and that USP7 and Ras/ERK pathway inhibitors potently synergize *in vitro* and *in vivo*. Surprisingly, while USP7 has been shown to regulate MDM2 stability and consequently p53 in other settings, here we show that USP7 inhibitors function in melanomas by suppressing USP7-EPOP-ELOB/C complexes, which control H2B ubiquitination and transcriptional elongation of a subset of genes, ultimately impinging on p63 and p73. Thus, in addition to identifying a promising new combination therapy for Ras-pathway driven melanomas, these studies have revealed a new tumor suppressor cascade that is regulated by USP7.

RESULTS

Genome-scale CRISPR screening identifies USP7 as a potential therapeutic target in NRAS-*mutant melanomas*

To identify dependencies in *NRAS*-mutant melanomas in the presence of MEK inhibitors, we performed a genome-scale CRISPR-Cas9 loss-of-function screen in the *NRAS*-mutant melanoma cell line SKMEL2. We designed this screen differently that other analogous screens in order to enrich for cytotoxic hits and possibly identify more genes outside of the Ras/ERK pathway. Typically, negative selection screens 1) utilize inhibitors at IC50 concentrations and 2) are analyzed after cells have been treated for many population doublings (2-3 weeks). However, this experimental design tends to enrich for cytostatic hits because guides that slow the rate of proliferation will “drop out” after 3 weeks. Moreover, if MEK inhibitors are used at an IC50 concentration, genes that improve the “on target” cytostatic effect of these agents, such as MEK, BRAF, and ERK, often predominate the list of hits. Therefore, we used a

concentration of the MEK inhibitor trametinib (10nM) that exerted maximal cytostatic effects (Figure 2-1A, left panel, top). This concentration also stably suppressed ERK phosphorylation and did not induce feedback activation of the Ras/ERK pathway (Figure 2-1A, left panel, bottom). Finally, we concluded our screen after only 4 days of trametinib treatment because we have previously shown that cytotoxic combinations can exert their effects in melanoma within this time frame (Maertens et al. 2019). We reasoned that this amended strategy would reduce the number of cytostatic hits and would enrich for cytotoxic hits.

We used two previously unpublished single vector CRISPR lentiviral libraries that contained 4-5 pairs of guide RNAs per gene: one “druggable” library that targets 7,564 genes and one “undruggable” library that targets 11,347 genes. The cell line was infected with a MOI of <0.3 and allowed to recover over one day (Figure 2-1A, right panel). After three days of puromycin selection, cells were then passaged for an additional 7 days to allow sufficient gene knock out to occur. We then collected a “day 0” time point in triplicate before treating with either DMSO (vehicle) or the cytostatic dose of the MEK inhibitor trametinib (10nM) in triplicate. After 4 days of treatment, we determined the relative enrichment or depletion of guides using massively parallel sequencing and compared day 4 treatments with the initial day 0 plasmid pool. Data were normalized across replicates, and a gene-level dependency score was calculated using edgeR algorithm (Dai et al. 2014). As expected, we observed several previously identified essential genes drop out in both the MEKi and vehicle treatment arms, including the cell-type-specific gene *NRAS*, highlighting that we waited long enough for sufficient drop out to occur (Supplemental figure 2-1A, B) (Hart et al. 2015).

We identified preferential genetic dependencies by first focusing on “druggable” hits, focusing first on hits that have promising inhibitors in preclinical or clinical development. From the “druggable” library, we identified several positive controls that have previously been found in

Figure 2-1. Genome-scale CRISPR screening identifies USP7 as a potential therapeutic target in NRAS-mutant melanomas

(A) (Left panel) MEK inhibitor trametinib (10nM) alone produces a cytostatic response in NRAS mutant melanoma cell line SKMEL2. Graph depicts log_2 transformation of the fold change in cell number at days 1, 3, 4, and 5 versus day 0. Right axis shows percent change in cell number relative to day 0. Negative values represent a decrease in cell number over time and positive values represent an increase in cell number. Immunoblots show levels of phosphorylated ERK (pERK), total ERK, and GAPDH over time with treatment of MEK inhibitor trametinib. To the right is a schematic of the negative selection screen. SKMEL2 cells were infected with library, selected and allowed to grow over 10 days before harvesting a day 0 time point and then treating with either DMSO or 10nM trametinib for 4 days.
(B) For our screen, we focused on "druggable" genes that were depleted more in the MEKi arm than in the vehicle, with a difference<-1. Screen was done in the *NRAS*-mutant melanoma cell line SKMEL2. As expected, 2 hits within the RAS/ERK pathway, RAF1 and BRAF, were significant hits from the screen. Graph depicts Log_2 fold change (MEKi treatment over 4 days / Day 0 timepoint – Vehicle treatment over 4 days / Day 0 time point) for "druggable" library only. Highlighted in red are other significant hits (FDR<0.25) from our screen that have been found in other publications to synergize with MEK inhibitors in RAS driven malignancies, such as MCL1, MTOR, and CDK4.
(C) *NRAS*-mutant melanoma line SKMEL2 was infected with shRNA against control or *USP7.* After knockdown was confirmed, cells were treated with DMSO or trametinib (MEKi, 10nM) for 96 hours. Graphs represent log2 transformation of the fold change in cell number at day 4 versus day 0. Right axis shows percent change in cell number relative to day 0. Negative values represent a decrease in cell number over time and positive values represent an increase in cell number. Immunoblots show levels of USP7, phosphorylated ERK (pERK), and total ERK (ERK) after 24 hours of indicated treatment. *, p<0.05 when comparing shControl+MEKi to shUSP7+MEKi; **, p<0.05 when comparing shUSP7+vehicle to shUSP7+MEKi.
(D) *NRAS*-mutant melanoma line SKMEL2 was infected with siRNA against control or *RAF1.* After knockdown was confirmed, cells were treated with DMSO or trametinib (MEKi, 10nM) for 96 hours. Graphs represent log2 transformation of the fold change in cell number at day 4 versus day 0. Right axis shows percent change in cell number relative to day 0. Negative values represent a decrease in cell number over time and positive values represent an increase in cell number. Immunoblots show levels of RAF1, phosphorylated ERK (pERK), and total ERK (ERK) after 24 hours of indicated treatment. *, p<0.05 when comparing siControl+MEKi to siRAF1+MEKi; **, p<0.05 when comparing siRAF1+vehicle to siRAF1+MEKi.
(E) Response of different *NRAS*-mutant cell lines to shRNA knock down of Control or *USP7* and 4 days of the indicated treatment. After knockdown was confirmed, cells were treated with DMSO or trametinib (MEKi, 10nM) for 96 hours. Graphs represent log2 transformation of the fold change in cell number at day 4 versus day 0. Right axis shows percent change in cell number relative to day 0. Negative values represent a decrease in cell number over time and positive values represent an increase in cell number. Immunoblots for one cell line (MM415) were also included (left), demonstrating the level of *USP7* knock-down. See Supplemental Figure A-1D for more immunoblots. *, p<0.05 when comparing between shControl+MEKi to shUSP7+MEKi.
(F) Log2 transformation in fold change of cell number at day 4 versus day 0 with 3 different sgRNAs targeting *USP7* in SKMEL2 and corresponding immunoblot demonstrating *USP7* knock-out. *, **, ***, p<0.05 when comparing each sgRNA targeting USP7 + MEKi to sgControl+MEKi.
(G) SKMEL2 cells were infected with 3' UTR-specific-shRNA targeting control or *USP7* as well as cDNA expressing *LACZ* or *USP7*. Immunoblot demonstrates corresponding USP7 and GAPDH levels. *, p<0.05; n.s., not statistically significant.

Figure 2-1 (continued)

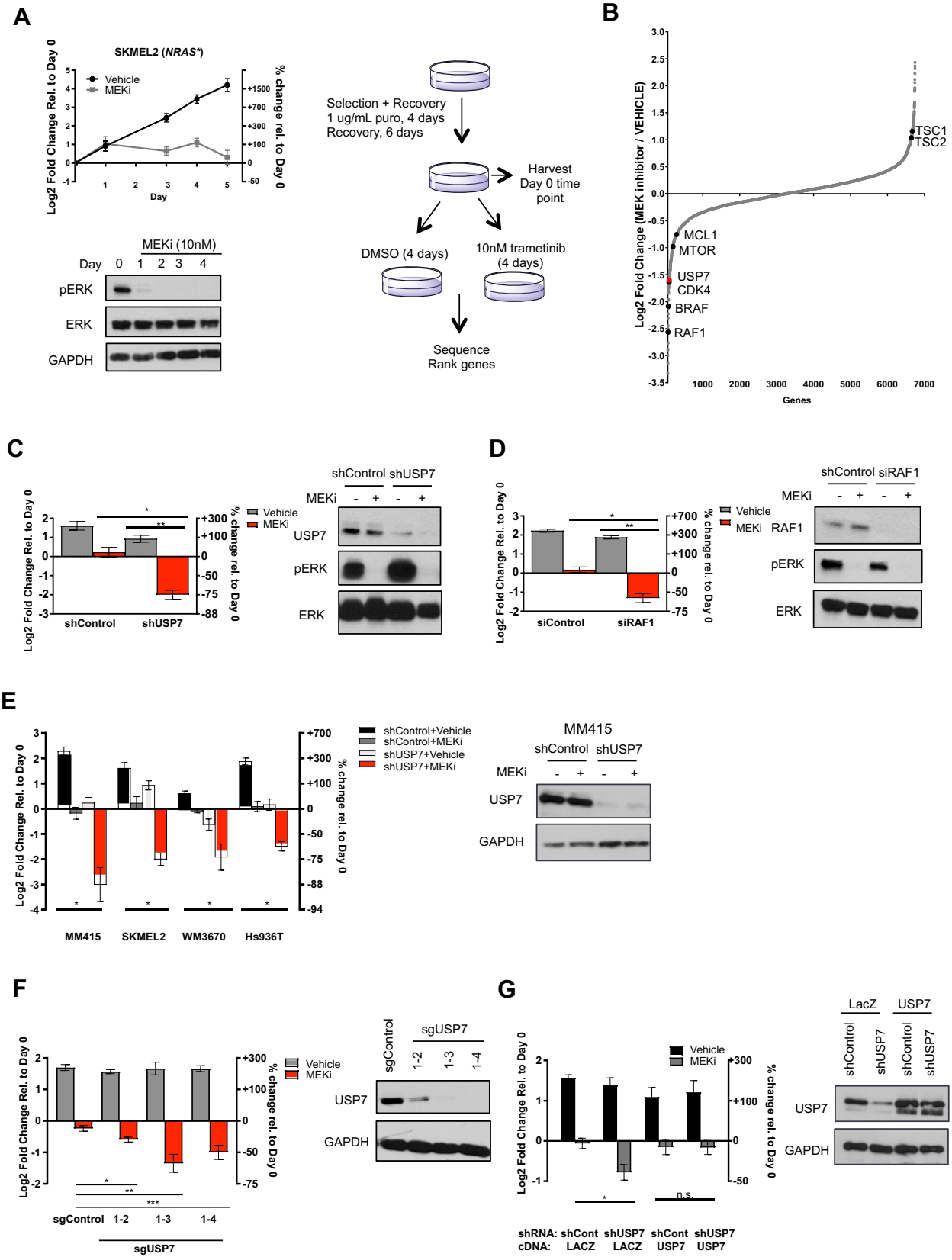

other studies in Ras-driven malignancies, including RAF1, BRAF, CDK4, MTOR, and MCL1 (Figure 1B) (Atefi et al. 2015; Nangia et al. 2018; Posch et al. 2013; Kwong et al. 2012). Interestingly, *USP7*, a deubiquitinase (DUB), ranked among the top 20 druggable genetic dependencies in the screen, with similar drop-out as compared to CDK4 and a significant FDR value of <0.25. We decided to focus on USP7 because there are promising inhibitors in development at multiple pharmaceutical companies and academic sites (Kategaya et al. 2017; Chauhan et al. 2012; Weinstock et al. 2012; Turnbull et al. 2017; Lamberto et al. 2017; Schauer et al. 2020).

Genetic suppression of USP7 kills multiple NRAS*-mutant melanoma cell lines when combined with the MEK inhibitor trametinib*

We next confirmed our pooled screen results by analyzing the effect of genetic deletion or suppression of USP7 in SKMEL2 cells, as well as 3 other *NRAS*-mutant melanoma cell lines. As a complementary approach, we first used USP7 shRNAs. Knockdown of *USP7* effectively reduced USP7 expression and exerted modest cytostatic response in SKMEL2 cells (Figure 2-1C). Trametinib alone induced a more potent cytostatic effect but did not cause a reduction in cell number over time. However, together USP7 ablation and MEK inhibition killed nearly 75% of cells within 4 days. As a comparison, when trametinib was combined with siRNA sequences that target RAF1 or BRAF, also identified in our screen, SKMEL2 cells also died, albeit to a somewhat lesser extent (Figure 2-1D; Supplemental Figure A-1C). Importantly, trametinib and USP7 depletion similarly killed 66-88% of cells in 3 additional *NRAS*-mutant melanoma cell lines (Figure 2-1E; Supplemental Figure A-1D). These findings were further confirmed in *NRAS*-mutant cell lines using 3 CRISPR guides comprised of sequences that were different than those used in the screen (Figure 2-1F; Supplemental figure A-1E). Finally, we found that ectopic expression of USP7 effectively rescued cell death conferred by trametinib and ablation of USP7 using UTR sequences (Figure 2-1G). These studies demonstrate that genetic suppression of

USP7 sensitizes *NRAS*-mutant melanoma cell lines to MEK inhibition, and together they exert potent cytotoxic effects.

MEK and USP7 inhibitors potently synergize, trigger apoptosis, and induce the regression of NRAS-*mutant melanomas* in vivo

To determine whether pharmacological agents could also mediate these effects, we evaluated four selective small molecule inhibitors of USP7: GNE6640, P5091, XL177A, and FT671 (Chauhan et al. 2012; Kategaya et al. 2017; Turnbull et al. 2017; Schauer et al. 2020). Currently, there are at least four USP7 inhibitors in preclinical development at Forma Therapeutics, Genentech, Progenra, Inc, and Dana-Farber Cancer Institute, with Progenra slated to enter Phase I clinical trials with an inhibitor based on the tool compound P5091. We first performed Incucyte live-cell imaging to concomitantly measure cell death and changes in cell number over time using a fluorescent assay that detects live and dead cells (Figure 2-2A). Similar to results observed with genetic suppression of USP7, USP7 inhibitors alone exerted cytostatic effects, the degree of which varied depending on the drug (Figure 2-2A, top panels). However, when combined with trametinib, these agents triggered a dramatic loss in viable cells (Figure 2-2A, top panels). Importantly, this reduction in cell number was accompanied by a potent cooperative increase in apoptosis, as determined by measuring caspase activity (Figure 2-2A, bottom panels). By extensively performing dose response assays, we found that the USP7 inhibitor P5091 and trametinib potently synergized in multiple *NRAS*-mutant melanoma cell lines as determined by the Gaddum model of non-interaction (Figure 2-2B) (Ianevski et al. 2017). We further showed that these cells were similarly sensitive to USP7 inhibition and another MEK inhibitor, binimetinib, which is in phase II clinical trials for *NRAS*-mutant melanomas (Supplemental Figure A-2A) (Dummer et al. 2017). Finally, we found that combined USP7 and MEK inhibitors caused cell death in a larger panel of *NRAS*-mutant melanoma cell lines (Figure 2-2B). Importantly, this combination is not generally cytotoxic,

Figure 2-2. ***MEK and USP7 inhibitors potently synergize, trigger apoptosis, and induce the regression of*** **NRAS-*mutant melanomas* in vivo**

(A) Real-time quantification of cell numbers (top) and cell death (bottom) using the live cell imager IncuCyte ZOOM. Red (nuclear restricted NucLight RFP for quantifiying live cells) and green (Cytotox Green reagent for quantifying dead cells) fluorescent cells were monitored every 4 hours (for 96 hours) after treatment with vehicle (DMSO) or drugs (MEK inhibitor, USP7 inhibitor) and then quantified with the IncuCyte integrated analysis software. GNE6640, 20uM; P5091, 10uM; FT671, 20uM, XL177A, 2uM.
(B) Synergy scores (to characterize the combination effects in Gaddum's model for non-interaction) for USP7 inhibitor P5091 combined with trametinib for SKMEL2 (3-D synergy map, left panel) and additional sensitive cell lines (right panel). Strong synergy is indicated in red.
(C) Waterfall plot of cell counting assay results after 4 days of treatment with MEKi trametinib (10nM) and USP7i P5091 (10uM) in 6 different NRAS-mutant melanoma cell lines. Cells were manually counted prior to the addition of compounds and 3 days after treatment. Graphs represent log2 transformation of the fold change in cell number at day 3 versus day 0. Right axis shows percent change in cell number relative to day 0. Negative values represent a decrease in cell number over time and positive values represent an increase in cell number.
(D) Waterfall plot depicting tumor volume change in NRAS-mutant melanoma xenograft model YUDOSO after 2 weeks of treatment. Each bar represents an individual tumor. MEKi= 0.6mg/kg/day trametinib, oral gavage; USP7i = 25mg/kg/day P5091, intraperitoneal injection. Mice were enrolled when tumors reached ~300mm3. Left axis indicates the log2 of fold change in tumor volume, and right axis indicates the percentage change in tumor volume relative to day 0.
(E) (Left) Waterfall plot depicting tumor volume change in NRAS-mutant melanoma xenograft model MM415 after 18 days of treatment. Each bar represents an individual tumor. (Right) Growth of MM415 tumors over time. Each data point is mean+/-SEM. MEKi= 0.6mg/kg/day trametinib, oral gavage; USP7i = 25mg/kg/day P5091, intraperitoneal injection. Mice were enrolled when tumors reached ~300mm3. Left axis indicates the log2 of fold change in tumor volume, and right axis indicates the percentage change in tumor volume relative to day 0. *, $p<0.05$ when comparing USP7i+MEKi treated tumors to MEKi treated tumors.
(F) Waterfall plot of cell counting assay results after 4 days of treatment with BRAFi dabrafenib (100nM), MEKi trametinib (10nM), and USP7i P5091 (10uM) in 6 different BRAF-mutant melanoma cell lines. Cells were manually counted prior to the addition of compounds and 3 days after treatment. Graphs represent log2 transformation of the fold change in cell number at day 3 versus day 0. Right axis shows percent change in cell number relative to day 0. Negative values represent a decrease in cell number over time and positive values represent an increase in cell number.
(G) (Left) Waterfall plot depicting tumor volume change in BRAF-mutant melanoma xenograft model A375 after 2 weeks of treatment. (Right) Growth of A375 tumors over time. Graph represent mean values +/- standard error of the mean. Left axis indicates the log2 of fold change in tumor volume, and right axis indicates the percentage change in tumor volume relative to day 0. BRAFi = 30mg/kg/day dabrafenib, oral gavage; MEKi = 0.6mg/kg/day trametinib, oral gavage; USP7i =25 mg/kg/day P5091, intraperitoneal injection. *, $p<0.05$ when comparing USP7i+MEKi treated tumors to MEKi treated tumors.

Figure 2-2 (continued)

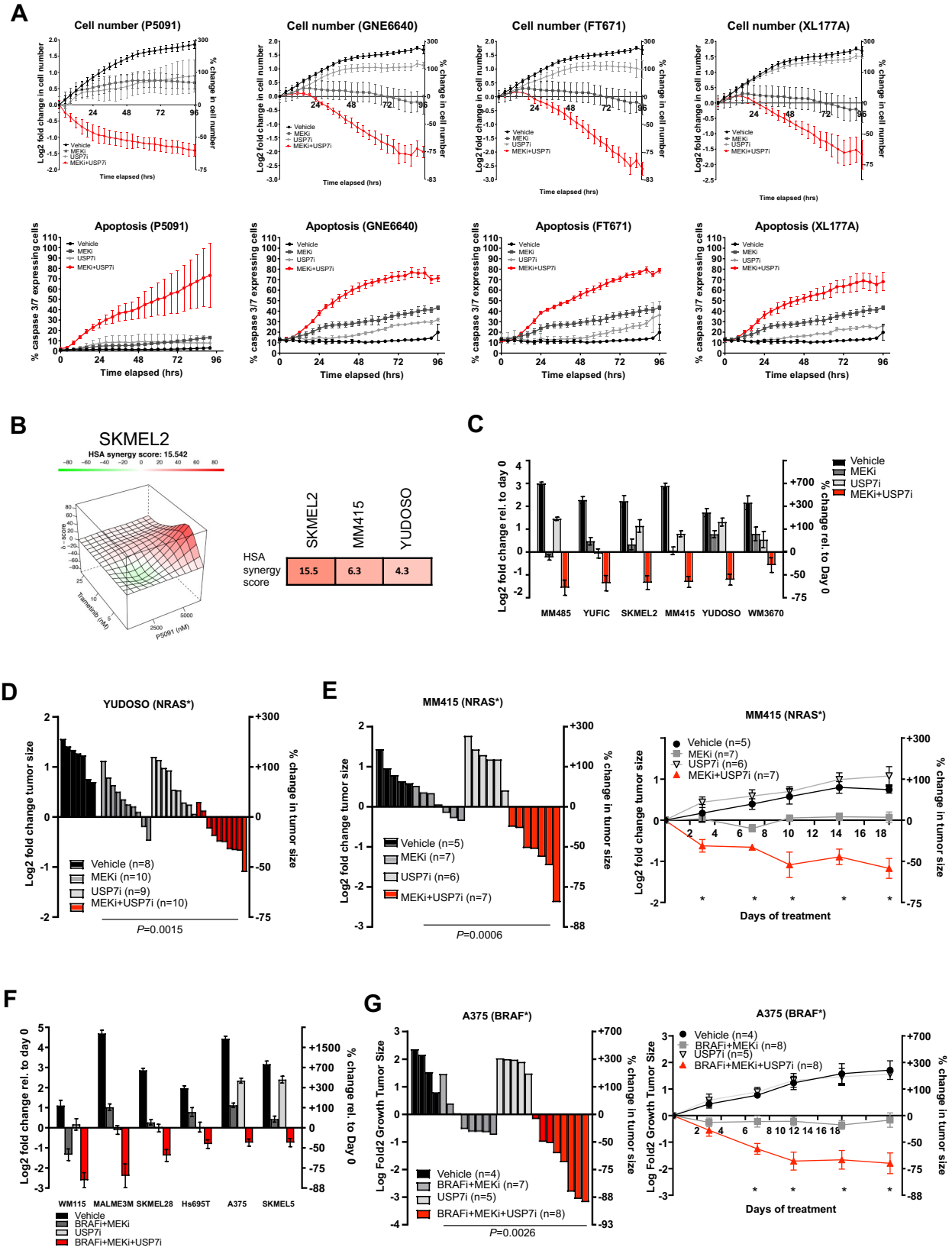

illustrated by its lack of effect on 293T cells (Supplemental Figure A-2B). Taken together, these observations demonstrate that USP7 and MEK inhibitors exert a potent synthetic lethal response in *NRAS*-mutant melanomas.

Next, we investigated whether these agents could exert similar cooperative effects *in vivo*. Importantly, we used a concentration of trametinib that mimics human exposures and a concentration of P5091 previously established for conducted *in vivo* studies (King et al. 2013; Chauhan et al. 2012; An et al. 2017). Cells were injected subcutaneously in immunocompromised mice, and once tumors reached 300mm^3, animals were randomly enrolled in either vehicle, MEKi (trametinib), USP7i (P5091), or combination treatment arms. Tumor size was measured twice a week by Vernier calipers. No toxicity was observed in animals treated with these combined agents (Supplemental Figures A-2C, D). Similar to clinical observations, trametinib alone exerted modest partial responses in a small subset of mice (Figures 2-2D, E). USP7 inhibitors alone did not affect tumor growth, but when combined with trametinib, USP7 inhibitors caused potent tumor regression in two distinct *NRAS*-mutant melanoma models, as depicted by waterfall plots and measurements of tumor volume over time (Figures 2-2D, E; p=0.0015 for YUDOSO, p=0.0006 for MM415). Together these data demonstrate that USP7 inhibitors dramatically enhance the effects of MEK inhibitors in *NRAS*-mutant melanomas *in* vivo, consistent with *in vitro* findings.

***USP7 inhibitors also potentiate the effects of BRAF/MEK inhibitors in* BRAF*-mutant melanomas* in vitro *and* in vivo**

We then investigated whether USP7 inhibitors might also potentiate the effects of Ras/ERK pathway inhibitors in *BRAF*-mutant melanomas. Currently, patients with *BRAF*-mutant melanomas are treated with a combination of BRAF and MEK inhibitors (Long et al. 2015). Therefore, we treated a panel of *BRAF*-mutant melanomas *in vitro* with a standard of care

combination (BRAFi dabrafenib and MEKi trametinib) along with USP7i P5091. Notably, we found that the effects of BRAF/MEK inhibitors were substantially potentiated by USP7 inhibitors (Figure 2-2F). This drug combination was also evaluated *in vivo* using clinically relevant concentrations of dabrafenib and trametinib in the *BRAF*-mutant A375 xenograft melanomas (King et al. 2013). Similar to results observed in *NRAS*-mutant melanomas, USP7 inhibitors substantially enhanced the effects of BRAF/MEK inhibitors and caused much greater tumor regression than with BRAF/MEK inhibitors alone (Figure 2-2G; p=0.0026). Notably, mice treated with all three agents also exhibited no signs of toxicity (Supplemental Figure 2-2FE). Thus, the addition of USP7 inhibitors kills more residual disease than BRAF/MEK inhibitors alone. This finding is highly significant since recurrence is caused by residual disease.

USP7 inhibitors function by suppressing the USP7-EPOP-ELOB/C complex in melanomas

USP7 has been reported to deubiquitinate a variety of substrates (Kim and Sixma 2017). The most well-studied is MDM2, an E3 ubiquitin ligase that ubiquitinates p53 and leads to its proteasomal degradation (Li et al. 2004; Cummins et al. 2004a). Accordingly, USP7 ablation can enhance the stability of p53, and the effects of USP7 inhibitors in some settings are dependent on p53 (Schauer et al. 2020; Stolte et al. 2018). However, SKMEL2 cells and several responding cell lines shown in Figure 2 are *TP53*-mutant and/or lack p53. Therefore, we speculated that USP7 might be working through an alternative mechanism in this therapeutic context. Nevertheless, we investigated whether cell death was dependent on p53 in tumor cell lines that retained wildtype p53. Notably, we found that genetic ablation of *TP53* did not rescue the effect of these agents in two different sensitive *NRAS*-mutant and one sensitive *BRAF*-mutant melanoma cell lines, one of which was *TP53*-mutant (SKMEL2) and two of which had intact *TP53* alleles (MM415, MALME3M) (Supplemental figure 2-3A). Additionally, the inhibitor nutlin-3A, which inhibits the interaction between MDM2 and p53, did not phenocopy the effects of USP7 inhibition (Supplemental figure 2-3B). Therefore, we conclude that Ras pathway-driven

melanomas are sensitive to USP7 and Ras/ERK pathway inhibition through a p53-independent mechanism.

To assist in identifying alternative pathways of interest, we examined the “undruggable” hits identified through the CRISPR-Cas9 screen. Interestingly, two top hits within the “undruggable” screen – EPOP (also known as C17orf96) and ELOB (also known as TCEB2) – have been reported to interact with USP7 in a complex that regulates H2B ubiquitination (H2Bub), a marker of transcriptional elongation (Figure 2-3A, B) (Liefke, Karwacki-Neisius, and Shi 2016). Specifically, EPOP is a chromatin binding protein that brings USP7 to H2Bub, allowing USP7 to deubiquitinate H2B and suppress transcriptional elongation at specific gene sites, whereas ELOB is a scaffolding protein within this complex (Figure 2-3B). To investigate this further, EPOP and ELOB were individually suppressed with siRNA and shRNA respectively (Figure 2-3C, D; Supplemental Figure A-3C, D). Strikingly, both EPOP and ELOB depletion phenocopied the loss of USP7 and triggered cell death in the presence of trametinib (Figure 2-3C, D; Supplemental Figure A-3C, D). Next, to verify that USP7-EPOP-ELOB/C complexes exist in these melanomas, we performed co-immunoprecipitations and found that endogenous ELOB is associated in a complex with endogenous USP7 (Figure 2-3E). Antibodies that recognize EPOP are not available, but epitope tagged EPOP also co-precipitated in this complex (Figure 2-3E). Finally, we found that the USP7 inhibitor resulted in an increase in total H2Bub levels at time points prior to apoptosis (Figure 2-3F). Taken together, these results suggest that USP7 critically functions in USP7-EPOP-ELOB/C complexes in melanoma and that suppression of this complex mediates cell death in response to MEK/USP7 inhibitors.

Figure 2-3. USP7 inhibitors function by suppressing the USP7-EPOP-ELOB/C complex in melanomas

(A) Genome-scale negative CRISPR screen results showing both “druggable” and “undruggable” targets. Two “undruggable” hits (FDR<0.25) were identified to form a complex with USP7 that affects H2Bub. Left axis Log2 fold change when comparing day 4 of MEK treatment to day 4 of vehicle treatment from screen.
(B) Schematic of USP7-EPOP-ELOB complex, adapted from Liefke et al., 2016. EPOP is a chromatin binding protein that recruits USP7 to chromatin, allowing USP7 to de-ubiquitinate H2B-ub, a marker of transcriptional elongation.
(C) (Left) Cell counting assays with two NRAS-mutant cell lines with or without siRNA against control or EPOP after 4 days of treatment with vehicle (DMSO) or MEKi trametinib (10nM). *, $p<0.05$ when comparing siControl+MEKi to siEPOP+MEKi; **, $p<0.05$ when comparing siEPOP+vehicle to siEPOP+MEKi. (Right) qPCR results demonstrating knock-down of EPOP with siRNA. We were not able to find an effective EPOP antibody for our cell lines.
(D) (Left) Cell counting assays with two NRAS-mutant cell lines with or without shRNA against control or ELOB after 4 days of treatment with vehicle (DMSO) or MEKi trametinib (10nM). *, $p<0.05$ when comparing shControl+MEKi to shELOB+MEKi; **, $p<0.05$ when comparing shELOB+vehicle to shELOB+MEKi. (Right) Immunoblots demonstrating knock-down of ELOB. E, Co-IP of ELOB identifies flag-tagged EPOP and USP7. MEKi = trametinib, 10nM, 24 hours treatment.
(E) Co-immunoprecipitation of endogenous ELOB precipitated other members of the complex, including endogenous USP7 and ectopically expressed Flag-tagged EPOP. SKMEL2 cells were treated with DMSO (vehicle) or trametinib (MEKi, 10nM) for 24 hours before collection.
(F) Immunoblot of H2Bub after 2 hours of treatment with USP7i P5091 (10uM) and MEKi trametinib (10nM) in SKMEL2 cell lines.

Figure 2-3 (continued)

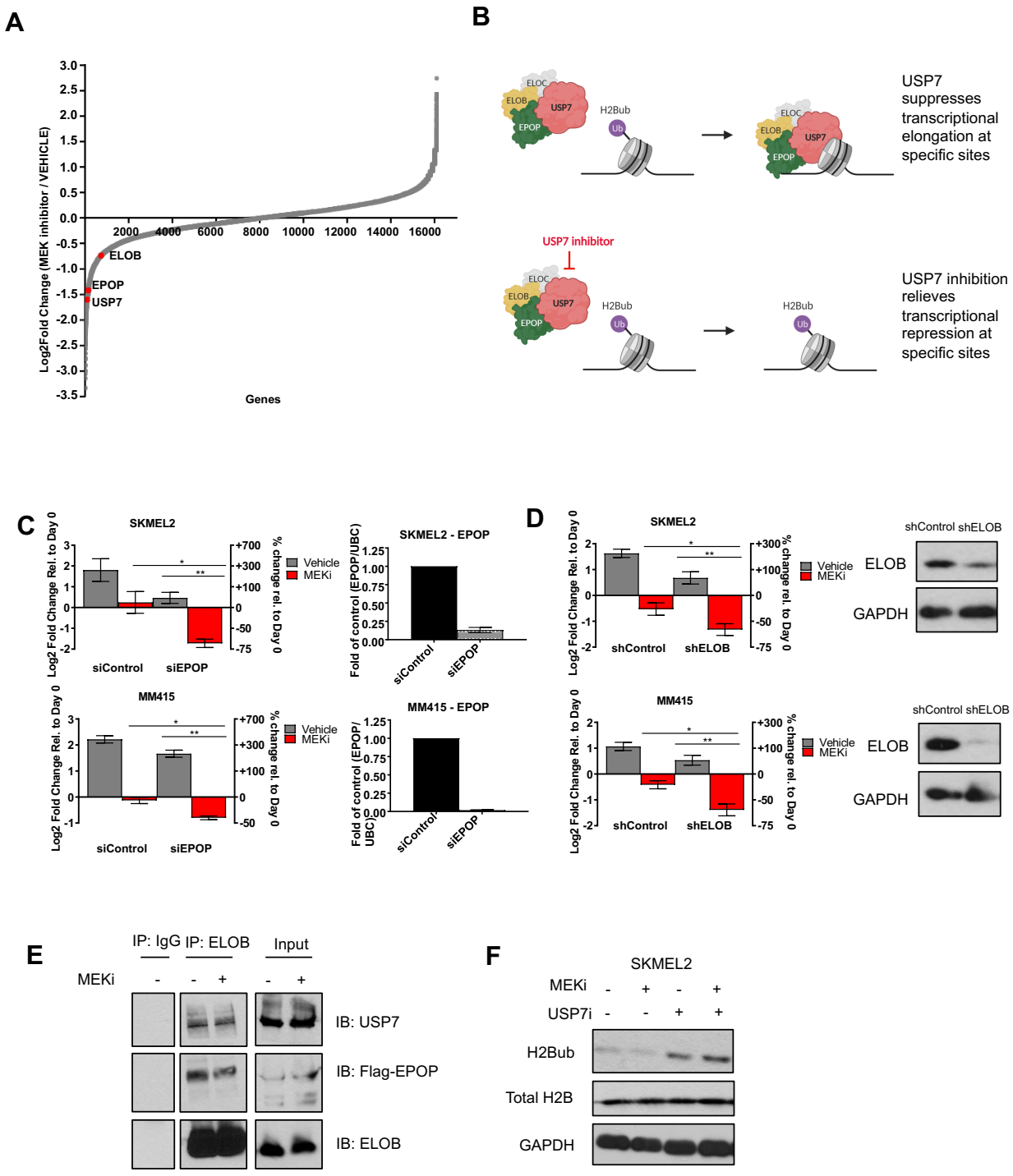

The CABLES1 tumor suppressor is an essential transcriptional target of the USP7-EPOP-ELOB/C complex in melanomas and is required for cell death

We next sought to identify the genes and pathways regulated by the USP7-EPOP-ELOB/C complex in melanomas. SKMEL2 cells lacking either USP7 or EPOP were generated. Control and knock-out cell lines were then treated for 24 hours with trametinib, a timepoint which precedes cell death, before collecting and processing for RNA sequencing (RNA-seq) and ChIP sequencing (ChIP-seq). We first examined the broad pathways that were affected by the loss of USP7 (in the presence of MEK inhibitors) by performing GSEA analysis of our RNA-seq results. Expression profiles associated with the activation of p63 and p53 were the top scoring signatures enriched in USP7-depleted cells using several MSigDB databases (Figure 2-4A). This was somewhat surprising because we had ruled out a requirement for p53 in previous functional experiments and SKMEL2 cells do not express functional p53. Nevertheless, we next sought to identify the direct transcriptional targets regulated by the USP7-EPOP-ELOB complex. Based on the model shown in Figure 2-3B, we were specifically looking for genes that were upregulated in response to USP7 and EPOP suppression in the presence of trametinib. We identified 115 genes that were significantly up-regulated by $\geq$ 2 fold in both USP7 and EPOP depleted cells (Figure 2-4A, B).

However, to identify genes that are directly regulated by the USP7-EPOP-ELOB/C complex, we performed ChIP sequencing using USP7 antibodies and observed 1400 promoter-region peaks (Figure 2-4B). We then compared the genes containing USP7 peaks in their promoter regions to the 138 genes upregulated in USP7 and EPOP depleted cells and discovered 23 overlapping genes (Figure 2-4B). These genes represent transcriptional targets that are directly regulated by USP7-EPOP complexes.

Figure 2-4. The CABLES1 tumor suppressor is an essential transcriptional target of the USP7-EPOP-ELOB/C complex in melanoma and is required for cell death

(A) Enrichment analysis (GSEA) was used to develop plots depicting the enrichment of p53 and p63 gene signatures using Oncogenic Signatures and Chemical and Genetic Perturbation (CGP) datasets in my RNA-sequencing data. FDR: false discovery rate, NES: normalized enrichment score.
(B) 1400 genes were identified as having USP7 peaks in the promoter regions in SKMEL2 sgControl+MEKi compared to sgUSP7+MEKi through ChIP seq and 138 genes were identified as significantly up-regulated (>2 fold) in expression through RNA-sequencing in SKMEL2 sgControl+MEKi compared to sgUSP7+MEKi. Of these, 23 genes were identified in both sets, with 1 genes of interest, CABLES1, having tumor suppressive functions and stabilizing p63 and p73.
(C) ChIP-seq results demonstrating USP7 peaks across the gene promoter of *CABLES1*.
(D) Interestingly, we saw that knock-out of CABLES1 rescued cell death observed with USP7 and MEK inhibition in two different *NRAS*-mutant cell lines. Cells were infected with either control or CABLES1 shRNA and treated for 4 days with P5091 (USP7i, 10uM) and trametinib (MEKi, 10nM).. Cell counting assay and corresponding immunoblot for SKMEL2 and MM415 with shControl or shCABLES1.
(E) Immunoblots demonstrating protein expression of CABLES1 in SKMEL2 and MM415 cells treated for 48 hours with the USP7 inhibitor P5091 (10uM) and MEK inhibitor trametinib (10nM).
(F) (Left panel) Immunoblot demonstrating protein expression of CABLES1 in SKMEL2 cells with shRNA against either Control or EPOP and with or without MEK inhibitor trametinib (10nM) for 48 hours. (Right panel) EPOP expression was quantified with qPCR.
(G) Immunoblot demonstrating USP7, CABLES1, p63, p73, and GAPDH expression in SKMEL2 after 48 hours of treatment. SKMEL2 were infected with either shRNA against Control or USP7 and then treated for 48 hours with MEK inhibitor trametinib (10nM).

Figure 2-4 (continued)

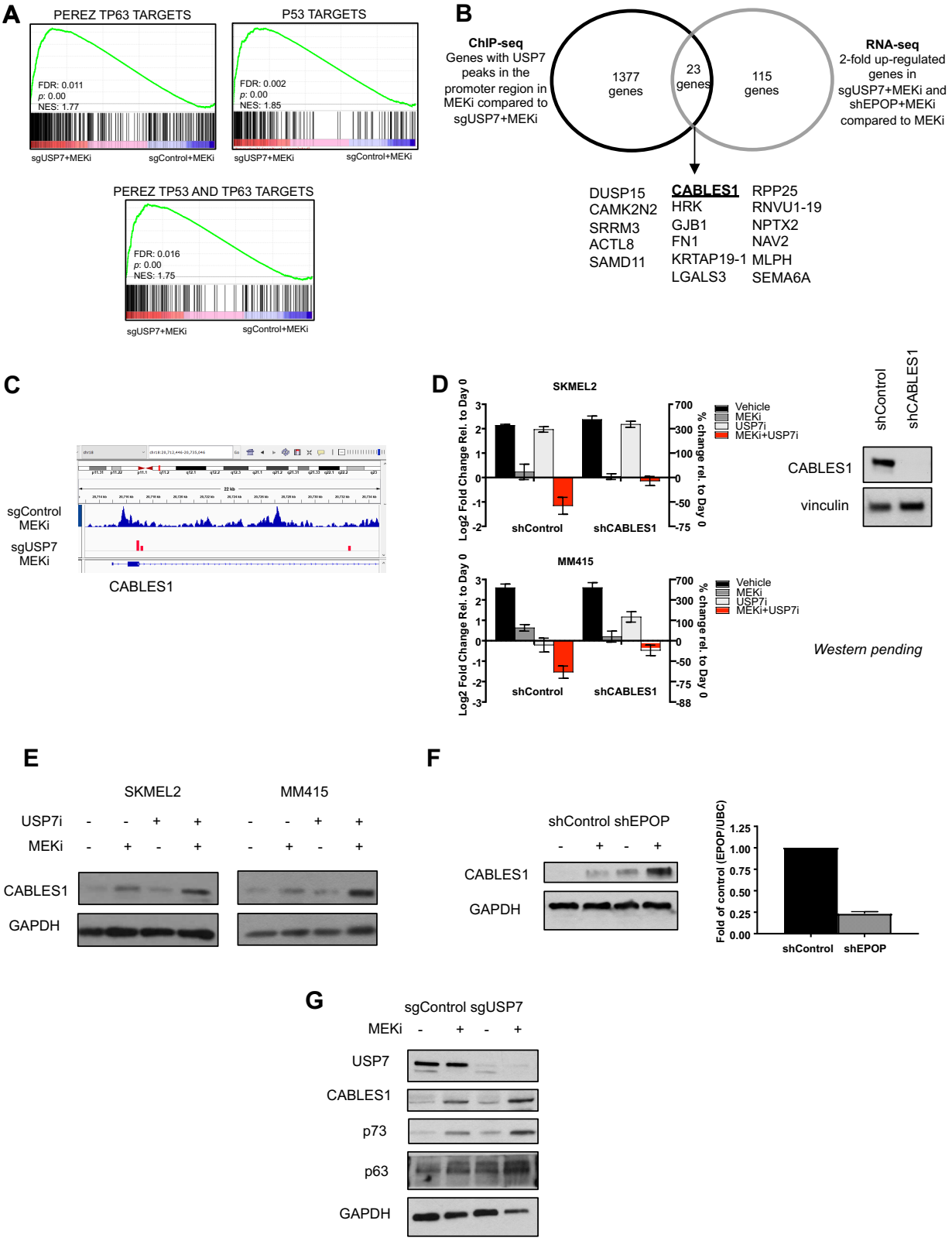

Within this gene set, a tumor suppressor known as CABLES1, has been shown to stabilize the p53 family members p63 and p73 (Wang et al. 2010; Huang et al. 2017). The USP7 ChIP peaks for this gene are shown in Figure 2-4C. As noted above, p63 and p53 signatures were significantly enriched in USP7 knock-out cells treated with trametinib (Figure 2-4A). However, while p53 is not intact in these cells, p53, p63 and p73 share many overlapping targets (De Laurenzi and Melino 2000; DeYoung and Ellisen 2007). Therefore, based on these observations, we investigated whether CABLES1 upregulation might be mediating the apoptotic effect of combined USP7 and MEK inhibition. Strikingly, genetic suppression of CABLES1 prevented the cytotoxic response to combined MEK and USP7 inhibitors in multiple responding cell lines (Figure 2-4D). Importantly, we found that CABLES1 expression was upregulated in response to combined USP7 and MEK inhibitors in multiple cell lines (Figure 2-4E). A similar expression pattern of CABLES1 was observed in cells in which EPOP was genetically suppressed (Figure 2-4F). These data suggest that CABLES1 is a direct transcriptional target of the USP7-EPOP-ELOB/C complex, and that loss of the complex increases CABLES1 gene and protein expression, causing cell death when combined with MEK inhibitors.

p63 and p73 are upregulated in response to USP7 and MEK suppression

The data thus far demonstrate that 1) p63 and p53 signatures are upregulated in melanomas treated with USP7 and MEK inhibitors, 2) USP7 and MEK inhibitors also lead to upregulation of CABLES1, which is a direct USP7 bound target, and 3) CABLES1 is known to stabilize p63 and p73. Therefore, we examined p63 and p73 expression in cells treated with USP7 shRNAs and trametinib. Notably, the expression of p63 and p73 mirrored the expression of CABLES1, which was highest in cells in which USP7 and MEK were both suppressed (Figure 2-4G).

Necessary Imminent Studies

Our hypothesis is that the upregulation of p63 and/or p73 by CABLES1 is required for cell death in response to USP7/MEK inhibition. Two essential experiments, both of which are in progress, will be required to make this conclusion. First, we need to demonstrate that the ablation of CABLES1 suppresses p63 and p73 induction. More importantly, we need to show that genetic suppression of p63 and/or p73 suppresses cell death**.** Preliminary studies exhibiting partial knock-down of these proteins suggest that this is the case, but definitive studies will be required.

DISCUSSION

Using a genome-scale negative-selection CRISPR-Cas9 screen, we identified USP7 as a target that, when suppressed, sensitizes *NRAS*- and *BRAF*-mutant melanomas to Ras/ERK pathway inhibitors both *in vitro* and *in vivo*. These findings have important clinical implications, as there are currently no effective therapies for *NRAS*-mutant melanomas, which represent a substantial fraction of melanomas. Additionally, a vast majority of *BRAF*-mutant melanoma patients relapse after treatment with BRAF and MEK inhibitors, and therefore improved therapies are needed in this setting as well. We further elucidated the mechanism of action of USP7/MEK inhibition in melanoma and identified a key transcriptional node regulated by USP7 deubiquitination. Overall, this study highlights the therapeutic potential of USP7 inhibitors, which are currently in various stages of clinical development, and also reveal a role for USP7 in protecting melanomas from the cytostatic effects of Ras pathway inhibitors..

While USP7 has been commonly associated with MDM2 deubiquitination, in melanomas, we found that USP7 affects transcription by inhibiting H2Bub, a marker of transcriptional elongation, through the USP7-EPOP-ELOB/C complex. Moreover, through transcriptional and epigenetic profiling, we identified *CABLES1* as a novel target of the USP7-EPOP-ELOB/C complex (Figure 2-5). Expression of CABLES1, also called ik3-1, has been

reported to be lost in lung, colon, ovarian, and endometrial cancers (Park et al. 2007; Sakamoto et al. 2008; Zukerberg et al. 2004; Tan et al. 2003; Dong et al. 2003). Conversely, its overexpression significantly inhibits the growth of these cancer cells, suggesting that it may function as a tumor suppressor. Interestingly, CABLES1 has been reported to bind to and stabilize p53 family proteins p63 and p73, which play a critical role in tumorigenesis (Orzol et al. 2015). For example, CABLES1 has been shown to protect p63 from proteasomal degradation, promoting cell death after genotoxic stress (Wang et al. 2010). Here we have shown that CABLES1 ablation protects melanoma cells from Ras pathway inhibitors. Ongoing studies will determine if CABLES1 indeed functions by stabilizing p63 and/or p73. Importantly, we have shown that both of these proteins become elevated in the presence of USP7 and MEK inhibitors and that the p63 pathway is activated, as determined by transcriptional evidence. Nevertheless, functional studies will be required to prove that these proteins are mediating cell death in melanoma. If true, these findings will reveal an unappreciated role for USP7 in broader regulation of the p53 protein family by distinct mechanisms.

While p63 and p73 are usually not mutationally inactivated in human cancer, both have been shown to regulate cell survival and apoptosis in human tumors (Moll and Slade 2004; DeYoung and Ellisen 2007). Genomic organization of p63 and p73 is complex, with alternative internal promoters generating NH2-terminally deleted dominant negative proteins that engage in inhibitory circuits within the family. Deregulated dominant-negative p73 isoforms, for example, have been shown to play an oncogenic role in some human cancers, including melanoma (Petrenko, Zaika, and Moll 2003; Steder et al. 2013; Zaika et al. 2002; Buhlmann and Putzer 2008). Nevertheless, p63 and p73 isoforms have been shown to regulate survival and apoptosis by transactivating subsets of known p53-regulated genes involved in cell-cycle arrest and apoptosis as well as independent sets of genes involved in development, differentiation, proliferation, and damage response (Zhu et al. 1998; Lee and La Thangue 1999; Suenaga et al.

2019; Awais et al. 2016; Prabhu et al. 1998). Through our RNA sequencing analysis, we found that USP7 and MEK inhibition significantly increased the expression of p63 and p53 regulated genes, and analysis of these genes found that the majority were tumor suppressive. For example, *BCL2L11, PERP,* and *BIK*, three pro-apoptotic genes, are significantly up-regulated within both p63 and p53 regulated gene sets. Therefore, in the future, we may also investigate the involvement of these downstream targets as well.

Together these studies have identified USP7 as an important therapeutic target in melanoma and have revealed a new therapeutic strategy for treating *NRAS*-mutant melanomas and enhancing responsiveness in *BRAF*-mutant melanomas. Our findings also suggest that USP7 plays an important role in protecting melanomas from Ras pathway inhibitors by regulating H2B ubiquitination at specific genomic sites in the genome. Finally, this work has revealed an unappreciated tumor suppressor cascade that is regulated by this DUB. A summary of our model is shown in Figure 2-5.

METHODS

Cell Lines and Reagents

All cell lines were purchased from ATCC, except for MALME3M (obtained from Levi Garraway, Dana-Farber Cancer Institute, Boston, MA), MELJUSO (obtained from William Hahn, Dana-Farber Cancer Institute, Boston, MA), YUFIC and YUDOSO (obtained from Yale Dermatology Center, New Haven, CT), WM3670 (obtained from Rockland Immunochemicals), and MM415 and MM485 (obtained from HPA Culture Collections through Sigma). No further authentication of these cell lines was performed. All cell lines were regularly tested for *Mycoplasma* using the MycoAlert Mycoplasma Detection Kit (Lonza, LT07-318). Cells were used for experiments within 15-20 passages from thawing. MM485, SKMEL2, MM415, WM3670, MALME3M, SKMEL28, and Hs695T were cultured in RPMI media supplemented with 10% FBS. HEK-293T, A375, and SKMEL5 were cultured in DMEM media supplemented with

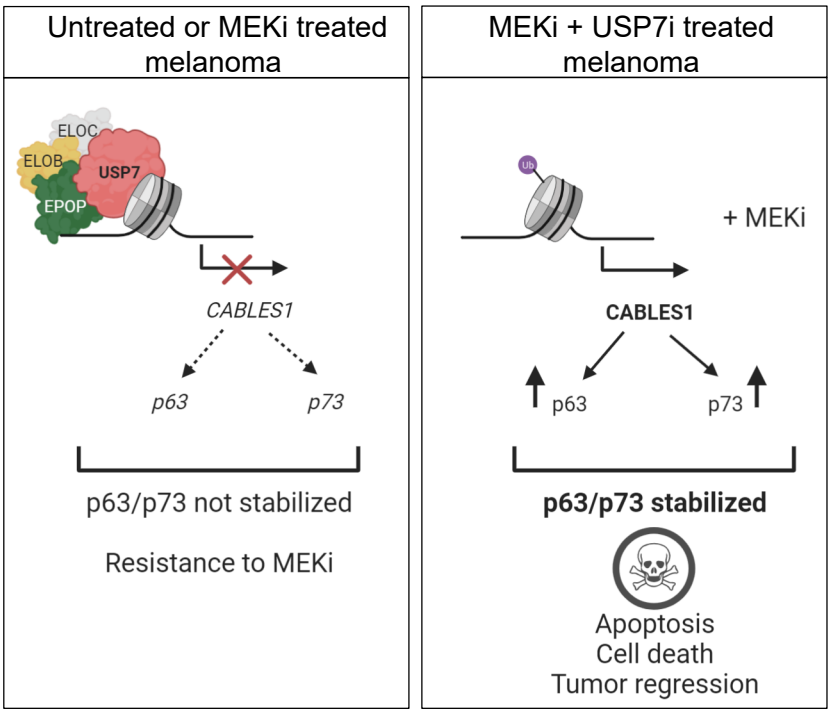

Figure 2-5: Summary of results observed in our study.
We found that in untreated or MEKi treated melanomas, the USP7-EPOP-ELOB/C complex inhibits expression of the tumor suppressor CABLES1, which downregulates p63 and p73 protein levels and leads to resistance to MEKi. When we treat these tumors with USP7/MEK inhibitors, then the USP7-EPOP-ELOB/C complex is inhibited, allowing transcriptional elongation of CABLES1. CABLES1 then stabilizes p63/p73, leading to apoptosis, cell death, and tumor regression.

10% FBS. WM115 was cultured in EMEM media supplemented with 10% FBS, and YUDOSO and YUFIC were cultured in Opti-mem media supplemented with 5% FBS. Antibodies were obtained from the following sources: Cell Signaling Technologies: pERK (4370), ERK (9102), c-RAF (9422), GAPDH (2118), vinculin (4650S), H2Bub (5546), p63 (13109); Sigma-Aldrich: Actin (A2066), Flag M2 (3165); Abcam: total H2B (1790), ELOB/TCEB2 (168836), CABLES1 (75535); Bethyl: USP7 (A300-034), p73 (A300-126A); Santa Cruz: P53 (126), Raf-B (5284). Trametinib and dabrafenib were purchased from LC Laboratories. P5091 and nutlin-3a were purchased from Selleck Chemicals. GNE6640 was purchased from MedChem Express LLC. FT671 was purchased from Glixx Laboratories. XL177A was a gift provided by Nathan Schauer and Sara Buhrlage.

Genome-scale Negative Selection CRISPR-Cas9 screen

sgRNAs were designed based on an Elledge lab algorithm (unpublished) with different scores including an evolutionary conservation score to predict important parts of a protein and DNA sequence parameters that can better predict identification of essential genes from previously published CRISPR studies. sgRNAs were synthesized via oligo chip and cloned into a derivative of lentiCRISPR V2 that contains a human and mouse U6 promoter to drive sgRNA expression as well as a puromycin resistance gene for selection. Two libraries of gRNAs (“druggable”: 27,525 gRNA pairs; “undruggable”: 47,230 gRNA pairs) targeting 18,911 genes in total with 4-5 gRNA pairs per gene were individually prepared and pooled together at equal molar ratios. 293T cells were transfected with the library plasmid pool with psPax2 and pMD2.G lentiviral packaging vectors to prepare pooled virus. Virus was then collected after 48 and 72 hours post transfection and concentrated with lenti-X concentrator solution (Clontech). SKMEL2 cells were infected at a low MOI (0.3) with a representation of 500 in triplicate. Cells were selected with puromycin (1 ug/mL) for 3

days and then cultured for an additional 7 days to allow complete knock out to occur. An initial cell pellet was then collected for a day 0 time point before cells were treated either with DMSO (vehicle) or trametinib (MEKi, 10nM) for 4 days. Genomic DNA was isolated by phenol:chloroform extraction, and the second sgRNA driven by the mouse U6 promoter was PCR amplified with barcoded primers for sequencing on an Illumina NextSeq 500. Sequencing reads were aligned to the initial library and counts were obtained for each sgRNA. EdgeR was used to calculate p-values, FDRs, and $\log_2$ fold changes for comparison between day 0 and day 4 samples.

RNAi

Short interfering RNAs (siRNAs) ON-TARGET SMARTpool siRNA were purchased from GE Healthcare/Dharmacon to target *BRAF*, *RAF1*, *TP53,* and *EPOP*, and transfected with lipofectamine RNAiMAX from Invitrogen. Cells were transfected approximately 24 hours before proliferation experiments were started. CRISPR guide RNAs (sgRNAs) for control and *USP7* were a gift from Isaac Harris and Joan Brugge and are describe in (Harris et al. 2019). Control, *ELOB, EPOP,* and *CABLES1* shRNAs were purchased from Sigma-Aldrich (SHC016, SHCLNG-NM_007108, SHCLNG-NM_001130677, and SHCLNG-NM_138375 respectively).

Expression Constructs

USP7 cDNA clones were obtained from Horizon Discovery, Dharmacon, sequence verified, and subsequently cloned into the pLX304 mammalian lentiviral expression vector (Addgene plasmid #25890).

Cell Growth Assays

For cell proliferation experiments, 50,000-70,000 cells per well were seeded in triplicate in 6-well plates and then day 0 time points were counted approximately 24 hours after plating

using a hemocytometer. Drug treatments were then started at this time, and final cell counts were taken 96 hours after day 0 to determine changes in cell number versus day 0. For synergy experiments, cells were plated in 96-well plates. At 24 hours, one plate of cells was frozen (-80C) representing the time 0 plate. Compounds were added to the remaining plates. After 96 hours, each of the plates were frozen. After freezing, all plates (day 0 and day 4) were thawed simultaneously and cells were quantified using CellTiter-Glo (Promega) as per the manufacturer's instructions. SynergyFinder was used to analyze drug combination dose-response matrix data. Gaddum's noninteraction HSA synergy score was used to determine the strength of synergistic interaction because at least one agent (trametinib) is cytostatic (Ianevski et al. 2017; Foucquier and Guedj 2015).

Live Cell Imaging

IncuCyte ZOOM (Essen Biosciences), a live cell imager, was used for multiplexed measurements of cell death and proliferation. The mKate2 red fluorescent protein (RFP; Essen Biosciences) was transfected into SKMEL2 melanoma cell line and selected with puromycin. Stably transfected cells were plated in 48-well plates and allowed to settle overnight at 37C. Compounds and Green IncuCyte Caspase 3/7 Apoptosis reagents were then added to the tissue culture growth media to assess real-time quantification of cell death. IncuCyte ZOOM acquired images every 4 hours for 96 hours after treatment with vehicle or compounds and then quantified with the IncuCyte integrated analysis software. Relative cell death is the ratio between cells with overlapping red and green cells (dead cells) and cells with red nuclei only (live cells).

Animal Studies and Treatments

Animal procedures were approved by the Center for Animal and Comparative Medicine in Harvard Medical School in accordance with the NIH Guide for Care and Use of Laboratory

Animals and the Animal Welfare Act. Immunodeficient NSG (YUDOSO, MM415) or Nu/Nu (A375) mice were inoculated subcutaneously with 3 x 10^6 *NRAS*- or *BRAF*-mutant human melanoma cells in 200uL PBS. Tumor volumes were measured twice a week and calculated using the formula [length x $(width)^2$ x 0.52]. Once tumor volume reached approximately 200-300mm^3, mice were randomly divided into treatment groups and treated daily with USP7 inhibitor P5091 (20mg/kg/day, intraperitoneal [i.p.] injection); MEK inhibitor GSK1120212/ trametinib (0.6mg/kg/day, oral gavage [o.g.]) and BRAF inhibitor GSK2118436/ dabrafenib (30 mg/kg/day, o.g.); or a combination of P5091, GSK1120212, and GSK2118436. To track changes in tumor volume, mice tumor size was measured at day 0 and subsequently every 3-5 days by Vernier calipers. Mice were treated daily for up to 45 days. Unpaired two-tailed *t* tests with unequal variance were used to compared datasets where indicated, and *P* values are shown.

RNA Extraction and Quantitative Real-Time PCR

Total RNA was isolated from cells after indicated treatments using Trizol (Invitrogen) and phenol:chloroform extraction. 50 ng of total RNA was used for each reaction, and cDNA synthesis and PCR amplification were performed using qScript One-Step SYBR Green Kit for Iq (Quanta Biosciences). Quantitative PCR (qPCR) reactions were run using a Bio-Rad iCycler iQ thermal cycler. Samples were run in triplicate, and expression levels were determined based on a standard curve run with each primer set; levels were normalized to an internal control, UBC. Primers for *EPOP* were (5'-3'): CAGGCCCAAGTCCATTCTT (forward) and AGGCCAAGAGTCCTTTCATTTA (reverse). Primers for *UBC* were (5'-3'): TGCCTTGACATTCTCGATGGT (forward) and ATTTGGGTCGCGGTTCTTG (reverse).

Immunoprecipitation experiments

Twenty million SKMEL2 cells were treated with either 10nM trametinib or DMSO for 24 hr. Cells were lysed in CHAPS buffer (50mM Tris pH7.8, 350mM NaCl, 1mM DTT, 10mM CHAPS) for 10 min at 4C and then lysate was clarified by spinning at max speed for 15 min. Lysate was pre-cleared twice for 30 min at 4C with Pierce Protein A magnetic beads (ThermoFisher, 88846) before 2 ug of TCEB2/ELOB antibody (Abcam, 168836) was added. Protein was immunoprecipitated rotating at 4C for 4 h. Subsequently, 20 ul washed Protein A beads were added and mixture was incubated for 2h rotating at 4C. Beads were washed three times with CHAPS buffer, and protein complexes were eluted by boiling in 2x SDS sample buffer. Samples were analyzed by western blot with antibodies against USP7 (Bethyl, A300-033), TCEB2/ELOB (Abcam, 168836), and Flag (Sigma, 3165).

RNA-seq and ChIP-seq sample preparation and data analysis

A subset of RNA-seq and ChIP-seq libraries were generated by the Center for Functional Cancer Epigenetics (CFCE) and Molecular Biology Core (MBC) at Dana-Farber Cancer Institute (DFCI) following manufacturer's protocols.

ChIP for USP7 was performed using antibody USP7 (Bethyl, A300-033). For ChIP-seq, 10 x 10^6 cells were fixed with 1% formaldehyde (Sigma, F8775) for 10 min at 37C. Crosslinking was quenched by adding glycine to a final concentration of 0.125M for 5 min at 37C. Cells were washed with ice-cold PBS. The nuclear fraction was extracted by first resuspending the pellet in Lysis Buffer 1 (50mM Hepes-KOH pH 7.5, 140mM NaCl, 1mM EDTA pH 8, 10% glycerol, 0.0033% NP-40, 0.25% Triton-X100) and rotating at 4C for 15 minutes before spinning down at 1,350xg for 5 min at 4C and aspirating supernatant. Next, the pellet was resuspended in Lysis Buffer 2 (10mM Tris-HCL pH8, 200mM NaCl, 1mM EDTA pH 8, 0.5mM EGTA pH8) and rotated at RT for 10 min, then pelleted at 1,350xg for 5 min at 4C. Then pellet was resuspended in Sonication Buffer (10mM Tris-HCl pH 8, 100mM NaCl, 1mM EDTA pH 8, 0.5mM EGTA pH8, 0.1% Na deoxycholate, 0.5% sarcosyl) and transferred to sonication tubes (Active Motif,

103842). Samples were sonicated in a Covaris sonicator. Lysate was centrifuged for 15 min at 20,000xg at 4C to purify debris. Then sample was incubated with 100 uL of Pierce Protein A/G Magnetic Beads (ThermoFisher, 88803) for 1 h at 4C. 10ug primary antibodies were added to each tube and immunoprecipitation (IP) was conducted overnight on a rotator at 4C. Cross-linked complexes were precipitated with Pierce Protein A/G magnetic beads for 2 h at 4C. The beads were then washed 3 times with low salt wash buffer (0.1% SDS, 1% Triton-X100, 2mM EDTA pH8, 20mM Tris-HCl pH 8, 150mM NaCl), 3 times with high salt wash buffer (0.1% SDS, 1% Triton-X100, 2mM EDTA pH8, 20mM Tris-HCl pH 8, 500mM NaCl), 3 times with LiCl wash buffer (0.25M LiCl, 1% NP-40, 1mM EDTA pH8, 10mM Tris-HCl pH 8, 1% Na deoxycholate), and 1 time with TE buffer (10mM Tris-HCl, 1mM EDTA pH 8) at 4C. DNA was eluted in elution buffer (50mM Tris-HCl pH8, 10mM EDTA pH8, 1% SDS) and samples were reverse cross-linked overnight at 65C with 0.2mg/ml proteinase K. RNA and protein were digested with 0.2mg/ml RNase A for 30 min at 37C. DNA was purified with phenol-chloroform extraction and isopropanol precipitation. ChIP-seq libraries were prepared according to manufacturer's protocol. We used Burrows-Wheeler Aligner (BWA) as a read mapping tool and Model-based Analysis of ChIP-Seq (MACS2) as a peak caller. Peak annotation was performed using annotatePeaks.pl of the HOMER package v4.9.1 with version hg19 of the human genome.

For RNA seq, RNA was extracted from cells after 24 hours of indicated treatments using RNEasy Mini kit (QIAGEN) according to manufacturer's instructions with an in-solution DNAse digestion step. RNA integrity was confirmed with an Agilent 2100 Bioanalyzer (Agilent Technologies). RNA (30 ng/uL) was submitted to the Molecular Biology Core (MBC) at DFCI. Library was prepared using Kapa stranded mRNA hyper prep and sequenced with Illumina NS500 single-end 75 base pair sequencing. Data was analyzed using Viper NextSeq Run by the MBC. To determine genes and gene sets differentially expressed between groups, GO and

GSEA analyses were performed using both the GenePattern server (The Broad Institute) and David Bioinformatics Resources (version 6.8).

Statistical Analysis for In Vitro Experiments

For quantitative measurements, graphs represent mean values +/- SD. Where indicated the data are presented as $\log_2$ fold (left axis) and percent change (right axis) over initial measurements. Changes in tumor volume are presented in a waterfall plot with each bar representing the change in tumor volume of an individual animal in the study. Unpaired two-tailed *t* tests with unequal variance were used to compare data-sets where indicated and *P* values are shown. A *P* value less than or equal to 0.05 was considered significant. Data were graphed and analyzed using GraphPad Prism v.6.

Acknowledgements

We thank Nathan Schauer and Sara Buhrlage for discussion and the use of XL177A for our experiments. We thank Isaac Harris and Joan Brugge for the USP7 CRISPR-Cas9 sgRNA plasmids. We thank Patrick Loi for discussions about ChIP sequencing. We thank Joao Paulo and Steve Gygi for experimental advice and for performing experiments that were not included in the manuscript.

Chapter 3 : MAPK Pathway Suppression Unmasks Latent DNA Repair Defects and Confers a Chemical Synthetic Vulnerability in *BRAF, NRAS,* and *NF1*-Mutant Melanomas

MAPK pathway suppression unmasks latent DNA repair defects and confers a chemical synthetic vulnerability in *BRAF*, *NRAS*, and *NF1* mutant melanomas

Ophélia Maertens[1,2,3], Ryan Kuzmickas[1,2], Haley E. Manchester[1,2], Chloe E. Emerson[1,2], Alessandra G. Gavin[1,2], Caroline J. Guild[1,2], Terence C. Wong[4,5], Thomas De Raedt[1,2], Christian Bowman-Colin[2,6], Elodie Hatchi[2,6], Levi A. Garraway[2,3,4,5], Keith T. Flaherty[2,7], Shailja Pathania[8], Stephen J. Elledge[1,2,3,9], Karen Cichowski[1,2,3]

[1]Genetics Division, Department of Medicine, Brigham and Women's Hospital, Boston, MA 02115, USA; [2]Harvard Medical School, Boston, MA 02115, USA; [3]Ludwig Center at Harvard, Boston, MA 02115, USA; [4]Department of Medical Oncology, Center for Cancer Precision Medicine, Dana-Farber Cancer Institute, Boston, MA 02115, USA; [5]Cancer Program, Broad Institute of MIT and Harvard, Cambridge, MA 02142, USA; [6]Department of Cancer Biology, Dana-Farber Cancer Institute, Boston, MA 02115, USA; [7]Department of Medical Oncology, Massachusetts General Hospital, Boston, MA 02114, USA; [8]Center for Personalized Cancer Therapy, University of Massachusetts, Boston, MA 02125, USA; [9]Department of Genetics, Howard Hughes Medical Institute, Boston, MA 02115, USA

Author Attributions:

Conception and design: O. Maertens, S.J. Elledge, K. Cichowski
Development of methodology: O. Maertens, T. De Raedt
Acquisition of data (provided animals, acquired and managed patients, provided facilities, etc.): O. Maertens, C.E. Emerson, A.G. Gavin, T.C. Wong, T. De Raedt, L.A. Garraway, K.T. Flaherty, S. Pathania
Analysis and interpretation of data (e.g., statistical analysis, biostatistics, computational analysis): O. Maertens, R. Kuzmickas, H.E. Manchester, C.E. Emerson, A.G. Gavin, T.C. Wong, T. De Raedt, K.T. Flaherty, S. Pathania, S.J. Elledge, K. Cichowski
Writing, review, and/or revision of the manuscript: O. Maertens, R. Kuzmickas, C. Bowman-Colin, E. Hatchi, K.T. Flaherty, S.J. Elledge, K. Cichowski
Administrative, technical, or material support (i.e., reporting or organizing data, constructing databases): H.E. Manchester, C.E. Emerson, C.J. Guild
Study supervision: L.A. Garraway, S.J. Elledge, K. Cichowski

ABSTRACT

While the majority of *BRAF*-mutant melanomas respond to BRAF/MEK inhibitors, these agents are not typically curative. Moreover, they are largely ineffective in *NRAS*- and *NF1*-mutant tumors. Here we report that genetic and chemical suppression of HDAC3 potently cooperates with MAPK pathway inhibitors in all three Ras pathway-driven tumors. Specifically, we show that entinostat dramatically enhances tumor regression when combined with BRAF/MEK inhibitors, both in models that are sensitive or relatively resistant to these agents. Interestingly, *MGMT* expression predicts responsiveness and marks tumors with latent defects in DNA repair. BRAF/MEK inhibitors enhance these defects by suppressing homologous recombination genes, inducing a BRCA-like state; however, entinostat addition triggers the concomitant suppression of NHEJ genes, resulting in a chemical synthetic lethality caused by excessive DNA damage. Together these studies identify melanomas with latent DNA repair defects, describe a promising drug combination that capitalizes on these defects, and reveal a tractable therapeutic biomarker.

INTRODUCTION

Melanomas can be classified into four genomic subtypes based on the presence or absence of mutations in Ras pathway genes: *BRAF*, *NRAS*, *NF1* and Triple-wild-type ('Genomic Classification of Cutaneous Melanoma' 2015). Fortunately, selective BRAF and MEK inhibitors, and more recently BRAF/MEK inhibitor combinations, have improved prognosis and overall survival in patients with metastatic *BRAF*-mutant disease (Luke et al. 2017). Nevertheless, all individuals ultimately relapse, and do so on average in 11 months (Robert, Schachter, et al. 2015; Robert, Karaszewska, et al. 2015). A fraction of *NRAS*-mutant tumors (15%) exhibit partial responses to MEK inhibitors, albeit with shorter durations (Dummer et al. 2017). The MEK pathway is also hyperactivated in *NF1*-mutant melanomas, however the clinical activity of MEK inhibitors in this subtype is not known. Regardless, these observations suggest that while

RAF/MEK pathway inhibition will remain an important cornerstone of melanoma treatment, improved combinations and/or sequential therapies are needed. Accordingly, additional meaningful targets must be identified.

Agents that target epigenetic enzymes are increasingly being developed as potential cancer therapies (Jones, Issa, and Baylin 2016). HDAC inhibitors are one such class of compounds and various drugs have been approved for use in hematopoietic malignancies (West and Johnstone 2014). While single agent efficacy in solid tumors has not been observed, HDAC inhibitors are currently being evaluated in combination with other targeted agents in several diseases (Falkenberg and Johnstone 2014). However, the key to discovering successful combinations, if they exist, will likely lie in 1) identifying the most selective/potent agent for the specified target to minimize potential toxicities; 2) elucidating the mechanism of action of the combination identified; and 3) using this insight to prospectively identify patients that are most likely to respond. While these criteria are important for developing any successful combination therapy, they may be critical for developing combinations with HDAC inhibitors, many of which inhibit numerous HDAC isoforms, and therefore have major effects on chromatin.

Here we identify an epigenetic-based combination therapy for *BRAF*-, *NRAS-,* and *NF1*-mutant melanomas. Specifically, we show that HDAC3 is an important therapeutic target in these tumors and that the selective Class I inhibitor, entinostat, not only dramatically enhances the in vivo efficacy of BRAF/MEK inhibitors in *BRAF*-mutant malignancies with varying sensitivities to these agents, but also cooperates with MEK inhibitors in *NRAS* and *NF1*-mutant tumors. We further demonstrate that these agents function by coordinately suppressing the transcription of homologous recombination (HR) and non-homologous end joining (NHEJ) genes, thereby triggering excessive DNA damage in sensitive tumors. Finally, we identify a tractable biomarker that marks melanomas with broad defects in DNA repair genes and predicts efficacy. Together these studies have identified a promising mechanism-based combinatorial

strategy for treating melanomas with several RAS/RAF pathway defects and have outlined a path for clinical translation.

RESULTS

HDAC inhibitors dramatically potentiate the effects of BRAF/MEK inhibitors in BRAF-, NRAS- and NF1-mutant melanomas

MITF is a lineage-specific survival gene that is amplified in a subset of melanomas and has been shown to confer resistance to MAPK pathway inhibition (Johannessen et al. 2013). Because HDAC inhibitors have been reported to suppress *MITF* expression (Yokoyama et al. 2008), we reasoned that these agents might potentiate the therapeutic effects of BRAF and/or MEK inhibitors. A panel of melanoma cell lines harboring mutations in *BRAF*, *NRAS* or *NF1* were examined in a CellTiter-Glo based screen. The MEK inhibitor, trametinib, was used to broadly suppress the MAPK pathway in all cell lines. Notably, the pan-HDAC inhibitor, vorinostat, dramatically potentiated the effects of trametinib in 6 out of 10 lines, including *BRAF*-, *NRAS*- and *NF1*-mutant cells (Figure 3-1A). These effects were determined to be synergistic using the Loewe excess additivity model (Figure 3-1B).

Cytotoxicity was confirmed by cell counting assays and live cell imaging in the presence of clinically relevant drug combinations. Combined BRAF and MEK inhibitors (dabrafenib/trametinib) were used to suppress the MAPK pathway in *BRAF*-mutant cells, as this represents the standard of care (Luke et al. 2017), whereas trametinib alone was used in *NRAS* and *NF1*-mutant cell lines. In both settings, combined MAPK/HDAC suppression resulted in a dramatic loss of viable cells in just 72 hours in sensitive lines representing all three genotypes (Figure 3-1C). Dabrafenib/trametinib and vorinostat effectively suppressed their respective targets in all cell lines and the combination did not further reduce ERK phosphorylation in sensitive cells nor attenuate phospho-ERK suppression in resistant cells

Figure 3-1: HDAC inhibitors potentiate the effects of BRAF/MEK pathway inhibitors in *BRAF*-, *NRAS*- and *NF1*-mutant melanoma. (A) Melanoma cell lines with specified genotypes (*BRAF*-mutant (B*), *NRAS*-mutant (N*), *NF1*-mutant (NF1) or wild-type for *BRAF*, *NRAS* and *NF1* (WT)) were treated with DMSO, 10nM trametinib (MEK inhibitor), 2μM vorinostat (HDAC inhibitor) or both agents. Graph depicts log2 transformation of the fold change in luminescence using a CellTiter-Glo assay in cells after 3 days of treatment versus day 0 (left axis) +/- SD. **(B)** Synergy scores (to characterize the combination effects in excess of Loewe additivity) for Vorinostat combined with Trametinib for SKMEL2 (3D synergy map, left) and additional sensitive cell lines from Fig. 3-1A (right). Strong synergy is indicated in red. **(C)** *BRAF*-, *NRAS*- and *NF1*-mutant melanoma cell lines were treated with DMSO, 100nM dabrafenib (D) and/or 10nM trametinib (T), 2μM vorinostat (V) or the specified agents combined, as indicated. Cells were manually counted prior to the addition of compounds and 3 days after treatment. Graphs represent log2 transformation of the fold change in cell number at day 3 versus day 0. Right axis shows percent change in cell number relative to day 0. Negative values represent a decrease in cell number over time and positive values represent an increase in cell number. Immunoblots show levels of phosphorylated ERK (p-ERK), total ERK, histone H3 acetylation at lysine 9 (H3K9Ac) and total H3 after 48 hours of indicated treatment. (Hs695T) *p=0.001896, **p=0.002332; (SKMEL5) *p=0.000011, **p=0.000077; (SKMEL2) *p=0.000007, **p=0.000074; (MEWO) *p=0.003025, **p=0.001545 **(D)** Normal melanocytes (melan-A) were treated with DMSO, 100nM dabrafenib and 10nM trametinib (MAPKi), 1μM HDAC inhibitor (HDACi) and the combination of MEK/BRAF and HDAC inhibitors. Cells were manually counted prior to the addition of compounds and 3 days after treatment. Graphs represent log2 transformation of the fold change in cell number at day 3 versus day 0. **(E)** Real-time quantification of cell death (left panel) and cell numbers (right panel) using the live cell imager IncuCyte Zoom. Red (nuclear restricted NucLight Red fluorescent protein for quantifiying live cells) and green (Cytotox Green reagent for quantifying dead cells) fluorescent objects were monitored in the Incucyte ZOOM acquiring images every 2 hours (for 72 hours) following treatment with vehicle (DMSO) or drugs (MEK inhibitor, BRAF inhibitor, HDAC inhibitor) and then quantified with the IncuCyte integrated analysis software. **(F)** Western blot depicting cleaved PARP protein levels after 48hrs of treatment with vehicle (-), MEK inhibitor (trametinib, T) and/or HDAC inhibitor (vorinostat, V). Alpha-tubulin serves as a loading control. Bar graphs represent quantification of cleaved PARP for different treatment arms, relative to untreated control. **(G)** Hs695T cells were treated with vorinostat (VOR, 1μM), mocetinostat (MOC, 1μM), nexturastat (NEX, 2μM) or entinostat (ENT, 2μM), alone (black) and in combination with 10nM trametinib (MEKi, red). Graph depicts the mean log2 fold change of cell number after 72 hours, relative to day 0. Right axis shows percent change in cell number relative to day 0. Immunoblot shows acetylated H3 at lysine 9 (H3K9Ac), acetylated H3 at lysine 56 (H3K56Ac) and acetylated tubulin (tubulin-Ac, surrogate marker for HDAC6 inhibition) after 48 hours of indicated treatment. GAPDH serves as a loading control. **(H-J)** Melanoma cell lines were treated with DMSO, 100nM dabrafenib (D) and/or 10nM trametinib (T), 1μM entinostat (ENT) or the specified drug combinations. Graphs represent log2 transformation of the fold change in cell number at day 3 versus day 0. Right axis shows percent change in cell number relative to day 0. Negative values represent cell death and a decrease in cell number. Immunoblots show levels of phosphorylated ERK (p-ERK), total ERK, histone H3 acetylation at lysine 9 (H3K9Ac) and total H3 after 48 hours of indicated treatment. (Hs695T) *p=0.005997, **p=0.005364; (SKMEL2) *p=0.008834, **p=0.017467; (MEWO) *p=0.003176, **p=0.000183 **(K)** Hs695T cells were transfected with pooled siRNAs targeting HDAC1, HDAC2, HDAC3, HDAC6 or control non-targeting siRNAs and treated with DMSO (black) or 10nM trametinib (MEKi, grey). Graph depicts the mean log2 fold change of cell number after 72 hours, relative to day 0. Right axis shows percent change in cell number relative to day 0. Immunoblot below depicts knockdown of the respective siRNAs. GAPDH serves as a loading control. **(L)** SKMEL2 cells were infected with lentiviral constructs targeting HDAC1, HDAC2, HDAC3, HDAC6 or control and treated with DMSO (black) or 10nM trametinib (MEKi, grey). Graph depicts the mean log2 fold change of cell number after 72 hours, relative to day 0. Right axis shows percent change in cell number relative to day 0. Immunoblot below depicts knockdown of the respective shRNAs. GAPDH serves as a loading control.

Figure 3-1 (continued)

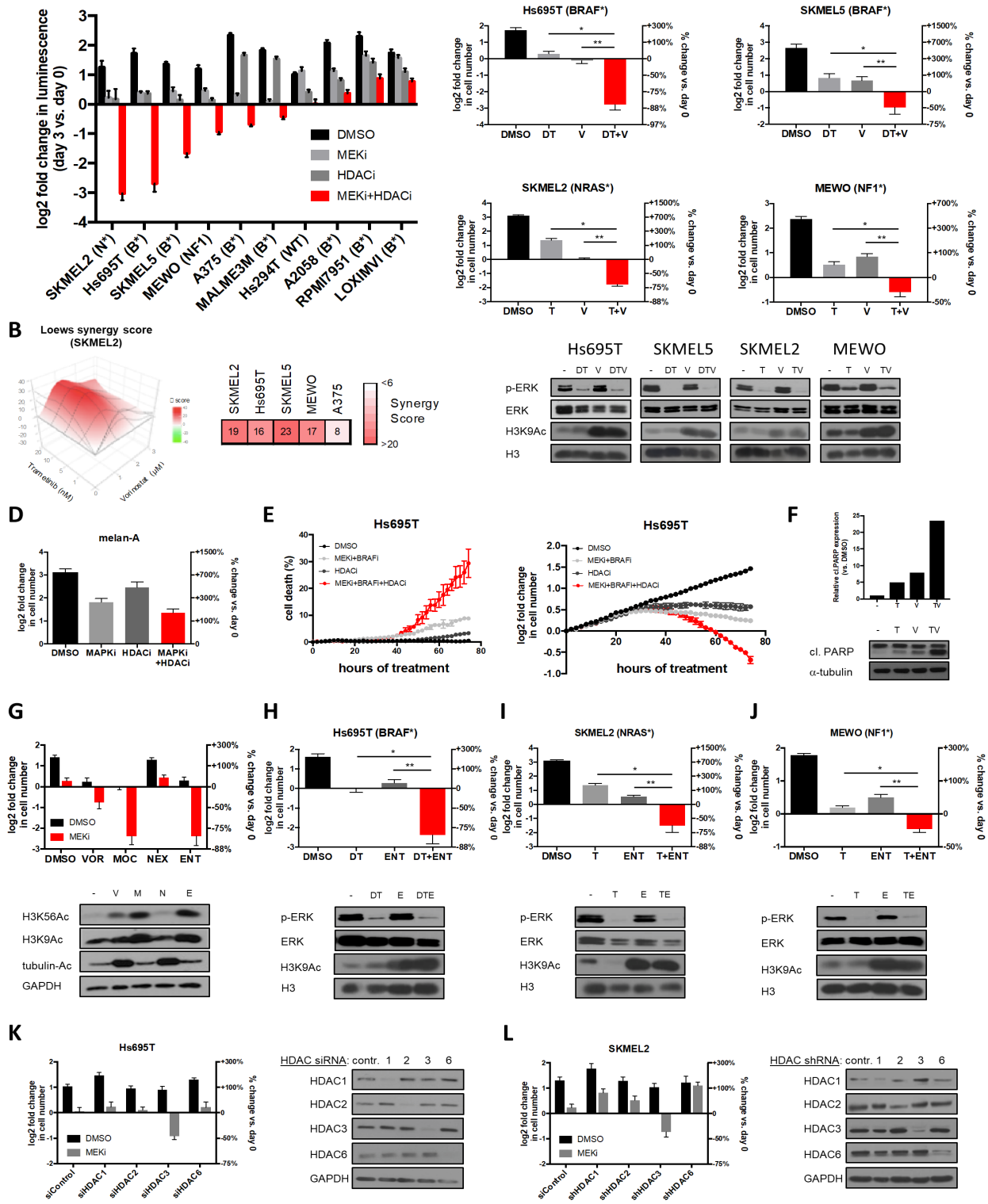

Figure 1

(Figure 3-1C and Supplementary Figure B-1A,B). These agents were not generally toxic, as they did not affect the viability of normal melanocytes, unresponsive melanoma cell lines, and a variety of other unrelated cell types (Figure 3-1D and Supplementary Figure B-1A-D).

Live-cell incucyte imaging was used to concomitantly measure cell death and changes in cell number over time, using a fluorescent assay that detects live and dead cells. BRAF/MEK inhibitors alone killed 9% of cells, consistent with previous reports (Figure 3-1E, left panel) (Tsai, 2008). However, while the HDAC inhibitor had little effect on its own, it dramatically potentiated cell death triggered by dabrafenib/trametinib, resulting in 29% cell death within just 72 hours (Figure 3-1E, left panel). Cell death was mediated by apoptosis, as confirmed by PARP cleavage and a fluorescent caspase reporter, which similarly revealed that one-third of the cell population was undergoing apoptosis within 72 hours (Figure 3-1F and Supplementary Figure A-1E). Importantly, the onset of cell death corresponded to a concomitant reduction in cell number (Figure 3-1E, right panel). Consistent with previous observations, BRAF/MEK inhibitors alone appeared to exert delayed cytostatic effects in vitro ; however, this apparent cytostasis was likely due to the net effects of concomitant proliferation and lower levels of cell death (Figure 3-1E). By contrast, BRAF/MEK and HDAC inhibitors together synergized to cause much more cell death, thereby eliminating more resistant tumor cells (Figure 3-1A-C,E).

Therapeutic responses are unrelated to MITF status or expression changes

Melanomas can either be categorized as $MITF^{high}$ or $MITF^{low}$ (Konieczkowski et al. 2014). Based on our original hypothesis we expected that $MITF^{high}$ cells might be more sensitive to these agents, and if so MITF suppression by HDAC inhibitors would correspond to sensitivity. Surprisingly however, sensitivity was unrelated to MITF status, as both $MITF^{high}$ and $MITF^{low}$ cells responded to this combination (Supplementary Figure B-1F). In addition, MITF suppression did not correlate with sensitivity (Supplementary Figure B-1G). Taken together

these observations suggest that HDAC inhibitors broadly potentiate the therapeutic effects of BRAF/MEK pathway inhibitors in a high percentage of melanomas harboring mutations in one of several genes affecting the RAS/RAF pathway, but that these effects are unrelated to MITF status or expression changes.

Suppression of HDAC3 is sufficient to kill melanomas when combined with MAPK pathway inhibitors

Before embarking on mechanistic studies we sought to identify the most clinically tractable agent(s). Vorinostat is a pan-HDAC inhibitor, however more selective inhibitors have been developed (West and Johnstone 2014). Importantly, the use of more selective compounds might minimize potential toxicities in humans, especially in the context of drug combinations. The effects of vorinostat were compared to mocetinostat (which inhibits Class I HDACs 1-3 and Class IV HDAC 11) (Fournel et al. 2008), nexturastat (a selective HDAC6 inhibitor that primarily affects acetylation of proteins other than histones) (Miyake et al. 2016), and entinostat (which inhibits Class I HDACs 1-3) (West and Johnstone 2014). Nexturastat did not kill cells when combined with MAPK pathway inhibitors, indicating that HDAC6 inhibition is not sufficient for these effects (Figure 3-1G). However, mocetinostat and entinostat, both cooperated with trametinib and were even more potent than vorinostat, demonstrating that the suppression of Class I HDAC proteins is sufficient for a maximal therapeutic response (Figure 3-1G).

We were particularly enthusiastic about entinostat because it is the most selective agent in this panel that exerted therapeutic effects, and it has shown promising responses in Phase 2 drug combination studies in breast cancer (Connolly et al. 2016). It is also currently being evaluated in a variety of solid tumors, underscoring the potential translatability of entinostat-based combinations. Importantly, entinostat also cooperated with MAPK pathway inhibitors in *BRAF*-, *NRAS*- and *NF1*-mutant cell lines (Figure 3-1H-J).

Entinostat suppresses the activity of HDAC1, 2 and 3, and does not affect protein expression, as previously reported (Supplementary Fig. B-1H) (Zhu et al. 2015). To determine whether the inhibition of a specific HDAC gene was mediating the therapeutic effects, individual HDACs were genetically suppressed using pooled siRNAs. Interestingly, only HDAC3 suppression was sufficient to kill melanomas when combined with trametinib, which was confirmed using an unrelated panel of shRNA sequences in a second sensitive cell line (Figure 3-1K,L). Because entinostat is currently the most selective, clinically available agent that suppresses HDAC3 and is well tolerated even when combined with other agents, we continued our analysis using entinostat. In addition, it should be noted that while pan-HDAC inhibitors also exert activity in this setting, toxicities associated with broad HDAC inhibition have limited their clinical utility in the context of some drug combinations (Oki et al. 2013), further supporting the selection of entinostat.

Entinostat potently cooperates with dabrafinib/trametinib in vivo in models with differing sensitivities to BRAF/MEK inhibitors

Next, we investigated whether these agents could exert similar cooperative effects in vivo, using drug concentrations that mimic human exposures (King et al. 2013). In clinical trials the BRAF inhibitor dabrafenib exhibits activity as a single agent in *BRAF*-mutant melanomas, however when combined with trametinib, efficacy is enhanced and toxicities are reduced, due to the suppression of feedback pathways (Robert, Schachter, et al. 2015; Robert, Karaszewska, et al. 2015). As such, combined BRAF/MEK inhibitors are now the standard of care in *BRAF*-mutant melanoma. Nevertheless, a range of therapeutic responses are observed in patients. Therefore, we examined several *BRAF*-mutant melanoma models with differing sensitivities to these agents. The A375 xenograft model was moderately sensitive to the standard of care; average tumor regression in response to dabrafenib/trametinib was 32% (Figure 3-2A). However, the inclusion of entinostat at 1mg/kg per week, a dose that is comparable to the

human dose of 5mg once weekly being used in other clinical combination studies, dramatically enhanced efficacy (p=0.004). While entinostat on its own had no effect on tumor growth, when combined with dabrafenib/trametinib, tumors regressed by 70% on average (Figure 3-2A).

Next, we examined the effects of entinostat in a human xenograft model that is more sensitive to dabrafenib/trametinib in vivo (Hs695T) (Figure 3-2B). In this study we were also interested in examining the durability of the response and therefore continued treatment for 6 weeks. Strikingly, even in this model entinostat substantially enhanced the therapeutic response to dabrafenib/trametinib, promoting deeper regressions (83% versus 57%, p=0.02), demonstrating that this combination is able to kill more residual disease. Moreover, regressions remained durable throughout the entire study.

Finally, the effects of these agents were evaluated in two different GEMM allograft models, with cooperating mutations in genes associated with resistance to BRAF inhibitors (Maertens et al. 2013; Paraiso et al. 2011). Importantly, the immune system is also intact in each of these models. The first model harbored mutations in *Braf* and *Nf1* (Maertens et al. 2013), as *NF1* mutations have been shown to functionally confer resistance to MAPK pathway inhibitors (Maertens et al. 2013; Whittaker et al. 2013). As predicted, MEK/BRAF inhibition did not cause any durable regressions in this model, and instead, tumors grew 18% on average; however, combined MEK/BRAF/HDAC suppression triggered tumor regression in every animal, and tumors shrunk by 43% (Figure 3-2C, p=0.03). *PTEN* mutations have been proposed to function by augmenting survival in response to MAPK pathway inhibition and are associated with smaller and less durable clinical responses in patients (Catalanotti et al. 2017)(Van Allen, 2014). Consistent with clinical observations, the effect of dabrafenib/trametinib on *Braf/Pten*-mutant GEMM allografts was also relatively modest in most tumors (Figure 3-2D, left), and these lesions ultimately became resistant (Figure 3-2D, right). Nevertheless, the inclusion of entinostat caused tumors to shrink by more than 73% and responses in all tumors were stable

Figure 3-2: Entinostat improves the efficacy of BRAF/MEK pathway inhibitors *in vivo*. (A) Waterfall plot (left panel) depicting change in tumor volume in a *BRAF*-mutant melanoma xenograft model (A375 cells) after 2 weeks of treatment with single and combined agents as indicated. Each bar represents an individual tumor (Vehicle n=9, DAB+TRAM n=8, ENT n=8, DAB+TRAM+ENT n=10). Left axis indicates the log2 of fold change in tumor volume, and right axis indicates the percentage change in tumor volume relative to day 0. Dabrafenib (DAB, BRAF inhibitor), trametinib (TRAM, MEK inhibitor), entinostat (ENT, Class I HDAC inhibitor). Growth curve for the entire duration of the study is shown on the right. Graphs represent mean values +/- standard error of the mean. **(B)** Growth curve of an additional human *BRAF*-mutant melanoma xenograft model (Hs695T) treated with single and combined agents as indicated (Vehicle n=6, DAB+TRAM n=8, ENT n=6, DAB+TRAM+ENT n=8). Left axis indicates the log2 of fold change in tumor volume relative to day 0. Graphs represent mean values +/- standard error of the mean. **(C)** Growth curve depicting change in tumor volume of GEMM-derived *Braf/Nf1*-mutant melanoma allografts after treatment with single and combined agents as indicated. (*Braf/Nf1*: Vehicle n=7, DAB+TRAM n=6, ENT n=6, DAB+TRAM+ENT n=5). Graphs represent mean values +/- standard error of the mean. **(D)** Waterfall plot (left panel) depicting change in tumor volume in a *Braf/Pten*-mutant melanoma allograft model after 2 weeks of treatment with single and combined agents as indicated. Each bar represents an individual tumor (Vehicle n=4, DAB+TRAM n=7, ENT n=2, DAB+TRAM+ENT n=7). Growth curve for the entire duration of the study is shown on the right. Graphs represent mean values +/- standard error of the mean. **(E)** Table summarizing in vitro sensitivity of 6 human *NRAS*-mutant cell lines against combined trametinib and entinostat treatment. **(F)** Waterfall plot depicting change in tumor volume of *NRAS*-mutant melanoma xenografts (YUDOSO cells) treated with single and combined agents as indicated (Vehicle n=7, TRAM n=9, ENT n=9, TRAM+ENT n=8). Each bar represents an individual tumor.

Figure 3-2 (continued)

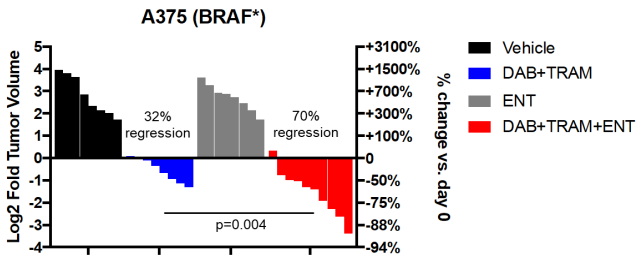

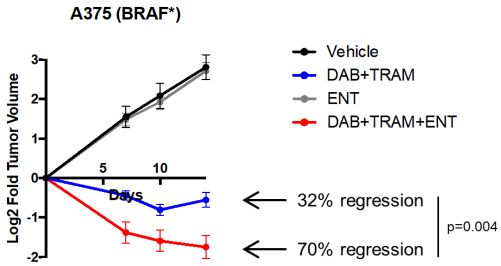

B

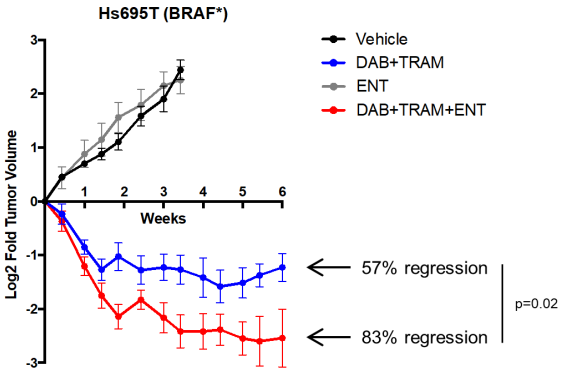

C

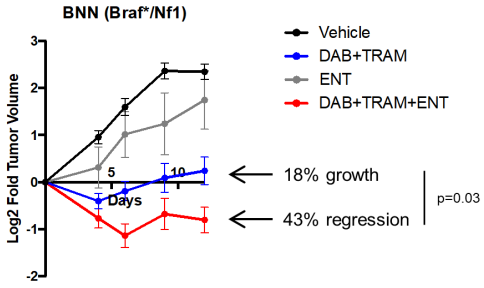

D

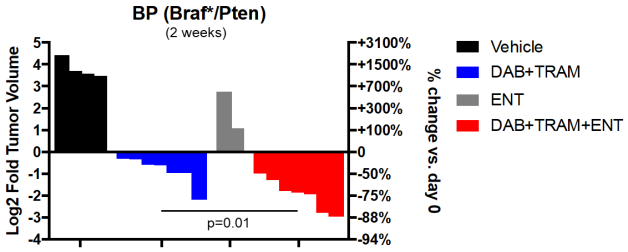

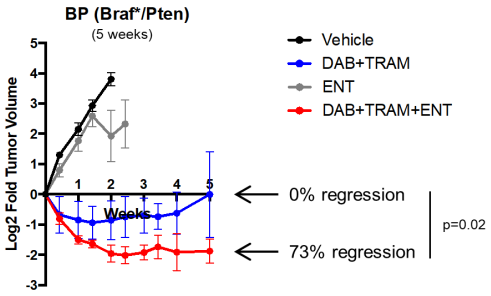

E

NRAS mutant cell line	Sensitivity to TRAM+ENT
YUGASP	++
Hs852T	+++
YUDOSO	+++
WM3670	-
WM3629	-
MELJUSO	--

F

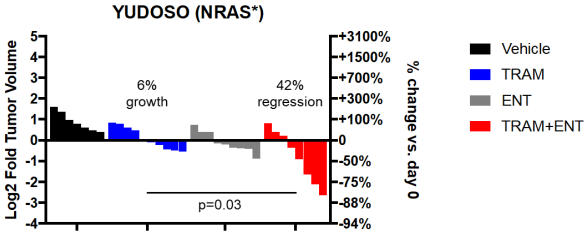

Figure 2

(Figure 3-2D; p=0.02). Altogether, preclinical studies in four distinct *BRAF*-mutant models, representing tumors with distinct genetic alterations and different sensitivities to BRAF/MEK inhibitors (sensitive, moderately sensitive, and resistant), suggest that entinostat can substantially enhance the therapeutic effects of BRAF/MEK pathway inhibitors in vivo in all of these settings. Figure 3-2C also demonstrates that this combination is effective in vivo in tumors that harbor *NF1* mutations.

Entinostat sensitizes NRAS-mutant melanomas to trametinib

We also expanded our analysis of *NRAS*-mutant melanomas. Using a panel of six additional *NRAS*-mutant lines we found that three were sensitive to combined MEK and HDAC inhibitors while three were not, consistent with the frequency of sensitivity to this combination overall (Figure 3-2E). Importantly, these agents also cooperatively enhanced the regression of *NRAS*-mutant xenografts (Figure 3-2F). Whereas trametinib alone exerted largely cytostatic effects (on average tumors grew by 6%), trametinib and entinostat together induced a 42% tumor regression (p=0.03). This observation is particularly important given that there are currently no effective treatments for *NRAS*-mutant tumors.

MGMT is a biomarker that predicts sensitivity to combined MAPK/HDAC inhibitors

While several genetically distinct melanoma cell lines and tumor models were sensitive to combined HDAC and MAPK pathway inhibitors, a subset were resistant to this combination (Figure 3-1A). Therefore, we hypothesized that these differential responses could be exploited to identify potential biomarkers of sensitivity or resistance. Extensive genomic analysis did not reveal any recurrent mutations or copy number alterations that distinguished sensitive or resistant cells. We therefore performed a two-class comparison of transcriptional profiles from the sensitive (n=6) and resistant (n=4) cell lines shown in Figure 3-1A. Eighteen genes that were differentially expressed (p<0.001) between these two populations were identified (Figure

3-3A, Supplementary Table B-1); however dramatic differences in expression were observed for only one of these genes, O^6-methylguanine DNA methyltransferase (*MGMT*), which was elevated in sensitive cells by almost 9-fold (Figure 3-3A and 3-3B, p=0.0005). Western blot analysis further revealed that MGMT protein was readily detected in sensitive cell lines whereas it was undetectable or minimally expressed in resistant cells (Figure 3-3C). Based on these observations two additional *BRAF*-mutant cell lines, predicted by the CCLE to have either high or low levels of *MGMT* mRNA, were selected for analysis. Immunoblots confirmed the expected differences in MGMT protein levels (Figure 3-3D). Importantly, the MGMT expressing cells were sensitive to dabrafenib/trametinib/entinostat, whereas the cell line that lacked MGMT expression was insensitive to this combination (Figure 3-3E). Similarly, the *NRAS*-mutant melanomas that were sensitive to these agents expressed MGMT, whereas insensitive cells did not (Supplementary Figure B-2). Altogether, analysis of 18 different sensitive and resistant cell lines indicates that MGMT expression is a strong predictive biomarker of sensitivity to this drug combination.

MGMT directly reverses the mutagenic DNA lesion O^6-methylguanine, which is caused by alkylating agents (Fu, Calvo, and Samson 2012). Accordingly, in glioblastomas, high MGMT levels are associated with resistance to alkylating chemotherapies such as temozolomide (Hegi et al. 2005; Weller et al. 2009). In a subset of glioblastomas, the *MGMT* promoter is epigenetically silenced by methylation, which is thought to be responsible for conferring sensitivity to temozolomide. Therefore, *MGMT* promoter methylation testing is routinely used in clinical practice as a predictive biomarker to guide patient management in glioblastoma. Consistent with this mechanism of regulation, we found that the *MGMT* promoter was differentially methylated in MGMT+ versus MGMT- melanoma cell lines (Figure 3-3F, p=0.00011) and that treatment with the DNA demethylating agent 5-azacitidine restored MGMT expression in MGMT- cells (Figure 3-3G). However, it is important to note that in this setting

Figure 3-3: MGMT expression predicts sensitivity to BRAF/MEK and HDAC inhibition but does not play a functional role. (A) Graph depicts fold difference in mRNA expression of 18 differentially expressed genes in cell lines sensitive (n=6) or resistant (n=4) to combined MAPK and HDAC inhibition (p<0.001). *MGMT* is upregulated by 8.6-fold in sensitive cells (p=0.0005). **(B)** Boxplot illustrating differential mRNA expression of *MGMT* in cell lines sensitive (n=6) or resistant (n=4) to combined MAPK and HDAC inhibition (p=0.0005). **(C)** Immunoblot depicting MGMT protein levels in sensitive and resistant cell lines. Order of cell lines is the same as in Fig. 3-1A. **(D)** Two additional melanoma cell lines characterized by the CCLE to have either high (UACC257) or low (A101D) *MGMT* mRNA levels were analyzed for MGMT protein levels by Western blot. Actin serves as a loading control. **(E)** Both cell lines were treated with either DMSO, 100nM dabrafenib and 10nM trametinib (DT), 1μM entinostat (ENT) or DT+ENT. Cells were manually counted prior to the addition of compounds and 3 days after treatment. Graphs represent log2 transformation of the fold change in cell number at day 3 versus day 0. Right axis shows percent change in cell number relative to day 0. Negative values represent cell death and a decrease in cell number. (UACC257) *p=0.002090, **p=0.002767; (A101D) n.s., not significant **(F)** Boxplot illustrating differential MGMT DNA methylation in cell lines sensitive (n=4) or resistant (n=3) to combined MAPK and HDAC inhibition (p=0.00011). **(G)** Western blot depicting MGMT protein levels before and after treatment with 5-azacitidine (5-aza) for 5 days in a cell line resistant to combined MEK and HDAC inhibition. **(H)** Hs695T cells were transfected with pooled siRNAs targeting MGMT or control non-targeting siRNAs and treated with drugs as indicated. Graphs represent log2 transformation of the fold change in cell number at day 3 versus day 0. Right axis shows percent change in cell number relative to day 0. Immunoblot depicts knockdown of MGMT. GAPDH serves as a loading control. n.s., not significant **(I)** A2058 cells were infected with a lentiviral construct expressing MGMT or lacZ control. Stable cell lines were treated with drugs as indicated. Graphs represent log2 transformation of the fold change in cell number at day 3 versus day 0. Right axis shows percent change in cell number relative to day 0. Immunoblot depicts ectopic expression of MGMT. GAPDH serves as a loading control. n.s., not significant

Figure 3-3 (continued)

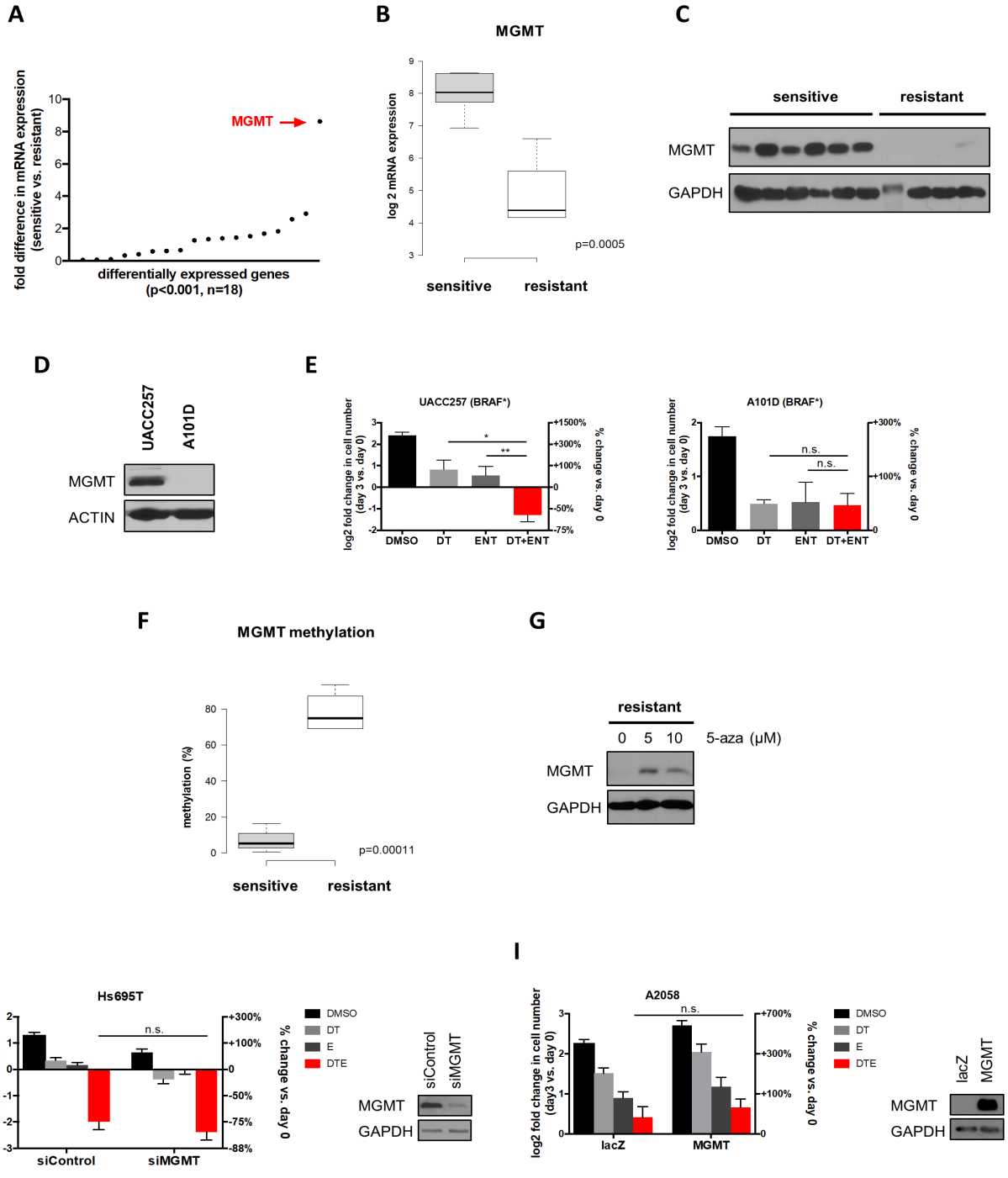

Figure 3

MGMT expression correlates with sensitivity, rather than resistance, to BRAF/MEK/HDAC inhibitors. Regardless, this pre-existing clinical test could be readily implemented to select patients for clinical trials. Importantly, two separate studies have shown that the *MGMT* promoter is methylated in only 21.5-26.0% of human metastatic melanomas using this clinical assay (Schraml et al. 2012; Tuominen et al. 2015). Therefore, these observations suggest that up to 79% of patients with RAS/RAF pathway mutations could benefit from this combination.

To determine whether MGMT was a functional or passive biomarker we genetically ablated it in sensitive cells and ectopically expressed it in resistant cells. Genetic ablation of MGMT did not make sensitive cells become resistant to these agents (Figure 3-3H) and ectopic MGMT expression did not confer sensitivity (Figure 3-3I). Therefore, we conclude that MGMT does not play a functional role in mediating sensitivity or resistance to this drug combination, but rather marks a distinct subset of melanomas. Regardless, the fact that a clinical test already exists makes this a clinically useful biomarker.

MGMT expressing melanomas exhibit broader defects in DNA repair genes

The strong association between MGMT expression and drug sensitivity prompted us to determine whether we could use a larger set of (primary) tumors to identify a specific genetic defect, responsible for sensitivity or resistance, that might co-segregate with high or low *MGMT* expression. To maximize potential differences we compared the top 10% of tumors in the TCGA database expressing the highest levels of *MGMT* mRNA (MGMT+) with the bottom 10% of tumors, expressing the lowest levels of *MGMT* mRNA (MGMT-). Similar to cell line studies, comparative analysis of mutations and copy number changes did not identify any recurrent genetic alterations that were enriched in MGMT+ or MGMT- tumors. However, these tumor cohorts exhibited distinct transcriptional profiles.

To identify potentially defective pathways and/or vulnerabilities in MGMT+ melanomas, we examined transcriptional signatures that were suppressed in these tumors using the GO:Biological Processes database. Interestingly, among the top 35 suppressed gene sets, numerous signatures associated with DNA repair, in particular double-strand break repair, were identified (Figure 3-4A and Supplementary Table B-2), suggesting that these tumors might possess inherent defects in DNA repair processes.

Concomitantly, we examined transcriptional profiles of sensitive cells exposed to MAPK/HDAC inhibitors, prior to the onset of cell death. In drug-treated cells, the Hallmark_DNA_Repair gene set was identified as one of the top significantly suppressed pathways in response to dabrafenib/trametinib/entinostat, suggesting that DNA repair processes were also being inhibited by this combination (Supplementary Table B-3). These observations raised the intriguing possibility that preexisting defects in DNA repair, compounded by the chemical suppression of these pathways, might be mediating cell death by causing excessive DNA damage. Of note, an oxidative phosphorylation signature was also observed, but we found that reactive oxygen species were not consistently elevated by these agents, and were neither necessary nor sufficient for this therapeutic response (Supplementary Figure B-3A-E).

To investigate a potential role for DNA repair defects in this response, we further characterized MGMT+ tumors and cell lines. The transcriptional signatures identified in Figure 3-4A suggested that MGMT+ tumors might harbor defects in homologous recombination (HR). Using a more specific transcriptional dataset we confirmed that MGMT+ tumors were, in fact, enriched for a common signature that is induced by RNAi-mediated ablation of many HR genes, termed the HR-defect gene signature (Figure 3-4B) (Peng et al. 2014). The HR-defect signature was also enriched in MGMT+ melanoma cell lines as compared to MGMT- cells (Figure 3-4C). However, to confirm that sensitive cells harbor functional defects in HR, we performed a Rad51 redistribution assay. In response to ionizing radiation, Rad51 normally accumulates in numerous

Figure 3-4: Baseline and drug induced suppression of DNA repair genes and consequential DNA damage in MGMT+ tumors/cells. (A) Gene sets from the GO:Biological Processes database involved in DNA repair and HR are significantly suppressed in MGMT "high" versus MGMT "low" samples. "High" expression was defined as the top 10% of tumors in the TCGA SKCM provisional dataset stratified by *MGMT* mRNA expression, whereas "low" was defined as the bottom 10%. Normalized Enrichment Scores (NES), p-values and False Discovery Rates (FDRs) calculated by Gene Set Enrichment Analysis (GSEA) software from the Broad Institute. The entire list of the top 35 suppressed gene sets are shown in Supplementary Table 2. **(B)** Gene Set Enrichment Analysis (GSEA) was used to develop a plot depicting the enrichment of the HR-defect (HRD) gene signature (Peng et al. 2014) in primary tumors with high versus low *MGMT* expression. "High" expression (MGMT+) was defined as the top 10% of tumors in the TCGA SKCM provisional dataset stratified by *MGMT* mRNA expression, whereas "low" (MGMT-) was defined as the bottom 10%. Note: The HRD gene signature is a compilation of genes that are significantly suppressed after single-gene ablation of HR components (Peng et al. 2014). MGMT+ tumors show a reduction of these same genes. FDR: false discovery rate, NES: normalized enrichment score. **(C)** Gene Set Enrichment Analysis (GSEA) was used to develop a plot depicting the enrichment of the HR-defect (HRD) gene signature (Peng et al. 2014) in cell lines with high versus low *MGMT* expression. "High" expression was defined as the top 10% of melanoma cell lines in the CCLE stratified by *MGMT* mRNA expression, whereas "low" was defined as the bottom 10%. Note: The HRD gene signature is a compilation of genes that are significantly suppressed after single-gene ablation of HR components (Peng et al. 2014). MGMT+ cells show a reduction of these same genes. FDR: false discovery rate, NES: normalized enrichment score. **(D)** Melanoma cells, transfected with control (siLuc) or pooled siRNAs targeting BRCA2 were irradiated with 10Gy. Cells were fixed 5 hours later and analyzed by immunofluorescence for RAD51 and gamma H2AX. The bar graph depicts the percentage of siLuc cells with RAD51 foci. Images are shown in Supp. Fig. A-4A. **(E)** Heatmap of differentially expressed DNA repair genes (significance level p=0.001) in (MGMT+) versus (MGMT-) melanomas. **(F)** Western blot depicting phospho-gamma H2AX levels in two sensitive cell lines in response to dabrafenib/trametinib (DT) plus entinostat (ENT) over time. GAPDH serves as a loading control. **(G)** Western blot comparing phospho-gamma H2AX levels in sensitive and resistant cell lines after treatment with DT+ENT. GAPDH serves as a loading control. **(H)** Western blot depicting phospho-gamma H2AX levels in sensitive cell line after treatment with either DMSO, 100nM dabrafenib and 10nM trametinib (DT), 1μM entinostat (E) or DT+E. GAPDH serves as a loading control. **(I)** Microarray analysis of sensitive and resistant cell lines after 24 hours of treatment with vehicle, 100nM dabrafenib/10nM trametinib (DT), 1μM entinostat (ENT), or DT+ENT. Heatmap (triplicate samples per treatment arm) depicts the upregulated (red) or downregulated (blue) non-cell cycle regulated DNA repair genes, reaching a significance level of p=0.001. Group A defines a subset of potently suppressed genes that cluster together in two groups in the DT treatment arm. A subset of these genes are listed. Group B defines an additional large set of DNA repair genes suppressed in DT+ENT arm. A subset of these genes are also listed.

Figure 3-4 (continued)

A

GO Biological processes	NES	NOM p-value	FDR q-value
CELLULAR RESPONSE TO DNA DAMAGE STIMULUS (GO:0006974)	-2.1977699	0	0.001659461
DNA SYNTHESIS INVOLVED IN DNA REPAIR (GO:0000731)	-2.0065343	0	0.016806431
DOUBLE-STRAND BREAK REPAIR VIA NONHOMOLOGOUS END JOINING (GO:0006303)	-1.9085537	0	0.03854989
DNA DOUBLE-STRAND BREAK PROCESSING (GO:0000729)	-1.9064397	0	0.034910116
DOUBLE-STRAND BREAK REPAIR (GO:0006302)	-1.8857639	0.00176991	0.038918607
DNA REPAIR (GO:0006281)	-1.8676513	0	0.04586939
DNA DAMAGE CHECKPOINT (GO:0000077)	-1.7732302	0.0017889087	0.0857029
DOUBLE-STRAND BREAK REPAIR VIA HOMOLOGOUS RECOMBINATION (GO:0000724)	-1.6111594	0	0.22490148

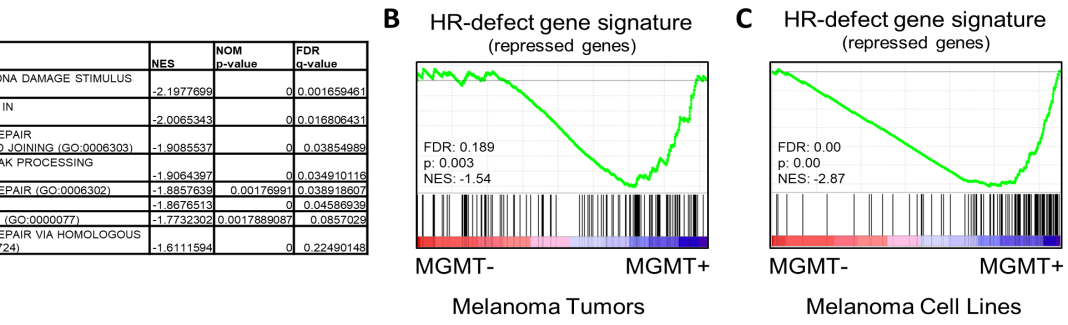

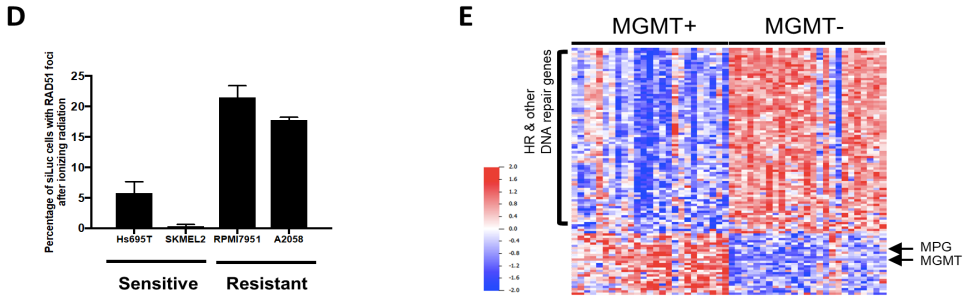

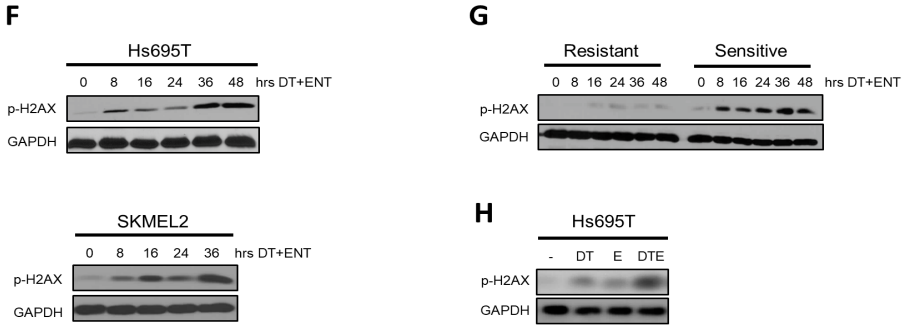

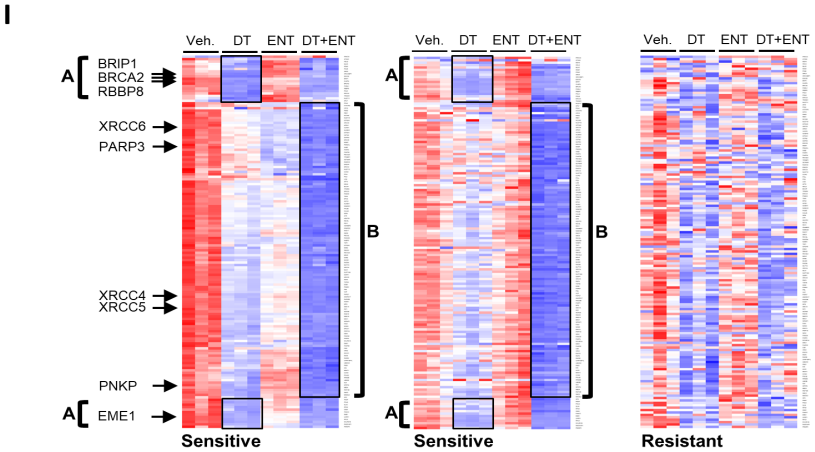

Figure 4

distinct foci at sites of DNA damage (Gildemeister, Sage, and Knight 2009). However, the appearance of these foci is prevented or reduced in cells with defects in various HR proteins (Gildemeister, Sage, and Knight 2009). Indeed, while ionizing radiation induced a dramatic increase in Rad51 foci that co-localized with phospho-gamma H2AX in the two resistant cell lines, the two sensitive cell lines were substantially impaired in their ability to form Rad51 foci (Figure 3-4D, Supplementary Figure A-4A). These observations demonstrate that sensitive cell lines harbor a preexisting impairment in HR.

MGMT+ melanomas exhibit a global reduction of DNA repair genes

In breast and ovarian cancers, *BRCA1/2* mutations are known to underlie defects in HR (Farmer et al. 2005). However, more recently castration-resistant prostate cancers have been shown to harbor alterations in any one of five different HR genes (Dhawan, Ryan, and Ashworth 2016). Therefore, we reanalyzed genomic data to determine whether we might have missed a similar heterogeneous mutational pattern of HR genes but did not find this to be the case.

Because there were no recurrent genetic alterations in HR genes, the relative expression levels of all genes implicated in DNA repair were examined in MGMT+ versus MGMT- tumors (list obtained from (Mjelle et al. 2015)). Strikingly, the majority of DNA repair genes were downregulated in MGMT+ tumors as compared to MGMT- tumors (Figure 3-4E). Genes known to be involved in HR as well as other DNA repair pathways were suppressed in MGMT+ tumors. Importantly, this observation held true even when known cell cycle-regulated genes were removed from the analysis, reinforcing that this is a true DNA repair effect, and not a by-product of cell cycle differences between treatments (Supplementary Figure B-4B) (Mjelle et al., 2015). A subset of repair genes, which included *MGMT* and *MPG*, both involved in the repair of alkylated bases, along with genes that repair hydrolyzed and oxidized bases, clustered together and exhibited the inverse expression pattern as compared to the broader group of

genes: these genes were expressed at higher levels in MGMT+ tumors and were lower in MGMT- tumors (Figure 3-4E). Importantly, this distinct expression pattern of DNA repair genes was not associated with prior exposure to therapy, suggesting that these genes were not selectively repressed or induced as a consequence of treatment. Therefore, there appears to be two potentially distinct populations of melanomas: DNA repair low$^{(MGMT+)}$ and DNA repair intact$^{(MGMT-)}$, which we hypothesize are differentially sensitive to BRAF/MEK/HDAC inhibitors. While the mechanisms that underlie the inverse expression pattern of these gene clusters could not be ascertained, it is well known that genes with similar functions are often co-regulated. We believe that this may be occurring in melanoma, especially given the related function of the co-regulated genes.

HDAC and MAPK pathway inhibitors cooperatively induce DNA damage

To determine whether the HDAC/MAPKi combination might be capitalizing on this potential defect and killing cells by triggering unresolvable DNA damage, we first compared phospho-gamma H2AX expression levels, a marker of double strand DNA breaks, in sensitive and resistant cells. In sensitive cell lines two waves of phospho-gamma H2AX induction were observed. Phospho-gamma H2AX initially increased within 8 hours of treatment, increased more dramatically between 24-36 hours, and remained elevated (Figure 3-4F). Importantly, gamma H2AX phosphorylation occurred prior to cell death, which begins at 40 hours (Figure 3-1E and Supplementary Figure B-1E), suggesting that this event precedes cell death and is not merely a consequence of DNA damage in dying cells. In contrast, phospho-gamma H2AX levels remained low in resistant cells (Figure 3-4G). Notably, both agents induced low levels of gamma H2AX phosphorylation as single agents; however, the drug combination was required to induce maximal DNA damage, demonstrating that these agents cooperatively induce DNA damage (Figure 3-4H).

BRAF/MEK and HDAC inhibitors coordinately suppress the expression of DNA repair genes

To investigate the molecular mechanism by which this combination was functioning, transcriptional profiles were examined in cells treated with vehicle, dabrafenib/trametinib, entinostat or all three agents at 24 hours, prior to the commencement of cell death. Striking changes in the expression of DNA repair genes in response to these agents were observed. As depicted in the heatmaps shown, dabrafenib/trametinib alone suppressed the expression of many DNA repair genes in sensitive cell lines, which clustered together in two groups, herein referred to as Group A genes (Figure 3-4I, left and middle panels). Interestingly, Group A genes included several HR pathway genes such as *BRCA2*, *BRIP1*, *EME1* and *RBBP8* (Mjelle et al. 2015; Moynahan and Jasin 2010). These four genes were suppressed between 60-84%. Entinostat had no effect on the expression of group A genes but in both sensitive cell lines, dabrafenib/trametinib/entinostat together not only inhibited Group A genes but also suppressed an additional large set of DNA repair genes (Group B) (Figure 3-4I, left and middle panels). Notably, the most potently suppressed genes in Group B (suppressed 65-80%) included genes that function in the NHEJ pathway (e.g. *XRCC4, XRCC5, XRCC6, PNKP* and *PARP3*). This striking pattern of transcriptional repression was not observed in resistant cells (Figure 3-4I, right panel).

It should be noted that HDAC inhibitors have previously been reported to induce DNA damage in cells through a variety of direct and indirect mechanisms (Robert and Rassool 2012; Thurn et al. 2013; Miller et al. 2010). Nevertheless, in this setting we observed a potent and broad suppression of DNA repair genes that only occurred in the presence of MAPK pathway inhibitors, which was quite unexpected. Therefore, while HDAC inhibitors may contribute to DNA damage via additional mechanisms, the deep suppression of numerous DNA repair genes that occurs in response to this combination is likely to play a major role in this response. The

observation that DNA repair gene networks are already impaired in sensitive cell lines further supports this model.

MAPK pathway inhibitors potently suppress HR pathway genes in sensitive but not resistant melanomas

As noted above, Group A genes included several HR pathway genes such as *BRCA2*, *BRIP1*, *EME1* and *RBBP8* (Figure 3-4I) (Myelle et al., Moynaham and Jasin, 2010). Western blot analysis confirmed that dabrafenib/trametinib potently suppressed BRIP1, BRCA2, RBBP8 and EME1 protein expression in sensitive cells (Figure 3-5A). BRIP1 and BRCA2 expression were further evaluated in two sensitive and resistant cell lines. Dabrafenib/trametinib nearly depleted the expression of BRIP1 and BRCA2 proteins in sensitive cell lines, but did not do so in resistant cells (Figure 3-5B). Quantitative PCR further confirmed that BRAF/MEK inhibitors suppressed the transcription of these HR genes, and did so in sensitive but not resistant cells (Figure 3-5C).

To exclude the possibility that differences in expression were a secondary consequence of effects on the cell cycle, sensitive cells were treated with vehicle or dabrafenib/trametinib and cells in G1, S and G2/M were separated by FACS. In both sensitive cell lines, *BRIP1* and *BRCA2* mRNA levels were suppressed in all phases of the cell cycle (Figure 3-5D), demonstrating that the suppression of these genes is not merely due to changes in cell cycle distribution.

MAPK pathway inhibitors induce a BRCAness phenotype by further suppressing the transcription of HR pathway genes

Figures 3-4A-E demonstrate that sensitive melanomas already have broad defects in the expression of DNA repair genes that result in HR defects, as inferred by transcriptional profiles

Figure 3-5: MAPK pathway inhibitors potently reduce the expression of HR pathway genes in sensitive melanomas. (A) Western blot depicting BRIP1, BRCA2, RBBP8 and EME1 protein levels in Hs695T cells after 48hrs of treatment with vehicle (Veh) or 100nM dabrafenib and 10nM trametinib (DT). GAPDH serves as a loading control. **(B)** Western blot depicting BRIP1 and BRCA2 protein levels in sensitive (Hs695T and SKMEL2) and resistant (A2058 and RPMI7951) cells after 48hrs of treatment with vehicle (Veh) or 100nM dabrafenib and 10nM trametinib (DT). GAPDH serves as a loading control. **(C)** mRNA levels of *BRIP1* and *BRCA2* in sensitive (Hs695T and SKMEL2) and resistant (A2058) cells after 24 hours of treatment with vehicle (Veh) or 100nM dabrafenib and 10nM trametinib (DT) as determined by quantitative PCR. **(D)** Cells from 2 sensitive cell lines (top and bottom panels, respectively) were separated in different phases of the cell cycle for subsequent gene expression analysis. Bar graphs show mRNA expression of *BRCA2* and *BRIP1* in specific cell subpopulations after 24 hours of treatment with Vehicle (Veh) or 100nM dabrafenib and 10nM trametinib (DT). **(E)** Plot of Gene Set Enrichment Analysis (GSEA) showing suppression of HRD associated genes (Peng et al. 2014) in melanoma cells in response to trametinib (10nM) and dabrafenib (100nM). Note: The HRD gene signature is a compilation of genes that are significantly suppressed after single-gene ablation of HR components (Peng et al. 2014). Cells treated with BRAF/MEKi show a reduction of these same genes. FDR: false discovery rate, NES: normalized enrichment score. **(F)** Single Sample Gene Set Enrichment Analysis (ssGSEA) depicting the relative expression of HRD signature genes in response to dabrafenib/trametinib (DT) treatment in sensitive and resistant cell lines. Note: The HRD gene signature is a compilation of genes that are significantly suppressed after single-gene ablation of HR components (Peng et al. 2014). **(G)** Sensitive cells (SKMEL5, Hs695T, SKMEL2 and YUDOSO) and resistant cells (A2058 and RPMI7951) were treated with DMSO, 100nM dabrafenib/10nM trametinib (DT), 5μM olaparib (PARP inhibitor) or the combination of DT + PARP inhibitor. As a positive control the *BRCA1*-mutant breast cancer cell line SUM149PT was treated with the PARP inhibitor. Cells were manually counted prior to the addition of compounds and 5 days after treatment. Graphs represent log2 transformation of the fold change in cell number at day 5 versus day 0. Negative values represent a net loss of cells. **(H)** Waterfall plot depicting change in tumor volume in a *Braf/Nf1*-mutant melanoma allograft model after 9 days of treatment with single and combined agents as indicated. Each bar represents an individual tumor (Vehicle n=7, DAB+TRAM n=6, PARPi n=5, DAB+TRAM+PARPi n=6). Left axis indicates the log2 of fold change in tumor volume, and right axis indicates the percentage change in tumor volume relative to day 0. Dabrafenib (DAB, BRAF inhibitor), trametinib (TRAM, MEK inhibitor), olaparib (PARPi, PARP inhibitor). **(I)** Overexpression of RAD51 suppresses death in response to MAPK/HDAC inhibition. Western blot confirms overexpression.

Figure 3-5 (continued)

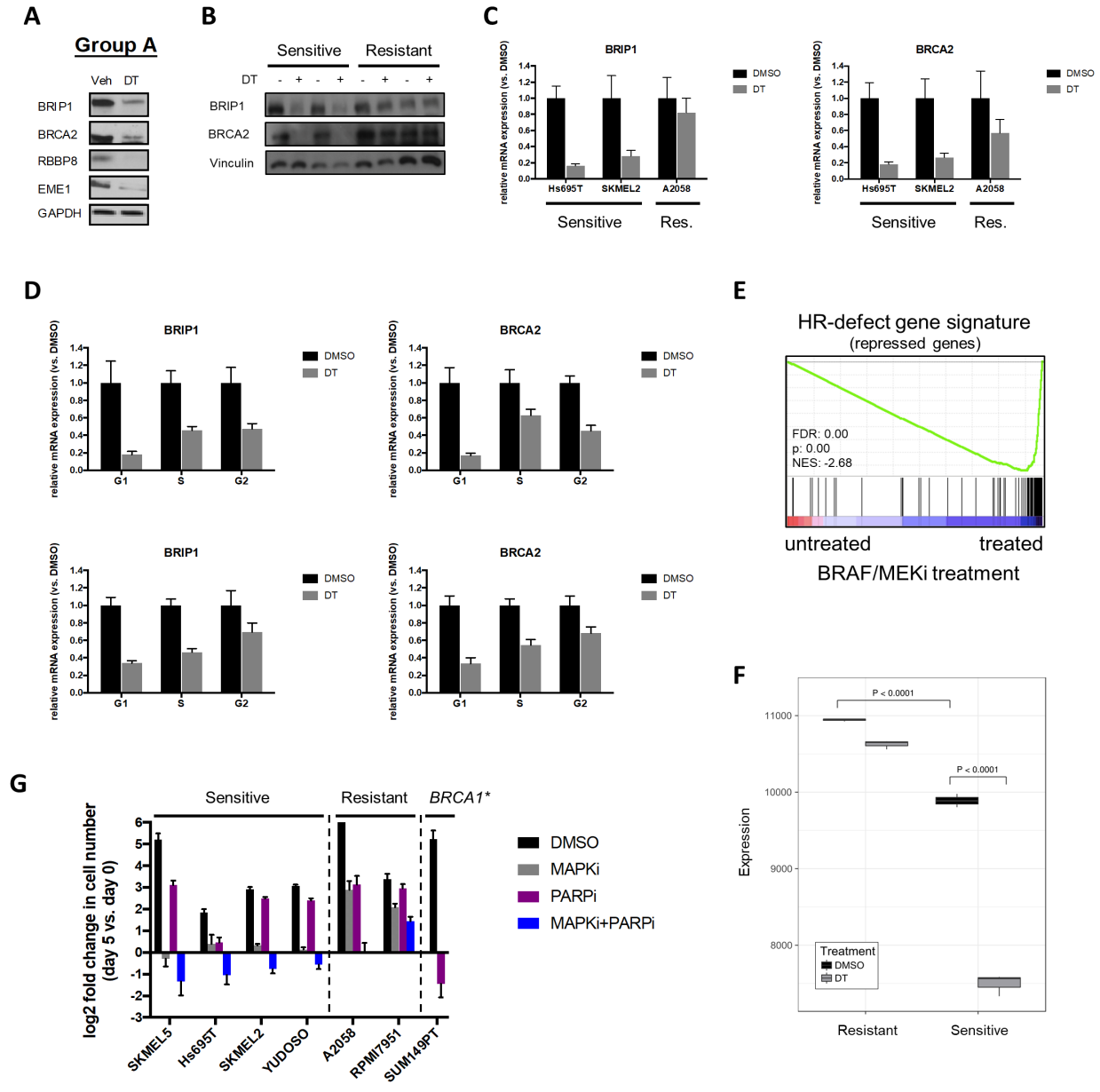

Figure 5

and validated by Rad51 redistribution assays. However, Figure 3-5A-C demonstrate that dabrafenib/trametinib causes a nearly complete suppression of a subset of these HR genes, which would presumably enhance these defects. Indeed, we found that dabrafenib/trametinib caused a potent enrichment of the HR-defect signature in sensitive cells (Figure 3-5E). In order to visualize the progressive suppression of this pathway, we performed ssGSEA analysis on sensitive and resistant cell lines. Figure 3-5F demonstrates that genes that are suppressed in response to HR defects are lower in (untreated) sensitive compared to resistant cells (sample 3 versus sample 1, $p<0.0001$). Moreover, dabrafenib/trametinib causes a further potent reduction of these genes in sensitive cells (sample 4 versus 3, $p<0.0001$). Taken together these observations suggest that BRAF/MEK inhibitors are potentiating inherent defects in the HR pathway by suppressing multiple HR pathway genes.

The Rad51 redistribution experiment confirmed that there are substantial defects in HR in untreated sensitive cells, however the dynamic range of this assay precluded us from determining whether BRAF/MEK inhibitors could further potentiate these defects. HR impairment can also be measured by a I-Sce-I-based double strand break repair assay, however this requires reporter integration into a single genomic site, specifically in sensitive cells, which was unachievable after extensive effort. However, it is well established that genetic defects in HR genes, such as *BRCA1* and *BRCA2*, confer sensitivity to PARP inhibitors, which has become a hallmark functional assay for measuring HR defects (Farmer et al. 2005). Given the potent suppression of HR gene expression, in particular *BRCA2*, we hypothesized that BRAF/MEK inhibitors would sensitize (or further sensitize) responsive cell lines to PARP inhibitors.

Interestingly, we found that the PARP inhibitor, olaparib, did not exert potent cytotoxic effects as a single agent in sensitive melanomas, in contrast to *BRCA1*-deficient breast cancer cells (Figure 3-5G). These observations suggest that the DNA repair defects present in these

melanomas are less pronounced than those in *BRCA1*-mutant tumor cells, consistent with the observation that these cells still express HR genes (Figure 3-5A). However, dabrafenib/trametinib potently sensitized melanomas to olaparib and together dabrafenib/trametinib/olaparib killed multiple sensitive cell lines and did not kill non-responsive cell lines (Figure 3-5G). Strikingly, these observations were also recapitulated in vivo. While the PARP inhibitor olaparib alone was unable to cause tumor regression, when combined with dabrafenib/trametinib, tumors regressed by 47% on average ($p=0.03$, Fig. 5H). Taken together these results suggest that while baseline defects in DNA repair gene expression prime sensitive cells, MAPK pathway inhibition is required to functionally impair the HR pathway in these melanomas to the extent observed in *BRCA1*-mutant breast cancers.

Finally, to prove that defects in HR functionally contribute to the therapeutic response to combined MAPK/HDAC inhibitors, we examined the effects of Rad51 overexpression. A key step in HR is the recruitment of the Rad51 recombinase to double strand breaks, which normally requires HR proteins such as BRCA2 (Moynahan, 2010). However it is well known that overexpression of Rad51 can override this regulatory step in cells with various upstream HR defects (Moynahan, 2010). Therefore we reasoned that Rad51 would be the one component that might rescue effects caused by the concomitant suppression of multiple HR proteins. Importantly, Rad51 overexpression suppressed death in response to MAPK/HDAC inhibition, confirming that defects in HR and consequently excessive DNA damage play critical functional roles in mediating the therapeutic response to these agents (Figure 3-5I). It should be noted that Rad51 did not rescue the limited response to BRAF/MEK inhibitors alone, indicating that these agents mediate their canonical effects through other pathways, as would be expected.

MAPK and HDAC inhibitors cooperatively suppress NHEJ genes in sensitive melanomas

We next sought to identify critical genes in Group B that might be responsible for the cooperativity between dabrafenib/trametinib and entinostat. Interestingly, the most potently suppressed Group B genes that could be ascribed to a specific DNA repair pathway are known to function in the NHEJ pathway (a subset listed in Figure 3-4I). Importantly, it is well established that when HR is impaired, NHEJ can compensate (Lord and Ashworth 2016). Therefore we examined a subset of genes in the NHEJ pathway that were the most transcriptionally suppressed, specifically XRCC5 (Lieber 2010; Mjelle et al. 2015), PNKP (Lieber 2010, Mjelle et al 2015), and PARP3 (Beck et al. 2014; Mjelle et al. 2015), and confirmed that protein expression was also potently inhibited by dabrafenib/trametinib/entinostat (Figure 3-6A). We also showed that suppression occurred at the level of transcription, occurred in different sensitive cell lines, and that these genes were not suppressed in insensitive cells (Figure 3-6B). Together, these results demonstrate that combined HDAC and MAPK inhibitors potently suppress both HR and NHEJ genes.

The cooperative effects of MAPK/HDAC inhibition are due to the coordinate suppression of HR and NHEJ pathways

To functionally determine whether the suppression of NHEJ pathways was required for cell death in response to this combination, we ectopically expressed Lig 4. Lig 4 directly mediates the NHEJ ligation step and its overexpression, analogous to Rad51 overexpression, is the one distal gene that can largely override deficiencies in (multiple) upstream components (Lieber, 2010). Importantly, Lig 4 substantially inhibited the cytotoxic effects of MAPK/HDAC suppression (Figure 3-6C; $p=0.009$). Taken together with the Rad51 overexpression experiment in Figure 3-5I, these studies demonstrate that the impairment of both HR and NHEJ are required for cell death in response to combined MAPK/HDAC inhibition.

Figure 3-6: Entinostat enhances dabrafenib/trametinib activity by cooperatively triggering the broad suppression of other DNA repair genes including NHEJ genes. (A) Western blot depicting XRCC5, PNKP and PARP3 protein levels in Hs695T cells after treatment with vehicle (Veh), 100nM dabrafenib/10nM trametinib (DT), 1μM entinostat (E) or DT+E. GAPDH serves as a loading control. **(B)** mRNA levels of *XRCC5*, *PARP3* and *PNKP* in sensitive (Hs695T and SKMEL2) and resistant (A2058) cells after 24 hours of treatment with vehicle (Veh) or 100nM dabrafenib, 10nM trametinib and 1μM entinostat (DTE) as determined by quantitative PCR. **(C)** Overexpression of LIG4 suppresses cell death in response to MAPK/HDAC inhibition. **(D)** Hs695T cells were transfected with pooled siRNAs targeting *XRCC5, PNKP, PARP3, XRCC4, XRCC6* or control non-targeting siRNAs and treated with DMSO (black) or 100nM dabrafenib and 10nM trametinib (DT, red). Graph depicts the mean log2 fold change of cell number after 72 hours, relative to day 0. Right axis shows percent change in cell number relative to day 0. Immunoblots in Supp Fig. A-5A confirm siRNA target suppression. **(E)** Model depicting the mechanism by which BRAF/MEK pathway and HDAC inhibitors promote excessive DNA damage, cell death and tumor regression of melanomas with a compromised DNA repair gene network (MGMT+ tumors). **(F)** Table depicting top scoring transcription factor binding sites enriched in genes suppressed by BRAF/MEK/HDACi, using the MSigDB Transcription Factor Motif database. (blue = ETS family transcription factor binding sites; bold: ELK1 binding sites) **(G)** Single Sample Gene Set Enrichment Analysis (ssGSEA) projection scores for ELK1 target genes following drug treatment. ssGSEA quantifies ELK1 target gene activation for each treatment group, showing a decrease in ELK1-driven transcription in single agent treatment (MAPKi (DT) and HDACi (E)) followed by further suppression of ELK1 targets by combination therapy (DTE). **(H)** Western blots depicting phosphor-ELK1 and total ELK1 protein levels in 2 sensitive cell lines treated with 100nM dabrafenib (D), 10nM trametinib (T) and/or 1μM entinostat (E). **(I)** Experimentally identified direct ETS family binding sites (ChIP-X data) in *BRIP1, BRCA2*, *XRCC5* and *PARP3*. **(J,K)** Western blots depicting PARP3, BRIP1, XRCC5 and ELK1 protein levels after knockdown of ELK1 and/or ELK3 using siRNA smartpools. **(L)** RNAi-mediated suppression of ELK1 and/or ELK3 cooperates with either MAPK (Dabrafenib/Trametinib, DT) or HDAC (Entinostat, E) inhibitors.

Figure 3-6 (continued)

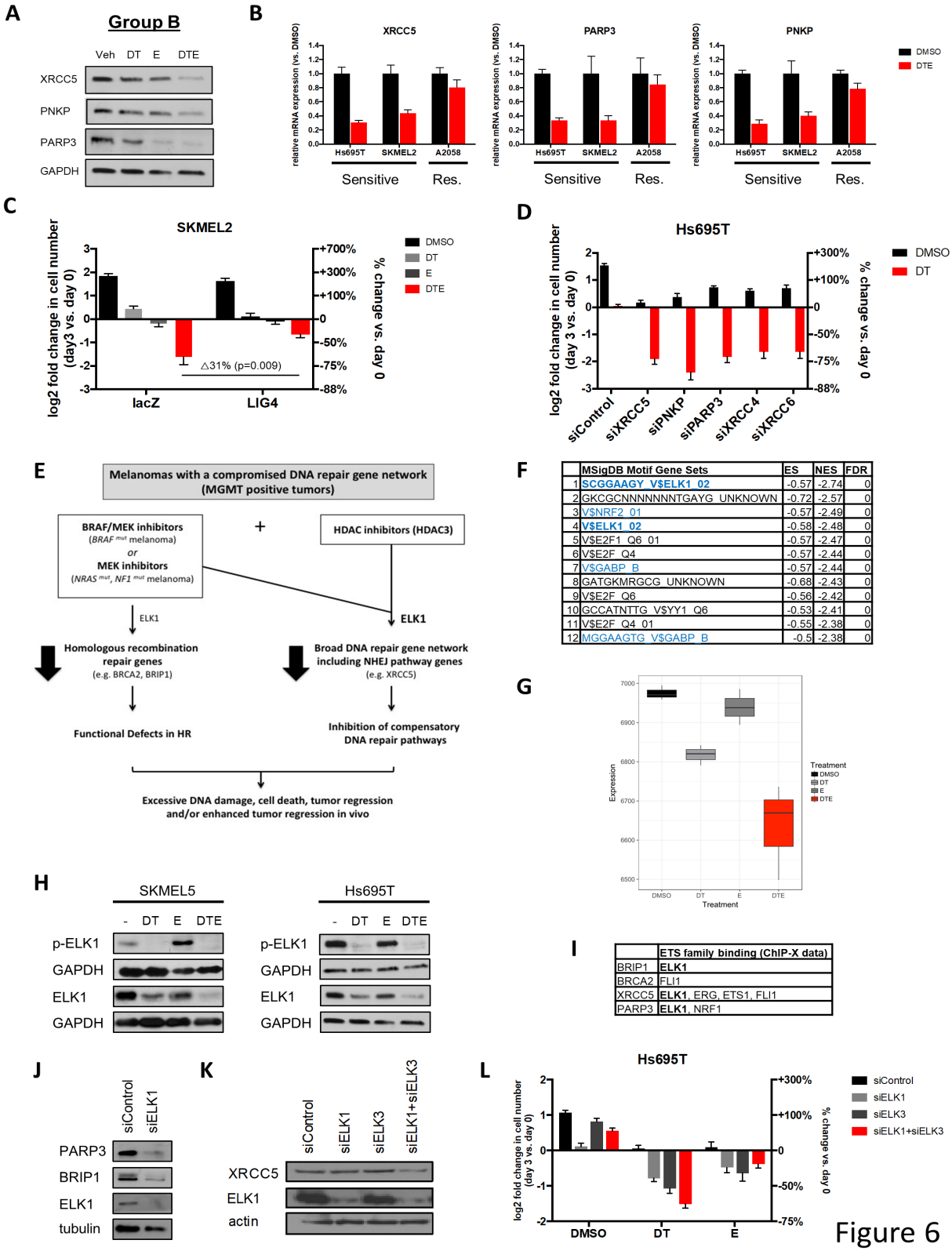

	MSigDB Motif Gene Sets	ES	NES	FDR
1	SCGGAAGY_V$ELK1_02	-0.57	-2.74	0
2	GKCGCNNNNNNNTGAYG_UNKNOWN	-0.72	-2.57	0
3	V$NRF2_01	-0.57	-2.49	0
4	V$ELK1_02	-0.58	-2.48	0
5	V$E2F1_Q6_01	-0.57	-2.47	0
6	V$E2F_Q4	-0.57	-2.44	0
7	V$GABP_B	-0.57	-2.44	0
8	GATGKMRGCG_UNKNOWN	-0.68	-2.43	0
9	V$E2F_Q6	-0.56	-2.42	0
10	GCCATNTTG_V$YY1_Q6	-0.53	-2.41	0
11	V$E2F_Q4_01	-0.55	-2.38	0
12	MGGAAGTG_V$GABP_B	-0.5	-2.38	0

	ETS family binding (ChIP-X data)
BRIP1	**ELK1**
BRCA2	FLI1
XRCC5	**ELK1**, ERG, ETS1, FLI1
PARP3	**ELK1**, NRF1

Figure 6

The converse experiment was also performed. We reasoned that if cell death was occurring because 1) MAPK pathway inhibitors suppress HR and 2) MAPK/HDAC inhibitors together suppress NHEJ, then ablation of NHEJ genes should kill cells in the presence of MAPK pathway inhibitors. Individual NHEJ genes were suppressed by pooled siRNA sequences and cells were treated with dabrafenib/trametinib. Suppression of any one of the NHEJ genes killed cells but only in the presence of dabrafenib/trametinib (Figure 3-6D and Supplementary Figure A-5A), suggesting that NHEJ pathway suppression was able to recapitulate the effects of entinostat in this context.

Taken altogether these observations suggest that BRAF/MEK inhibitors suppress DNA repair genes function in the HR pathway, resulting in a state that functionally resembles tumors with BRCA pathway defects (model shown in Figure 3-6E) (Lord and Ashworth 2016). However, when combined with entinostat, these agents now cooperatively and potently suppress a second broader set of DNA repair genes, including NHEJ pathway genes. Importantly, this broad transcriptional repression of these major DNA repair genes is lethal in tumors with a preexisting impairment in a DNA repair gene expression.

HDAC and MAPK pathway inhibitors cooperatively suppress ELK, which regulates the expression of key DNA repair genes

To investigate the molecular mechanism(s) by which MAPK and HDAC inhibitors might be cooperatively suppressing DNA repair genes, we first identified transcription factor binding sites that were enriched in genes suppressed by this combination, using the MSigDB Transcription factor targets database. ELK1 binding sites were the most significantly enriched in the suppressed genes and several other ETS family members binding sites were also identified (Figure 6F). ssGSEA analysis was then used to examine the pattern of ELK1 regulated transcriptional signatures in response to single and combined agents. MAPK suppression

partially inhibited these signatures, as expected, given that ERK phosphorylation contributes to the activation of ELK1 (Shaw and Saxton 2003) (Figure 3-6G). HDAC inhibitors slightly suppressed ELK1 signatures, however these signatures were maximally suppressed in the presence of combined MAPK/HDAC inhibitors (Figure 3-6G). We found that ELK1 phosphorylation was inhibited in response to BRAF/MEK inhibitors as would be predicted (Figure 3-6H). However, unexpectedly both agents individually and cooperatively suppressed total ELK1 protein expression. Microarray data indicated that this was occurring at the level of transcription, which was confirmed by Q-PCR (Supplementary Figure B-5B). The related gene, ELK3, showed a similar pattern of suppression (Supplementary Figure B-5B).

Twenty percent of the DNA repair genes suppressed by MAPK/HDAC inhibitors have been experimentally determined to be direct ELK1 targets (32/160 genes; (Lachmann et al. 2010)) and many more of these genes are targets of other ETS family proteins. For practical reasons we focused on determining whether ELK was controlling the expression of any of the most prominently suppressed group A and B genes (*BRIP1*, *BRCA2*, *XRCC5* and *PARP3*). Experimental ChIP data indicate that ETS family proteins directly bind sites in the promoters of all four genes, although only *BRIP1*, *XRCC5* and *PARP3* contain the ELK1 target sequence (Figure 3-6I). Because ELK1 and 3 bind the same DNA sequences and therefore may be redundant, we investigated the consequences of genetically ablating ELK1 and/or ELK3. Notably, ELK1 ablation was sufficient to potently suppress the expression of PARP3 and BRIP1 (Figure 3-6J), whereas XRCC5 expression was inhibited by the loss of both ELK1 and 3 (Figure 3-6K). The less dramatic effect on XRCC5 expression, as compared to PARP3 and BRIP1, may be due to the presence of several ETS family binding sites in its promoter (Figure 3-6I). Nevertheless, these observations demonstrate that ELK1 critically regulates the expression of these important HR and NHEJ proteins.

More importantly however, we found that RNAi-mediated suppression of ELK genes cooperates with either MAPK or HDAC inhibitors to kill these melanomas (Figure 3-6L), consistent with the observation that ELK regulates both types of genes (e.g. HR and NHEJ) (Figure 3-6I). The effects of ELK suppression were more pronounced when combined with MAPK inhibitors, versus HDAC inhibitors, as might be expected, since it is likely that other MAPK pathway targets are important in *BRAF*-mutant melanomas. Growth arrest triggered by ELK1 overexpression precluded rescue experiments. However the observation that 1) ELK activity and expression is potently suppressed in drug treated cells, 2) *BRIP1*, *PARP3*, *XRCC5* (and many other DNA repair genes) are direct ELK1 targets, 3) ELK suppression substantially inhibits the expression of these genes in melanomas and 4) ELK ablation can partially recapitulate the effects of both drugs, all support the conclusion that ELK critically regulates this DNA repair network in response to HDAC/MAPK inhibitors. Other ETS family members may play a cooperative role in this process as well. Taken together, these findings provide a mechanistic basis for understanding the cooperativity of MAPK and HDAC inhibitors on DNA repair pathways and cell death.

DISCUSSION

Using multiple animal models of *BRAF*-mutant melanoma we have shown that the Class I HDAC inhibitor, entinostat, dramatically enhances the efficacy of BRAF/MEK inhibitors, both in tumors that are sensitive and relatively resistant to these agents. In addition we have uncovered a strategy for treating *NRAS*- and *NF1*-mutant tumors, for which there are currently no approved targeted therapies. Finally, we have elucidated the mechanism by which these agents function and have discovered that a clinically available biomarker can be used to select patients that are most likely to benefit from MAPK/HDAC inhibitor combinations. Together these findings provide a promising and readily translatable strategy for improving treatments for these RAS/RAF pathway-driven melanomas.

Interestingly, in the course of this work we also discovered a population of melanomas that exhibit unconventional defects in DNA repair. Mutations in *BRCA1* or *BRCA2* represent examples of classical cancer-associated DNA repair defects, and confer sensitivity to agents that stall replication forks, such as PARP inhibitors (Farmer et al. 2005; Lord and Ashworth 2012). However, additional alterations have been proposed to phenocopy these mutations, resulting in a state sometimes referred to as 'BRCAness' (discussed in (Lord and Ashworth 2016)). Examples of this include mutations in other HR genes, hypermethylation of *BRCA* genes, amplification of genes that disrupt HR, and mutations in the transcriptional regulator CDK12. Here we observe a related, but more complex paradigm. "Sensitive" melanomas exhibit measureable defects in HR genes due to the transcriptional suppression of a broad group of DNA repair genes (Peng, 2014). Nevertheless, these defects are not potent enough to reach a functional threshold that confers sensitivity to PARP inhibitors alone. Intriguingly, BRAF/MEK pathway inhibitors unmask these defects, by further reducing the expression of several HR/BRCA pathway genes, thereby triggering a BRCA-like state (Lord and Ashworth 2016). Accordingly, these studies reveal a new type of 'priming' defect in melanomas. Moreover, they demonstrate that in this setting BRAF/MEK inhibitors can broadly suppress the expression of DNA repair genes, most notably in the HR/BRCA pathways, thereby creating a new therapeutic vulnerability.

Importantly, we show that combined suppression of BRAF/MEK and HDAC3 capitalizes on this vulnerability. While BRAF/MEK pathway inhibitors suppress one set of DNA repair genes, most notably HR pathway genes, the addition of entinostat induces a potent suppression of a broader set of genes including essential NHEJ genes. It should be noted that these effects are not due to an additive effect of MAPK and HDAC inhibition, but rather these agents cooperate by potently suppressing a broad transcriptional network of DNA repair genes. We have shown that key nodes of this network are regulated by ELK1, which is cooperatively

suppressed by combined MAPK/HDAC suppression, via effects on phosphorylation and expression. Notably, ELK1 has been shown to directly bind and regulate 20% of the DNA repair genes that are suppressed by these agents, suggesting a broader role for ELK1 in maintaining this network. Other ETS family members may also contribute to this response.

It is well established that the NHEJ pathway can compensate for defects in HR. As such, synthetic lethal interactions between HR genes and NHEJ genes have been observed (Hemann 2014; Lord and Ashworth 2016). Here we have discovered a chemical synthetic lethality between BRAF/MEK inhibitors and Class I HDAC inhibitors, which when combined coordinately suppress these pathways. Importantly, we have experimentally demonstrated that suppression of both HR and NHEJ pathways are required for cell death.

While the molecular basis for the priming defect in melanomas is not known, it could be related to an epigenetic event or state, or alternatively caused by specific defects in transcriptional regulatory proteins. Fortunately however, this defect consistently segregates with MGMT expression, which has already proven to be a tractable clinical biomarker in other settings (Hegi et al. 2005; Weller et al. 2009). In this respect it is interesting to note that there are two clusters of DNA repair genes that show inverse expression patterns; a broad set of genes that are suppressed in MGMT+ tumors, and a smaller set of genes, several of which are also involved in directly repairing base modifications, that are high in MGMT+ tumors (and vice versa). This observation further supports the notion that these gene clusters are co-regulated in melanomas. Regardless, the identification of this potent therapeutic combination, coupled with the elucidation of its mechanism of action and a tractable predictive biomarker of efficacy, will enable new mechanism-based combination trials that have the potential to improve treatments for these three major melanoma subtypes.

METHODS

Cell lines and reagents

All cell lines were purchased from ATCC, except for MALME3M (obtained from Levi Garraway, Dana-Farber Cancer Institute), Meljuso (obtained from William Hahn, Dana-Farber Cancer Institute), SUM149PT (obtained from Frank McCormick, University of California, San Francisco), Yugasp and Yudoso (obtained from Yale Dermatology Center) and WM3670 and WM3629 (obtained from Rockland Immunochemicals). No further authentication of these cell lines was performed. All of the cell lines were determined to be negative for mycoplasma using the MycoAlert Mycoplasma Detection Kit (Lonza, LT07-318). Cells were used for experiments within 15 to 20 passages from thawing. Antibodies were obtained from the following sources: Cell Signaling Technologies: p-ERK (4370), ERK (9102), GAPDH (2118), BRIP1 (4578), XRCC5 (2753), H3K56-Ac (4243), HDAC1 (5356), HDAC2 (5113), HDAC3 (3949), HDAC6 (7612), RAD51 (8875), p-ELK1 (9181), HA (3724), cleaved PARP (9541); Sigma Aldrich: Actin (A2066); EMD Millipore: H3K9-Ac (06-942), BRCA2 (OP95), p-H2AX (05-636); Santa Cruz Biotechnology: XRCC4 (365055), XRCC6 (17789), PARP3 (390771), EME1 (53275); Bethyl Laboratories: RBBP8 (A300-488A-M); Novus Biologicals: PNKP (NBP1-87257); BD Pharmingen: MGMT (557045); Abcam: ELK1 (32106), LIG4 (26039). Trametinib, dabrafenib and olaparib were purchased from LC labs. Vorinostat, mocetinostat, nexturastat and entinostat were purchased from Selleck Chemicals. 5-azacytidine, NAC, Vitamin C and BSO were purchased from Sigma-Aldrich. Carboxy-H2DCFDA was purchased from Life Technologies (#C400).

RNAi

Non-targeting, HDAC1, HDAC2, HDAC3, HDAC6, XRCC4, XRCC5, XRCC6, PARP3, PNKP, BRCA2, MGMT, ELK1 and ELK3 siRNA pools were purchased from GE Healthcare/Dharmacon (D-001810-10, L-003493-00, L-003495-02, L-003496-00, L-003499-00,

L-004494-00, L-010491-00, L-005084-00, L-009297-00, L-006783-00, L-003462-00, L-008856-01, L-003885-00, L-010320-00, respectively). SiRNAs were transfected into cells using RNAiMax lipofectamine from Invitrogen. Cells were transfected approximately 24 hours before starting proliferation experiments. Control, HDAC1, HDAC2, HDAC3, and HDAC6 shRNAs were purchased from Sigma-Aldrich (SHC016, SHCLNG-NM_004964, SHCLNG-NM_008229, SHCLNG-NM_010411 and SHCLNG-NM_006044, respectively).

Expression constructs

cDNA clones were obtained from Sino Biologicals (MGMT) and the PlasmID Repository at Harvard Medical School (LIG4 and RAD51), sequence verified and subsequently cloned into the pHAGE-FLAG-HA mammalian lentiviral expression vector.

Cell growth assays

For the initial MAPK/HDACi screen and the dose-response matrix assay, cells were plated in 96-well plates. 5 replicates were done for each condition. At 24 hours, one plate of cells was frozen (-80ºC) representing the time 0 plate. At this time compounds were added to the remaining plates. After 72 hours each of the plates was frozen. After freezing, the plates (day 0 and 3) were thawed simultaneously and cells were quantified using CellTiter-Glo (Promega) as per manufacturer's instructions. SynergyFinder (Ianevski et al. 2017) was used to analyze drug combination dose-response matrix data. To determine the combination effects in excess of Loewe additivity, a Synergy Score was calculated to characterize the strength of synergistic interaction. For all other proliferation experiments, cells were seeded in triplicate into 6-well plates. Approximately 24 hours after plating, day 0 counts were taken using a hemocytometer. For inhibitor experiments, drug treatments were started at this time. Final cell counts were taken 72 hours after day 0 to determine changes in cell number versus day 0. For

western blots to determine drug efficacy or efficient knockdown, lysates were collected 48 hours following the addition of inhibitors.

Live cell imaging

The live cell imager IncuCyte ZOOM (Essen Biosciences, Ann Arbor, MI, USA) was used for multiplexed measurements of cell proliferation alongside cell death in a single well. The mKate2 red fluorescent protein (Essen Biosciences) was transfected into the Hs695T melanoma cell line and selected for RFP-infected cells using puromycin. Successful insertion of the nuclear-restricted RFP was confirmed via direct visualization of transfected cells on the IncuCyte ZOOM fluorescent microscope. For proliferation experiments, stably transfected cells were plated in 96-well plates and allowed to settle overnight at 37ºC. The green Incucyte Cytotox or Caspase-3/7 Apoptosis reagents were then added to the tissue culture growth media to assess real-time quantification of cell death. Red and green fluorescent objects were monitored in the Incucyte ZOOM acquiring images every 2 hours (for 72 hours) following treatment with vehicle or drugs and then quantified with the IncuCyte integrated analysis software. Relative cell death was defined as the ratio between cells with overlapping red and green cells (dead cells) and cells with red nuclei only (live cells).

Animal Studies and Treatments

Animal procedures were approved by the Center for Animal and Comparative Medicine in Harvard Medical School in accordance with the NIH Guide for the Care and Use of Laboratory Animals and the Animal Welfare Act. For cancer cell xenograft experiments immunodeficient Nu/Nu (A375 and Hs695T) or NSG (YUDOSO) mice were inoculated subcutaneously with 3×10^6 human *BRAF*- or *NRAS*-mutant melanoma cells. For allograft experiments, immunocompetent C56/Bl6 mice were inoculated subcutaneously with 1.5×10^5 murine *Braf/Nf1*-mutant melanoma cells or 4×10^5 murine *Braf/Pten*-mutant melanoma cells.

Tumor volumes were calculated by measuring length and width of the lesions and with the formula [(length) x $(width)^2$ x 0.52]. When tumors reached approximately 200-300mm^3, mice were randomly divided into different treatment groups that were administered either the MEK inhibitor trametinib (0.6mg/kg QD, oral gavage (OG)), the BRAF inhibitor dabrafenib (30mg/kg QD, OG), the HDAC inhibitor entinostat (1mg/kg QW, intraperitoneal injection (IP)), the PARP inhibitor olaparib (10mg/kg, QD IP) or their combinations as indicated. To track changes in tumor volume, tumor size was measured at day 0 and subsequently every 3-5 days by Vernier calipers. Unpaired 2-tailed t-tests with unequal variance were used to compare data sets where indicated and p-values are shown.

MGMT methylation assay

MGMT methylation analysis was performed using the OneStep qMethyl kit (Zymo Research, D5310). Briefly, DNA from 7 different melanoma cell lines was digested with methylation sensitive restriction enzymes in the test reaction while DNA in the reference reaction was not. Following digestion, DNA from both samples was amplified using real-time PCR in the presence of fluorescent dye and quantified. Investigator was blinded to group allocation and when assessing outcome. MGMT primer sequences used: Forward: 5'-GCGCTCTCTTGCTTTTCTCA-3', Reverse: 5'-CTGCAGGACCACTCGAGG-3'.

RAD51 foci assay

Melanoma cells transfected with control (siLuc) or siRNA pools against BRCA2 were irradiated with 10Gy. Cells were fixed 5 hours later and analyzed by immunofluorescence for RAD51 foci and gamma H2AX.

DCFDA staining

Cells were treated as indicated and then stained with H2DCFDA at 10μM and analyzed by flow cytometry.

Cell cycle phase separation

Live cells were separated in different phase of the cell cycle for subsequent gene expression analysis. Cells treated with vehicle or drugs were incubated with 10µg/ml Hoechst33342 for 1 hour at 37ºC in the dark. After trypsinization, cells were resuspended at a concentration of $10x10^6$ cells per ml for sorting. Cells were sorted based on the amount of DNA by defining two regions for sorting: one for G1 and the other for G2/M. The separated cells were collected in RNAse free conditions and further processed for RNA extraction.

Microarray and gene set enrichment analysis

RNA was isolated from Hs695T, SKMEL2 and A2058 cells 24 hours after treatment with indicated drugs. Prior to RNA extraction ERCC spike-in control mix was added to Trizol and RNA isolation was performed following the manufacturer's protocol. RNA clean-up was performed using the Qiagen RNeasy kit (74201). The Molecular Biology Core Facility at Dana-Farber Cancer Institute hybridized RNA to the Affymetrix Human 2.0 ST array chip. Analyses used BRB-ArrayTools developed by R. Simon and the BRB-ArrayTools development team. Thresholds were set at p=0.001. Microarray data can be accessed from the Gene Expression Omnibus (GEO) database (accession number: GSE125565). Gene set enrichment analysis (GSEA) and ssGSEA was performed using the Broad Institute interface (http://software.broadinstitute.org/gsea/index.jsp). The signature of Homologous Recombination-associated genes (PENG_HRD_SIGNATURE) was developed from genome-wide transcriptome profiling of Homologous Recombination DNA Repair (Peng, 2014) and added to the KEGG signature file from MSIGDB for subsequent analysis (http://software.broadinstitute.org/gsea/msigdb/genesets.jsp?collection=CP:KEGG). Tumor sample transcriptional profiles were obtained from the TCGA SKCM provisional dataset (http://firebrowse.org/?cohort=SKCM) and stratified based on median-centered z-scores of *MGMT* mRNA expression. The top 10% of *MGMT* expressors comprised the "MGMT+" cohort,

whereas the bottom 10% of *MGMT* expressors comprised the “MGMT-” cohort used in GSEA analyses. Melanoma cell line transcriptional profiles were obtained from CCLE (https://portals.broadinstitute.org/ccle/home) and stratified based on gene-centric RMA-normalized *MGMT* mRNA expression. The top 10% of MGMT expressors comprised the “MGMT+” cohort, whereas the bottom 10% of MGMT expressors comprised the “MGMT-” cohort used in GSEA analyses. Experimental ChIP data were obtained from the ChIP-X database (http://amp.pharm.mssm.edu/Harmonizome/).

Statistical analysis for in vitro experiments

For quantitative measurements, graphs represent mean values +/- standard deviation. Where indicated the data is presented as log2 fold (left axis) and percent change (right axis) over initial measurements. Unpaired 2-tailed t-tests with unequal variance were used to compare data sets where indicated and p-values are shown. Data were graphed and analyzed using GraphPad Prism v.6.

Statement of replication

All proliferation studies in Figures 1, 3, 4, 5 and Supplementary Figures 1 and 3 were performed $\geqq$ 3 times. Synergy studies were performed in 5 cell lines at different times with qualitatively similar findings. The large preclinical animal studies were performed one time, however qualitatively similar results were obtained in 5 different animal models and responses mimicked effects observed numerous times in vitro. The gamma H2AX experiment (Figure 3-4D) is shown in 3 cell lines and has been repeated in a separate set of cell lines. The microarray experiment was performed once (3 technical replicates) in 3 different cell lines and key targets were confirmed by qPCR and western blot (n>3) as shown throughout Figures 3-5 and 3-6.

Acknowledgements

This work was supported by grants from the NCI R01CA111754 (to K. Cichowski), the Ludwig Center at Harvard (to K. Cichowski and S.J. Elledge), and the NF Research Initiative at Boston Children's Hospital made possible by an anonymous gift (to O. Maertens).

Chapter 4 : Melanoma Therapeutic Strategies That Select Against Resistance by Exploiting MYC-Driven Evolutionary Convergence

Melanoma therapeutic strategies that select against resistance by exploiting MYC-driven evolutionary convergence

Katherine R. Singleton[1,†], Lorin Crawford[2,†], Elizabeth Tsui[1] Haley E. Manchester,[3,4] Ophelia Maertens,[3,4] Xiaojing Liu,[1] Maria V. Liberti,[1,5] Anniefer N. Magpusao,[6] Elizabeth M. Stein,[1] Jennifer P. Tingley,[1] Dennie T. Frederick,[4,7] Genevieve M. Boland,[4,7] Keith T. Flaherty,[4,7] Shannon J. McCall,[8] Clemens Krepler,[9] Katrin Sproesser,[9] Meenhard Herlyn,[9] Drew J. Adams,[6] Jason W. Locasale,[1] Karen Cichowski,[3,4,10] Sayan Mukherjee,[2,11] and Kris C. Wood[1,*]

[1]Department of Pharmacology and Cancer Biology, Duke University, Durham, NC 27710, USA [2]Department of Statistical Science, Duke University, Durham, NC 27708, USA [3]Genetics Division, Department of Medicine, Brigham and Women's Hospital, Boston, MA 02115, USA [4]Harvard Medical School, Boston, MA 02115, USA [5]Department of Molecular Biology and Genetics, Graduate Field of Biochemistry, Molecular and Cell Biology, Cornell University, Ithaca, NY 14853, USA [6]Department of Genetics, Case Western Reserve University, Cleveland, OH 44106, USA [7]Massachusetts General Hospital Cancer Center, Boston, MA 02114, USA [8]Department of Pathology, Duke University, Durham, NC 27710, USA [9]Molecular and Cellular Oncogenesis Program, The Wistar Institute, Philadelphia, PA 19104, USA [10]Ludwig Center at Harvard, Boston, MA 02115 [11]Departments of Mathematics, and Computer Science, Duke University, Durham, NC 27708, USA

[†]These authors contributed equally to this work

Author Attributions:
Conceptualization: K.R. Singleton, L. Crawford, S.Mukherjee, and K.C. Wood
Methodology: K.R. Singleton and L. Crawford
Software: L. Crawford and S. Mukherjee
Validation: K.R. Singleton, H.E. Manchester, E. Tsui, A.N. Magpusao, E.M. Stein, J.P. Tingley, and K. Sproesser
Formal Analysis: L. Crawford, X. Liu and M.V. Liberti
Investigation: K.R. Singleton, H.E. Manchester, E. Tsui, A.N. Magpusao., E.M. Stein, J.P. Tingley, X. Liu, and K. Sproesser
Resources: M. Herlyn, D.J. Adams, J.W. Locasale, K. Cichowski, and K.C. Wood
Data Curation: L. Crawford, X. Liu, M.V. Liberti, A.N. Magpusao
Writing – Original Draft: K.R. Singleton, L. Crawford, and K.C. Wood
Writing – Review & Editing: all authors
Visualization: K.R. Singleton, L. Crawford
Supervision: M. Herlyn, D.J. Adams, J.W. Locasale, K. Cichowski, S. Mukherjee, and K.C. Wood
Funding Acquisition: M. Herlyn, D.J. Adams, K. Cichowski, and K.C. Wood

ABSTRACT

Diverse pathways drive resistance to BRAF/MEK inhibitors in *BRAF*-mutant melanoma, suggesting that durable control of resistance will be a challenge. By combining statistical modeling of genomic data from matched pre-treatment and post-relapse patient tumors with functional interrogation of over 20 *in vitro* and *in vivo* resistance models, we discovered that major pathways of resistance converge to activate the transcription factor, c-MYC (MYC). MYC expression and pathway gene signatures were suppressed following drug treatment, then rebounded during progression. Critically, MYC activation was necessary and sufficient for resistance, and suppression of MYC activity using genetic approaches or BET bromodomain inhibition was sufficient to resensitize cells and delay BRAFi resistance. Finally, MYC-driven, BRAFi-resistant cells are hypersensitive to the inhibition of MYC synthetic lethal partners, including SRC family and c-KIT tyrosine kinases as well as glucose, glutamine, and serine metabolic pathways. These insights enable the design of combination therapies that select against resistance evolution.

INTRODUCTION

Recently, the treatment of metastatic *BRAF* mutant melanoma has been revolutionized by two major new therapeutic modalities: targeted therapies (e.g., BRAF and MEK inhibitors, BRAFi/MEKi) and immune checkpoint blockade (e.g., PD-1/PD-L1 and CTLA-4 inhibitors) (Wargo, Cooper, and Flaherty 2014). Therapy with BRAFi/MEKi yields high objective response rates, but diverse mechanisms of acquired resistance limit therapeutic duration (Alcala and Flaherty 2012; Robert, Karaszewska, et al. 2015; Solit and Rosen 2014; Wargo, Cooper, and Flaherty 2014). In contrast, checkpoint inhibitors yield lower response rates, but are often durable (Wargo, Cooper, and Flaherty 2014; Larkin et al. 2015). Ongoing clinical trials are investigating combinations of BRAFi/MEKi with checkpoint inhibitors, hoping to improve their durations and rates of response, respectively. However, emerging evidence suggests that

mechanisms driving resistance to BRAFi/MEKi may also drive cross-resistance to checkpoint blockade through the suppression of tumor immune surveillance, underscored by observations that patients who fail first-line treatment with BRAFi/MEKi appear to respond poorly to subsequent checkpoint blockade (Ackerman et al. 2014; Frederick et al. 2013; Peng et al. 2016; Wargo, Cooper, and Flaherty 2014)(Puzanov et al., 2015, *Pigment Cell Melanoma Res.*, abstract; Ramanujam et al., 2015, *Pigment Cell Melanoma Res.*, abstract; Simeone et al., 2015, *Pigment Cell Melanoma Res.*, abstract). These findings suggest that innovative and robust strategies for preventing resistance to BRAFi/MEKi may not only increase the durability of responses to first-line therapy but also improve the activity of emerging checkpoint blockade and combination strategies.

Extensive studies have identified diverse mechanisms of resistance to BRAFi/MEKi in *BRAF*-mutant melanomas, including those that function by modulating the initial adaptive tumor response (intrinsic resistance) and those selected for over time (acquired resistance). Many resistance mechanisms, including activating mutations in *NRAS*, *MEK*, and *ERK, NF1* loss, and amplification or alternative splicing of mutant *BRAF*, result in reactivation of the ERK pathway in the presence of BRAFi/MEKi (Alcala and Flaherty 2012; Corcoran et al. 2010; Hugo et al. 2015; Maertens et al. 2013; Nazarian et al. 2010; Poulikakos et al. 2011; Rizos et al. 2014; Shi, Hong, et al. 2014; Shi et al. 2012; Van Allen et al. 2014; Solit and Rosen 2014; Whittaker et al. 2013). Additionally, bypass mechanisms, including activation of the phosphoinositide-3-kinase (PI3K) pathway through mutations or altered expression of *IGF-1R, PIK3CA, PTEN*, and *AKT*, as well as through microenvironmental changes, can drive resistance (Alcala and Flaherty 2012; Fedorenko and Smalley 2015; Hugo et al. 2015; Paraiso et al. 2011; Rizos et al. 2014; Shi, Hong, et al. 2014; Shi, Hugo, et al. 2014; Solit and Rosen 2014; Villanueva et al. 2010). Similarly, bypass signaling through the Notch1 pathway via altered expression of Notch1 and other pathway members drives resistance in a third, distinct subset of

patients (Martz et al. 2014). Importantly, these three pathways—ERK, PI3K and Notch1—have been shown to drive resistance to both single agent and combined BRAFi/MEKi, and together they appear to account for ~75% of acquired resistance cases while also playing important roles in intrinsic resistance (Hugo et al. 2015; Martz et al. 2014; Moriceau et al. 2015; Wagle et al. 2014). Finally, a “long tail” of alternative, rare resistance mutations and non-genomic (transcriptional) alterations, including those affecting the WNT/LEF1 and Hippo/YAP pathways, are likely to play roles in resistance, although the fractions of tumors affected have yet to be defined. In sum, the presence of multiple distinct pathways of resistance, sometimes within the same patient or even the same tumor (Shi, Hugo, et al. 2014), suggests that the therapeutic inhibition of individual resistance pathways is likely to have only limited clinical value, and that robust therapies may require simultaneous inhibition of multiple resistance pathways (Robert, Karaszewska, et al. 2015; Solit and Rosen 2014). Unfortunately, such higher order combination therapies are expected to frequently produce unacceptable toxicities in patients, necessitating the development of conceptually new approaches to circumvent resistance.

One such approach is based on the hypothesis that the seemingly distinct pathways driving resistance to BRAFi/MEKi may actually converge on one or more “common effectors”: downstream signaling targets that are required for the development and maintenance of resistance. This hypothesis is consistent with the notion of oncogene addiction (Settleman 2012), which asserts that cancers develop dependencies on signaling downstream of driver oncogenes, implying that resistance may require the reactivation of these key downstream target(s). In melanoma, the ‘common effector’ hypothesis is also consistent with the observation that BRAFi/MEKi-resistant tumors driven by diverse upstream signaling alterations exhibit highly recurrent transcriptional programs (Hugo et al. 2015). Finally, this hypothesis is supported by recent data from our group and others demonstrating that distinct mechanisms of resistance to receptor tyrosine kinase inhibitors in lung and colorectal cancers converge on a single

downstream signaling axis, the targeting of which can forestall resistance (Hrustanovic et al. 2015; Misale et al. 2015; Tricker et al. 2015).

In this study, we integrate genomic and biochemical data from two cohorts of *BRAF* mutant melanoma patients with acquired resistance to BRAF/MEK pathway blockade, alongside diverse cellular and animal models of BRAFi resistance, to identify the transcription factor MYC as a convergent downstream effector of multiple major resistance pathways that is both necessary and sufficient for resistance. By leveraging this insight alongside the concept of synthetic lethality, we define combination therapies that, by selectively targeting the MYC-activated, BRAFi/MEKi-resistant state, have the unique property of selecting against resistance evolution and thereby represent promising strategies to durably control resistance.

RESULTS

MYC is commonly reactivated in patients with acquired resistance to BRAF inhibitors

To search a potential convergent effector of resistance, we began by reasoning that such an effector should follow two rules: (1) it should be regulated downstream of the driver oncogene and (2) it should rebound to at least pre-treatment expression or activation states at resistance. To identify genes that obey (1), we used a nonlinear classification model that allows for the inference of differential gene expression by estimating effect sizes (Crawford et al. 2018) to identify a set of genes, termed the BRAF response signature, that are most transcriptionally altered by BRAFi/MEKi treatment in cell lines and human tumors from recent published studies (local false sign rate (LFSR) < 0.01; see Supplemental C text for details) (Nazarian et al. 2010; Stephens 2017; Pratilas et al. 2009; Rizos et al. 2014). Gene Set Enrichment Analysis (GSEA) of these 68 genes revealed numerous enriched signatures associated with the canonical RAS-RAF-MEK-ERK cascade (Supplemental Table C-1). Next, we winnowed the signature to genes that return to their pre-treatment states during relapse in a panel of 29 human melanoma tumors

sampled before and after the development of resistance (Rizos et al. 2014). We used Bayes Factors (BF; see Appendix C Text for details) as a metric describing a gene's return toward its pre-treatment state. The BF is a Bayesian alternative to classical likelihood ratio testing. Here, a large BF indicates signature genes useful for classifying a relapsed sample, whereas a $\log_{10}$BF less than or equal to zero indicates a gene that does not discriminate between treated and resistant tumors. We considered all signature genes with $\log_{10}$BF greater than zero to be potential convergent effectors of resistance. Thirty-three genes were associated with positive $\log_{10}$BF values (Figure 4-1A and Supplemental Table C-1). We observed that *MYC* returned the highest $\log_{10}$BF value. Correspondingly, GSEA of the 33-gene panel revealed numerous *MYC*-related, enriched gene sets (Supplemental Table C-1). By comparing the change in *MYC* mRNA levels in matched pre-treatment and post-relapse tumors with the expected change in the same following BRAFi treatment, we calculated the probability of *MYC* rebound in each resistant tumor (see Supplemental C Text for details). Strikingly, this analysis revealed ≥90% probability of *MYC* rebound in 23 of 29 resistant tumors, and ≥50% probability of *MYC* rebound in all 29 tumors despite the fact that resistance in these tumors was putatively driven by a range of mechanisms including activation of the ERK, PI3K, and Notch1 pathways (Figure 4-1B and Supplemental Table C-2) (Martz et al. 2014; Rizos et al. 2014). At the protein level, immunohistochemical analysis of formalin-fixed tumor samples from an independent cohort of *BRAF* mutant melanoma patients showed a similar pattern of MYC suppression on treatment followed by reactivation upon progression (Figure 4-1C–D).

To assess the functional role of MYC activation in BRAFi-resistance, we used step-wise selection in several *BRAF* mutant melanoma cell lines to establish a panel of clonal derivatives with acquired resistance to BRAF pathway blockade. Functionally, these lines exhibited an array

Figure 4-1: MYC is a potential convergent effector of diverse resistance pathways in BRAF mutant melanoma tumors that have progressed on treatment with BRAF/MEK inhibitors. (A) Bayes Factor (BF) values for BRAF response signature genes. (**B)** Probability of MYC rebound to pretreatment or greater expression levels in each of 29 patient tumors with acquired resistance to vemurafenib. (**C)** Matched patient samples pre-treatment (PRE), on treatment (ON) with RAF and/or MEK inhibitor, or after progression on treatment (POST). Nuclear MYC staining scored 0: none to 3: maximum (left panel) and percent nuclei staining positive for MYC (right panel). (**D)** Representative images from the data shown in C) at 40X magnification. **(E)** MYC mRNA transcript levels in cell lines with evolved resistance. Data are means of 3 experiments in clonal cell lines normalized to β-actin transcript levels and parental MYC levels. Parental cells were treated with 1μM PLX4720 or DMSO for 72 hrs. **(F)** MYC protein levels shown by immunoblotting. Parental lines (P) were treated with DMSO or 1 μM PLX4720 for 24 hrs and resistant lines (annotated as R(A), PI3K-AKT-mTOR-driven resistance; R(N), Notch1-driven resistance; R(M), ERK reactivation-driven resistance; R(O), other/unknown resistance mechanism; R(Mi), evolved resistance to MEK inhibitor, AZD6244; R(Ei), evolved resistance to ERK inhibitor, VX-11E) were treated with 3 μM PLX4720. Quantification of MYC protein normalized to total protein is shown in the bottom panel and total protein staining is shown in Figure S1C. *P < 0.05. See also Supplemental Figure C-1 and Supplemental Table C-1.

Figure 4-1 (continued)

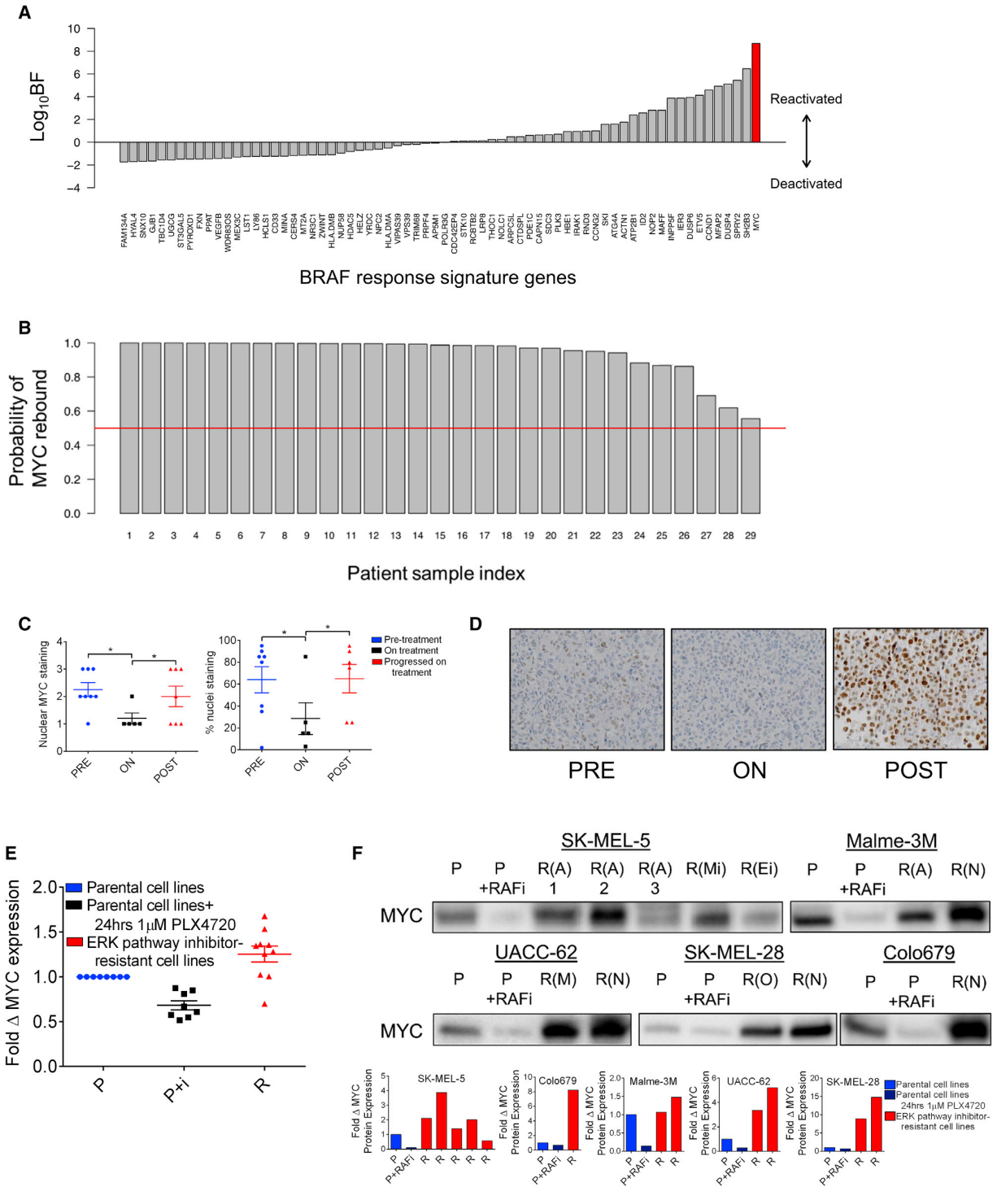

of resistance mechanisms including ERK re-activation and bypass of ERK signaling through PI3K or Notch1 pathway activation. Additionally, the resistance mechanism of one resistant cell line could not be determined (Supplemental Figure C-1A) (Martz et al. 2014). Like their human tumor counterparts, *MYC* mRNA and protein levels in these models were decreased following initial BRAFi treatment, then rebounded to pre-treatment or greater levels on resistance despite the continued presence of BRAFi (Figures 4-1E–F and Supplemental Figure C-1B–C). Together, these data suggest that MYC may play an important role in the development of resistance.

MYC expression is necessary and sufficient for resistance in diverse models

To determine whether *MYC* activation is functionally driving resistance or simply a marker of the proliferative state, we first ectopically expressed a degradation-resistant MYC^{T58A} mutant in sensitive (treatment naïve) cells, revealing that MYC expression alone is sufficient to confer resistance to BRAFi, MEKi, ERKi, and BRAFi+MEKi (Figure 4-2A and Supplemental Figure C-2A). Next, to determine whether MYC activation is necessary for resistance, we partially suppressed MYC expression with two independent shRNAs in a panel of resistant cell lines (Supplemental Figure C-2B). In each case, MYC knockdown sensitized cells to BRAFi at growth inhibition-50% (GI_{50}) values near or below those of parental, sensitive cells (Figure 4-2B). By comparison, MYC knockdown had modest effects on BRAFi sensitivity in parental cells (Supplemental Figure C-2C). Also, MYC levels in parental and resistant lines were uncoupled from doubling time (Supplemental Figure C-2D), consistent with the observation that resistant cells, which have higher MYC levels that their parental counterparts, also tend to grow more slowly. To explore whether resistant cells could be sensitized to BRAFi/MEKi using pharmacological methods, we used JQ1, a small molecule BET bromodomain inhibitor that suppresses *MYC* expression alongside other targets (Supplemental Figure C-2E) (Delmore et al. 2011). JQ1 treatment phenocopied genetic *MYC* suppression (Figure 4-

Figure 4-2: MYC activation is necessary and sufficient for resistance to BRAF/MEK pathway inhibitors in diverse BRAF-mutant melanoma cell lines.

(A) Fold change in GI50 values for cells expressing MYCT58A and treated with either PLX4720, AZD6244, VX-11E, or the combination of PLX4720 and AZD6244 at a 1:1 dose ratio as compared to cells expressing an empty vector control (pBABE-puro). **(B)** Fold change in GI50 values for PLX4720 between cell lines expressing shGFP compared to each of two independent shRNAs targeting MYC. P values denote significance between the response of shGFP and each shMYC expressing cell line. Parental lines are shaded blue, resistant lines, red/yellow. **(C)** Clonogenic growth assay of A375 line derivatives treated with DMSO, 100 nM, 300 nM or 1 μM PLX4720 +/− 300 nM JQ1. **(D)** WM793 cells expressing ectopic MYC or luciferase control were treated with DMSO or 100nM JQ1 and their PLX4720 GI50 value was determined. JQ1+PLX4720 treated cells are normalized to the viability of cells treated with JQ1 alone to account for nonspecific toxicity. P values denote significance between DMSO and JQ1 treatment in each cell line. **(E)** Clonogenic growth of SK-MEL-5 cells with resistance to VX-11E (VX) in DMSO or 100 nM JQ1. JQ1+VX-11E treated cells are normalized to the viability of cells treated with JQ1 alone to account for nonspecific toxicity. P values denote significance between DMSO and JQ1 treatment. **(F)** JQ1 GI50 values for the indicated PLX-resistant lines compared to matched parental controls. Significance is between the parental cell line and each matched resistant derivative. Data are means (SD) from 3 experiments. *P < 0.05; **P < 0.01; ***P < 0.005; ****P < 0.001. See also Supplemental Figure C-2.

Figure 4-2 (continued)

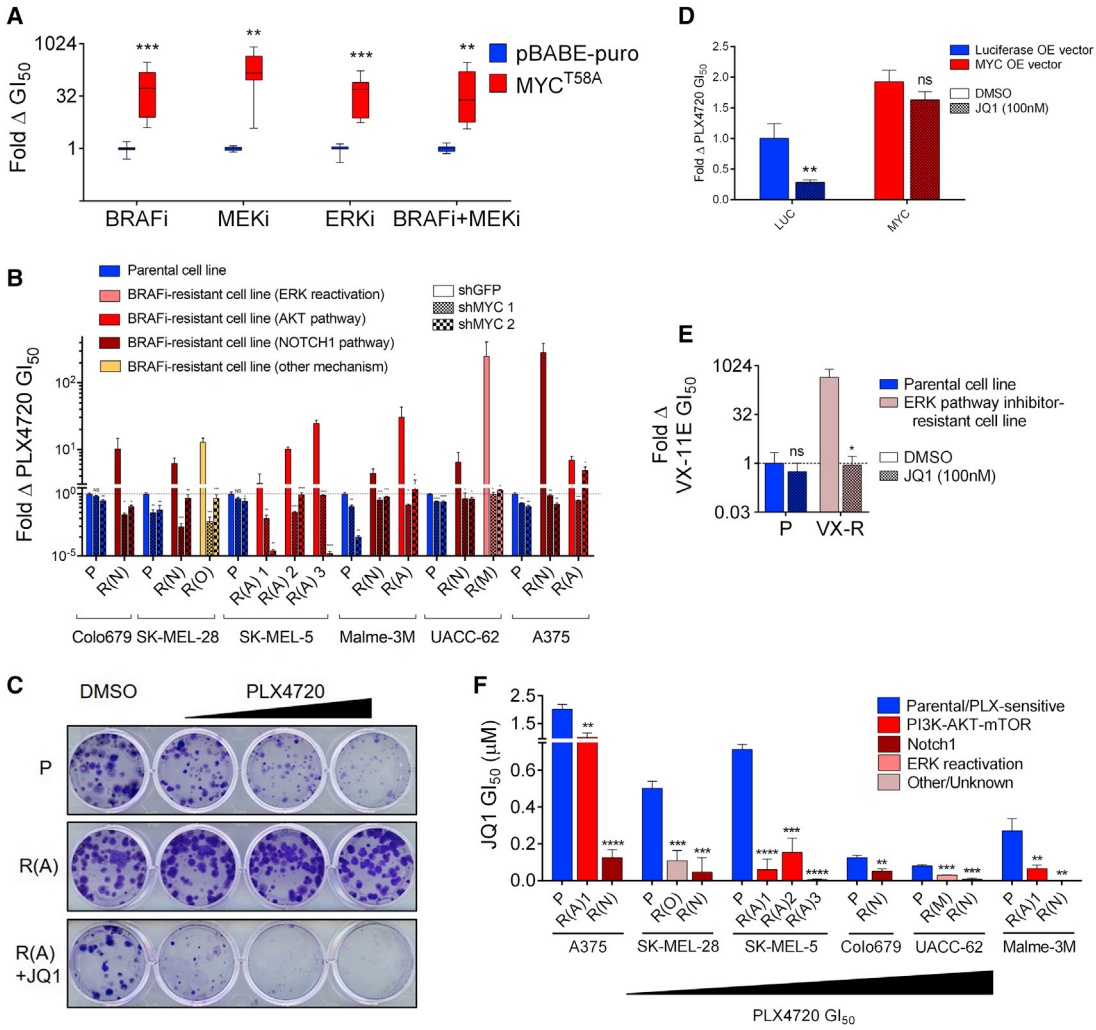

2C and Supplemental Figure C-2E–G). As JQ1 blocks the endogenous transcription of multiple genes, we tested its MYC-specific effects using a virally-expressed MYC construct lacking its native promoter (Zuber et al., Nature, 2011). We found that while JQ1 could sensitize control, luciferase expressing cells to BRAFi, it lost this ability upon ectopic expression of MYC, indicating that JQ1's effects are largely due to on-target inhibition of MYC expression (Figure 4-2D). Additionally, JQ1 could re-sensitize cell lines with evolved resistance to the ERKi VX-11E (Figure 4-2E). Finally, consistent with a shift away from BRAF-dependence and toward MYC-dependence, we found that evolved resistant lines were always more sensitive to JQ1 monotherapy than their parental counterparts, and that the sensitivity of parental cell lines to JQ1 was inversely related to their basal sensitivity to BRAFi (Figure 4-2F). Together, these data demonstrate that MYC activation is both necessary and sufficient for resistance to ERK pathway inhibition in diverse models and suggest that *BRAF* mutant melanoma cell lines exist along a continuum between BRAF- and MYC-driven states.

MYC functions downstream of common resistance pathways

Although the finding that MYC knockdown could reverse resistance in evolved cell lines exhibiting diverse resistance mechanisms suggests that MYC functions as a convergent downstream effector of resistance, we sought to further investigate this in a controlled genetic system. We stably expressed lentiviral cDNAs constitutively activating the ERK, PI3K, and Notch1 resistance pathways in a treatment-naïve, BRAFi-sensitive cell line, UACC-62. Activation of the ERK pathway (through expression of activated KRASG12V, activated HRASG12V, or activated MEK1(S218D/S222D) (MEK1 DD)), the PI3K pathway (through expression of activated, myristoylated AKT1), and the Notch1 pathway (through expression of the Notch1 intracellular domain (ICD)) each increased MYC protein levels relative to cells expressing a negative control construct (luciferase) or activators of pathways that fail to confer resistance (the Janus kinase-Signal Transducer and Activator of Transcription (JAK-STAT)

pathway (JAK2V617F) and Hedgehog pathway (truncated Gli2)) (Figures 4-3A and Supplemental Figure C-3A–B)

We next investigated the mechanisms by which each resistance pathway was causing increased MYC expression. It has previously been demonstrated that the ERK and PI3K pathways can increase MYC levels by enhancing protein stability through phosphorylation (Wang et al. 2011). Consistent with these findings, expression of MEK1 DD and myrAKT1 increased MYC protein levels, but not MYC mRNA levels, relative to luciferase expressing cells (Figure 4-3A–C and Supplemental Figure C-3B). Further, MEK1 DD and myrAKT1 expression increased MYC stability in a cycloheximide chase assay (Figure 4-3C and Supplemental Figure C-3C). Separately, Notch1 is known to activate MYC through transcriptional upregulation (Palomero et al. 2006; Konieczkowski et al. 2014; Martz et al. 2014; Wood et al. 2012), consistent with our findings that cells expressing the Notch1 intracellular domain exhibit increased MYC mRNA levels without evidence of increased MYC protein stability (Figure 4-3A–C and Supplemental Figure C-3B–C). Resistance caused by ERK pathway reactivation can be reversed with MEKi and/or ERKi treatment. Consistent with this, we found that both ERK pathway activating constructs and evolved cell line models with ERK pathway reactivation lost MYC expression upon treatment with MEKi+ERKi, while AKT-driven resistance models retained partial MYC expression (Supplemental Figure C-3D). Resistance driven by each of these upstream pathways was MYC-dependent, as both shRNA-mediated MYC knockdown and treatment with JQ1 were sufficient to fully reverse resistance (Figures 4-3D–E and Supplemental Figure C-3E). Finally, cells with forced activation of resistance pathways displayed increased sensitivity to JQ1 relative to controls (Figure 4-3F). Collectively, these findings demonstrate that major pathways of resistance function through convergent, downstream MYC activation and suggest that resistant cells, which have shifted their

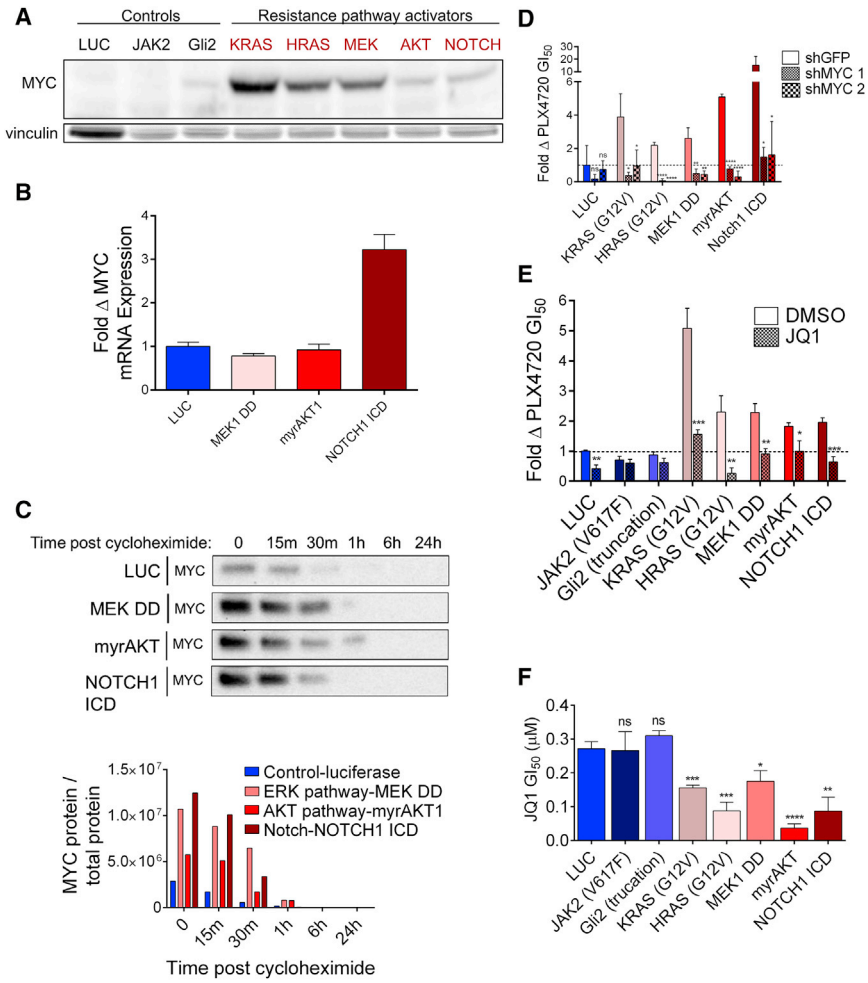

Figure 4-3: MYC activation drives resistance to BRAF pathway inhibition downstream of common resistance pathways.

(A) Immunoblot of MYC levels in UACC-62 cells expressing luciferase (luc) or the indicated pathway activating constructs. Vinculin levels are shown as a loading control. Quantification shown in Figure S3B. **(B)** MYC mRNA transcript levels in UACC-62 cells expressing the indicated constructs. Data are means of 3 experiments normalized to TUBB3 transcript levels and UACC-62-luc MYC levels**. (C)** Immunoblot of MYC levels in UACC-62 cells expressing luc or the indicated pathway activating constructs at the indicated times post treatment with 20 μg/mL cycloheximide. Quantification of MYC protein normalized to total protein is shown in the bottom panel and total protein staining is shown in Figure S3C. **(D)** Change in sensitivity to PLX4720 for lines in A) by expression of two independent shRNAs targeting MYC. P values are the comparison of shGFP to each shMYC-expressing cell line. **(E)** Sensitization to PLX4720 for lines in A) by the addition of 100 nM JQ1. JQ1+PLX4720 treated cells are normalized to the viability of cells treated with JQ1 alone to account for nonspecific toxicity. P values indicate difference between DMSO and JQ1 treatment**. (F)** JQ1 GI50 values of lines in A) that do not (blue shades) or do (red shades) provide resistance to PLX4720. P values indicate significance relative to luc-expressing cells. All data are means (SD) from 3 *experiments. *P < 0.05; **P < 0.01; ***P < 0.005; ****P < 0.001. See also Supplemental Figure C-3*

dependencies from BRAF to MYC, may be selectively sensitive to therapeutic strategies that disrupt MYC function.

BRAF mutant cell lines with intrinsic resistance to BRAFi rapidly upregulate MYC upon treatment

Previously, we and others have described BRAF mutant melanoma cell lines that, like a minority of patients, exhibit intrinsic resistance to BRAFi/MEKi (Konieczkowski et al. 2014; Martz et al. 2014; Wood et al. 2012). Given our finding that evolved resistant cell lines have increased MYC expression relative to their parental counterparts, we expected that intrinsically resistant lines would have similarly elevated MYC levels. Surprisingly, however, we found no clear correlation between MYC expression level and intrinsic resistance status (Figure 4-4A–C and Supplemental Figure C-4A–B). However, in contrast to sensitive cells, which tend to lose MYC expression following short-term treatment with PLX4720 (24h), intrinsically resistant cell lines increase MYC expression following the same treatment (Figure 4-4A–C). Accordingly, sensitivity to JQ1 could be potentiated in intrinsically resistant cell lines, but not in sensitive cell lines, following a brief, 4-day pre-treatment with PLX4720 (Figure 4-4D). To further investigate MYC dynamics, we chronically cultured both a sensitive cell line, A375, and an intrinsically resistant line, WM793, in 1 μM PLX4720, measuring JQ1 and PLX4720 GI50 values over time. A375 gradually developed resistance over the course of 60 days while concurrently developing increased sensitivity to JQ1 (Figure 4-4E), changes that correlated with MYC expression over time and are consistent with the hypothesis of selection for MYC-driven clones (Figures 4-4F and Supplemental Figure C-4C). In contrast, the intrinsically resistant cell line exhibited rapid decreases in JQ1 GI50 values that were already apparent at the first measurable time point (3d) and remained stable thereafter, while modestly increasing in PLX4720 resistance (Figure 4-4G). Changes in drug sensitivity were mirrored by a rapid upregulation of MYC expression over 24 hours of PLX4720 exposure, which then remained constant for the remaining duration of the

experiment (Figures 4-4H and Supplemental Figure C-4D). Additionally, MYC expression remained stably elevated following removal of PLX4720 (Figure S4E). MYC knockdown could reverse resistance to BRAFi in the intrinsically resistant cell lines (Figure 4-4I), a result that could be phenocopied with JQ1 (Supplemental Figure C-4F). Finally, we recently reported that these intrinsically resistant cell lines could be re-sensitized to ERKi using combinations of inhibitors directed against the upstream PI3K and Notch1 pathways, with minor contributions from the estrogen receptor alpha (ERα) pathway (Figure 4-4J) (Martz et al., 2014). Consistent with the hypothesis that MYC is a convergent downstream effector of these resistance pathways, MYC overexpression fully rescued the sensitizing effects caused by upstream inhibition of these pathways (Figure 4-4K). Together, these findings demonstrate that intrinsic resistance, like evolved resistance, is driven by MYC activation, that a key distinguishing feature of intrinsically resistant lines is their ability to rapidly upregulate MYC expression in response to BRAFi, and that dynamic MYC upregulation in these cells results in corresponding changes in sensitivity to pharmacological MYC suppression with JQ1.

.

Figure 4-4: Melanoma cell lines with intrinsic resistance to BRAFi derive resistance by rapidly upregulating MYC following drug treatment. (A) The indicated cell lines were incubated with DMSO or 1 μM PLX4720 for 24 hrs, then immunoblotted for MYC. Total protein staining is shown in Figure S4A. **(B)** As in A). Total protein staining is shown in Figure S4B. **(C)** Quantification of immunoblots shown in A) and B) showing MYC protein levels normalized to total protein. **(D)** JQ1 GI50 values for the indicated lines following pre-incubation with either DMSO or 1 μM PLX4720 for four days. P values indicate significance between DMSO and PLX4720 pre-treatment. **(E)** GI50 values in A375 cells for either PLX4720 (solid line) or JQ1 (dashed line), measured at intervals during continuous culture in 1 μM PLX4720. **(F)** MYC levels in A375 at several time points while in culture with 1 μM PLX4720. Quantification shown in Figure S4C. **(G)** As in E), for the intrinsically resistant line, WM793. **(H)** As in F) for WM793. Quantification shown in Figure S4D. **(I)** Sensitization of the indicated lines to PLX4720 by expression of two shRNAs targeting MYC. Differences between shGFP and shMYC are denoted by P values. **(J)** Signaling pathways controlling intrinsic resistance to BRAFi/MEKi in intrinsically resistant cell lines and their convergence on downstream MYC activation. As indicated, previous findings demonstrate that inhibition of the PI3K-AKT-mTOR and NOTCH1 pathways can sensitize these lines to ERK pathway inhibition. **(K)** Sensitivity of indicated lines to the ERKi VX-11E following expression of luc or MYC and treatment DMSO or a combination of inhibitors (200 nM BEZ235 (PI3K/mTOR inhibitor) for the PI3K-AKT-mTOR pathway and shNotch1 for the Notch1 pathway for Hs 294T cells; 200 nM BEZ235, shNotch1, and 1 μM fulvestrant for Lox IMVI, A2058 and WM793 cells). Viabilities of cells treated with pathway inhibitors plus VX-11E are normalized to the viability of the same cells treated with pathway inhibitors alone to account for nonspecific toxicity. All data are means (SD) from 3 experiments. *P < 0.05; **P < 0.01; ***P < 0.005; ****P < 0.001; #, the upper bound of the assay was reached. See also Supplemental Figure C-4

Figure 4-4 (continued)

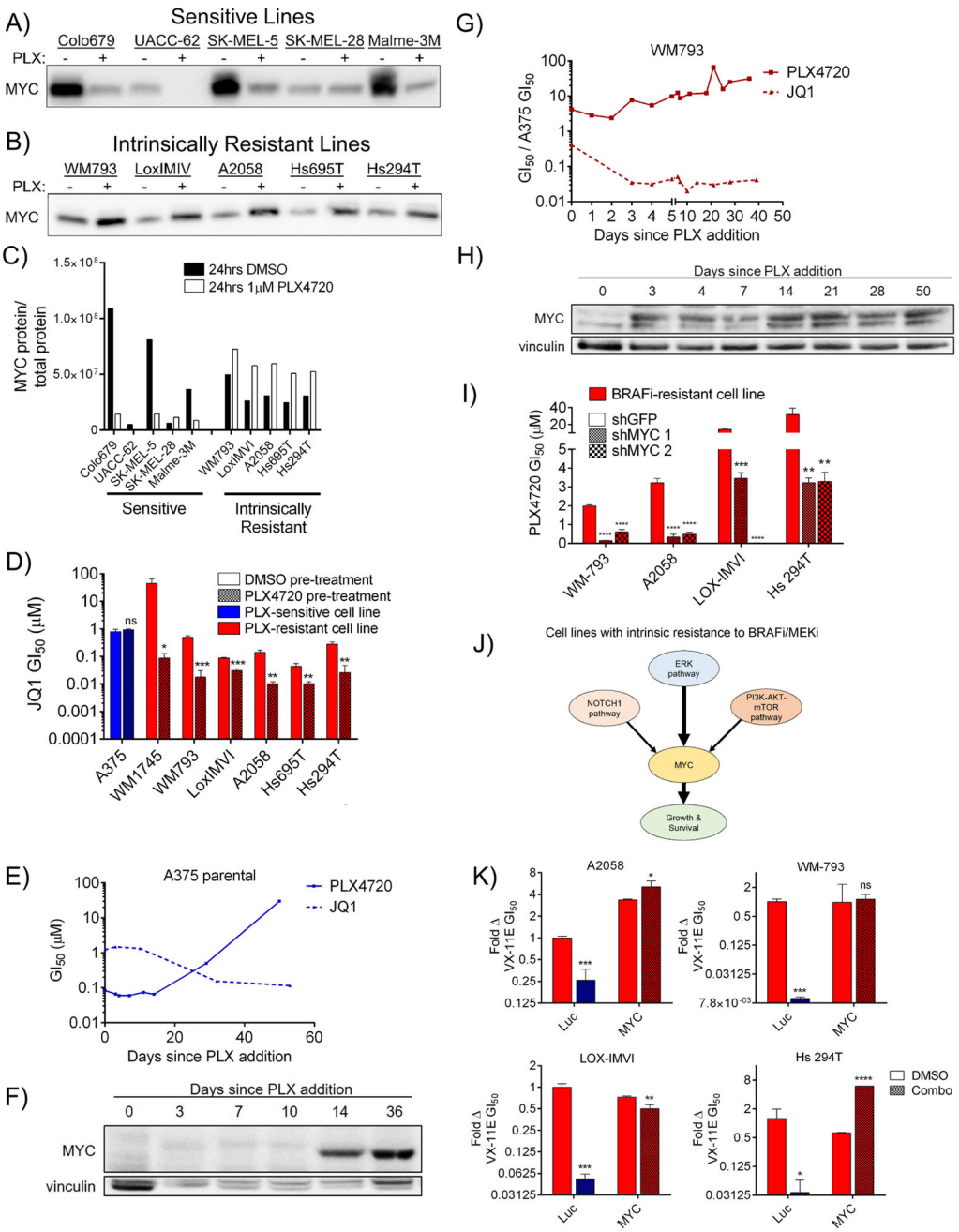

Combined BRAFi and MYC suppression delays the emergence of resistance in vitro and in vivo

The finding that multiple pathways converge to drive resistance through MYC suggests that pairing BRAFi/MEKi with MYC suppression may delay the emergence of resistance. To test this hypothesis, we stably expressed shRNAs against either MYC or a negative control (GFP) in A375 cells, then cultured the cells in 3μM PLX4720 with weekly counting until acquired resistance was observed, as indicated by the recovery of exponential growth. As in Figure 4-4E–F, cells expressing shGFP began proliferating in PLX4720 after three weeks, at which time they also began expressing MYC (Figures 4-5A and Supplemental Figure C-5A). In contrast, the growth of cells expressing shMYC in PLX4720 was delayed until week 6 of culture, despite the fact that these cells proliferated normally in the absence of drug (Figures 4-5A and Supplemental Figure C-5A). Given the possibility that clones with incomplete MYC knockdown could have been selected to drive resistance, we measured MYC expression over the experimental time course. Indeed, cells expressing shMYC began to exhibit high MYC expression around week 6, in concordance with their acquisition of exponential grow in PLX4720 (Figures 4-5A). To determine if these results could be extended to pharmacologic inhibition of MYC expression, we serially passaged A375 cells in PLX4720, JQ1, or the combination. Cells treated with JQ1 alone quickly regained nearly normal proliferation rates, while cells treated with the combination began proliferating at 7–9 weeks, not recovering a population size equal to that of initial seeding until 12 weeks (Figures 4-5B and Supplemental

Figure 4-5: MYC suppression delays the emergence of resistance to BRAF inhibition in vitro and in vivo. (A) Lines indicate cell numbers calculated from weekly measured growth of A375 cells expressing shGFP or shMYC and cultured in 3μM PLX4720 (left axis). Bars indicate quantification of MYC levels in extracts made at the indicated times normalized to β-actin levels (right axis). **(B)** Cell numbers calculated from growth rates of A375 cells cultured in 3 μM PLX4720, 100 nM JQ1, or the combination. **(C)** Immunoblot of MYC in cell lines generated in B), D) and F). **(D)** Cell numbers calculated from growth rates of A375-PLX+JQ1 dual resistant cells cultured in 3 μM PLX4720 or 100 nM JQ1 and 3 μM PLX4720. **(E)** GI50 values of cell lines generated in B) and D) treated with PLX4720 or JQ1. Quantification of MYC protein normalized to total protein and total protein staining is shown in Figure S5C. **(F)** Cell numbers calculated from growth rates of A375-PLX resistant cells cultured in 3 μM PLX4720 and 1 μM AZD6244 (MEKi), 100 nM JQ1, or the combination. **(G)** Growth of A375 xenograft tumors treated with vehicle, JQ1 (45 mg/kg/d), dabrafenib (Dab, 30 mg/kg/d) plus trametinib (Tram, 0.6 mg/kg/d), or the combination over time. Data shown are mean tumor volume +/− SEM, with n=6–8 mice per group. P values were calculated using the one-sided Mann-Whitney test, *p<0.05. **(H)** Waterfall plot showing tumor sizes in the indicated groups from panel G) on day 45 of treatment. For B) and F), dashed line indicates initial seeding number. All data are means (SD) from 3 experiments. *P < 0.05; **P < 0.01; ***P < 0.005; ****P < 0.001. See also Supplemental Figure C-5.

Figure 4-5 (continued)

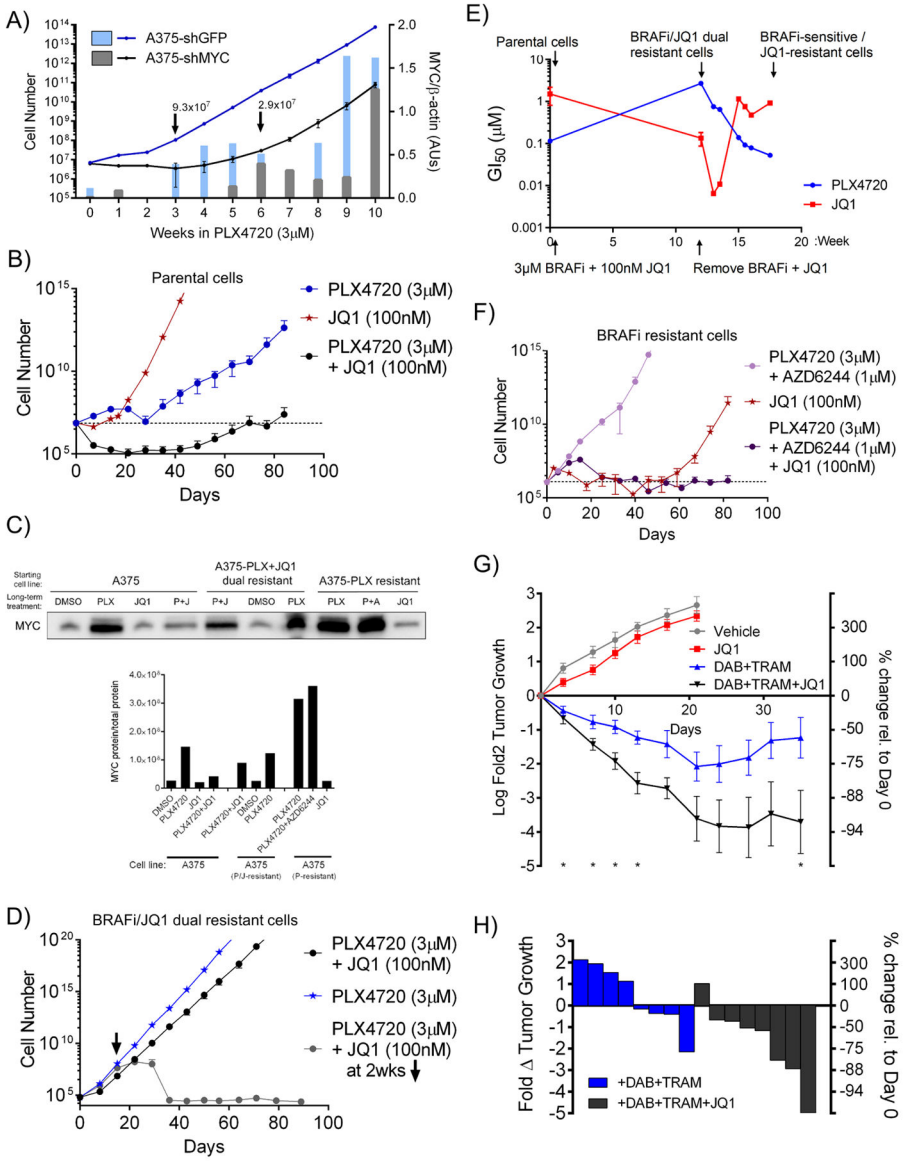

Figure C-5B). Further, as in the case of shRNA-mediated MYC suppression, cells that emerged with resistance to BRAFi + JQ1 escaped JQ1-mediated MYC suppression (Figure 4-5C and Supplemental C-5C). To investigate cells in the PLX4720+JQ1 dual resistant state ('dual cells'), we treated the dual cells with DMSO, PLX4720 or the combination of PLX4720 and JQ1, while measuring the cells' GI50 values to PLX4720 and JQ1 (Figures 4-5D–E). Once both drugs were removed, the population gradually shifted back to a BRAFi-sensitive, JQ1-resistant state (Figures 4-5E). By contrast, if JQ1 was reintroduced after a two-week holiday, cells could be resensitized to the combination, with no outgrowth of resistant clones over 12 weeks (Figure 4-5D). MYC protein expression was observed in the PLX4720-resistant populations and in the dual resistant cells, suggesting that the dual resistance arises through failure of JQ1 to durably inhibit MYC expression (Figure 4-5C and Supplemental Figure C-5C). PLX4720-resistant cells acquired resistance to the addition of a MEK inhibitor very quickly, although these cells' increased dependency on MYC led to eradication of cells when JQ1 was included in the combination (Figure 4-5F). Further, unlike parental cells, PLX4720-resistant cells were highly sensitive to JQ1 alone (Figure 4-5F). Both BRAFi- and BRAFi+MEKi-resistant cells exhibited high-level MYC expression, while those treated only with JQ1 lost both their BRAFi resistance and MYC expression (Figure 4-5C). These results demonstrate that MYC suppression is a viable strategy to delay resistance to BRAFi, and further, are consistent with the hypothesis that resistance evolution requires MYC activation. Although we were able to generate cells resistant to dual BRAF+MYC inhibition, this state was 1) highly unstable, 2) caused by failure of JQ1 to inhibit MYC expression, and 3) reversible with a short JQ1 drug holiday.

In order to investigate the relationship between MYC and resistance in vivo, we established xenografts from A375 cells in immunocompromised mice. After formation of a palpable tumor, mice were treated with either diluent control, the BRAFi/MEKi combination dabrafenib (BRAFi, 30 mg/kg/d) and trametinib (MEKi, 0.6 mg/kg/d), JQ1 (45 mg/kg/d), or the

combination of dabrafenib, trametinib and JQ1. While tumors were able to grow similarly to control in the presence of JQ1, their growth was inhibited by the combination of dabrafenib and trametinib, and substantial tumor regressions were observed when JQ1 was added to this combination (Figure 4-5G–H). Furthermore, while tumors treated with the dabrafenib/trametinib combination began increasing in size after approximately 20 days of treatment, the addition of JQ1 led to sustained tumor regression throughout the experimental time course (Figure 5G). To assess the ability of JQ1 to sensitize a BRAFi-resistant model to BRAFi+MEKi, we established xenografts using a cell line with intrinsic resistance to BRAFi, Hs695T. We observed substantial decreases in tumor size when JQ1 was added to the combination of dabrafenib and trametinib (Supplemental Figure C-5D).

MYC activation creates targetable vulnerabilities in resistant cells

The fact that BRAFi resistant cells exhibit increased MYC dependency suggests that synthetic lethal drugging strategies that target the MYC activated state may be selectively toxic to resistant cells. Numerous potential MYC synthetic lethal partners have been identified, but their applicability to melanomas is unclear given the tissue-specific nature of MYC-driven expression programs (Cermelli et al. 2014; Dang 2012). Therefore, to target MYC-driven resistance, we leveraged both unbiased and candidate-based methods. First, we screened a library of ~1700 bioactive compounds, including diverse targeted inhibitors, natural products, and chemotherapeutics, to identify those differentially lethal to PLX4720-resistant A375 cells relative to parental cells (Supplemental Table C-3). As expected, compounds targeting the ERK pathway were highly selective for sensitive cells (Figure 4-6A, $p < 10^{-12}$ by one-sided Kolmogorov-Smirnov (K-S) test). Conversely, resistant cells exhibited increased sensitivity to many compounds, including annotated inhibitors of SRC family kinases ($p = 2 \times 10^{-3}$), c-KIT ($p = 3 \times 10^{-4}$), the Hedgehog pathway ($p = 0.03$), and Aurora kinases ($p = 9 \times 10^{-6}$), the latter of which have been previously implicated as MYC synthetic lethal partners (Dang 2012; den

Hollander et al. 2010; Yang, Liu, et al. 2010) (Figure 4-6A and Supplemental Figure C-6A–D). Another interesting compound identified in the screen was Tigecycline, whose selectivity could be extended to several BRAFi-resistant models (Supplemental Figure C-6E). In parallel, we examined candidate MYC synthetic lethal partners previously identified in other cancer types using a panel of matched parental and BRAFi-resistant cells (Chipumuro et al. 2014; Goga et al. 2007; Martins et al. 2015; Toledo et al. 2011; Truman et al. 2012; Yang, Liu, et al. 2010). Of these candidates, the multi-targeted tyrosine kinase inhibitor, dasatinib, was selectively lethal in 6 out of 6 MYC-dependent, PLX4720-resistant clones relative to matched parental cells (Figures 4-6B and Supplemental Figure C-6F). Given that dasatinib inhibits SRC family and other kinases with nanomolar efficiency (Steinberg 2007), we examined this compound in greater detail. The combination of dasatinib and PLX4720 yielded an increase in apoptosis and synergistic growth inhibition in PLX4720-resistant cells (Figures 4-6C and Supplemental Figure C-6G). Further, by simultaneously targeting both sensitive and resistant cells using PLX4720 and dasatinib, respectively, it was possible to block the emergence of resistance in long-term culture (Figures 4-6D and Supplemental Figure C-6H). Dasatinib is estimated to have over 50 targets with an IC50 of 1 μM or less. In order to begin to elucidate the contributions of these targets to MYC synthetic lethality, we examined gene expression data for dasatinib targets (“das-genes”) in A375 parental cells, PLX4720-resistant A375 cells, and resistant A375 cells expressing a MYC-targeted shRNA. Twenty-eight of 71 das-genes were upregulated in resistant cells in a MYC-dependent fashion (Supplemental Table C-4 and Figure 4-6E). Among the agents in the screen of 1,700 small molecules, those targeting das-genes upregulated in MYC-active cells were enriched for selectivity against resistant cells ($p = 2 \times 10{-}6$), while compounds that inhibit non-upregulated das-genes showed no selectivity ($p = 1.0$) (Figure 4-6F). Together, these results: (1) identify families of compounds that selectively target MYC-activated, BRAFi-resistant melanoma cells, (2) identify dasatinib as a high priority polypharmacology-based strategy to target resistant cells, and (3) suggest that the protein products of das-genes with

Figure 6. The BRAF/MEK Inhibitor-Resistant, MYC-Activated State Is Associated with Targetable Vulnerabilities. Average differential viability between parental A375 and PLX4720-resistant A375 cells treated at 2 and 10 mM with each of a 1,753-member compound library. Compounds targeting SRC family members, c-KIT, and ERK pathway members are indicated. **(A)** Fold change in dasatinib GI50 values in the indicated PLX-resistant lines relative to matched parental lines. The p values indicate significance between parental and resistant derivatives. (**B)** Fold change compared with DMSO treatment in the annexin V+ cell population fraction in parental or resistant A375 cells treated with 1 mM PLX4720, 100 nM dasatinib, or the combination for 3 days. The p values indicate significance between each treatment and PLX4720 treatment alone. **(C)** Numbers of A375 cells over time during continuous culture in 3 mM PLX4720, 1 mM dasatinib, or the combination. Dashed line indicates initial seeding number. **(D)** Change in expression of dasatinib targets as measured by RNA sequencing (RNA-seq) in A375 parental cells, PLX4720-resistant A375 cells, and resistant cells expressing shMYC. The approximate IC50 of dasatinib for each target is shown. **(E)** Average differential viability between parental A375 and PLX4720-resistant A375 cells treated at 2 mM and 10 mM with each of a 1,753-member compound library. Compounds targeting dasatinib-target genes with differential expression in MYC-active versus non-MYC-active cells are indicated. **(F)** Change in expression of canonical MYC targets as measured by RNA-seqin A375 parental cells, PLX4720-resistant A375 cells, andresistantcells expressing shMYC. All data are mean (SD) from three experiments. *$p < 0.05$, **$p < 0.01$, ***$p < 0.005$, and ****$p < 0.001$. See also Figure S6 and Tables S3, S4, and S5.

Figure 4-6 (continued)

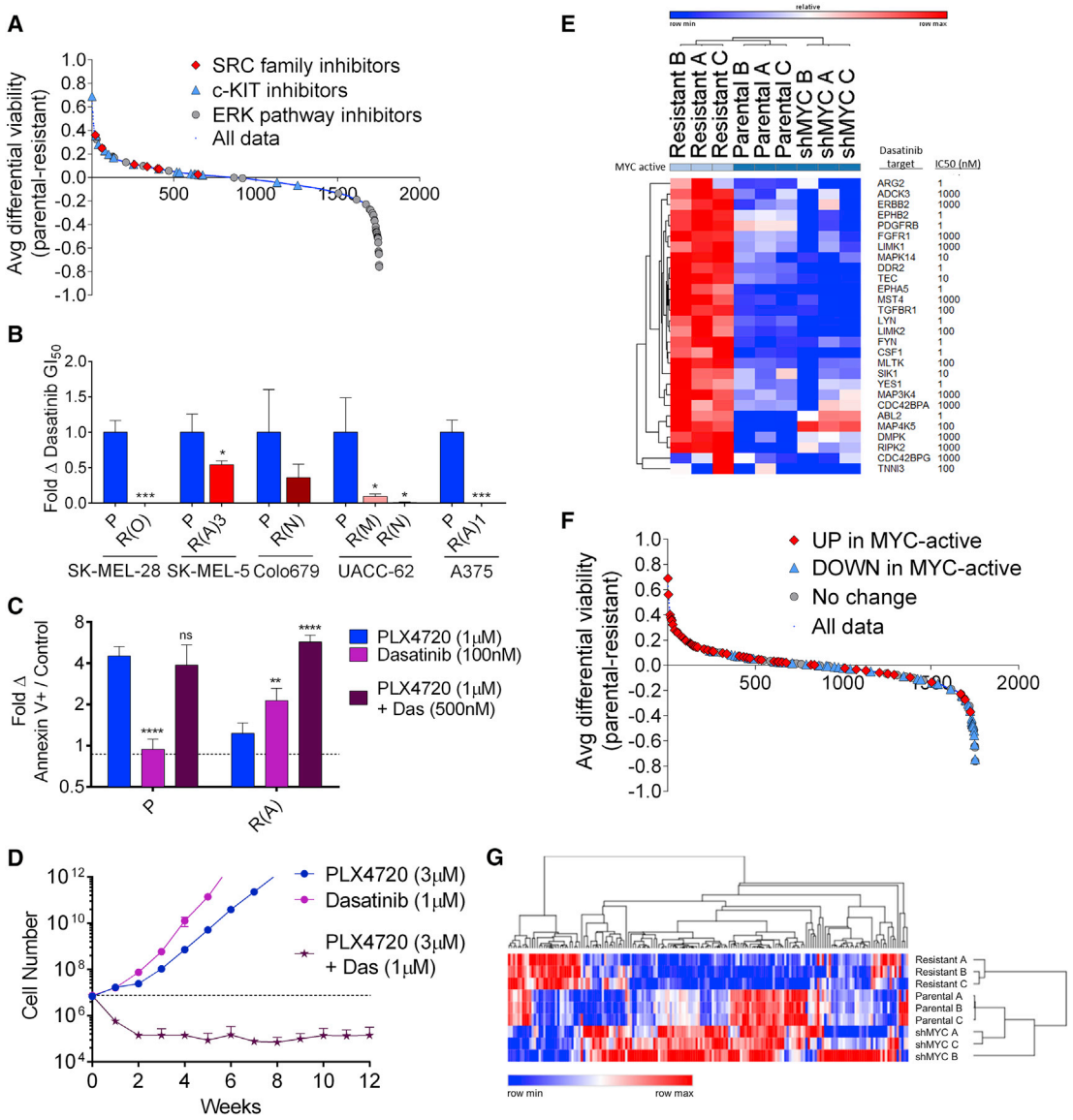

increased expression in MYC-activated cells, including LYN, ERBB2, and PDGFRB, warrant individual examination as potentially specific targets. Finally, to nominate additional candidate targets, we defined expression changes in genes that have been identified as canonical, direct MYC targets by combined ChIP-seq and gene expression analysis (Zeller et al. 2003). We examined the set of genes whose promotor is bound by MYC and whose expression is changed following MYC activation to identify those with changed expression in sensitive versus resistant cell lines. Parental and resistant-shMYC samples clustered together (Figure 4-6G), and the genes with increased or decreased expression in resistant cells relative to parental and resistant-shMYC cells are listed in Figure S6I. Expression changes for all MYC target genes are listed in Table S5, including those like the dasatinib target ERBB2 that are upregulated in a MYC-dependent fashion in resistant cells and may represent high-priority candidate therapeutic targets.

MYC activation in resistant cells creates targetable metabolic dependencies

A wide body of work has linked MYC activation, oncogenic progression, and cellular metabolic re-wiring (Stine et al. 2015). Further, our statistical analysis outlined in Figure 1 implicated several metabolic pathways as altered on progression (Supplemental Table C-1). To examine if MYC activation drives metabolic changes as cells develop BRAFi resistance, we performed integrated gene expression profiling, alongside metabolomics, in PLX4720-sensitive A375 cells expressing GFP-targeted shRNA (‘parental cells’), parental A375 cells expressing MYCT58A (‘MYCT58A cells’), PLX4720-resistant A375-shGFP (‘resistant cells’) and PLX4720-resistant A375-shMYC (‘shMYC cells’) (see Materials and Methods). Consistent with the concept that MYC drives global gene expression changes, unbiased hierarchical clustering of expression data showed that shMYC cells clustered more closely with parental cells than resistant, MYC activated cells (Supplemental Figure C-7A). Analysis of steady state metabolite levels using pathway enrichment revealed a diverse set of metabolic pathways altered in a

MYC-dependent fashion in resistant cells relative to parental cells, as evidenced by the fact that reciprocal changes between the resistant and shMYC cells were observed (Figure 4-7A). Of note were alterations in glycolysis, serine, and glutamine metabolism, each of which has been implicated in MYC-driven oncogenesis (Jin, Alesi, and Kang 2016; Pavlova and Thompson 2016; Stine et al. 2015). Glycolysis-related gene sets were enriched in BRAFi/MEKi-resistant cell lines and human patient tumors (Figure 4-7B), and we observed modest MYC-dependent (as well as MYC-independent) changes in the expression of key early glycolytic enzymes (e.g., hexokinase 2 (HK2)) and in the steady-state levels of glycolytic intermediates, in particular, lactate (Figures 4-7B and Supplemental Figure C-7B–D). Consistent with increases in lactate production, observed in a wide panel of parental and resistant derivative cell lines (Figure 4-7B, right panel), there was little change in the incorporation of 13C from glucose into citrate and other TCA cycle intermediates, indicating that the resistant cells are increasing aerobic glycolysis, similar to the switch away from anaerobic glycolysis observed during oncogenesis (Supplementary Figure C-7D). For serine synthesis, which occurs through oxidation of the glycolytic intermediate 3-phospho-D-glycerate (3PG), we observed enrichment of serine-synthesis related gene sets in resistant cell lines and human tumors, increased MYC-dependent expression of enzymes involved in the metabolism of serine into glycine to fuel one carbon metabolism in resistant cells, and corresponding MYC-dependent increases in 13C incorporation from glucose into serine, glycine and the purine precursor, IMP, in resistant cells (Figure 4-7C) (Locasale 2013). Lastly, glutaminolysis has been shown to be provide important biosynthetic precursors in cancer cells that are primarily performing aerobic glycolysis (Filipp et al. 2012). We observed increases in glutamine pathway gene sets in resistant cell lines and tumors, increased MYC-dependent expression of key enzymes in glutaminolysis and the TCA cycle, and increased MYC-dependent incorporation of 13C into glutamate, aspartate, duhydroorotate, UTP and TCA cycle intermediates in cells grown in 13C-glutamine (13C-gln) media (but not in 13C-glucose media), indicative of preferential use of glutamine to supply

Figure 4-7: MYC activation in BRAFi resistant cells induces changes in the activities and dependencies associated with targetable metabolic pathways. (A) Top scoring metabolic pathways (Metaboanalyst) enriched in either resistant A375-shGFP (R) relative to parental A375-shGFP (P) cells or enriched in R relative to resistant A375-shMYC (shM) cells. Pathways are ranked by impact score in the former comparison. **(B)** GSEA analysis (left) of differential gene expression in patient tumors and cell lines, in each case comparing resistant samples to their sensitive counterparts. Fold change (middle) in lactate levels in resistant and shMYC cells relative to parental. Fold change (right) in extracellular lactate in a panel of PLX-sensitive (blue) and PLX-resistant (red) cell lines normalized to cell number. **(C)** GSEA analysis as in B) (left). Fold change in mRNA transcript levels for the indicated serine metabolism genes in P, R and shM cells (middle). 13C-glucose incorporation in the indicated metabolites in P, R and shM cells cultured after 24 hours in 13C-glucose (13C-Glc) (right). **(D)** GSEA as in B) (upper left). Fold change in mRNA transcript levels for the indicated glutaminolysis pathways in P, R and shM cells (upper right). Relative abundance of 13C-glutamine (13C-Gln) for glutamate, aspartate and all TCA cycle intermediates (except citrate/isocitrate and dihydroorotate, m+4, and UTP, m+3) in P, R and shM cells cultured for 24 hours in 13C-Gln (lower left and right, respectively). **(E)** GI50 values in multiple cell line models treated with the glycolysis inhibitor, 2-deoxy-D-glucose. **(F)** GI50 values of lines treated with 5-FU. **(G)** GI50 values of lines treated BPTES. Data in E), F) and G) are means of 3 experiments. P values denote significance between parental and each of the resistant groups measured by ordinary one-way ANOVA. PLX4720-sensitive cell lines are in blue and resistant cell lines are in red. **(H)** Projected numbers of A375 cells over time during continuous culture in 3 μM PLX4720, 5 mM 2-DG, 10 μM BPTES, the double combinations, or the triple combination. **(I)** A375 cell numbers during continuous culture in 3 μM PLX4720 in either normal DMEM containing 4.5 g/L glucose and 2mM glutamine, DMEM containing 0.45 g/L glucose and 2 mM glutamine, DMEM containing 4.5 g/L glucose and 200 μM glutamine, or DMEM containing 0.45 g/L glucose and 200 μM glutamine. In H) and I), a dashed line indicates initial seeding number. **(J)** Fold change compared to DMSO in the annexin V+ cell population fraction in parental (P) or resistant (R(A)) A375 cells treated with 1 μM PLX4720, 1 mM 2-DG, 10 μM BPTES or the combinations for 3 days. P values are shown comparing each treatment to PLX4720 treatment. **(K)** Summary of metabolic changes found between P, R and shM cell lines. Red arrows indicate metabolic flux increased in resistant cells and returned to parental levels upon MYC knock down. NADPH: Nicotinamide adenine dinucleotide phosphate GSH: glutathione ATP: Adenosine triphosphate NADH: Nicotinamide adenine dinucleotide G6P: glucose-6-phosphate 3PG: 3-phospho-glycerate 3P pyruvate: 3-phospho-pyruvate 3P ser: 3-phospho-serine Ser: serine Gly: glycine Gln: glutamine Glu: glutamate α-KG: α-ketoglutarate. Relationships are derived from a combination of gene expression, metabolite levels and glucose and glutamine 13C isotope tracing data. All data except E), F) and G) are means (SD) from 3 experiments. *P < 0.05; **P < 0.01; ***P < 0.005; ****P < 0.001. See also Supplemental Figure C-7.

Figure 4-7 (continued)

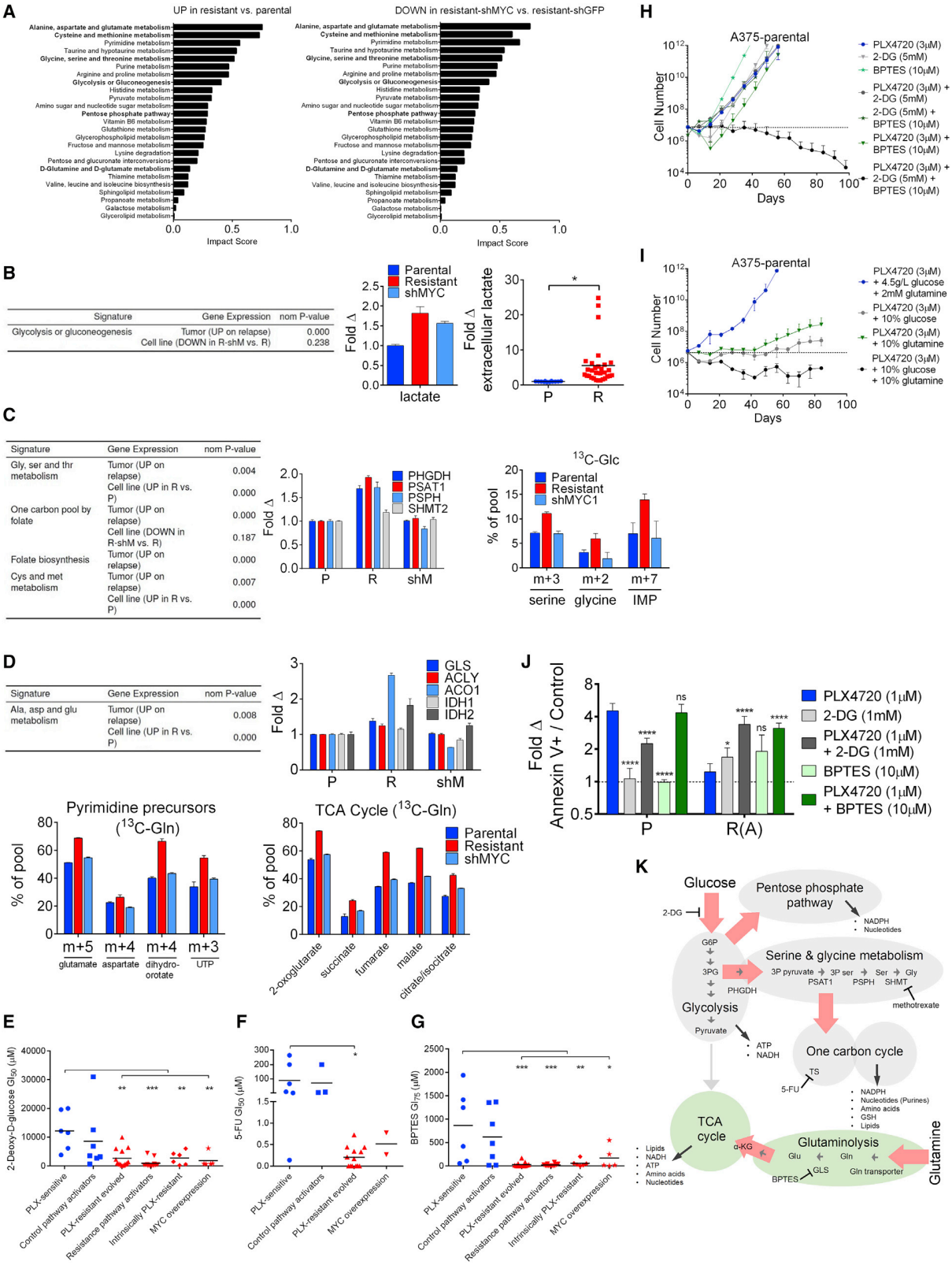

biosynthetic building blocks, particularly those for fatty acid synthesis and pyrimidine synthesis (Figures 4-7D and Supplemental Figure C-7D). Importantly, the increased activities of the glycolysis, serine, and glutamine pathways created new, MYC-dependent vulnerabilities, as diverse models of resistance were hypersensitive to the glycolysis inhibitor 2-deoxy-D-glucose (2-DG), the thymidylate synthase (TS) inhibitor fluorouracil (5-FU), the serine hydroxymethyltransferase (SHMT) inhibitor methotrexate, and the glutaminase inhibitor BPTES relative to sensitive cell lines (Figures 7E–G and S7E). We hypothesized that inhibition of these pathways may select against the development of resistance to BRAFi. For these experiments, we utilized BPTES and 2-DG, the latter of which was chosen for its potential to suppress both the glycolysis and serine pathways. While alone, 2-DG and BPTES treatment could delay resistance to PLX4720 by 1–2 weeks, their combination completely forestalled resistance (Figures 4-7H and Supplemental Figure C-7F). This finding, which could be phenocopied using media containing glucose and/or glutamine at 10% of their standard concentrations (Figure 4-7I and Supplemental Figure C-7G). At these concentrations, 2-DG, BPTES, and low glucose/glutamine media only modestly affected cell growth (Supplemental Figure C-7F–H). (Similarly delayed resistance was observed in cells treated with PLX4720 and low dose methotrexate (10nM) (Supplemental Figure C-7I).) Finally, the combination of 2DG and PLX4720 or BPTES and PLX4720 led to synergistic growth inhibition and apoptosis in PLX4720-resistant cells (Figures 4-7J and Supplemental Figure C-7J). MYC-dependent metabolic changes described here, and their associated targetable vulnerabilities, are summarized in Figure 4-7K.

DISCUSSION

The importance of MYC in tumorigenesis has long been appreciated, dating to its initial discovery through the investigation of oncogenic retroviruses (Sheiness, Fanshier, and Bishop 1978). One of the most commonly deregulated oncogenes, MYC's activity is tightly linked to

major oncogenic signaling pathways. For example, the ERK and PI3K pathways are believed to regulate MYC protein levels through direct modulation of protein stability, while MYC activation downstream of Notch1 occurs via transcriptional activation (Dang 2012; Palomero et al. 2006; Sears 2004). MYC activation is linked to therapeutic resistance, for example in breast cancer cells treated with PI3K pathway inhibitors and in c-Met-addicted cancers treated with c-Met inhibitors (Ilic et al. 2011; Muellner et al. 2011; Shen et al. 2015). In melanoma, our finding that MYC is a nexus of convergent resistance is consistent with a recent report that used network modeling to nominate MYC as a synergistic target with BRAF, then verified this finding by demonstrating synergy between JQ1 and vemurafenib treatment in a cell line (Korkut et al. 2015). Our findings are also interesting in light of a report suggesting that the eukaryotic initiation factor 4F (eIF4F) complex may act as a point of convergence between the ERK and PI3K resistance pathways in melanoma, as MYC and eIF4F interact in a well-characterized synthetic lethal feedforward loop to support tumorigenesis (Boussemart et al. 2014; Lin et al. 2008; Lin et al. 2012). The molecular mechanisms by which MYC is regulated by the major pathways of resistance in melanoma are therefore important areas for future study.

The finding that MYC is a convergent downstream effector of resistance in melanoma reconciles disparate observations from the literature. First, it provides a mechanistic explanation for the observation that diverse resistance pathways can lead to a phenotypically convergent state and clarifies why certain oncogenic pathways can drive resistance while others seemingly cannot (Hugo et al. 2015; Martz et al. 2014; Rizos et al. 2014). Second, the fact that MYC is regulated both transcriptionally and post-translationally, and its activation downstream of major resistance pathways does not require alteration of its genomic locus, provides an explanation for why it was not uncovered in previous, in-depth genomic investigations of therapeutic resistance (Hugo et al., 2015; Moriceau et al., 2015; Rizos et al., 2014; Shi et al., 2014b; Van Allen et al., 2014; Wagle et al., 2014). Third, the concept of MYC-driven convergent resistance

provides a rationale for the recent observations that cells with NRAS-driven resistance exhibit increased glutamine dependence and synergy between BRAF and glycolysis inhibition (Baenke et al. 2016; Hernandez-Davies et al. 2015; Parmenter et al. 2014). Finally, this work demonstrates that cells with intrinsic versus acquired resistance – which are driven by similar pathways (Martz et al., 2014) – are distinguished by their differential abilities to mobilize MYC following BRAF inhibition.

The data here reveal that as melanomas become resistant to BRAFi/MEKi, they become more dependent on MYC, suggesting that combination therapies that simultaneously target both states may have the unique property of selecting against resistance. The observation that combined BRAF/MEK/BET bromodomain inhibition exerts a more potent and durable effect in tumor models in vivo further supports this idea. Although BRD4/BET bromodomain targeting is one promising approach to block MYC activity, we also demonstrated that the MYC-dependent state in resistant melanomas can be targeted by exploiting other co-dependencies. However, it is clear that additional MYC synthetic lethal partners are likely to exist and may include regulators of transcription, nucleotide biosynthesis, the SUMOylation machinery, and the spliceosome, among other targets (Cunningham et al. 2014; Hsu et al. 2015; Kessler et al. 2012; Wang, Zhang, et al. 2015). Systematic studies to define and credential these MYC-dependent synthetic lethal partners in the specific context of BRAFi/MEKi-resistant melanoma are therefore warranted. Finally, it is tempting to speculate that other oncogene-driven cancers, including BRAF-driven non-melanoma tumors, may also exhibit convergent resistance to targeted therapy, and as such, this concept may provide a generalizable framework for designing robust therapies that select against resistance evolution.

METHODS

Statistical modeling of genomic data

See Extended Experimental Methods in Appendix C for details.

Cell lines

Malme-3M, WM793, WM1745, SK-MEL-28, Lox IMVI, Hs294T, A2058 and RPMI-7951 cell lines were obtained from L. Garraway (Harvard University, Dana-Farber Cancer Institute). All other cell lines were purchased from the American Type Culture Collection. All lines were submitted to STR profiling by the Duke University DNA Analysis Facility to confirm their authenticity. See Extended Experimental Methods in Appendix C for culture conditions.

Chemicals

2-Deoxy-D-glucose (2-DG) and BPTES were purchased from Sigma-Aldrich. JQ1 and dasatinib were purchased from Apexbio Technology (Houston, TX). BS-181 was purchased from MedChem Express (Monmouth Junction, NJ). All other inhibitors were purchased from Selleck Chemicals (Houston, TX). For stock preparations, see Extended Experimental Methods in Appendix C.

GI50 and sensitization assays

In order to measure the GI50 values of specific inhibitors and quantify the effect of resistance pathway inhibition on the sensitivity of cell lines to ERK pathway inhibition, small molecule sensitization assays were performed as previously described (Martz et al., 2014). For details, see Extended Experimental Methods in Appendix C.

Combinatorial index value calculation

In order to assess synergy, the GI50 value of each inhibitor in the indicated cell lines was determined. 5,000 cells were plated per well in 96-well cell culture plates. Twenty-four

hours later, the cells were treated with a 2-fold dilution series ranging from 4(GI50) to ¼(GI50) singly and in combination at a fixed ration of GI50 of inhibitor1: GI50 of inhibitor2. After 36 hours of treatment, cell viability relative to control was assessed and CI values were calculated according to the Chou and Talalay method (Chou and Talalay 1984), using CompuSyn software (ComboSyn, Inc., Paramus, NJ).

Immunoblotting

To measure protein levels, aliquots of cell extracts prepared in lysis buffer (see Extended Experimental Methods in Appendix C) were submitted to SDS-PAGE. After electrophoretic transfer to PDMF, filters were blocked in 5% BSA and probed overnight at 4°C with primary antibodies (see Extended Experimental Methods in Appendix C). After washing in TBS-T, filters were incubated for 1 hour at room temperature with alkaline phosphatase-coupled goat anti-rabbit antibodies (Santa Cruz) and developed with Western Lightning Plus (Perkin Elmer, Inc., Waltham, MA).

Immunohistochemistry Staining

Melanoma patient samples (paraffin embedded slices) were obtained from Harvard (Dennie Frederick) and were then sent to the Duke Pathology Research Immunohistology Lab for c-MYC (Abcam 32072) staining. Samples were then sent to a pathologist (Shannon McCall) to be scored for nuclear c-MYC. Scoring was performed blinded to the staging of the samples.

Lentivirus preparation and DNA constructs

All expression clones were prepared in lentiviral form as previously described (Martz et al., 2014). See Extended Experimental Methods in Appendix C.

In vitro adaption of inhibitor resistant cells

PLX4720 or VX-11E-resistant cell lines were produced by 1 of 2 methods as previously described (Martz et al., 2014). See Extended Experimental Methods in Appendix C.

Clonogenic growth assay

To measure the ability of cell lines to form colonies from a single cell, clonogenic growth assays were performed as previously described (Singleton et al. 2015). Briefly, 100 cells were seeded per well in 12-well plates. After 24 hours, the indicated treatments were added and the assay was incubated for 14 days with the addition of fresh media and inhibitors after 7 days. Cells were fixed and stained with 0.5% (w/v) crystal violet in 6.0% (v/v) glutaraldehyde (Thermo Fisher Scientific, Waltham, MA).

Time to progression assay

To evaluate the relative ability of treatments to delay the reemergence of logarithmic cell growth in vitro (i.e. resistance), cells were plated in triplicate in 15 cm plates at 3,000,000 cells per plate in normal growth media. After 24 hours, the growth media was replaced with the indicated treatment. Seven days later, the cells were lifted with 0.25% trypsin (Life Technologies) and counted using a Z2 Coulter Particle Count and Size Analyzer (Beckman Coulter, Pasadena, CA). All cells up to 3,000,000 were centrifuged at 1200 RPM for 5 minutes and resuspended in 1 mL of media and then plated in a 15 cm plate with fresh treatment. This procedure was repeated weekly for 8–20 weeks, depending on the kinetics of resistance. Weekly growth rates (μ) were calculated from the number of cells plated the previous week (N0) and the number counted the current week (N) according to the formula:

$$\ln N = \ln N0 + \mu.t$$

where t = elapsed time or 168 hours. These growth rates were then used to project total cell number as if no cells had been discarded.

Annexin V apoptosis assay

The induction of apoptosis was quantified as described previously (Martz et al., 2014). See Extended Experimental Methods in Appendix C.

Xenograft model

Animal procedures were approved by the Center for Animal and Comparative Medicine in Harvard Medical School in accordance with the NIH Guild for Care and Use of Laboratory Animals and the Animal Welfare Act. Nude mice were inoculated subcutaneously with 3 × 106 human melanoma A375 or Hs695T cells in 200 µL PBS. Tumor volumes were measure twice a week and calculated with the formula [(length) × (width)2 × 0.52]. Once tumor volume reached ~300 mm3, mice were randomly divided into treatment groups and treated daily with BET inhibitor, JQ1 [45 mg/kg/day, intraperitoneal (i.p.) injection]; MEK inhibitor, GSK1120212 [0.6 mg/kg/day, oral gavage (o.g.)] and BRAF inhibitor, GSK2118436 (30mg/kg/day, o.g.); or a combination of JQ1, GSK1120212, and GSK2118436. Mice were treated daily for up to 45 days.

RNA extraction and quantitative real-time PCR

The total RNA of cells was isolated with QIAshredder Homogenizers and the RNEasy Mini kit (Qiagen) according to the manufacture's instruction after a 72-hr treatment with DMSO or 1µM PLX4720. cDNA was then synthesized from 1µg RNA using iScript cDNA Synthesis kit (BioRad). Quantitative real-time PCR was conducted with iQ SYBR Green Supermix and a CFX384 Touch Real-Time PCR Detection System (BioRad). For PCR primers and conditions, see Extended Experimental Methods in Appendix C.

Gene expression analysis

RNA was isolated from whole cells with QIAshredder Homogenizers and the RNEasy Mini kit (Qiagen). RNA integrity was confirmed with an Agilent 2100 Bioanalyzer (Agilent Technologies, Inc., Santa Clara, CA). RNA [20ng/μL] was submitted to the Duke University Sequencing and Genomic Technologies Core Facility. For sequencing conditions and data processing details, see Extended Experimental Methods in Appendix C.

Patient tumor samples

Serial tumor and blood samples were collected from male and female adult patients with Stage IV BRAF mutant melanoma under an IRB approved protocol at the Massachusetts General Hospital (DFHCC 11-181; PI: Boland). Patients were treated with combined BRAF + MEK inhibition. All patients provided written consent for both tissue acquisition and analysis, including all analyses performed in this study.

Metabolomics analysis

Cells were seeded in 6-well plates at an initial seeding density such that 1×106 cells would be harvested after 48 hours in culture. After 24-hrs growth, cells were rinsed with PBS and RPMI-1640 (Life Technologies), RPMI-1640 with 1g/L D-glucose 13C6 (Cambridge Isotope Laboratories, Inc., Tewksbury, MA) or RPMI-1640 with 300mg/L L-glutamine 13C5 (Sigma-Aldridge) was added in triplicate. After 24 hours, cells were harvested in 80% methanol. Cell extracts were pelleted and dried by speed vacuum. Metabolomics study was performed on liquid chromatography-high resolution mass spectrometer (LC-HRMS) Q Exactive plus (Liu, Ser, and Locasale 2014). The peak area was used to present relative abundance and to calculate the isotopologue distribution. The natural abundance correction was done based on previously published method (Yuan, Bennett, and Rabinowitz 2008).

Chemical Screen

A375 cells or a PLX4720-resistant A375 derivative were plated into a 384 well-plate (Corning 3707) at 200 cells/well using an automated liquid dispenser (BioTek EL406). The next day, 50 nL of bioactive compounds in DMSO were added to the assay plate via pin transfer to give a final compound concentration of 10 and 2 μM, respectively. Three days after compound treatment, cell viability was measured with CellTiter-Glo (Promega). Luminescence values were obtained using a multimode plate reader, and percent viability was calculated by comparison to DMSO-treated cells.

Statistics

All results are shown as means±SD. Unless noted otherwise, P values were determined using unpaired, two-tailed Student's t tests. Unless otherwise noted, n=3 independent, biological replicates.

Acknowledgements

We thank Ashwini Jambhekar for critical reading of the manuscript. We thank the members of the Y.S. lab for discussion, Andres Blanco and Andrew Elia for performing experiments that were not included in the final manuscript, and Sebastian Dango and Benoıˆt Laurent for experimental advice. We thank Luciano Di Croce and Malte Beringer for data and antibody sharing and discussion.

This work is supported by the National Cancer Institute (R01 CA118487) toY.S. and the German Research Foundation (DFG, LI 2057/1-1) to R.L. Y.S. is an American Cancer Society Research Professor. Y.S. is a co-founder of Constellation Pharmaceuticals, Inc. and a member of its scientific advisory board.

Chapter 5 : Conclusions and Future Directions

SUMMARY

The goal of my thesis work has been to identify novel combination therapies for patients with Ras pathway-driven cutaneous melanomas. Despite recent advances in therapies for these patients, the current standard of care is often not curative, and thus there is an unmet clinical need for more effective therapies.

In Chapter 2, I identified combined USP7 and Ras/ERK pathway inhibition as a novel targeted treatment regimen for *NRAS*- and *BRAF*-mutant melanomas. Importantly, this therapeutic combination has the potential to be translated to patients, as USP7 inhibitors are currently in development at several biotech companies. Through transcriptional and epigenetic analyses, we show that the mechanism of action is through the deregulation of USP7-EPOP-ELOB/C complexes, which regulate H2B ubiquitination. Moreover, loss of either USP7 or EPOP triggers an increase in RNA and protein expression of CABLES1, a tumor suppressing protein that stabilizes p53 family proteins. Interestingly, GSEA analysis of our RNA sequencing data revealed that p63 and p53 transcriptional targets increase in response to USP7 and MEK inhibitors, even in *TP53*-mutant cell lines. P63 and p73 have both been shown to transcriptionally regulate p53 targets, and therefore, we hypothesize that CABLES1 causes apoptosis in melanomas through p63 and/or p73 stabilization. Importantly, we have shown that USP7/MEK inhibitors cause an increase in p63 and p73 protein levels. Ongoing functional genomic studies investigating the effects of p63 and p73 ablation will determine if they are in fact mediating these effects. Nevertheless, we have shown that USP7 critically regulates USP7-EPOP-ELOB/C complexes, H2Bub, and the expression of the CABLES1 tumor suppressor, which is required for cell death.

In Chapter 3, we show that genetic and chemical inhibition of HDAC3 potently cooperates with Ras/ERK pathway inhibition in *BRAF-, NRAS-,* and *NF1*-mutant melanomas. Specifically, we found that entinostat, which inhibits HDAC1 and HDAC3, synergizes with

Ras/ERK pathway inhibitors, causing apoptosis to occur and profound tumor regression in multiple mouse models of melanoma. Additionally, we identified *MGMT* expression as a biomarker that predicts sensitivity to Ras/ERK pathway and HDAC1/3 inhibition. Because *MGMT* expression is already used in clinical practice as a predictive biomarker for treatment response in glioblastoma, this preexisting clinical test can be readily implemented to select melanoma patients for clinical trials. Interestingly, *MGMT*-expressing melanomas that respond to Ras/ERK pathway and HDAC1/3 inhibition exhibit broad defects in DNA repair genes, and the combination therapy cooperates by inducing irreparable DNA damage due to coordinated suppression of HR and NHEJ repair pathways.

In Chapter 4, we found through statistical modeling of genomic *BRAF*-mutant melanoma patient data that major pathways of BRAF and MEK inhibitor resistance converge to activate the transcription factor *MYC*, and that *MYC* activation is necessary and sufficient for resistance. The combination of Ras/ERK pathway and BET inhibition suppressed *MYC* expression and caused profound tumor regression in two xenograft models of *BRAF*-mutant melanomas. Additionally, we found that Ras/ERK pathway inhibitor resistant melanomas with *MYC* activation are also sensitive to suppression of targetable metabolic pathways, such as glycolysis, serine, and glutamine pathways.

In conclusion, this thesis (1) describes a novel unbiased negative-selection genome-scale CRISPR-Cas9 screen that identifies dependencies in *NRAS*-mutant melanomas, (2) provides a strong base of evidence for pursuing Ras/ERK pathway and USP7, HDAC3, or BET inhibition in three types of Ras pathway-driven melanomas, and (3) explores important transcriptional nodes and dependencies in melanoma. From this work, I hope that further clinical investigation of these three combination therapies will continue, particularly in *NRAS*-mutant melanomas where there is an urgent need for more effective therapies.

DISCUSSION

CRISPR-Cas9 screens to identify synthetic lethal drug targets

In Chapter 2, we performed a negative selection, genome-scale CRISPR-Cas9 screen using a strategy that differs from other previously published screens. To enrich for hits that are outside of the Ras/ERK pathway, we used a predetermined cytostatic dose of the MEK inhibitor trametinib instead of a dose based on IC50 results. Previously published screens typically determine their screen dose based on IC50 study results, not through cell proliferation assays that directly visualize cell death. In these circumstances, incomplete inhibition or over-inhibition of the Ras/ERK pathway (which can trigger feedback activation) often results in the identification of hits that are primarily components of the Ras/ERK pathway. Dr. Ryan Corcoran highlighted this issue in a public seminar hosted by The Society of Translational Oncology, where he showed results from an unpublished screen in *KRAS*-mutant colorectal cancer performed by his lab (Corcoran 2019). In this study, his laboratory used a high dose of the MEK inhibitor AZD6244 and found that aberrant pathway feedback occurred, leading to an increase in phosphorylated ERK after a few days of treatment. After performing a negative selection screen with this dose of AZD6244, the most significantly depleted hits were all within the Ras/ERK pathway. Therefore, we sought to avoid this issue by using a minimal cytostatic dose of the MEK inhibitor trametinib and by making sure that sufficient suppression of phosphorylated ERK occurred during the four days of treatment.

Additionally, we shortened the treatment time within our screen to four days instead of extending the study to allow many cell population doublings so that we would specifically enrich for cytotoxic, and not cytostatic, hits. Previous work from our lab has found that three to four days of treatment is sufficient to observe a cytotoxic effect in melanoma cell lines *in vitro* (Maertens et al. 2019). Additionally, we believe that treating cells for a longer time period selects

for both cytostatic and cytotoxic targets because cytostatic targets will continue to drop out over time when compared to targets that do not affect cell proliferation. Therefore, we believe that these longer studies will increase the identification of false-positive hits that do not actually cause cell death. We believe that this point is particularly important because therapies that induce cytotoxic rather than cytostatic responses are likely to be more effective in the clinic.

There are additional challenges that remain with any negative selection whole genome CRISPR-Cas9 screen, despite the efficiency of many CRISPR systems, and we addressed these challenges through further validation of our hits (Yin, Xue, and Anderson 2019). First, despite improved sgRNA design, libraries still have off-target effects, and in this way, false-positives emerge. We mitigated this by validating any screen hits and were able to successfully validate many of our top hits, including the positive controls RAF1 and BRAF. Secondly, aberrant genomic copy number can cause false-positive results in CRISPR screening studies. For example, a number of labs have found that sgRNAs targeting amplified genes can lead to replication stress and G2-M cell cycle arrest, likely owing to excessive DNA damage induced by CRISPR cutting (Sheel and Xue 2016; Aguirre et al. 2016; Munoz et al. 2016). To address this concern, we verified that any hit identified in our screen was not amplified in our cell line. Lastly, another shortcoming of genome-wide CRISPR-Cas9 screens is that CRISPR-mediated targeting of exons encoding functional protein domains can increase the occurrence of null mutations, therefore decreasing the likelihood of functional gene disruption (Shi et al. 2015). We addressed this concern by thoroughly validating our hits with additional CRISPR guides, shRNA, siRNA, and chemical perturbation.

Finally, the cell line that we chose for the screen, SKMEL2, has previously been shown to have defects in genes important for homology-directed repair (Maertens et al. 2019). Because of this, we hypothesize that we will have improved knock-out of CRISPR targets in our screen, and therefore, this will also mitigate some of the off-target effects highlighted in this

section. It should also be noted that our goal was to perform a rigorous genomic screen in one cell line, and then confirm hits in a panel of cell lines. Based on all of the combinatorial therapeutic studies that our laboratory has conducted in many different tumor types, any given therapeutic combination tends only to be effective in 30-60% of the cell lines. Our goal was to identify a combination and then confirm efficacy in at least 50% of genetically defined cell lines (e.g. *NRAS*-mutant). This goal was achieved and surpassed. We believe that this strategy was more cost-effective and perhaps superior than performing a screen with multiple cell lines, which would have likely eliminated many important hits due to this heterogeneity.

In conclusion, through informed screen design and further validation of screen hits, pooled CRISPR-Cas9 negative selection screens are indeed powerful tools to identify drug targets that cause cell death with other drugs that, on their own, only cause a cytostatic effect.

Novel combination therapies for* NRAS*-mutant melanomas

Treatment of *NRAS*-mutant melanoma is challenging because NRAS-GTPase is difficult to target directly and efforts to inhibit its downstream pathways are limited by feedback activation of the Ras/ERK pathway as well as parallel pathways such as the PI3K/AKT pathway. Therefore, compared to *BRAF*-mutant melanomas, there is an unmet need for new therapies that potentiate the effect of MEK inhibition in *NRAS*-mutant melanomas. In this thesis, we identified three novel combination therapies that are clinically relevant to *NRAS*-mutant melanomas. Exclusively considering *NRAS*-mutant melanomas, in Chapter 2, we demonstrated that combined USP7 and MEK inhibition is efficacious in six different *NRAS*-mutant melanoma cell lines, and that tumor regression is observed *in vivo* with no apparent toxicities in two different *NRAS*-mutant xenograft mouse models. Additionally, with our CRISPR-Cas9 screen, we identified other hits that cooperate with MEK inhibitors, which I will highlight briefly in the future directions section of this thesis. In Chapter 3, we found that combined HDAC and MEK

inhibition is efficacious in *NRAS*-mutant melanoma cell lines and xenograft models. Finally, in Chapter 4, though we did not explore whether MYC-driven convergent resistance occurs in *NRAS*-mutant melanomas in our publication, previous studies have found that cells with *NRAS*-driven resistance to Ras/ERK pathway inhibitors exhibit increased glutamine dependence and synergy between BRAF and glycolysis inhibition (Parmenter et al. 2014; Rao et al. 2016; Kimmelman 2015). Therefore, we hypothesize that *NRAS*-mutant melanomas may inherently be sensitive to the combination of MEK and BET inhibitors. In fact, in the future directions section of this thesis, I briefly summarize unpublished results where I found that MEK and BET inhibitors do cooperate to induce potent cell death and tumor regression in *NRAS*-mutant melanomas. Overall, these three chapters highlight exciting combination therapies for clinical development for *NRAS*-mutant melanomas.

USP7 loss may lead to stabilization of p63 and p73 through CABLES1

In Chapter 2, to identify the mechanism of action of USP7 inhibition, we performed a global transcriptional analysis and found that loss of USP7 causes an upregulation of p63 and p53 transcriptional targets. Additionally, we performed USP7 ChIP sequencing to identify where USP7 binds in the genome and whether this correlates with genes that are upregulated with USP7 perturbation. Interestingly, we found that *CABLES1*, which stabilizes p53 family proteins p63 and p73, was upregulated with USP7 perturbation and was additionally bound by USP7 at the promoter region in control cells. CABLES1, also known as ik3-1, has been shown to stabilize p63 and p73, preventing them from proteasomal degradation (Wang et al. 2010; Tsuji et al. 2002). For example, CABLES1 directly stabilizes TAp63 during genotoxic stress after ionizing radiation exposure in mouse oocyte cells (Wang et al. 2010). CABLES1 is frequently lost in cancer, and Cables1$^{-/-}$ mice have an increased incidence of endometrial cancer (Dong et al. 2003; Zukerberg et al. 2004; Tan et al. 2003; Park et al. 2007). *CABLES1* has also been shown to act as a tumor suppressor by inhibiting intestinal tumor progression in Apc^{Min} mice

(Arnason et al. 2013). Importantly, I found that *CABLES1* suppression rescued cell death in response to combined MEK and USP7 inhibition in *NRAS*-mutant melanoma cell lines, revealing an unappreciated role for CABLES1 in melanoma.

While USP7 regulates MDM2 stability in other settings, we have shown that the effects of USP7 inhibition in this therapeutic context are p53 independent. First, three cell lines (SKMEL2 [*NRAS*-mutant], MM485 [*NRAS*-mutant], and SKMEL28 [*BRAF*-mutant]) that respond to the combination of Ras/ERK pathway and USP7 inhibition are either *TP53*-mutant or do not express *TP53*. Secondly, when we knock down *TP53* with siRNA, we still observe cell death in response to combined USP7 and MEK inhibitors in *NRAS*- and *BRAF*-mutant cell lines. Finally, disruption of the MDM2-p53 interaction using nutlin-3a does not phenocopy USP7 inhibition, further demonstrating that the observed cell death from USP7 and MEK inhibition is not due to effects of USP7 on the MDM2/p53 axis.

Accordingly, we hypothesize that CABLES1 stabilizes p63 and/or p73 proteins in response to combined USP7/MEK inhibition. The activation of p63 is further supported by GSEA analysis of our RNA-sequencing studies. P63, p53, and p73 contain similar protein domains, including an N-terminal transactivation (TA) domain, a central DNA-binding domain (DBD), and an oligomerization domain (OD) (DeYoung and Ellisen 2007). The highest degree of homology among the three proteins are observed within the DBD, with a 60% amino-acid (AA) identity between p53 and both p63 and p73, and a 85% AA identity between p63 and p73, including conservation of all essential DNA contact residues (De Laurenzi and Melino 2000). All three members of the p53 gene family give rise to multiple protein products resulting from alternative promoter usage and mRNA splicing. For p63 and p73, TAp63 and TAp73 isoforms are capable of transactivating subsets of p53-regulated genes involved in cell-cycle arrest and apoptosis as well as gene sets independent of p53 targets (Zhu et al. 1998; Dohn, Zhang, and Chen 2001;

Harms, Nozell, and Chen 2004). In contrast, ΔNp73 and ΔNp63 isoforms can sometimes act as dominant negatives of TAp63 and TAp73, inhibiting these proteins.

Notably, the p53 and p63 transcriptional target genes that are up-regulated by USP7 and MEK inhibition in our *NRAS*-mutant cell line are all associated with the tumor suppressive functions of p53 and p63. For example, three prominent p53-regulated targets that are up-regulated are the pro-apoptotic genes *BIK, PERP,* and *BCL2L11*. In other cancers, similar findings have been observed – for example, in uveal melanoma, p63 has been found to induce PERP-mediated apoptosis (Awais et al. 2016). Additionally, *TP53* upregulation and subsequent transcriptional activation of p53-regulated pro-apoptotic genes have been found to cooperate with MEK inhibition in *NRAS*-mutant melanomas (Najem et al. 2017). Therefore, we hypothesize that CABLES1 is stabilizing the tumor suppressive isoforms of p63 and/or p73, and that these isoforms are transcriptionally regulating p53 targets. Our data demonstrate that total p63 and p73 protein levels increase after USP7 and MEK inhibition. We are now teasing out the effect of CABLES1 upregulation on the tumor suppressive isoforms of p63 and p73 specifically. If true, these studies will reveal a new mechanism by which USP7 regulates other p53 family proteins. This is especially interesting because USP7 inhibitors have been found to reduce cell viability in *TP53*-mutant cancers in other studies, and thus our study may demonstrate how this might occur (Tavana, Sun, and Gu 2018; Wang et al. 2017).

If USP7 inhibition increases *CABLES1* expression and causes the subsequent stabilization of p63 and/ or p73, then why does this sensitize melanoma cells to Ras/ERK pathway inhibitors? The presence of genotoxic stress in cells has been shown to correlate with increased phosphorylation of p63, preventing its ubiquitination and degradation by the proteasome (Li, Zhou, and Chen 2008). Increased stabilization then leads to apoptosis and cell death. Interestingly, previous work in the Cichowski lab has demonstrated that melanomas exhibit unconventional defects in DNA repair, and Ras/ERK pathway inhibitors further contribute

to this by reducing the expression of several key homologous repair and BRCA pathway genes, triggering a “BRCA-like” state (Lord and Ashworth 2016; Maertens et al. 2019). Therefore, I hypothesize that Ras/ERK pathway inhibitors increase genotoxic stress in melanoma cells, and that USP7 inhibitors, by further stabilizing p63, contribute to further activation of apoptotic pathways, leading to irreversible cell death. However, more studies are needed to further elucidate this vulnerability.

Identifying and targeting epigenetic regulators in melanoma

Overall, my thesis highlights three exciting therapeutic strategies that combine the current standard of care for melanomas (Ras/ERK pathway inhibitors) with agents that target transcriptional nodes important for melanoma. This further emphasizes the promise of targeting epigenetic regulators in melanomas and other Ras-driven malignancies. As mentioned in my introduction, epigenetic dysregulation occurs in melanoma and has been found to drive tumor progression. For example, work using zebrafish models to study melanoma initiation identified that some melanoma progenitor cells may be epigenetically primed to be cancerous (Kaufman et al. 2016). MEK inhibition has been associated with epigenetic reprogramming in melanomas, with inhibition resulting in widespread SOX10 recruitment through the genome, increasing melanocyte lineage specific and pigmentation genes and potentially contributing to MEK inhibitor resistance (Fufa et al. 2019). Mutations in epigenetic regulators have been observed in melanoma as well, further highlighting the importance of studying and potentially targeting the epigenetic landscape. Recently, activating mutations within the SET domain of the histone methyl transferase G9a were identified and found to lead to repression of a negative regulator of the WNT pathway (Kato et al. 2020). In my thesis, I focus on three targets that also affect the epigenetic landscape of melanoma, contributing to resistance to Ras/ERK pathway inhibitors.

Although many oncogenes are frequently mutated and activated in melanoma, we and others have found that targeting their associated downstream pathways does not necessarily lead to cell death. Therefore, identifying and targeting nodes that are synthetic lethal with inhibitors of oncogenic pathways is critical. This concept is known as “non-oncogene addiction,” in that the tumorigenic state depends on the activities of a wide variety of genes and pathways, many of which are not inherently oncogenic themselves (Luo, Solimini, and Elledge 2009). BRD4, HDAC3, and USP7 are all genes that are expressed in both melanoma cells and normal cells and targeting these three proteins individually does not kill cells. However, when combined with Ras/ERK pathway inhibitors, BRD4, HDAC3, or USP7 inhibition cooperate to cause potent cell death through stress overload. In the case of USP7 inhibitors, they target pro-survival pathways important for tumorigenesis. HDAC3 inhibition increases DNA damage stress by inhibiting proteins important for NHEJ, which then cooperates with HR dysregulation caused by Ras/ERK pathway inhibitors. Finally, BRD4 inhibition targets MYC and inhibits alternative metabolic pathways important for melanoma growth and escape from Ras/ERK pathway inhibitors.

FUTURE DIRECTIONS

Clinical outlook

Despite the existence of clinical trials investigating the combination of Ras/ERK pathway inhibitors with other small molecule therapies, I believe there still is an unmet need for new combination therapies to enter the clinic, especially therapies for which biomarkers exist. Additionally, preliminary data from some of the current combination therapy clinical trials, such as the combination of MEK and CDK4/6 inhibitors, is not promising, with many patients still not responding to these combination therapies. Out of the three combination therapies highlighted in this thesis, the combination of Ras/ERK pathway inhibitor and HDAC inhibitors could be the

most straightforward to translate as 1) HDAC inhibitors are approved for other indications and 2) we identified a clear biomarker, *MGMT* expression, which already is used in the clinic to identify treatment-resistant glioblastomas. The existence of a biomarker will make clinical trials easier to organize. Additionally, a common reason for failure of clinical trials is the lack of a clear biomarker, which we would be able to avoid (Townsend and Arron 2016). It should be noted that while we emphasized entinostat in our study, we also showed that pan-HDAC inhibitors were also very effective. Because entinostat is no longer being developed, these broader HDAC inhibitors could be tested instead in the clinic. In addition, in the course of this work, we also showed that PARP and MEK inhibitors are effective in these melanomas, and this therapeutic combination could also be developed into a clinical trial.

The combination of Ras/ERK pathway inhibitors and BET inhibitors additionally represent a promising clinical option, as there are currently BET inhibitors in clinical trials as single agents, which I summarized in the introduction of this thesis. Notably, we have initiated trials combining AZD6244 and AZD5153 (MEK/BETi) with our clinical collaborators and AstraZeneca in another tumor type. Therefore, the tolerability and initial efficacy of this combination may be known soon. Finally, the combination of USP7 and Ras/ERK pathway inhibitors is very promising, but of course will depend on the successful introduction of USP7 inhibitors into clinical trials and its tolerability in humans.

An additional future direction related to all three of these inhibitor combinations could also be to determine if they cooperate with current immunotherapies. Treatment of melanoma cells with HDAC inhibitors has been shown to rapidly reduce the expression of multiple HDAC proteins as well as levels of PD-L1, PD-L2, and ODC, thus enhancing the anti-tumor efficacy of anti-PD-1 and anti-CTLA4 antibodies (Booth et al. 2017). BET and USP7 inhibition have also been linked to antitumor immunity – pharmacological inhibition of USP7 impairs regulatory T cells, and BET inhibition has been found to block PD-L1 signaling (Zhu et al. 2016; Wang,

Kumar, et al. 2016). Therefore, these combination therapies might cooperate with anti-PD-1 and anti-CTLA4 antibodies in the clinic, however, more research is needed in immune-competent mouse models of melanoma.

Targeting other Ras-driven malignancies

Additional future directions for the therapies outlined in my thesis are to investigate if these therapies are efficacious in other Ras-driven malignancies, such as *KRAS*-mutant colorectal cancer. The combination of USP7 and MEK inhibitors may cooperate in other Ras-driven cancers, especially in cancers with low expression of *CABLES1.* For example, 45% of non-small cell lung cancers and 65% of colorectal cancers have low expression of *CABLES1*, and these two cancers frequently are driven by *KRAS* mutations (Tan et al. 2003; Park et al. 2007). Therefore, inhibition of USP7 and subsequent upregulation of *CABLES1* may lead to cell death in these tumors when combined with MEK inhibition.

Members of the Cichowski laboratory have also found that the combination of BET and MEK inhibitors are efficacious in *KRAS*-mutant lung cancer and the *NF1*-driven malignancies (De Raedt et al. 2014; Guerra et al. 2020). However, the mechanism of response is not through the regulation of *MYC*, but rather through alternative pathways regulated by BRD4, such as the transcription of Ras signature genes and the transcription factor *HOXC10* in non-small cell lung cancer. This hints at a tissue-specific role of BRD4, and more studies are needed to investigate the observed differences in responses to MEK and BET inhibition.

Though in our initial publication we did not investigate the effect of BET and MEK inhibition in *NRAS*-mutant melanoma (Katherine R. Singleton 2017), one project that I pursued briefly in addition to my work on the CRISPR-Cas9 screen was to determine whether *NRAS*-mutant melanomas were indeed sensitive to this combination. Interestingly, I found that *NRAS*-mutant melanoma cell lines responded to this combination *in vitro,* with potent cell death after 3

days of treatment (Figure 5-1A). Additionally, I found that the combination caused a cytotoxic effect in a *NRAS*-mutant tumor xenograft mouse model, although this combination could be more potent in other models, which should be tested (Figure 5-1B). Based on this preliminary data, further research is needed to determine if this response is through *MYC*, or if it is through a different pathway as has been observed in other Ras-driven malignancies.

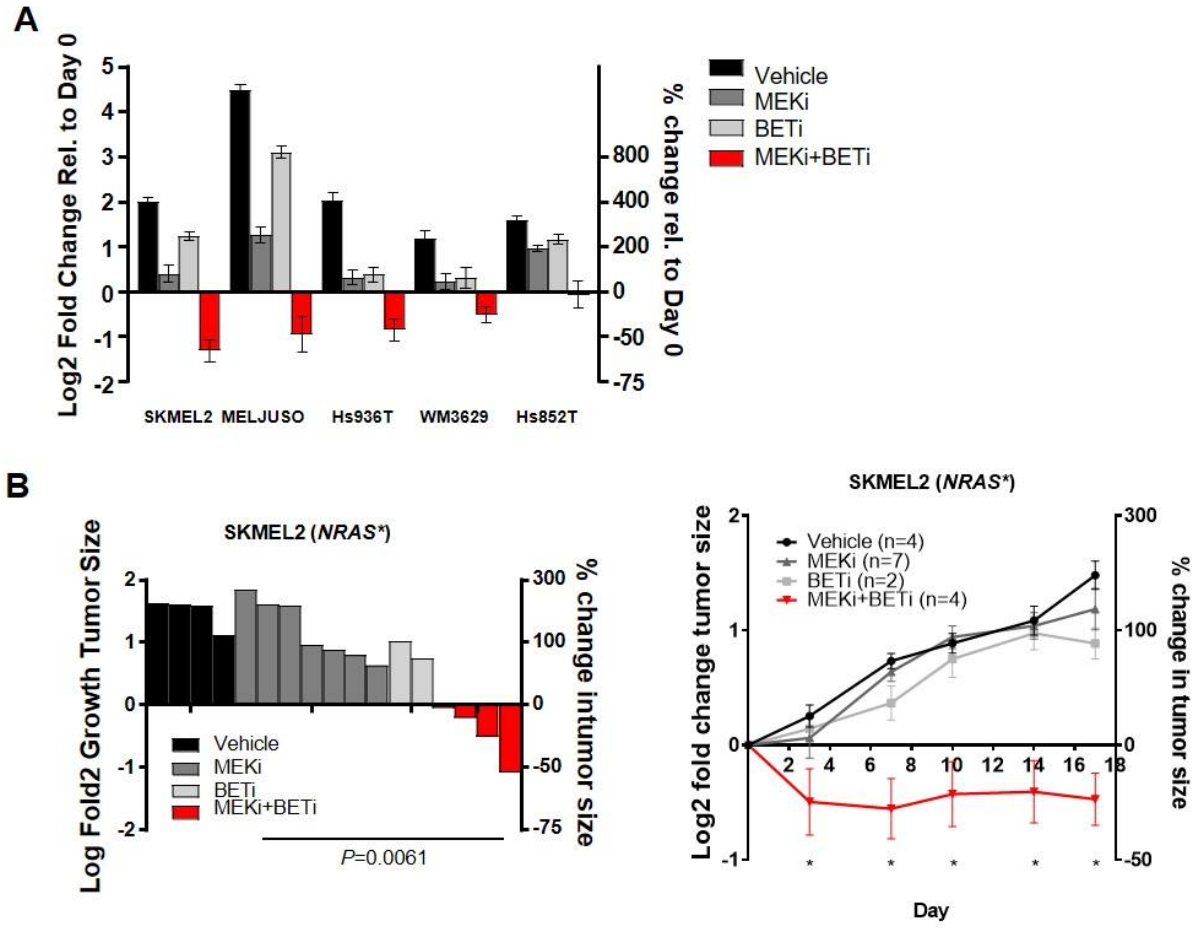

Figure 5-1: BET/MEK inhibition in *NRAS*-mutant melanomas *in vitro* and *in vivo*

(A) Waterfall plot of cell counting assay results after 3 days of treatment with MEKi trametinib and BETi JQ1 in 5 different NRAS-mutant melanoma cell lines.

(B) (Left) Waterfall plot depicting tumor volume change in NRAS-mutant melanoma xenograft model SKMEL2 after 17 days of treatment. Each bar represents an individual tumor. (Right) Growth of SKMEL2 tumors over time. Each data point is mean+/-SEM. MEKi= 0.6mg/kg/day trametinib, oral gavage; BETi = 45mg/kg/day JQ1, intraperitoneal injection. Mice were enrolled when tumors reached ~300mm3. * p>0.05

Future questions about CABLES1 and p63/p73 regulation

Within Chapter 2, several important questions remain for investigation, most importantly with respect to the functions of CABLES1, p63, and p73. I found that *CABLES1* is a bona fide USP7-EPOP-ELOB/C complex target in melanoma and that it is significantly upregulated in response to USP7/MEK inhibitors in *NRAS*-mutant melanomas. Moreover, this upregulation correlated with upregulation of p53 and p63 transcriptional targets. Interestingly, CABLES1 protein is normally very lowly expressed in melanoma cell lines. Therefore, these studies reveal a previously unstudied dependency in *NRAS*- and *BRAF*-melanomas that contributes to *de novo* resistance to Ras/ERK pathway inhibitors. Prior work has shown that CABLES1 acts as a tumor suppressor by stabilizing p53 family proteins, and therefore, we surmise that CABLES1 is causing apoptosis by stabilizing p63 and/or p73. However, additional ongoing studies need to be completed to confirm this hypothesis. For example, an important experiment is to prove that p63 and/or p73 are necessary to cause apoptosis in melanoma cell lines treated with USP7/MEK inhibitors. Additionally, we need to tease out the intricacies of how p63 and p73 are expressed and regulated – is CABLES1 stabilizing the apoptotic TAp63 and/or TAp73 isoforms? Or is it stabilizing all p63 and p73 isoforms? What functions downstream of p63 and p73 to cause apoptosis, and why does it synergize with MEK inhibition? As noted earlier, our RNA sequencing results indicate that common pro-apoptotic p53 and p63 transcriptional targets are up-regulated with MEK and USP7 inhibition, such as *PERP, BIK,* and *BCL2L11.* Therefore, I also plan to verify the increased expression of these targets and determine whether they are necessary for cell death.

Further investigation of CRISPR-Cas9 screen targets

Lastly, from my negative selection CRISPR-Cas9 screen, we identified many other targets of interest which I decided not to pursue further in the course of my dissertation, but will

be investigated in future projects in the Cichowski laboratory. Two hits in particular, MARCH5 and CDC7, scored strongly in my screen, have been validated in different *NRAS*-mutant melanoma cell lines, and would be extremely interesting to follow up in the future (Figure 5-2).

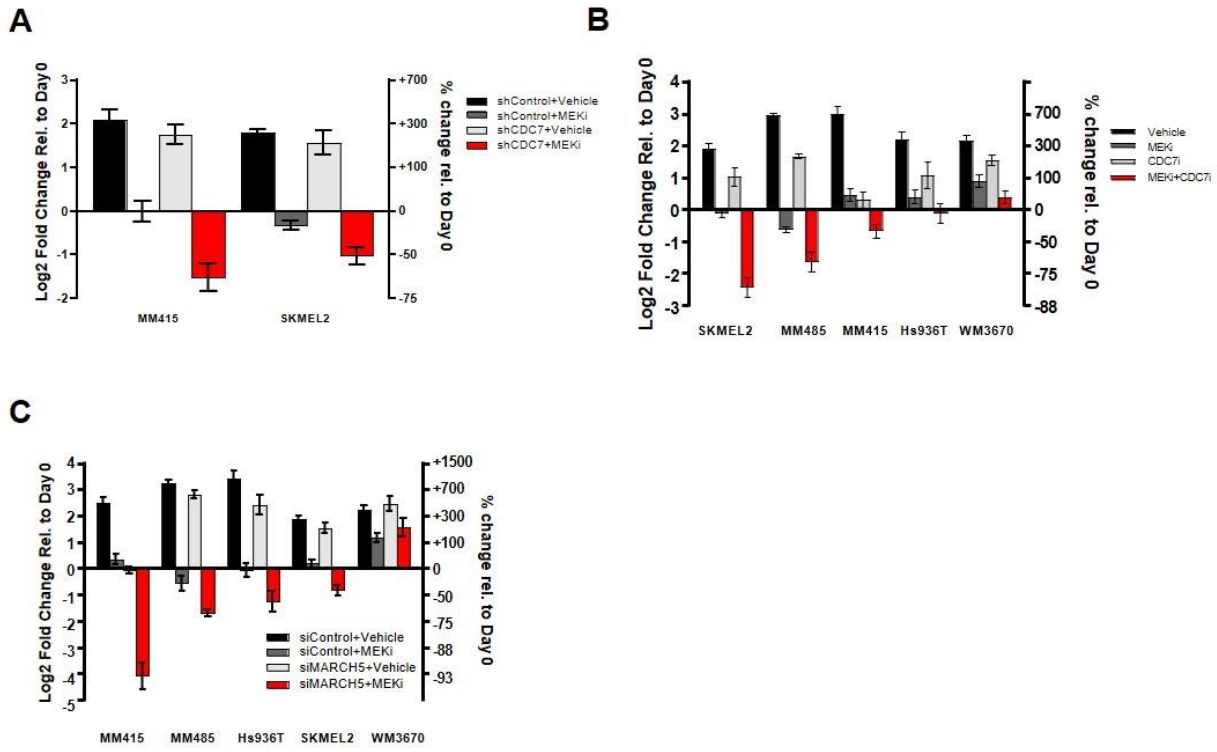

Figure 5-2: CDC7 and MARCH5 are validated as potential hits from CRISPR-Cas9 screen

(A) Cell counting assay results after 4 days of treatment with or without knock-down of CDC7 with shRNA and MEKi trametinib in 2 different NRAS-mutant melanoma cell lines.
(B) Waterfall plot depicting cell counting assay results in 5 NRAS-mutant melanomas cell lines treated with MEKi and/or CDC7i XL413.
(C) Waterfall plot depicting cell counting assay results in 5 NRAS-mutant melanomas cell lines with siRNA against control or MARCH5 and treated with or without MEKi over 4 days.

References

Ackerman, A., O. Klein, D. F. McDermott, W. Wang, N. Ibrahim, D. P. Lawrence, A. Gunturi, K. T. Flaherty, F. S. Hodi, R. Kefford, A. M. Menzies, M. B. Atkins, G. V. Long, and R. J. Sullivan. 2014. 'Outcomes of patients with metastatic melanoma treated with immunotherapy prior to or after BRAF inhibitors', *Cancer*, 120: 1695-701.

ACS. 2020. 'Cancer Facts & Figures 2020'.

Aguirre, A. J., R. M. Meyers, B. A. Weir, F. Vazquez, C. Z. Zhang, U. Ben-David, A. Cook, G. Ha, W. F. Harrington, M. B. Doshi, M. Kost-Alimova, S. Gill, H. Xu, L. D. Ali, G. Jiang, S. Pantel, Y. Lee, A. Goodale, A. D. Cherniack, C. Oh, G. Kryukov, G. S. Cowley, L. A. Garraway, K. Stegmaier, C. W. Roberts, T. R. Golub, M. Meyerson, D. E. Root, A. Tsherniak, and W. C. Hahn. 2016. 'Genomic Copy Number Dictates a Gene-Independent Cell Response to CRISPR/Cas9 Targeting', *Cancer Discov*, 6: 914-29.

Ahmadian, M. R., T. Zor, D. Vogt, W. Kabsch, Z. Selinger, A. Wittinghofer, and K. Scheffzek. 1999. 'Guanosine triphosphatase stimulation of oncogenic Ras mutants', *Proc Natl Acad Sci U S A*, 96: 7065-70.

Alcala, A. M., and K. T. Flaherty. 2012. 'BRAF inhibitors for the treatment of metastatic melanoma: clinical trials and mechanisms of resistance', *Clin Cancer Res*, 18: 33-9.

Allis, C. David, and Thomas Jenuwein. 2016. 'The molecular hallmarks of epigenetic control', *Nature Reviews Genetics*, 17: 487-500.

Alonso-de Vega, I., Y. Martin, and V. A. Smits. 2014. 'USP7 controls Chk1 protein stability by direct deubiquitination', *Cell Cycle*, 13: 3921-6.

An, T., Y. Gong, X. Li, L. Kong, P. Ma, L. Gong, H. Zhu, C. Yu, J. Liu, H. Zhou, B. Mao, and Y. Li. 2017. 'USP7 inhibitor P5091 inhibits Wnt signaling and colorectal tumor growth', *Biochem Pharmacol*, 131: 29-39.

Arnason, Thomas, Maria S. Pino, Omer Yilmaz, Sandra D. Kirley, Bo R. Rueda, Daniel C. Chung, and Lawrence R. Zukerberg. 2013. 'Cables1 is a tumor suppressor gene that regulates intestinal tumor progression in ApcMin mice', *Cancer Biol Ther*, 14: 672-78.

Atefi, Mohammad, Bjoern Titz, Earl Avramis, Charles Ng, Deborah J. L. Wong, Amanda Lassen, Michael Cerniglia, Helena Escuin-Ordinas, David Foulad, Begonya Comin-Anduix, Thomas G. Graeber, and Antoni Ribas. 2015. 'Combination of pan-RAF and MEK inhibitors in NRAS mutant melanoma', *Molecular Cancer*, 14: 27.

Awais, R., D. G. Spiller, M. R. White, and L. Paraoan. 2016. 'p63 is required beside p53 for PERP-mediated apoptosis in uveal melanoma', *Br J Cancer*, 115: 983-92.

Baenke, F., B. Chaneton, M. Smith, N. Van Den Broek, K. Hogan, H. Tang, A. Viros, M. Martin, L. Galbraith, M. R. Girotti, N. Dhomen, E. Gottlieb, and R. Marais. 2016. 'Resistance to BRAF inhibitors induces glutamine dependency in melanoma cells', *Mol Oncol*, 10: 73-84.

Beck, C., C. Boehler, J. Guirouilh Barbat, M. E. Bonnet, G. Illuzzi, P. Ronde, L. R. Gauthier, N. Magroun, A. Rajendran, B. S. Lopez, R. Scully, F. D. Boussin, V. Schreiber, and F. Dantzer. 2014. 'PARP3 affects the relative contribution of homologous recombination and nonhomologous end-joining pathways', *Nucleic Acids Res*, 42: 5616-32.

Bedford, L., J. Lowe, L. R. Dick, R. J. Mayer, and J. E. Brownell. 2011. 'Ubiquitin-like protein conjugation and the ubiquitin-proteasome system as drug targets', *Nat Rev Drug Discov*, 10: 29-46.

Berger, M. F., E. Hodis, T. P. Heffernan, Y. L. Deribe, M. S. Lawrence, A. Protopopov, E. Ivanova, I. R. Watson, E. Nickerson, P. Ghosh, H. Zhang, R. Zeid, X. Ren, K. Cibulskis, A. Y. Sivachenko, N. Wagle, A. Sucker, C. Sougnez, R. Onofrio, L. Ambrogio, D. Auclair, T. Fennell, S. L. Carter, Y. Drier, P. Stojanov, M. A. Singer, D. Voet, R. Jing, G. Saksena, J. Barretina, A. H. Ramos, T. J. Pugh, N. Stransky, M. Parkin, W. Winckler, S. Mahan, K. Ardlie, J. Baldwin, J. Wargo, D. Schadendorf, M. Meyerson, S. B. Gabriel, T. R. Golub, S. N. Wagner, E. S. Lander, G. Getz, L. Chin, and L. A. Garraway. 2012. 'Melanoma genome sequencing reveals frequent PREX2 mutations', *Nature*, 485: 502-6.

Bhattacharya, Seemana, Dipankar Chakraborty, Malini Basu, and Mrinal K. Ghosh. 2018. 'Emerging insights into HAUSP (USP7) in physiology, cancer and other diseases', *Signal Transduction and Targeted Therapy*, 3: 17.

Booth, L., J. L. Roberts, A. Poklepovic, J. Kirkwood, and P. Dent. 2017. 'HDAC inhibitors enhance the immunotherapy response of melanoma cells', *Oncotarget*, 8: 83155-70.

Bos, J. L. 1989. 'ras oncogenes in human cancer: a review', *Cancer Res*, 49: 4682-9.

Bourne, H. R., D. A. Sanders, and F. McCormick. 1990. 'The GTPase superfamily: a conserved switch for diverse cell functions', *Nature*, 348: 125-32.

Boussemart, Lise, Hélène Malka-Mahieu, Isabelle Girault, Delphine Allard, Oskar Hemmingsson, Gorana Tomasic, Marina Thomas, Christine Basmadjian, Nigel Ribeiro, Frédéric Thuaud, Christina Mateus, Emilie Routier, Nyam Kamsu-Kom, Sandrine Agoussi, Alexander M. Eggermont, Laurent Désaubry, Caroline Robert, and Stéphan Vagner. 2014. 'eIF4F is a nexus of resistance to anti-BRAF and anti-MEK cancer therapies', *Nature*, 513: 105-09.

Bryant, H. E., N. Schultz, H. D. Thomas, K. M. Parker, D. Flower, E. Lopez, S. Kyle, M. Meuth, N. J. Curtin, and T. Helleday. 2005. 'Specific killing of BRCA2-deficient tumours with inhibitors of poly(ADP-ribose) polymerase', *Nature*, 434: 913-7.

Buhlmann, S., and B. M. Putzer. 2008. 'DNp73 a matter of cancer: mechanisms and clinical implications', *Biochim Biophys Acta*, 1785: 207-16.

Catalanotti, Federica, Donavan T. Cheng, Alexander N. Shoushtari, Douglas B. Johnson, Katherine S. Panageas, Parisa Momtaz, Catherine Higham, Helen H. Won, James J. Harding, Taha Merghoub, Neal Rosen, Jeffrey A. Sosman, Michael F. Berger, Paul B. Chapman, and David B. Solit. 2017. 'PTEN Loss-of-Function Alterations Are Associated With Intrinsic Resistance to BRAF Inhibitors in Metastatic Melanoma', *JCO Precision Oncology*: 1-15.

Cermelli, S., I. S. Jang, B. Bernard, and C. Grandori. 2014. 'Synthetic lethal screens as a means to understand and treat MYC-driven cancers', *Cold Spring Harb Perspect Med*, 4.

Chapman, P. B., A. Hauschild, C. Robert, J. B. Haanen, P. Ascierto, J. Larkin, R. Dummer, C. Garbe, A. Testori, M. Maio, D. Hogg, P. Lorigan, C. Lebbe, T. Jouary, D. Schadendorf, A. Ribas, S. J. O'Day, J. A. Sosman, J. M. Kirkwood, A. M. Eggermont, B. Dreno, K. Nolop, J. Li, B. Nelson, J. Hou, R. J. Lee, K. T. Flaherty, and G. A. McArthur. 2011. 'Improved survival with vemurafenib in melanoma with BRAF V600E mutation', *N Engl J Med*, 364: 2507-16.

Chauhan, D., Z. Tian, B. Nicholson, K. G. Kumar, B. Zhou, R. Carrasco, J. L. McDermott, C. A. Leach, M. Fulcinniti, M. P. Kodrasov, J. Weinstock, W. D. Kingsbury, T. Hideshima, P. K. Shah, S. Minvielle, M. Altun, B. M. Kessler, R. Orlowski, P. Richardson, N. Munshi, and K. C. Anderson. 2012. 'A small molecule inhibitor of ubiquitin-specific protease-7 induces apoptosis in multiple myeloma cells and overcomes bortezomib resistance', *Cancer Cell*, 22: 345-58.

Cheng, C., C. Niu, Y. Yang, Y. Wang, and M. Lu. 2013. 'Expression of HAUSP in gliomas correlates with disease progression and survival of patients', *Oncol Rep*, 29: 1730-6.

Cheon, K. W., and K. H. Baek. 2006. 'HAUSP as a therapeutic target for hematopoietic tumors (review)', *Int J Oncol*, 28: 1209-15.

Chipumuro, E., E. Marco, C. L. Christensen, N. Kwiatkowski, T. Zhang, C. M. Hatheway, B. J. Abraham, B. Sharma, C. Yeung, A. Altabef, A. Perez-Atayde, K. K. Wong, G. C. Yuan, N. S. Gray, R. A. Young, and R. E. George. 2014. 'CDK7 inhibition suppresses super-enhancer-linked oncogenic transcription in MYCN-driven cancer', *Cell*, 159: 1126-39.

Chou, T. C., and P. Talalay. 1984. 'Quantitative analysis of dose-effect relationships: the combined effects of multiple drugs or enzyme inhibitors', *Adv Enzyme Regul*, 22: 27-55.

Cong, L., F. A. Ran, D. Cox, S. Lin, R. Barretto, N. Habib, P. D. Hsu, X. Wu, W. Jiang, L. A. Marraffini, and F. Zhang. 2013. 'Multiplex genome engineering using CRISPR/Cas systems', *Science*, 339: 819-23.

Connolly, R. M., H. Li, R. C. Jankowitz, Z. Zhang, M. A. Rudek, S. C. Jeter, S. A. Slater, P. Powers, A. C. Wolff, J. H. Fetting, A. Brufsky, R. Piekarz, N. Ahuja, P. W. Laird, H. Shen, D. J. Weisenberger, L. Cope, J. G. Herman, G. Somlo, A. A. Garcia, P. A. Jones, S. B. Baylin, N. E. Davidson, C. A. Zahnow, and V. Stearns. 2016. 'Combination Epigenetic Therapy in Advanced Breast Cancer with 5-Azacitidine and Entinostat: A Phase II National Cancer Institute/Stand Up to Cancer Study', *Clin Cancer Res*.

Cooper, Z. A., A. Reuben, C. N. Spencer, P. A. Prieto, J. L. Austin-Breneman, H. Jiang, C. Haymaker, V. Gopalakrishnan, M. T. Tetzlaff, D. T. Frederick, R. J. Sullivan, R. N. Amaria, S. P. Patel, P. Hwu, S. E. Woodman, I. C. Glitza, A. Diab, L. M. Vence, J. Rodriguez-Canales, E. R. Parra, Wistuba, II, L. M. Coussens, A. H. Sharpe, K. T. Flaherty, J. E. Gershenwald, L. Chin, M. A. Davies, K. Clise-Dwyer, J. P. Allison, P. Sharma, and J. A. Wargo. 2016. 'Distinct clinical patterns and immune infiltrates are observed at time of progression on targeted therapy versus immune checkpoint blockade for melanoma', *Oncoimmunology*, 5: e1136044.

Corcoran, R. B. 2019. "Optimal MAPK inhibition as a key component of therapeutic strategies for KRAS mutant cancers." In.: The Society for Translational Oncology.

Corcoran, R. B., D. Dias-Santagata, K. Bergethon, A. J. Iafrate, J. Settleman, and J. A. Engelman. 2010. 'BRAF gene amplification can promote acquired resistance to MEK inhibitors in cancer cells harboring the BRAF V600E mutation', *Sci Signal*, 3: ra84.

Crawford, L., K. C. Wood, X. Zhou, and S. Mukherjee. 2018. 'Bayesian Approximate Kernel Regression with Variable Selection', *J Am Stat Assoc*, 113: 1710-21.

Cristescu, R., R. Mogg, M. Ayers, A. Albright, E. Murphy, J. Yearley, X. Sher, X. Q. Liu, H. Lu, M. Nebozhyn, C. Zhang, J. K. Lunceford, A. Joe, J. Cheng, A. L. Webber, N. Ibrahim, E. R. Plimack, P. A. Ott, T. Y. Seiwert, A. Ribas, T. K. McClanahan, J. E. Tomassini, A. Loboda, and D. Kaufman. 2018. 'Pan-tumor genomic biomarkers for PD-1 checkpoint blockade-based immunotherapy', *Science*, 362.

Cummins, J. M., C. Rago, M. Kohli, K. W. Kinzler, C. Lengauer, and B. Vogelstein. 2004a. 'Tumour suppression: disruption of HAUSP gene stabilizes p53', *Nature*, 428: 1 p following 486.

Cummins, Jordan M., Carlo Rago, Manu Kohli, Kenneth W. Kinzler, Christoph Lengauer, and Bert Vogelstein. 2004b. 'Disruption of HAUSP gene stabilizes p53', *Nature*, 428: 1-2.

Cunningham, J. T., M. V. Moreno, A. Lodi, S. M. Ronen, and D. Ruggero. 2014. 'Protein and nucleotide biosynthesis are coupled by a single rate-limiting enzyme, PRPS2, to drive cancer', *Cell*, 157: 1088-103.

Curtin, J. A., J. Fridlyand, T. Kageshita, H. N. Patel, K. J. Busam, H. Kutzner, K. H. Cho, S. Aiba, E. B. Brocker, P. E. LeBoit, D. Pinkel, and B. C. Bastian. 2005. 'Distinct sets of genetic alterations in melanoma', *N Engl J Med*, 353: 2135-47.

Dai, Z., J. M. Sheridan, L. J. Gearing, D. L. Moore, S. Su, S. Wormald, S. Wilcox, L. O'Connor, R. A. Dickins, M. E. Blewitt, and M. E. Ritchie. 2014. 'edgeR: a versatile tool for the analysis of shRNA-seq and CRISPR-Cas9 genetic screens', *F1000Res*, 3: 95.

Dang, C. V. 2012. 'MYC on the path to cancer', *Cell*, 149: 22-35.

Dankort, D., D. P. Curley, R. A. Cartlidge, B. Nelson, A. N. Karnezis, W. E. Damsky, Jr., M. J. You, R. A. DePinho, M. McMahon, and M. Bosenberg. 2009. 'Braf(V600E) cooperates with Pten loss to induce metastatic melanoma', *Nat Genet*, 41: 544-52.

Davies, H., G. R. Bignell, C. Cox, P. Stephens, S. Edkins, S. Clegg, J. Teague, H. Woffendin, M. J. Garnett, W. Bottomley, N. Davis, E. Dicks, R. Ewing, Y. Floyd, K. Gray, S. Hall, R. Hawes, J. Hughes, V. Kosmidou, A. Menzies, C. Mould, A. Parker, C. Stevens, S. Watt, S. Hooper, R. Wilson, H. Jayatilake, B. A. Gusterson, C. Cooper, J. Shipley, D. Hargrave, K. Pritchard-Jones, N. Maitland, G. Chenevix-Trench, G. J. Riggins, D. D. Bigner, G. Palmieri, A. Cossu, A. Flanagan, A. Nicholson, J. W. Ho, S. Y. Leung, S. T. Yuen, B. L. Weber, H. F. Seigler, T. L. Darrow, H. Paterson, R. Marais, C. J. Marshall, R. Wooster, M. R. Stratton, and P. A. Futreal. 2002. 'Mutations of the BRAF gene in human cancer', *Nature*, 417: 949-54.

Dawson, M. A., R. K. Prinjha, A. Dittmann, G. Giotopoulos, M. Bantscheff, W. I. Chan, S. C. Robson, C. W. Chung, C. Hopf, M. M. Savitski, C. Huthmacher, E. Gudgin, D. Lugo, S. Beinke, T. D. Chapman, E. J. Roberts, P. E. Soden, K. R. Auger, O. Mirguet, K. Doehner, R. Delwel, A. K. Burnett, P. Jeffrey, G. Drewes, K. Lee, B. J. Huntly, and T. Kouzarides. 2011. 'Inhibition of BET recruitment to chromatin as an effective treatment for MLL-fusion leukaemia', *Nature*, 478: 529-33.

Dawson, Mark A, and Tony Kouzarides. 2012. 'Cancer Epigenetics: From Mechanism to Therapy', *Cell*, 150: 12-27.

De Laurenzi, V., and G. Melino. 2000. 'Evolution of functions within the p53/p63/p73 family', *Ann N Y Acad Sci*, 926: 90-100.

De Raedt, T., E. Beert, E. Pasmant, A. Luscan, H. Brems, N. Ortonne, K. Helin, J. L. Hornick, V. Mautner, H. Kehrer-Sawatzki, W. Clapp, J. Bradner, M. Vidaud, M. Upadhyaya, E. Legius, and K. Cichowski. 2014. 'PRC2 loss amplifies Ras-driven transcription and confers sensitivity to BRD4-based therapies', *Nature*, 514: 247-51.

Delmore, J. E., G. C. Issa, M. E. Lemieux, P. B. Rahl, J. Shi, H. M. Jacobs, E. Kastritis, T. Gilpatrick, R. M. Paranal, J. Qi, M. Chesi, A. C. Schinzel, M. R. McKeown, T. P. Heffernan, C. R. Vakoc, P. L. Bergsagel, I. M. Ghobrial, P. G. Richardson, R. A. Young, W. C. Hahn, K. C. Anderson, A. L. Kung, J. E. Bradner, and C. S. Mitsiades. 2011. 'BET bromodomain inhibition as a therapeutic strategy to target c-Myc', *Cell*, 146: 904-17.

den Hollander, J., S. Rimpi, J. R. Doherty, M. Rudelius, A. Buck, A. Hoellein, M. Kremer, N. Graf, M. Scheerer, M. A. Hall, A. Goga, N. von Bubnoff, J. Duyster, C. Peschel, J. L. Cleveland, J. A. Nilsson, and U. Keller. 2010. 'Aurora kinases A and B are up-regulated by Myc and are essential for maintenance of the malignant state', *Blood*, 116: 1498-505.

Der, C. J., T. Finkel, and G. M. Cooper. 1986. 'Biological and biochemical properties of human rasH genes mutated at codon 61', *Cell*, 44: 167-76.

Devitt, B., W. Liu, R. Salemi, R. Wolfe, J. Kelly, C. Y. Tzen, A. Dobrovic, and G. McArthur. 2011. 'Clinical outcome and pathological features associated with NRAS mutation in cutaneous melanoma', *Pigment Cell Melanoma Res*, 24: 666-72.

DeYoung, M. P., and L. W. Ellisen. 2007. 'p63 and p73 in human cancer: defining the network', *Oncogene*, 26: 5169-83.

Dhanjal, J. K., N. Radhakrishnan, and D. Sundar. 2017. 'Identifying synthetic lethal targets using CRISPR/Cas9 system', *Methods*, 131: 66-73.

Dhawan, M., C. J. Ryan, and A. Ashworth. 2016. 'DNA Repair Deficiency Is Common in Advanced Prostate Cancer: New Therapeutic Opportunities', *Oncologist*, 21: 940-5.

Dhomen, N., J. S. Reis-Filho, S. da Rocha Dias, R. Hayward, K. Savage, V. Delmas, L. Larue, C. Pritchard, and R. Marais. 2009. 'Oncogenic Braf induces melanocyte senescence and melanoma in mice', *Cancer Cell*, 15: 294-303.

Ding, L., G. Getz, D. A. Wheeler, E. R. Mardis, M. D. McLellan, K. Cibulskis, C. Sougnez, H. Greulich, D. M. Muzny, M. B. Morgan, L. Fulton, R. S. Fulton, Q. Zhang, M. C. Wendl, M.

S. Lawrence, D. E. Larson, K. Chen, D. J. Dooling, A. Sabo, A. C. Hawes, H. Shen, S. N. Jhangiani, L. R. Lewis, O. Hall, Y. Zhu, T. Mathew, Y. Ren, J. Yao, S. E. Scherer, K. Clerc, G. A. Metcalf, B. Ng, A. Milosavljevic, M. L. Gonzalez-Garay, J. R. Osborne, R. Meyer, X. Shi, Y. Tang, D. C. Koboldt, L. Lin, R. Abbott, T. L. Miner, C. Pohl, G. Fewell, C. Haipek, H. Schmidt, B. H. Dunford-Shore, A. Kraja, S. D. Crosby, C. S. Sawyer, T. Vickery, S. Sander, J. Robinson, W. Winckler, J. Baldwin, L. R. Chirieac, A. Dutt, T. Fennell, M. Hanna, B. E. Johnson, R. C. Onofrio, R. K. Thomas, G. Tonon, B. A. Weir, X. Zhao, L. Ziaugra, M. C. Zody, T. Giordano, M. B. Orringer, J. A. Roth, M. R. Spitz, Wistuba, II, B. Ozenberger, P. J. Good, A. C. Chang, D. G. Beer, M. A. Watson, M. Ladanyi, S. Broderick, A. Yoshizawa, W. D. Travis, W. Pao, M. A. Province, G. M. Weinstock, H. E. Varmus, S. B. Gabriel, E. S. Lander, R. A. Gibbs, M. Meyerson, and R. K. Wilson. 2008. 'Somatic mutations affect key pathways in lung adenocarcinoma', *Nature*, 455: 1069-75.

Dohn, M., S. Zhang, and X. Chen. 2001. 'p63alpha and DeltaNp63alpha can induce cell cycle arrest and apoptosis and differentially regulate p53 target genes', *Oncogene*, 20: 3193-205.

Dong, Q., S. Kirley, B. Rueda, C. Zhao, L. Zukerberg, and E. Oliva. 2003. 'Loss of cables, a novel gene on chromosome 18q, in ovarian cancer', *Mod Pathol*, 16: 863-8.

Downward, J. 2003. 'Targeting RAS signalling pathways in cancer therapy', *Nat Rev Cancer*, 3: 11-22.

Du, Zhanwen, Jing Song, Yong Wang, Yiqing Zhao, Kishore Guda, Shuming Yang, Hung-Ying Kao, Yan Xu, Joseph Willis, Sanford D. Markowitz, David Sedwick, Robert M. Ewing, and Zhenghe Wang. 2010. 'DNMT1 Stability Is Regulated by Proteins Coordinating Deubiquitination and Acetylation-Driven Ubiquitination', *Sci Signal*, 3: ra80-ra80.

Dumaz, N. 2011. 'Mechanism of RAF isoform switching induced by oncogenic RAS in melanoma', *Small GTPases*, 2: 289-92.

Dumaz, N., R. Hayward, J. Martin, L. Ogilvie, D. Hedley, J. A. Curtin, B. C. Bastian, C. Springer, and R. Marais. 2006. 'In melanoma, RAS mutations are accompanied by switching signaling from BRAF to CRAF and disrupted cyclic AMP signaling', *Cancer Res*, 66: 9483-91.

Dummer, R., D. Schadendorf, P. A. Ascierto, A. Arance, C. Dutriaux, A. M. Di Giacomo, P. Rutkowski, M. Del Vecchio, R. Gutzmer, M. Mandala, L. Thomas, L. Demidov, C. Garbe, D. Hogg, G. Liszkay, P. Queirolo, E. Wasserman, J. Ford, M. Weill, L. A. Sirulnik, V. Jehl, V. Bozon, G. V. Long, and K. Flaherty. 2017. 'Binimetinib versus dacarbazine in patients with advanced NRAS-mutant melanoma (NEMO): a multicentre, open-label, randomised, phase 3 trial', *Lancet Oncol*, 18: 435-45.

Ellerhorst, J. A., V. R. Greene, S. Ekmekcioglu, C. L. Warneke, M. M. Johnson, C. P. Cooke, L. E. Wang, V. G. Prieto, J. E. Gershenwald, Q. Wei, and E. A. Grimm. 2011. 'Clinical correlates of NRAS and BRAF mutations in primary human melanoma', *Clin Cancer Res*, 17: 229-35.

Engelman, J. A., J. Luo, and L. C. Cantley. 2006. 'The evolution of phosphatidylinositol 3-kinases as regulators of growth and metabolism', *Nat Rev Genet*, 7: 606-19.

Everett, R. D., M. Meredith, A. Orr, A. Cross, M. Kathoria, and J. Parkinson. 1997. 'A novel ubiquitin-specific protease is dynamically associated with the PML nuclear domain and binds to a herpesvirus regulatory protein', *Embo j*, 16: 1519-30.

Falkenberg, K. J., and R. W. Johnstone. 2014. 'Histone deacetylases and their inhibitors in cancer, neurological diseases and immune disorders', *Nat Rev Drug Discov*, 13: 673-91.

Farmer, H., N. McCabe, C. J. Lord, A. N. Tutt, D. A. Johnson, T. B. Richardson, M. Santarosa, K. J. Dillon, I. Hickson, C. Knights, N. M. Martin, S. P. Jackson, G. C. Smith, and A. Ashworth. 2005. 'Targeting the DNA repair defect in BRCA mutant cells as a therapeutic strategy', *Nature*, 434: 917-21.

Faustrup, H., S. Bekker-Jensen, J. Bartek, J. Lukas, and N. Mailand. 2009. 'USP7 counteracts SCFbetaTrCP- but not APCCdh1-mediated proteolysis of Claspin', *J Cell Biol*, 184: 13-9.

Fedorenko, I. V., and K. S. Smalley. 2015. 'The complexity of microenvironment-mediated drug resistance', *Genes Cancer*, 6: 367-8.

Filipp, F. V., B. Ratnikov, J. De Ingeniis, J. W. Smith, A. L. Osterman, and D. A. Scott. 2012. 'Glutamine-fueled mitochondrial metabolism is decoupled from glycolysis in melanoma', *Pigment Cell Melanoma Res*, 25: 732-9.

FitzGerald, M. G., D. P. Harkin, S. Silva-Arrieta, D. J. MacDonald, L. C. Lucchina, H. Unsal, E. O'Neill, J. Koh, D. M. Finkelstein, K. J. Isselbacher, A. J. Sober, and D. A. Haber. 1996. 'Prevalence of germ-line mutations in p16, p19ARF, and CDK4 in familial melanoma: analysis of a clinic-based population', *Proc Natl Acad Sci U S A*, 93: 8541-5.

Flaherty, K. T., J. R. Infante, A. Daud, R. Gonzalez, R. F. Kefford, J. Sosman, O. Hamid, L. Schuchter, J. Cebon, N. Ibrahim, R. Kudchadkar, H. A. Burris, 3rd, G. Falchook, A. Algazi, K. Lewis, G. V. Long, I. Puzanov, P. Lebowitz, A. Singh, S. Little, P. Sun, A. Allred, D. Ouellet, K. B. Kim, K. Patel, and J. Weber. 2012. 'Combined BRAF and MEK inhibition in melanoma with BRAF V600 mutations', *N Engl J Med*, 367: 1694-703.

Foucquier, J., and M. Guedj. 2015. 'Analysis of drug combinations: current methodological landscape', *Pharmacol Res Perspect*, 3: e00149.

Fournel, M., C. Bonfils, Y. Hou, P. T. Yan, M. C. Trachy-Bourget, A. Kalita, J. Liu, A. H. Lu, N. Z. Zhou, M. F. Robert, J. Gillespie, J. J. Wang, H. Ste-Croix, J. Rahil, S. Lefebvre, O. Moradei, D. Delorme, A. R. Macleod, J. M. Besterman, and Z. Li. 2008. 'MGCD0103, a novel isotype-selective histone deacetylase inhibitor, has broad spectrum antitumor activity in vitro and in vivo', *Mol Cancer Ther*, 7: 759-68.

Frederick, D. T., A. Piris, A. P. Cogdill, Z. A. Cooper, C. Lezcano, C. R. Ferrone, D. Mitra, A. Boni, L. P. Newton, C. Liu, W. Peng, R. J. Sullivan, D. P. Lawrence, F. S. Hodi, W. W. Overwijk, G. Lizee, G. F. Murphy, P. Hwu, K. T. Flaherty, D. E. Fisher, and J. A. Wargo. 2013. 'BRAF inhibition is associated with enhanced melanoma antigen expression and a more favorable tumor microenvironment in patients with metastatic melanoma', *Clin Cancer Res*, 19: 1225-31.

Fu, D., J. A. Calvo, and L. D. Samson. 2012. 'Balancing repair and tolerance of DNA damage caused by alkylating agents', *Nat Rev Cancer*, 12: 104-20.

Fufa, T. D., L. L. Baxter, J. C. Wedel, D. E. Gildea, S. K. Loftus, and W. J. Pavan. 2019. 'MEK inhibition remodels the active chromatin landscape and induces SOX10 genomic recruitment in BRAF(V600E) mutant melanoma cells', *Epigenetics Chromatin*, 12: 50.

Gao, J., B. A. Aksoy, U. Dogrusoz, G. Dresdner, B. Gross, S. O. Sumer, Y. Sun, A. Jacobsen, R. Sinha, E. Larsson, E. Cerami, C. Sander, and N. Schultz. 2013. 'Integrative analysis of complex cancer genomics and clinical profiles using the cBioPortal', *Sci Signal*, 6: pl1.

Garrett, W. S. 2015. 'Cancer and the microbiota', *Science*, 348: 80-6.

'Genomic Classification of Cutaneous Melanoma'. 2015. *Cell*, 161: 1681-96.

Gildemeister, O. S., J. M. Sage, and K. L. Knight. 2009. 'Cellular redistribution of Rad51 in response to DNA damage: novel role for Rad51C', *J Biol Chem*, 284: 31945-52.

Goga, Andrei, Dun Yang, Aaron D. Tward, David O. Morgan, and J. Michael Bishop. 2007. 'Inhibition of CDK1 as a potential therapy for tumors over-expressing MYC', *Nat Med*, 13: 820-27.

Gray-Schopfer, V. C., S. C. Cheong, H. Chong, J. Chow, T. Moss, Z. A. Abdel-Malek, R. Marais, D. Wynford-Thomas, and D. C. Bennett. 2006. 'Cellular senescence in naevi and immortalisation in melanoma: a role for p16?', *Br J Cancer*, 95: 496-505.

Guerra, S. L., O. Maertens, R. Kuzmickas, T. De Raedt, R. O. Adeyemi, C. J. Guild, S. Guillemette, A. J. Redig, E. S. Chambers, M. Xu, H. Tiv, S. Santagata, P. A. Janne, S. J. Elledge, and K. Cichowski. 2020. 'A Deregulated HOX Gene Axis Confers an Epigenetic Vulnerability in KRAS-Mutant Lung Cancers', *Cancer Cell*.

Haigis, K. M., K. R. Kendall, Y. Wang, A. Cheung, M. C. Haigis, J. N. Glickman, M. Niwa-Kawakita, A. Sweet-Cordero, J. Sebolt-Leopold, K. M. Shannon, J. Settleman, M. Giovannini, and T. Jacks. 2008. 'Differential effects of oncogenic K-Ras and N-Ras on proliferation, differentiation and tumor progression in the colon', *Nat Genet*, 40: 600-8.

Harms, K., S. Nozell, and X. Chen. 2004. 'The common and distinct target genes of the p53 family transcription factors', *Cell Mol Life Sci*, 61: 822-42.

Harrigan, Jeanine A., Xavier Jacq, Niall M. Martin, and Stephen P. Jackson. 2018. 'Deubiquitylating enzymes and drug discovery: emerging opportunities', *Nature Reviews Drug Discovery*, 17: 57-78.

Harris, I. S., J. E. Endress, J. L. Coloff, L. M. Selfors, S. K. McBrayer, J. M. Rosenbluth, N. Takahashi, S. Dhakal, V. Koduri, M. G. Oser, N. J. Schauer, L. M. Doherty, A. L. Hong, Y. P. Kang, S. T. Younger, J. G. Doench, W. C. Hahn, S. J. Buhrlage, G. M. DeNicola, W. G. Kaelin, Jr., and J. S. Brugge. 2019. 'Deubiquitinases Maintain Protein Homeostasis and Survival of Cancer Cells upon Glutathione Depletion', *Cell Metab*, 29: 1166-81.e6.

Hart, T., M. Chandrashekhar, M. Aregger, Z. Steinhart, K. R. Brown, G. MacLeod, M. Mis, M. Zimmermann, A. Fradet-Turcotte, S. Sun, P. Mero, P. Dirks, S. Sidhu, F. P. Roth, O. S. Rissland, D. Durocher, S. Angers, and J. Moffat. 2015. 'High-Resolution CRISPR

Screens Reveal Fitness Genes and Genotype-Specific Cancer Liabilities', *Cell*, 163: 1515-26.

He, Y., S. Wang, J. Tong, S. Jiang, Y. Yang, Z. Zhang, Y. Xu, Y. Zeng, B. Cao, M. F. Moran, and X. Mao. 2020. 'The deubiquitinase USP7 stabilizes Maf proteins to promote myeloma cell survival', *J Biol Chem*, 295: 2084-96.

Hegi, M. E., A. C. Diserens, T. Gorlia, M. F. Hamou, N. de Tribolet, M. Weller, J. M. Kros, J. A. Hainfellner, W. Mason, L. Mariani, J. E. Bromberg, P. Hau, R. O. Mirimanoff, J. G. Cairncross, R. C. Janzer, and R. Stupp. 2005. 'MGMT gene silencing and benefit from temozolomide in glioblastoma', *N Engl J Med*, 352: 997-1003.

Heidorn, S. J., C. Milagre, S. Whittaker, A. Nourry, I. Niculescu-Duvas, N. Dhomen, J. Hussain, J. S. Reis-Filho, C. J. Springer, C. Pritchard, and R. Marais. 2010. 'Kinase-dead BRAF and oncogenic RAS cooperate to drive tumor progression through CRAF', *Cell*, 140: 209-21.

Hemann, M. T. 2014. 'From breaking bad to worse: exploiting homologous DNA repair deficiency in cancer', *Cancer Discov*, 4: 516-8.

Hernandez-Davies, J. E., T. Q. Tran, M. A. Reid, K. R. Rosales, X. H. Lowman, M. Pan, G. Moriceau, Y. Yang, J. Wu, R. S. Lo, and M. Kong. 2015. 'Vemurafenib resistance reprograms melanoma cells towards glutamine dependence', *J Transl Med*, 13: 210.

Hodi, F. S., V. Chiarion-Sileni, R. Gonzalez, J. J. Grob, P. Rutkowski, C. L. Cowey, C. D. Lao, D. Schadendorf, J. Wagstaff, R. Dummer, P. F. Ferrucci, M. Smylie, A. Hill, D. Hogg, I. Marquez-Rodas, J. Jiang, J. Rizzo, J. Larkin, and J. D. Wolchok. 2018. 'Nivolumab plus ipilimumab or nivolumab alone versus ipilimumab alone in advanced melanoma (CheckMate 067): 4-year outcomes of a multicentre, randomised, phase 3 trial', *Lancet Oncol*, 19: 1480-92.

Hodis, E., I. R. Watson, G. V. Kryukov, S. T. Arold, M. Imielinski, J. P. Theurillat, E. Nickerson, D. Auclair, L. Li, C. Place, D. Dicara, A. H. Ramos, M. S. Lawrence, K. Cibulskis, A. Sivachenko, D. Voet, G. Saksena, N. Stransky, R. C. Onofrio, W. Winckler, K. Ardlie, N. Wagle, J. Wargo, K. Chong, D. L. Morton, K. Stemke-Hale, G. Chen, M. Noble, M. Meyerson, J. E. Ladbury, M. A. Davies, J. E. Gershenwald, S. N. Wagner, D. S. Hoon, D. Schadendorf, E. S. Lander, S. B. Gabriel, G. Getz, L. A. Garraway, and L. Chin. 2012. 'A landscape of driver mutations in melanoma', *Cell*, 150: 251-63.

Holowaty, M. N., Y. Sheng, T. Nguyen, C. Arrowsmith, and L. Frappier. 2003. 'Protein interaction domains of the ubiquitin-specific protease, USP7/HAUSP', *J Biol Chem*, 278: 47753-61.

Holzel, M., S. Huang, J. Koster, I. Ora, A. Lakeman, H. Caron, W. Nijkamp, J. Xie, T. Callens, S. Asgharzadeh, R. C. Seeger, L. Messiaen, R. Versteeg, and R. Bernards. 2010. 'NF1 is a tumor suppressor in neuroblastoma that determines retinoic acid response and disease outcome', *Cell*, 142: 218-29.

Honma, K., S. Tsuzuki, M. Nakagawa, H. Tagawa, S. Nakamura, Y. Morishima, and M. Seto. 2009. 'TNFAIP3/A20 functions as a novel tumor suppressor gene in several subtypes of non-Hodgkin lymphomas', *Blood*, 114: 2467-75.

Howlader N, Noone AM, Krapcho M, et al. 2019. 'SEER Cancer Statistics Review, 1975-2016'.

Hrustanovic, G., V. Olivas, E. Pazarentzos, A. Tulpule, S. Asthana, C. M. Blakely, R. A. Okimoto, L. Lin, D. S. Neel, A. Sabnis, J. Flanagan, E. Chan, M. Varella-Garcia, D. L. Aisner, A. Vaishnavi, S. H. Ou, E. A. Collisson, E. Ichihara, P. C. Mack, C. M. Lovly, N. Karachaliou, R. Rosell, J. W. Riess, R. C. Doebele, and T. G. Bivona. 2015. 'RAS-MAPK dependence underlies a rational polytherapy strategy in EML4-ALK-positive lung cancer', *Nat Med*, 21: 1038-47.

Hsu, Tiffany Y. T., Lukas M. Simon, Nicholas J. Neill, Richard Marcotte, Azin Sayad, Christopher S. Bland, Gloria V. Echeverria, Tingting Sun, Sarah J. Kurley, Siddhartha Tyagi, Kristen L. Karlin, Rocio Dominguez-Vidaña, Jessica D. Hartman, Alexander Renwick, Kathleen Scorsone, Ronald J. Bernardi, Samuel O. Skinner, Antrix Jain, Mayra Orellana, Chandraiah Lagisetti, Ido Golding, Sung Y. Jung, Joel R. Neilson, Xiang H. F. Zhang, Thomas A. Cooper, Thomas R. Webb, Benjamin G. Neel, Chad A. Shaw, and Thomas F. Westbrook. 2015. 'The spliceosome is a therapeutic vulnerability in MYC-driven cancer', *Nature*, 525: 384-88.

Hu-Lieskovan, S., S. Mok, B. Homet Moreno, J. Tsoi, L. Robert, L. Goedert, E. M. Pinheiro, R. C. Koya, T. G. Graeber, B. Comin-Anduix, and A. Ribas. 2015. 'Improved antitumor activity of immunotherapy with BRAF and MEK inhibitors in BRAF(V600E) melanoma', *Sci Transl Med*, 7: 279ra41.

Huang, A., L. A. Garraway, A. Ashworth, and B. Weber. 2020. 'Synthetic lethality as an engine for cancer drug target discovery', *Nat Rev Drug Discov*, 19: 23-38.

Huang, J. R., G. M. Tan, Y. Li, and Z. Shi. 2017. 'The Emerging Role of Cables1 in Cancer and Other Diseases', *Mol Pharmacol*, 92: 240-45.

Hugo, W., H. Shi, L. Sun, M. Piva, C. Song, X. Kong, G. Moriceau, A. Hong, K. B. Dahlman, D. B. Johnson, J. A. Sosman, A. Ribas, and R. S. Lo. 2015. 'Non-genomic and Immune Evolution of Melanoma Acquiring MAPKi Resistance', *Cell*, 162: 1271-85.

Ianevski, A., L. He, T. Aittokallio, and J. Tang. 2017. 'SynergyFinder: a web application for analyzing drug combination dose-response matrix data', *Bioinformatics*, 33: 2413-15.

Ilic, Nina, Tamara Utermark, Hans R. Widlund, and Thomas M. Roberts. 2011. 'PI3K-targeted therapy can be evaded by gene amplification along the MYC-eukaryotic translation initiation factor 4E (eIF4E) axis', *Proceedings of the National Academy of Sciences*, 108: E699-E708.

Jenkins, Russell W., David A. Barbie, and Keith T. Flaherty. 2018. 'Mechanisms of resistance to immune checkpoint inhibitors', *British Journal of Cancer*, 118: 9-16.

Ji, Z., K. T. Flaherty, and H. Tsao. 2010. 'Molecular therapeutic approaches to melanoma', *Mol Aspects Med*, 31: 194-204.

Jin, L., G. N. Alesi, and S. Kang. 2016. 'Glutaminolysis as a target for cancer therapy', *Oncogene*, 35: 3619-25.

Johannessen, C. M., J. S. Boehm, S. Y. Kim, S. R. Thomas, L. Wardwell, L. A. Johnson, C. M. Emery, N. Stransky, A. P. Cogdill, J. Barretina, G. Caponigro, H. Hieronymus, R. R. Murray, K. Salehi-Ashtiani, D. E. Hill, M. Vidal, J. J. Zhao, X. Yang, O. Alkan, S. Kim, J. L. Harris, C. J. Wilson, V. E. Myer, P. M. Finan, D. E. Root, T. M. Roberts, T. Golub, K. T. Flaherty, R. Dummer, B. L. Weber, W. R. Sellers, R. Schlegel, J. A. Wargo, W. C. Hahn, and L. A. Garraway. 2010. 'COT drives resistance to RAF inhibition through MAP kinase pathway reactivation', *Nature*, 468: 968-72.

Johannessen, C. M., L. A. Johnson, F. Piccioni, A. Townes, D. T. Frederick, M. K. Donahue, R. Narayan, K. T. Flaherty, J. A. Wargo, D. E. Root, and L. A. Garraway. 2013. 'A melanocyte lineage program confers resistance to MAP kinase pathway inhibition', *Nature*, 504: 138-42.

Jones, P. A., and S. B. Baylin. 2002. 'The fundamental role of epigenetic events in cancer', *Nat Rev Genet*, 3: 415-28.

Jones, P. A., J. P. Issa, and S. Baylin. 2016. 'Targeting the cancer epigenome for therapy', *Nat Rev Genet*, 17: 630-41.

Kaplan, F. M., C. H. Kugel, 3rd, N. Dadpey, Y. Shao, E. V. Abel, and A. E. Aplin. 2012. 'SHOC2 and CRAF mediate ERK1/2 reactivation in mutant NRAS-mediated resistance to RAF inhibitor', *J Biol Chem*, 287: 41797-807.

Kategaya, L., P. Di Lello, L. Rouge, R. Pastor, K. R. Clark, J. Drummond, T. Kleinheinz, E. Lin, J. P. Upton, S. Prakash, J. Heideker, M. McCleland, M. S. Ritorto, D. R. Alessi, M. Trost, T. W. Bainbridge, M. C. M. Kwok, T. P. Ma, Z. Stiffler, B. Brasher, Y. Tang, P. Jaishankar, B. R. Hearn, A. R. Renslo, M. R. Arkin, F. Cohen, K. Yu, F. Peale, F. Gnad, M. T. Chang, C. Klijn, E. Blackwood, S. E. Martin, W. F. Forrest, J. A. Ernst, C. Ndubaku, X. Wang, M. H. Beresini, V. Tsui, C. Schwerdtfeger, R. A. Blake, J. Murray, T. Maurer, and I. E. Wertz. 2017. 'USP7 small-molecule inhibitors interfere with ubiquitin binding', *Nature*, 550: 534-38.

Katherine R. Singleton, Lorin Crawford, Haley E. Manchester, Xiaojing Liu, Maria V. Liberti, Elizabeth Tsui, Anniefer N. Magpusao, Elizabeth M. Stein, Jennifer P. Tingley, Clemens Krepler, Katrin Sproesser, Meenhard Herlyn, Drew J. Adams, Jason W. Locasale, Karen Cichowski, Sayan Mukherjee, Kris C. Wood. 2017. "Melanoma therapeutic strategies that select against resistance by exploiting MYC-driven evolutionary convergence." In. Cancer Cell.

Kato, S., Q. Y. Weng, M. L. Insco, K. Y. Chen, S. Muralidhar, J. Pozniak, J. M. S. Diaz, Y. Drier, N. Nguyen, J. A. Lo, E. van Rooijen, L. V. Kemeny, Y. Zhan, Y. Feng, W. Silkworth, C. T. Powell, B. B. Liau, Y. Xiong, J. Jin, J. Newton-Bishop, L. I. Zon, B. E. Bernstein, and D. E. Fisher. 2020. 'Gain-of-function genetic alterations of G9a drive oncogenesis', *Cancer Discov*.

Kaufman, Charles K., Christian Mosimann, Zi Peng Fan, Song Yang, Andrew J. Thomas, Julien Ablain, Justin L. Tan, Rachel D. Fogley, Ellen van Rooijen, Elliott J. Hagedorn, Christie Ciarlo, Richard M. White, Dominick A. Matos, Ann-Christin Puller, Cristina Santoriello, Eric C. Liao, Richard A. Young, and Leonard I. Zon. 2016. 'A zebrafish melanoma model reveals emergence of neural crest identity during melanoma initiation', *Science*, 351: aad2197.

Kessler, Jessica D., Kristopher T. Kahle, Tingting Sun, Kristen L. Meerbrey, Michael R. Schlabach, Earlene M. Schmitt, Samuel O. Skinner, Qikai Xu, Mamie Z. Li, Zachary C. Hartman, Mitchell Rao, Peng Yu, Rocio Dominguez-Vidana, Anthony C. Liang, Nicole L. Solimini, Ronald J. Bernardi, Bing Yu, Tiffany Hsu, Ido Golding, Ji Luo, C. Kent Osborne, Chad J. Creighton, Susan G. Hilsenbeck, Rachel Schiff, Chad A. Shaw, Stephen J. Elledge, and Thomas F. Westbrook. 2012. 'A SUMOylation-Dependent Transcriptional Subprogram Is Required for Myc-Driven Tumorigenesis', *Science*, 335: 348-53.

Kim, K., A. D. Skora, Z. Li, Q. Liu, A. J. Tam, R. L. Blosser, L. A. Diaz, Jr., N. Papadopoulos, K. W. Kinzler, B. Vogelstein, and S. Zhou. 2014. 'Eradication of metastatic mouse cancers resistant to immune checkpoint blockade by suppression of myeloid-derived cells', *Proc Natl Acad Sci U S A*, 111: 11774-9.

Kim, R. Q., and T. K. Sixma. 2017. 'Regulation of USP7: A High Incidence of E3 Complexes', *J Mol Biol*, 429: 3395-408.

Kimmelman, A. C. 2015. 'Metabolic Dependencies in RAS-Driven Cancers', *Clin Cancer Res*, 21: 1828-34.

King, A. J., M. R. Arnone, M. R. Bleam, K. G. Moss, J. Yang, K. E. Fedorowicz, K. N. Smitheman, J. A. Erhardt, A. Hughes-Earle, L. S. Kane-Carson, R. H. Sinnamon, H. Qi, T. R. Rheault, D. E. Uehling, and S. G. Laquerre. 2013. 'Dabrafenib; preclinical characterization, increased efficacy when combined with trametinib, while BRAF/MEK tool combination reduced skin lesions', *PLoS One*, 8: e67583.

Komander, D., M. J. Clague, and S. Urbe. 2009. 'Breaking the chains: structure and function of the deubiquitinases', *Nat Rev Mol Cell Biol*, 10: 550-63.

Konieczkowski, D. J., C. M. Johannessen, O. Abudayyeh, J. W. Kim, Z. A. Cooper, A. Piris, D. T. Frederick, M. Barzily-Rokni, R. Straussman, R. Haq, D. E. Fisher, J. P. Mesirov, W. C. Hahn, K. T. Flaherty, J. A. Wargo, P. Tamayo, and L. A. Garraway. 2014. 'A melanoma cell state distinction influences sensitivity to MAPK pathway inhibitors', *Cancer Discov*, 4: 816-27.

Korkut, A., W. Wang, E. Demir, B. A. Aksoy, X. Jing, E. J. Molinelli, O. Babur, D. L. Bemis, S. Onur Sumer, D. B. Solit, C. A. Pratilas, and C. Sander. 2015. 'Perturbation biology nominates upstream-downstream drug combinations in RAF inhibitor resistant melanoma cells', *Elife*, 4.

Kwong, L. N., J. C. Costello, H. Liu, S. Jiang, T. L. Helms, A. E. Langsdorf, D. Jakubosky, G. Genovese, F. L. Muller, J. H. Jeong, R. P. Bender, G. C. Chu, K. T. Flaherty, J. A. Wargo, J. J. Collins, and L. Chin. 2012. 'Oncogenic NRAS signaling differentially regulates survival and proliferation in melanoma', *Nat Med*, 18: 1503-10.

Lachmann, A., H. Xu, J. Krishnan, S. I. Berger, A. R. Mazloom, and A. Ma'ayan. 2010. 'ChEA: transcription factor regulation inferred from integrating genome-wide ChIP-X experiments', *Bioinformatics*, 26: 2438-44.

Lahtz, C., R. Stranzenbach, E. Fiedler, P. Helmbold, and R. H. Dammann. 2010. 'Methylation of PTEN as a prognostic factor in malignant melanoma of the skin', *J Invest Dermatol*, 130: 620-2.

Lamberto, I., X. Liu, H. S. Seo, N. J. Schauer, R. E. Iacob, W. Hu, D. Das, T. Mikhailova, E. L. Weisberg, J. R. Engen, K. C. Anderson, D. Chauhan, S. Dhe-Paganon, and S. J. Buhrlage. 2017. 'Structure-Guided Development of a Potent and Selective Non-covalent Active-Site Inhibitor of USP7', *Cell Chem Biol*, 24: 1490-500.e11.

Laporte, A. N., J. J. Barrott, R. J. Yao, N. M. Poulin, B. A. Brodin, K. B. Jones, T. M. Underhill, and T. O. Nielsen. 2017. 'HDAC and Proteasome Inhibitors Synergize to Activate Pro-Apoptotic Factors in Synovial Sarcoma', *PLoS One*, 12: e0169407.

Larkin, J., V. Chiarion-Sileni, R. Gonzalez, J. J. Grob, C. L. Cowey, C. D. Lao, D. Schadendorf, R. Dummer, M. Smylie, P. Rutkowski, P. F. Ferrucci, A. Hill, J. Wagstaff, M. S. Carlino, J. B. Haanen, M. Maio, I. Marquez-Rodas, G. A. McArthur, P. A. Ascierto, G. V. Long, M. K. Callahan, M. A. Postow, K. Grossmann, M. Sznol, B. Dreno, L. Bastholt, A. Yang, L. M. Rollin, C. Horak, F. S. Hodi, and J. D. Wolchok. 2015. 'Combined Nivolumab and Ipilimumab or Monotherapy in Untreated Melanoma', *N Engl J Med*, 373: 23-34.

Larkin, James, Vanna Chiarion-Sileni, Rene Gonzalez, Jean-Jacques Grob, Piotr Rutkowski, Christopher D. Lao, C. Lance Cowey, Dirk Schadendorf, John Wagstaff, Reinhard Dummer, Pier F. Ferrucci, Michael Smylie, David Hogg, Andrew Hill, Ivan Márquez-Rodas, John Haanen, Massimo Guidoboni, Michele Maio, Patrick Schöffski, Matteo S. Carlino, Céleste Lebbé, Grant McArthur, Paolo A. Ascierto, Gregory A. Daniels, Georgina V. Long, Lars Bastholt, Jasmine I. Rizzo, Agnes Balogh, Andriy Moshyk, F. Stephen Hodi, and Jedd D. Wolchok. 2019. 'Five-Year Survival with Combined Nivolumab and Ipilimumab in Advanced Melanoma', *New England Journal of Medicine*, 381: 1535-46.

Lau, K. S., and K. M. Haigis. 2009. 'Non-redundancy within the RAS oncogene family: insights into mutational disparities in cancer', *Mol Cells*, 28: 315-20.

Lee, C. W., and N. B. La Thangue. 1999. 'Promoter specificity and stability control of the p53-related protein p73', *Oncogene*, 18: 4171-81.

Lee, J. H., J. W. Choi, and Y. S. Kim. 2011. 'Frequencies of BRAF and NRAS mutations are different in histological types and sites of origin of cutaneous melanoma: a meta-analysis', *Br J Dermatol*, 164: 776-84.

Leevers, S. J., and C. J. Marshall. 1992. 'MAP kinase regulation--the oncogene connection', *Trends Cell Biol*, 2: 283-6.

Leevers, S. J., H. F. Paterson, and C. J. Marshall. 1994. 'Requirement for Ras in Raf activation is overcome by targeting Raf to the plasma membrane', *Nature*, 369: 411-4.

Lemmon, M. A., and J. Schlessinger. 2010. 'Cell signaling by receptor tyrosine kinases', *Cell*, 141: 1117-34.

Levy, C., M. Khaled, and D. E. Fisher. 2006. 'MITF: master regulator of melanocyte development and melanoma oncogene', *Trends Mol Med*, 12: 406-14.

Li, Muyang, Christopher L. Brooks, Ning Kon, and Wei Gu. 2004. 'A Dynamic Role of HAUSP in the p53-Mdm2 Pathway', *Molecular Cell*, 13: 879-86.

Li, Muyang, Delin Chen, Ariel Shiloh, Jianyuan Luo, Anatoly Y. Nikolaev, Jun Qin, and Wei Gu. 2002. 'Deubiquitination of p53 by HAUSP is an important pathway for p53 stabilization', *Nature*, 416: 648-53.

Li, P., and H. M. Liu. 2020. 'Recent advances in the development of ubiquitin-specific-processing protease 7 (USP7) inhibitors', *Eur J Med Chem*, 191: 112107.

Li, X., L. Kong, Q. Yang, A. Duan, X. Ju, B. Cai, L. Chen, T. An, and Y. Li. 2020. 'Parthenolide inhibits ubiquitin-specific peptidase 7 (USP7), Wnt signaling, and colorectal cancer cell growth', *J Biol Chem*, 295: 3576-89.

Li, Y., and E. Seto. 2016. 'HDACs and HDAC Inhibitors in Cancer Development and Therapy', *Cold Spring Harb Perspect Med*, 6.

Li, Y., Z. Zhou, and C. Chen. 2008. 'WW domain-containing E3 ubiquitin protein ligase 1 targets p63 transcription factor for ubiquitin-mediated proteasomal degradation and regulates apoptosis', *Cell Death Differ*, 15: 1941-51.

Lieber, M. R. 2010. 'The mechanism of double-strand DNA break repair by the nonhomologous DNA end-joining pathway', *Annu Rev Biochem*, 79: 181-211.

Liefke, R., V. Karwacki-Neisius, and Y. Shi. 2016. 'EPOP Interacts with Elongin BC and USP7 to Modulate the Chromatin Landscape', *Mol Cell*, 64: 659-72.

Lim, K. H., and K. H. Baek. 2013. 'Deubiquitinating enzymes as therapeutic targets in cancer', *Curr Pharm Des*, 19: 4039-52.

Lin, C. J., Z. Nasr, P. K. Premsrirut, J. A. Porco, Jr., Y. Hippo, S. W. Lowe, and J. Pelletier. 2012. 'Targeting synthetic lethal interactions between Myc and the eIF4F complex impedes tumorigenesis', *Cell Rep*, 1: 325-33.

Lin, Chen-Ju, Regina Cencic, John R. Mills, Francis Robert, and Jerry Pelletier. 2008. 'c-Myc and eIF4F Are Components of a Feedforward Loop that Links Transcription and Translation', *Cancer Res*, 68: 5326-34.

Liu, Xiaojing, Zheng Ser, and Jason W. Locasale. 2014. 'Development and Quantitative Evaluation of a High-Resolution Metabolomics Technology', *Analytical Chemistry*, 86: 2175-84.

Locasale, Jason W. 2013. 'Serine, glycine and one-carbon units: cancer metabolism in full circle', *Nature Reviews Cancer*, 13: 572-83.

Long, G. V., D. Stroyakovskiy, H. Gogas, E. Levchenko, F. de Braud, J. Larkin, C. Garbe, T. Jouary, A. Hauschild, J. J. Grob, V. Chiarion-Sileni, C. Lebbe, M. Mandala, M. Millward, A. Arance, I. Bondarenko, J. B. Haanen, J. Hansson, J. Utikal, V. Ferraresi, N. Kovalenko, P. Mohr, V. Probachai, D. Schadendorf, P. Nathan, C. Robert, A. Ribas, D. J. DeMarini, J. G. Irani, S. Swann, J. J. Legos, F. Jin, B. Mookerjee, and K. Flaherty. 2015. 'Dabrafenib and trametinib versus dabrafenib and placebo for Val600 BRAF-mutant melanoma: a multicentre, double-blind, phase 3 randomised controlled trial', *Lancet*, 386: 444-51.

Lord, C. J., and A. Ashworth. 2012. 'The DNA damage response and cancer therapy', *Nature*, 481: 287-94.

———. 2016. 'BRCAness revisited', *Nat Rev Cancer*, 16: 110-20.

Luise, C., M. Capra, M. Donzelli, G. Mazzarol, M. G. Jodice, P. Nuciforo, G. Viale, P. P. Di Fiore, and S. Confalonieri. 2011. 'An atlas of altered expression of deubiquitinating enzymes in human cancer', *PLoS One*, 6: e15891.

Luke, J. J., K. T. Flaherty, A. Ribas, and G. V. Long. 2017. 'Targeted agents and immunotherapies: optimizing outcomes in melanoma', *Nat Rev Clin Oncol*, 14: 463-82.

Luke, J. J., and G. K. Schwartz. 2013. 'Chemotherapy in the management of advanced cutaneous malignant melanoma', *Clin Dermatol*, 31: 290-7.

Luo, J., N. L. Solimini, and S. J. Elledge. 2009. 'Principles of cancer therapy: oncogene and non-oncogene addiction', *Cell*, 136: 823-37.

Ma, M., and N. Yu. 2016. 'Ubiquitin-specific protease 7 expression is a prognostic factor in epithelial ovarian cancer and correlates with lymph node metastasis', *Onco Targets Ther*, 9: 1559-69.

Maertens, O., B. Johnson, P. Hollstein, D. T. Frederick, Z. A. Cooper, L. Messiaen, R. T. Bronson, M. McMahon, S. Granter, K. Flaherty, J. A. Wargo, R. Marais, and K. Cichowski. 2013. 'Elucidating distinct roles for NF1 in melanomagenesis', *Cancer Discov*, 3: 338-49.

Maertens, O., R. Kuzmickas, H. E. Manchester, C. E. Emerson, A. G. Gavin, C. J. Guild, T. C. Wong, T. De Raedt, C. Bowman-Colin, E. Hatchi, L. A. Garraway, K. T. Flaherty, S. Pathania, S. J. Elledge, and K. Cichowski. 2019. 'MAPK pathway suppression unmasks latent DNA repair defects and confers a chemical synthetic vulnerability in BRAF, NRAS, and NF1 mutant melanomas', *Cancer Discov*.

Malone, C. F., C. Emerson, R. Ingraham, W. Barbosa, S. Guerra, H. Yoon, L. L. Liu, F. Michor, M. Haigis, K. F. Macleod, O. Maertens, and K. Cichowski. 2017. 'mTOR and HDAC Inhibitors Converge on the TXNIP/Thioredoxin Pathway to Cause Catastrophic Oxidative Stress and Regression of RAS-Driven Tumors', *Cancer Discov*, 7: 1450-63.

Marais, R., Y. Light, H. F. Paterson, and C. J. Marshall. 1995. 'Ras recruits Raf-1 to the plasma membrane for activation by tyrosine phosphorylation', *Embo j*, 14: 3136-45.

Martins, M. M., A. Y. Zhou, A. Corella, D. Horiuchi, C. Yau, T. Rakhshandehroo, J. D. Gordan, R. S. Levin, J. Johnson, J. Jascur, M. Shales, A. Sorrentino, J. Cheah, P. A. Clemons, A. F. Shamji, S. L. Schreiber, N. J. Krogan, K. M. Shokat, F. McCormick, A. Goga, and S. Bandyopadhyay. 2015. 'Linking tumor mutations to drug responses via a quantitative chemical-genetic interaction map', *Cancer Discov*, 5: 154-67.

Martz, C. A., K. A. Ottina, K. R. Singleton, J. S. Jasper, S. E. Wardell, A. Peraza-Penton, G. R. Anderson, P. S. Winter, T. Wang, H. M. Alley, L. N. Kwong, Z. A. Cooper, M. Tetzlaff, P. L. Chen, J. C. Rathmell, K. T. Flaherty, J. A. Wargo, D. P. McDonnell, D. M. Sabatini,

and K. C. Wood. 2014. 'Systematic identification of signaling pathways with potential to confer anticancer drug resistance', *Sci Signal*, 7: ra121.

McCubrey, J. A., L. S. Steelman, W. H. Chappell, S. L. Abrams, E. W. Wong, F. Chang, B. Lehmann, D. M. Terrian, M. Milella, A. Tafuri, F. Stivala, M. Libra, J. Basecke, C. Evangelisti, A. M. Martelli, and R. A. Franklin. 2007. 'Roles of the Raf/MEK/ERK pathway in cell growth, malignant transformation and drug resistance', *Biochim Biophys Acta*, 1773: 1263-84.

McGillicuddy, L. T., J. A. Fromm, P. E. Hollstein, S. Kubek, R. Beroukhim, T. De Raedt, B. W. Johnson, S. M. Williams, P. Nghiemphu, L. M. Liau, T. F. Cloughesy, P. S. Mischel, A. Parret, J. Seiler, G. Moldenhauer, K. Scheffzek, A. O. Stemmer-Rachamimov, C. L. Sawyers, C. Brennan, L. Messiaen, I. K. Mellinghoff, and K. Cichowski. 2009. 'Proteasomal and genetic inactivation of the NF1 tumor suppressor in gliomagenesis', *Cancer Cell*, 16: 44-54.

Meyer, Julia A., Jinhua Wang, Laura E. Hogan, Jun J. Yang, Smita Dandekar, Jay P. Patel, Zuojian Tang, Paul Zumbo, Sheng Li, Jiri Zavadil, Ross L. Levine, Timothy Cardozo, Stephen P. Hunger, Elizabeth A. Raetz, William E. Evans, Debra J. Morrison, Christopher E. Mason, and William L. Carroll. 2013. 'Relapse-specific mutations in NT5C2 in childhood acute lymphoblastic leukemia', *Nat Genet*, 45: 290-94.

Michaloglou, C., L. C. Vredeveld, M. S. Soengas, C. Denoyelle, T. Kuilman, C. M. van der Horst, D. M. Majoor, J. W. Shay, W. J. Mooi, and D. S. Peeper. 2005. 'BRAFE600-associated senescence-like cell cycle arrest of human naevi', *Nature*, 436: 720-4.

Miller, K. M., J. V. Tjeertes, J. Coates, G. Legube, S. E. Polo, S. Britton, and S. P. Jackson. 2010. 'Human HDAC1 and HDAC2 function in the DNA-damage response to promote DNA nonhomologous end-joining', *Nat Struct Mol Biol*, 17: 1144-51.

Min, A., S. A. Im, D. K. Kim, S. H. Song, H. J. Kim, K. H. Lee, T. Y. Kim, S. W. Han, D. Y. Oh, T. Y. Kim, M. J. O'Connor, and Y. J. Bang. 2015. 'Histone deacetylase inhibitor, suberoylanilide hydroxamic acid (SAHA), enhances anti-tumor effects of the poly (ADP-ribose) polymerase (PARP) inhibitor olaparib in triple-negative breast cancer cells', *Breast Cancer Res*, 17: 33.

Mirmohammadsadegh, A., A. Marini, S. Nambiar, M. Hassan, A. Tannapfel, T. Ruzicka, and U. R. Hengge. 2006. 'Epigenetic silencing of the PTEN gene in melanoma', *Cancer Res*, 66: 6546-52.

Misale, S., I. Bozic, J. Tong, A. Peraza-Penton, A. Lallo, F. Baldi, K. H. Lin, M. Truini, L. Trusolino, A. Bertotti, F. Di Nicolantonio, M. A. Nowak, L. Zhang, K. C. Wood, and A. Bardelli. 2015. 'Vertical suppression of the EGFR pathway prevents onset of resistance in colorectal cancers', *Nat Commun*, 6: 8305.

Miyake, Y., J. J. Keusch, L. Wang, M. Saito, D. Hess, X. Wang, B. J. Melancon, P. Helquist, H. Gut, and P. Matthias. 2016. 'Structural insights into HDAC6 tubulin deacetylation and its selective inhibition', *Nat Chem Biol*, 12: 748-54.

Mjelle, R., S. A. Hegre, P. A. Aas, G. Slupphaug, F. Drablos, P. Saetrom, and H. E. Krokan. 2015. 'Cell cycle regulation of human DNA repair and chromatin remodeling genes', *DNA Repair (Amst)*, 30: 53-67.

Moll, U. M., and N. Slade. 2004. 'p63 and p73: roles in development and tumor formation', *Mol Cancer Res*, 2: 371-86.

Moriceau, G., W. Hugo, A. Hong, H. Shi, X. Kong, C. C. Yu, R. C. Koya, A. A. Samatar, N. Khanlou, J. Braun, K. Ruchalski, H. Seifert, J. Larkin, K. B. Dahlman, D. B. Johnson, A. Algazi, J. A. Sosman, A. Ribas, and R. S. Lo. 2015. 'Tunable-combinatorial mechanisms of acquired resistance limit the efficacy of BRAF/MEK cotargeting but result in melanoma drug addiction', *Cancer Cell*, 27: 240-56.

Moynahan, M. E., and M. Jasin. 2010. 'Mitotic homologous recombination maintains genomic stability and suppresses tumorigenesis', *Nat Rev Mol Cell Biol*, 11: 196-207.

Muellner, Markus K., Iris Z. Uras, Bianca V. Gapp, Claudia Kerzendorfer, Michal Smida, Hannelore Lechtermann, Nils Craig-Mueller, Jacques Colinge, Gerhard Duernberger, and Sebastian M. B. Nijman. 2011. 'A chemical-genetic screen reveals a mechanism of resistance to PI3K inhibitors in cancer', *Nat Chem Biol*, 7: 787-93.

Muñoz-Couselo, E., E. Z. Adelantado, C. Ortiz, J. S. García, and J. Perez-Garcia. 2017. 'NRAS-mutant melanoma: current challenges and future prospect', *Onco Targets Ther*, 10: 3941-47.

Munoz, D. M., P. J. Cassiani, L. Li, E. Billy, J. M. Korn, M. D. Jones, J. Golji, D. A. Ruddy, K. Yu, G. McAllister, A. DeWeck, D. Abramowski, J. Wan, M. D. Shirley, S. Y. Neshat, D. Rakiec, R. de Beaumont, O. Weber, A. Kauffmann, E. R. McDonald, 3rd, N. Keen, F. Hofmann, W. R. Sellers, T. Schmelzle, F. Stegmeier, and M. R. Schlabach. 2016. 'CRISPR Screens Provide a Comprehensive Assessment of Cancer Vulnerabilities but Generate False-Positive Hits for Highly Amplified Genomic Regions', *Cancer Discov*, 6: 900-13.

Najem, A., M. Krayem, F. Sales, N. Hussein, B. Badran, C. Robert, A. Awada, F. Journe, and G. E. Ghanem. 2017. 'P53 and MITF/Bcl-2 identified as key pathways in the acquired resistance of NRAS-mutant melanoma to MEK inhibition', *Eur J Cancer*, 83: 154-65.

Nalepa, G., M. Rolfe, and J. W. Harper. 2006. 'Drug discovery in the ubiquitin-proteasome system', *Nat Rev Drug Discov*, 5: 596-613.

Nangia, V., F. M. Siddiqui, S. Caenepeel, D. Timonina, S. J. Bilton, N. Phan, M. Gomez-Caraballo, H. L. Archibald, C. Li, C. Fraser, D. Rigas, K. Vajda, L. A. Ferris, M. Lanuti, C. D. Wright, K. A. Raskin, D. P. Cahill, J. H. Shin, C. Keyes, L. V. Sequist, Z. Piotrowska, A. F. Farago, C. G. Azzoli, J. F. Gainor, K. A. Sarosiek, S. P. Brown, A. Coxon, C. H. Benes, P. E. Hughes, and A. N. Hata. 2018. 'Exploiting MCL1 Dependency with Combination MEK + MCL1 Inhibitors Leads to Induction of Apoptosis and Tumor Regression in KRAS-Mutant Non-Small Cell Lung Cancer', *Cancer Discov*, 8: 1598-613.

Nazarian, R., H. Shi, Q. Wang, X. Kong, R. C. Koya, H. Lee, Z. Chen, M. K. Lee, N. Attar, H. Sazegar, T. Chodon, S. F. Nelson, G. McArthur, J. A. Sosman, A. Ribas, and R. S. Lo.

2010. 'Melanomas acquire resistance to B-RAF(V600E) inhibition by RTK or N-RAS upregulation', *Nature*, 468: 973-7.

Network, Cancer Genome Atlas Research. 2008. 'Comprehensive genomic characterization defines human glioblastoma genes and core pathways', *Nature*, 455: 1061-8.

Nissan, Moriah H., Christine A. Pratilas, Alexis M. Jones, Ricardo Ramirez, Helen Won, Cailian Liu, Shakuntala Tiwari, Li Kong, Aphrothiti J. Hanrahan, Zhan Yao, Taha Merghoub, Antoni Ribas, Paul B. Chapman, Rona Yaeger, Barry S. Taylor, Nikolaus Schultz, Michael F. Berger, Neal Rosen, and David B. Solit. 2014. 'Loss of NF1 in Cutaneous Melanoma Is Associated with RAS Activation and MEK Dependence', *Cancer Res*, 74: 2340-50.

Oh, Y. M., S. J. Yoo, and J. H. Seol. 2007. 'Deubiquitination of Chfr, a checkpoint protein, by USP7/HAUSP regulates its stability and activity', *Biochem Biophys Res Commun*, 357: 615-9.

Oki, Y., D. Buglio, M. Fanale, L. Fayad, A. Copeland, J. Romaguera, L. W. Kwak, B. Pro, S. de Castro Faria, S. Neelapu, N. Fowler, F. Hagemeister, J. Zhang, S. Zhou, L. Feng, and A. Younes. 2013. 'Phase I study of panobinostat plus everolimus in patients with relapsed or refractory lymphoma', *Clin Cancer Res*, 19: 6882-90.

Orzol, P., J. Holcakova, M. Nekulova, R. Nenutil, B. Vojtesek, and P. J. Coates. 2015. 'The diverse oncogenic and tumour suppressor roles of p63 and p73 in cancer: a review by cancer site', *Histol Histopathol*, 30: 503-21.

Palomero, T., W. K. Lim, D. T. Odom, M. L. Sulis, P. J. Real, A. Margolin, K. C. Barnes, J. O'Neil, D. Neuberg, A. P. Weng, J. C. Aster, F. Sigaux, J. Soulier, A. T. Look, R. A. Young, A. Califano, and A. A. Ferrando. 2006. 'NOTCH1 directly regulates c-MYC and activates a feed-forward-loop transcriptional network promoting leukemic cell growth', *Proc Natl Acad Sci U S A*, 103: 18261-6.

Paraiso, K. H., Y. Xiang, V. W. Rebecca, E. V. Abel, Y. A. Chen, A. C. Munko, E. Wood, I. V. Fedorenko, V. K. Sondak, A. R. Anderson, A. Ribas, M. D. Palma, K. L. Nathanson, J. M. Koomen, J. L. Messina, and K. S. Smalley. 2011. 'PTEN loss confers BRAF inhibitor resistance to melanoma cells through the suppression of BIM expression', *Cancer Res*, 71: 2750-60.

Park, D. Y., H. Sakamoto, S. D. Kirley, S. Ogino, T. Kawasaki, E. Kwon, M. Mino-Kenudson, G. Y. Lauwers, D. C. Chung, B. R. Rueda, and L. R. Zukerberg. 2007. 'The Cables gene on chromosome 18q is silenced by promoter hypermethylation and allelic loss in human colorectal cancer', *Am J Pathol*, 171: 1509-19.

Parmenter, T. J., M. Kleinschmidt, K. M. Kinross, S. T. Bond, J. Li, M. R. Kaadige, A. Rao, K. E. Sheppard, W. Hugo, G. M. Pupo, R. B. Pearson, S. L. McGee, G. V. Long, R. A. Scolyer, H. Rizos, R. S. Lo, C. Cullinane, D. E. Ayer, A. Ribas, R. W. Johnstone, R. J. Hicks, and G. A. McArthur. 2014. 'Response of BRAF-mutant melanoma to BRAF inhibition is mediated by a network of transcriptional regulators of glycolysis', *Cancer Discov*, 4: 423-33.

Parsons, D. W., S. Jones, X. Zhang, J. C. Lin, R. J. Leary, P. Angenendt, P. Mankoo, H. Carter, I. M. Siu, G. L. Gallia, A. Olivi, R. McLendon, B. A. Rasheed, S. Keir, T. Nikolskaya, Y. Nikolsky, D. A. Busam, H. Tekleab, L. A. Diaz, Jr., J. Hartigan, D. R. Smith, R. L. Strausberg, S. K. Marie, S. M. Shinjo, H. Yan, G. J. Riggins, D. D. Bigner, R. Karchin, N. Papadopoulos, G. Parmigiani, B. Vogelstein, V. E. Velculescu, and K. W. Kinzler. 2008. 'An integrated genomic analysis of human glioblastoma multiforme', *Science*, 321: 1807-12.

Pavlova, N. N., and C. B. Thompson. 2016. 'The Emerging Hallmarks of Cancer Metabolism', *Cell Metab*, 23: 27-47.

Peng, G., C. Chun-Jen Lin, W. Mo, H. Dai, Y. Y. Park, S. M. Kim, Y. Peng, Q. Mo, S. Siwko, R. Hu, J. S. Lee, B. Hennessy, S. Hanash, G. B. Mills, and S. Y. Lin. 2014. 'Genome-wide transcriptome profiling of homologous recombination DNA repair', *Nat Commun*, 5: 3361.

Peng, W., J. Q. Chen, C. Liu, S. Malu, C. Creasy, M. T. Tetzlaff, C. Xu, J. A. McKenzie, C. Zhang, X. Liang, L. J. Williams, W. Deng, G. Chen, R. Mbofung, A. J. Lazar, C. A. Torres-Cabala, Z. A. Cooper, P. L. Chen, T. N. Tieu, S. Spranger, X. Yu, C. Bernatchez, M. A. Forget, C. Haymaker, R. Amaria, J. L. McQuade, I. C. Glitza, T. Cascone, H. S. Li, L. N. Kwong, T. P. Heffernan, J. Hu, R. L. Bassett, Jr., M. W. Bosenberg, S. E. Woodman, W. W. Overwijk, G. Lizee, J. Roszik, T. F. Gajewski, J. A. Wargo, J. E. Gershenwald, L. Radvanyi, M. A. Davies, and P. Hwu. 2016. 'Loss of PTEN Promotes Resistance to T Cell-Mediated Immunotherapy', *Cancer Discov*, 6: 202-16.

Petrenko, O., A. Zaika, and U. M. Moll. 2003. 'deltaNp73 facilitates cell immortalization and cooperates with oncogenic Ras in cellular transformation in vivo', *Mol Cell Biol*, 23: 5540-55.

Pleasance, E. D., R. K. Cheetham, P. J. Stephens, D. J. McBride, S. J. Humphray, C. D. Greenman, I. Varela, M. L. Lin, G. R. Ordonez, G. R. Bignell, K. Ye, J. Alipaz, M. J. Bauer, D. Beare, A. Butler, R. J. Carter, L. Chen, A. J. Cox, S. Edkins, P. I. Kokko-Gonzales, N. A. Gormley, R. J. Grocock, C. D. Haudenschild, M. M. Hims, T. James, M. Jia, Z. Kingsbury, C. Leroy, J. Marshall, A. Menzies, L. J. Mudie, Z. Ning, T. Royce, O. B. Schulz-Trieglaff, A. Spiridou, L. A. Stebbings, L. Szajkowski, J. Teague, D. Williamson, L. Chin, M. T. Ross, P. J. Campbell, D. R. Bentley, P. A. Futreal, and M. R. Stratton. 2010. 'A comprehensive catalogue of somatic mutations from a human cancer genome', *Nature*, 463: 191-6.

Pollock, P. M., U. L. Harper, K. S. Hansen, L. M. Yudt, M. Stark, C. M. Robbins, T. Y. Moses, G. Hostetter, U. Wagner, J. Kakareka, G. Salem, T. Pohida, P. Heenan, P. Duray, O. Kallioniemi, N. K. Hayward, J. M. Trent, and P. S. Meltzer. 2003. 'High frequency of BRAF mutations in nevi', *Nat Genet*, 33: 19-20.

Posch, Christian, Homayoun Moslehi, Luzviminda Feeney, Gary A. Green, Anoosheh Ebaee, Valentin Feichtenschlager, Kim Chong, Lily Peng, Michelle T. Dimon, Thomas Phillips, Adil I. Daud, Timothy H. McCalmont, Philip E. LeBoit, and Susana Ortiz-Urda. 2013. 'Combined targeting of MEK and PI3K/mTOR effector pathways is necessary to effectively inhibit NRAS mutant melanoma in vitro and in vivo', *Proceedings of the National Academy of Sciences*, 110: 4015-20.

Poulikakos, P. I., Y. Persaud, M. Janakiraman, X. Kong, C. Ng, G. Moriceau, H. Shi, M. Atefi, B. Titz, M. T. Gabay, M. Salton, K. B. Dahlman, M. Tadi, J. A. Wargo, K. T. Flaherty, M. C. Kelley, T. Misteli, P. B. Chapman, J. A. Sosman, T. G. Graeber, A. Ribas, R. S. Lo, N. Rosen, and D. B. Solit. 2011. 'RAF inhibitor resistance is mediated by dimerization of aberrantly spliced BRAF(V600E)', *Nature*, 480: 387-90.

Prabhu, N. S., K. Somasundaram, K. Satyamoorthy, M. Herlyn, and W. S. El-Deiry. 1998. 'p73beta, unlike p53, suppresses growth and induces apoptosis of human papillomavirus E6-expressing cancer cells', *Int J Oncol*, 13: 5-9.

Pratilas, C. A., B. S. Taylor, Q. Ye, A. Viale, C. Sander, D. B. Solit, and N. Rosen. 2009. '(V600E)BRAF is associated with disabled feedback inhibition of RAF-MEK signaling and elevated transcriptional output of the pathway', *Proc Natl Acad Sci U S A*, 106: 4519-24.

Prives, C. 1998. 'Signaling to p53: breaking the MDM2-p53 circuit', *Cell*, 95: 5-8.

Raimondi, S., F. Sera, S. Gandini, S. Iodice, S. Caini, P. Maisonneuve, and M. C. Fargnoli. 2008. 'MC1R variants, melanoma and red hair color phenotype: a meta-analysis', *Int J Cancer*, 122: 2753-60.

Rao, Aparna D., Lorey K. Smith, Tiffany J. Parmenter, and Grant A. McArthur. 2016. 'Abstract B23: Mutant NRAS regulates glycolysis in melanoma through ERK, mTOR and the MYC/HIF1α/MondoA network of transcriptional regulators', *Molecular Cancer Research*, 14: B23-B23.

Reyes-Turcu, F. E., K. H. Ventii, and K. D. Wilkinson. 2009. 'Regulation and cellular roles of ubiquitin-specific deubiquitinating enzymes', *Annu Rev Biochem*, 78: 363-97.

Ribas, A., R. Gonzalez, A. Pavlick, O. Hamid, T. F. Gajewski, A. Daud, L. Flaherty, T. Logan, B. Chmielowski, K. Lewis, D. Kee, P. Boasberg, M. Yin, I. Chan, L. Musib, N. Choong, I. Puzanov, and G. A. McArthur. 2014. 'Combination of vemurafenib and cobimetinib in patients with advanced BRAF(V600)-mutated melanoma: a phase 1b study', *Lancet Oncol*, 15: 954-65.

Rizos, H., A. M. Menzies, G. M. Pupo, M. S. Carlino, C. Fung, J. Hyman, L. E. Haydu, B. Mijatov, T. M. Becker, S. C. Boyd, J. Howle, R. Saw, J. F. Thompson, R. F. Kefford, R. A. Scolyer, and G. V. Long. 2014. 'BRAF inhibitor resistance mechanisms in metastatic melanoma: spectrum and clinical impact', *Clin Cancer Res*, 20: 1965-77.

Robert, C., B. Karaszewska, J. Schachter, P. Rutkowski, A. Mackiewicz, D. Stroiakovski, M. Lichinitser, R. Dummer, F. Grange, L. Mortier, V. Chiarion-Sileni, K. Drucis, I. Krajsova, A. Hauschild, P. Lorigan, P. Wolter, G. V. Long, K. Flaherty, P. Nathan, A. Ribas, A. M. Martin, P. Sun, W. Crist, J. Legos, S. D. Rubin, S. M. Little, and D. Schadendorf. 2015. 'Improved overall survival in melanoma with combined dabrafenib and trametinib', *N Engl J Med*, 372: 30-9.

Robert, C., and F. V. Rassool. 2012. 'HDAC inhibitors: roles of DNA damage and repair', *Adv Cancer Res*, 116: 87-129.

Robert, C., J. Schachter, G. V. Long, A. Arance, J. J. Grob, L. Mortier, A. Daud, M. S. Carlino, C. McNeil, M. Lotem, J. Larkin, P. Lorigan, B. Neyns, C. U. Blank, O. Hamid, C. Mateus,

R. Shapira-Frommer, M. Kosh, H. Zhou, N. Ibrahim, S. Ebbinghaus, and A. Ribas. 2015. 'Pembrolizumab versus Ipilimumab in Advanced Melanoma', *N Engl J Med*, 372: 2521-32.

Robert, Caroline, Jean J. Grob, Daniil Stroyakovskiy, Boguslawa Karaszewska, Axel Hauschild, Evgeny Levchenko, Vanna Chiarion Sileni, Jacob Schachter, Claus Garbe, Igor Bondarenko, Helen Gogas, Mario Mandalá, John B.A.G. Haanen, Celeste Lebbé, Andrzej Mackiewicz, Piotr Rutkowski, Paul D. Nathan, Antoni Ribas, Michael A. Davies, Keith T. Flaherty, Paul Burgess, Monique Tan, Eduard Gasal, Maurizio Voi, Dirk Schadendorf, and Georgina V. Long. 2019. 'Five-Year Outcomes with Dabrafenib plus Trametinib in Metastatic Melanoma', *New England Journal of Medicine*, 381: 626-36.

Sakamoto, H., A. M. Friel, A. W. Wood, L. Guo, A. Ilic, M. V. Seiden, D. C. Chung, M. P. Lynch, T. Serikawa, E. Munro, E. Oliva, S. Orsulic, S. D. Kirley, R. Foster, L. R. Zukerberg, and B. R. Rueda. 2008. 'Mechanisms of Cables 1 gene inactivation in human ovarian cancer development', *Cancer Biol Ther*, 7: 180-88.

Sarkisian, S., and D. Davar. 2018. 'MEK inhibitors for the treatment of NRAS mutant melanoma', *Drug Des Devel Ther*, 12: 2553-65.

Schadendorf, D., D. E. Fisher, C. Garbe, J. E. Gershenwald, J. J. Grob, A. Halpern, M. Herlyn, M. A. Marchetti, G. McArthur, A. Ribas, A. Roesch, and A. Hauschild. 2015. 'Melanoma', *Nat Rev Dis Primers*, 1: 15003.

Schauer, N. J., X. Liu, R. S. Magin, L. M. Doherty, W. C. Chan, S. B. Ficarro, W. Hu, R. M. Roberts, R. E. Iacob, B. Stolte, A. O. Giacomelli, S. Perera, K. McKay, S. A. Boswell, E. L. Weisberg, A. Ray, D. Chauhan, S. Dhe-Paganon, K. C. Anderson, J. D. Griffin, J. Li, W. C. Hahn, P. K. Sorger, J. R. Engen, K. Stegmaier, J. A. Marto, and S. J. Buhrlage. 2020. 'Selective USP7 inhibition elicits cancer cell killing through a p53-dependent mechanism', *Sci Rep*, 10: 5324.

Schraml, P., A. von Teichman, D. Mihic-Probst, M. Simcock, A. Ochsenbein, R. Dummer, O. Michielin, B. Seifert, M. Schlappi, H. Moch, and R. von Moos. 2012. 'Predictive value of the MGMT promoter methylation status in metastatic melanoma patients receiving first-line temozolomide plus bevacizumab in the trial SAKK 50/07', *Oncol Rep*, 28: 654-8.

Sears, R. C. 2004. 'The life cycle of C-myc: from synthesis to degradation', *Cell Cycle*, 3: 1133-7.

Segura, M. F., B. Fontanals-Cirera, A. Gaziel-Sovran, M. V. Guijarro, D. Hanniford, G. Zhang, P. Gonzalez-Gomez, M. Morante, L. Jubierre, W. Zhang, F. Darvishian, M. Ohlmeyer, I. Osman, M. M. Zhou, and E. Hernando. 2013. 'BRD4 sustains melanoma proliferation and represents a new target for epigenetic therapy', *Cancer Res*, 73: 6264-76.

Settleman, J. 2012. 'Oncogene addiction', *Curr Biol*, 22: R43-4.

Shalem, O., N. E. Sanjana, E. Hartenian, X. Shi, D. A. Scott, T. Mikkelson, D. Heckl, B. L. Ebert, D. E. Root, J. G. Doench, and F. Zhang. 2014. 'Genome-scale CRISPR-Cas9 knockout screening in human cells', *Science*, 343: 84-87.

Shaw, P. E., and J. Saxton. 2003. 'Ternary complex factors: prime nuclear targets for mitogen-activated protein kinases', *Int J Biochem Cell Biol*, 35: 1210-26.

Sheel, A., and W. Xue. 2016. 'Genomic Amplifications Cause False Positives in CRISPR Screens', *Cancer Discov*, 6: 824-6.

Sheiness, D, L Fanshier, and J M Bishop. 1978. 'Identification of nucleotide sequences which may encode the oncogenic capacity of avian retrovirus MC29', *Journal of Virology*, 28: 600-10.

Shen, Aijun, Lu Wang, Min Huang, Jingya Sun, Yi Chen, Yan-Yan Shen, Xinying Yang, Xin Wang, Jian Ding, and Meiyu Geng. 2015. 'c-Myc Alterations Confer Therapeutic Response and Acquired Resistance to c-Met Inhibitors in MET-Addicted Cancers', *Cancer Res*, 75: 4548-59.

Shi, H., A. Hong, X. Kong, R. C. Koya, C. Song, G. Moriceau, W. Hugo, C. C. Yu, C. Ng, T. Chodon, R. A. Scolyer, R. F. Kefford, A. Ribas, G. V. Long, and R. S. Lo. 2014. 'A novel AKT1 mutant amplifies an adaptive melanoma response to BRAF inhibition', *Cancer Discov*, 4: 69-79.

Shi, H., W. Hugo, X. Kong, A. Hong, R. C. Koya, G. Moriceau, T. Chodon, R. Guo, D. B. Johnson, K. B. Dahlman, M. C. Kelley, R. F. Kefford, B. Chmielowski, J. A. Glaspy, J. A. Sosman, N. van Baren, G. V. Long, A. Ribas, and R. S. Lo. 2014. 'Acquired resistance and clonal evolution in melanoma during BRAF inhibitor therapy', *Cancer Discov*, 4: 80-93.

Shi, H., G. Moriceau, X. Kong, M. K. Lee, H. Lee, R. C. Koya, C. Ng, T. Chodon, R. A. Scolyer, K. B. Dahlman, J. A. Sosman, R. F. Kefford, G. V. Long, S. F. Nelson, A. Ribas, and R. S. Lo. 2012. 'Melanoma whole-exome sequencing identifies (V600E)B-RAF amplification-mediated acquired B-RAF inhibitor resistance', *Nat Commun*, 3: 724.

Shi, J., E. Wang, J. P. Milazzo, Z. Wang, J. B. Kinney, and C. R. Vakoc. 2015. 'Discovery of cancer drug targets by CRISPR-Cas9 screening of protein domains', *Nat Biotechnol*, 33: 661-7.

Siegel, Rebecca L., Kimberly D. Miller, and Ahmedin Jemal. 2019. 'Cancer statistics, 2019', *CA Cancer J Clin*, 69: 7-34.

Simanshu, Dhirendra K., Dwight V. Nissley, and Frank McCormick. 2017. 'RAS Proteins and Their Regulators in Human Disease', *Cell*, 170: 17-33.

Singh, H., D. L. Longo, and B. A. Chabner. 2015. 'Improving Prospects for Targeting RAS', *J Clin Oncol*, 33: 3650-9.

Singleton, Katherine R., Trista K. Hinz, Emily K. Kleczko, Lindsay A. Marek, Jeff Kwak, Taylor Harp, Jihye Kim, Aik Choon Tan, and Lynn E. Heasley. 2015. 'Kinome RNAi Screens Reveal Synergistic Targeting of MTOR and FGFR1 Pathways for Treatment of Lung Cancer and HNSCC', *Cancer Res*, 75: 4398-406.

Solit, D. B., L. A. Garraway, C. A. Pratilas, A. Sawai, G. Getz, A. Basso, Q. Ye, J. M. Lobo, Y. She, I. Osman, T. R. Golub, J. Sebolt-Leopold, W. R. Sellers, and N. Rosen. 2006. 'BRAF mutation predicts sensitivity to MEK inhibition', *Nature*, 439: 358-62.

Solit, D. B., and N. Rosen. 2011. 'Resistance to BRAF inhibition in melanomas', *N Engl J Med*, 364: 772-4.

———. 2014. 'Towards a unified model of RAF inhibitor resistance', *Cancer Discov*, 4: 27-30.

Song, M. S., L. Salmena, A. Carracedo, A. Egia, F. Lo-Coco, J. Teruya-Feldstein, and P. P. Pandolfi. 2008. 'The deubiquitinylation and localization of PTEN are regulated by a HAUSP-PML network', *Nature*, 455: 813-7.

Sosman, Jeffrey Alan, Muaiad Kittaneh, Martijn P. J. K. Lolkema, Michael Andrew Postow, Gary Schwartz, Catherine Franklin, Alessandro Matano, Suraj Bhansali, Sudha Parasuraman, and Kevin Kim. 2014. 'A phase 1b/2 study of LEE011 in combination with binimetinib (MEK162) in patients with NRAS-mutant melanoma: Early encouraging clinical activity', *Journal of Clinical Oncology*, 32: 9009-09.

Souroullas, George P., William R. Jeck, Joel S. Parker, Jeremy M. Simon, Jie-Yu Liu, Joshiawa Paulk, Jessie Xiong, Kelly S. Clark, Yuri Fedoriw, Jun Qi, Christin E. Burd, James E. Bradner, and Norman E. Sharpless. 2016. 'An oncogenic Ezh2 mutation induces tumors through global redistribution of histone 3 lysine 27 trimethylation', *Nat Med*, 22: 632-40.

Spugnardi, M., S. Tommasi, R. Dammann, G. P. Pfeifer, and D. S. Hoon. 2003. 'Epigenetic inactivation of RAS association domain family protein 1 (RASSF1A) in malignant cutaneous melanoma', *Cancer Res*, 63: 1639-43.

Srivastava, Mitul, Charu Suri, and Shailendra Asthana. 2019. 'What Modulates the Usp7 Function...A Dynamic Pocket or Inter-Regulatory Domains?', *Biophysical Journal*, 116: 340a-41a.

Steder, M., V. Alla, C. Meier, A. Spitschak, J. Pahnke, K. Furst, B. S. Kowtharapu, D. Engelmann, J. Petigk, F. Egberts, S. G. Schad-Trcka, G. Gross, D. M. Nettelbeck, A. Niemetz, and B. M. Putzer. 2013. 'DNp73 exerts function in metastasis initiation by disconnecting the inhibitory role of EPLIN on IGF1R-AKT/STAT3 signaling', *Cancer Cell*, 24: 512-27.

Steinberg, M. 2007. 'Dasatinib: a tyrosine kinase inhibitor for the treatment of chronic myelogenous leukemia and philadelphia chromosome-positive acute lymphoblastic leukemia', *Clin Ther*, 29: 2289-308.

Stephens, M. 2017. 'False discovery rates: a new deal', *Biostatistics*, 18: 275-94.

Stine, Zachary E., Zandra E. Walton, Brian J. Altman, Annie L. Hsieh, and Chi V. Dang. 2015. 'MYC, Metabolism, and Cancer', *Cancer Discov*, 5: 1024-39.

Stolte, B., A. B. Iniguez, N. V. Dharia, A. L. Robichaud, A. S. Conway, A. M. Morgan, G. Alexe, N. J. Schauer, X. Liu, G. H. Bird, A. Tsherniak, F. Vazquez, S. J. Buhrlage, L. D. Walensky, and K. Stegmaier. 2018. 'Genome-scale CRISPR-Cas9 screen identifies druggable dependencies in TP53 wild-type Ewing sarcoma', *J Exp Med*, 215: 2137-55.

Suenaga, Y., M. Yamamoto, T. Sakuma, M. Sasada, F. Fukai, M. Ohira, Y. Yamaguchi, T. Yamamoto, K. Ando, T. Ozaki, and A. Nakagawara. 2019. 'TAp63 represses transcription of MYCN/NCYM gene and its high levels of expression are associated with favorable outcome in neuroblastoma', *Biochem Biophys Res Commun*, 518: 311-18.

Tan, D., S. Kirley, Q. Li, N. Ramnath, H. K. Slocum, J. S. Brooks, C. L. Wu, and L. R. Zukerberg. 2003. 'Loss of cables protein expression in human non-small cell lung cancer: a tissue microarray study', *Hum Pathol*, 34: 143-9.

Tavana, O., H. Sun, and W. Gu. 2018. 'Targeting HAUSP in both p53 wildtype and p53-mutant tumors', *Cell Cycle*, 17: 823-28.

Thurn, K. T., S. Thomas, P. Raha, I. Qureshi, and P. N. Munster. 2013. 'Histone deacetylase regulation of ATM-mediated DNA damage signaling', *Mol Cancer Ther*, 12: 2078-87.

Toledo, Luis I., Matilde Murga, Rafal Zur, Rebeca Soria, Antonio Rodriguez, Sonia Martinez, Julen Oyarzabal, Joaquin Pastor, James R. Bischoff, and Oscar Fernandez-Capetillo. 2011. 'A cell-based screen identifies ATR inhibitors with synthetic lethal properties for cancer-associated mutations', *Nat Struct Mol Biol*, 18: 721-27.

Townsend, Michael J., and Joseph R. Arron. 2016. 'Reducing the risk of failure: biomarker-guided trial design', *Nature Reviews Drug Discovery*, 15: 517-18.

Tricker, E. M., C. Xu, S. Uddin, M. Capelletti, D. Ercan, A. Ogino, C. A. Pratilas, N. Rosen, N. S. Gray, K. K. Wong, and P. A. Janne. 2015. 'Combined EGFR/MEK Inhibition Prevents the Emergence of Resistance in EGFR-Mutant Lung Cancer', *Cancer Discov*, 5: 960-71.

Truman, A. W., K. Kristjansdottir, D. Wolfgeher, N. Hasin, S. Polier, H. Zhang, S. Perrett, C. Prodromou, G. W. Jones, and S. J. Kron. 2012. 'CDK-dependent Hsp70 Phosphorylation controls G1 cyclin abundance and cell-cycle progression', *Cell*, 151: 1308-18.

Tsuji, K., K. Mizumoto, T. Yamochi, I. Nishimoto, and M. Matsuoka. 2002. 'Differential effect of ik3-1/cables on p53- and p73-induced cell death', *J Biol Chem*, 277: 2951-7.

Tuominen, R., R. Jewell, J. J. van den Oord, P. Wolter, U. Stierner, C. Lindholm, C. Hertzman Johansson, D. Linden, H. Johansson, M. Frostvik Stolt, C. Walker, H. Snowden, J. Newton-Bishop, J. Hansson, and S. Egyhazi Brage. 2015. 'MGMT promoter methylation is associated with temozolomide response and prolonged progression-free survival in disseminated cutaneous melanoma', *Int J Cancer*, 136: 2844-53.

Turnbull, A. P., S. Ioannidis, W. W. Krajewski, A. Pinto-Fernandez, C. Heride, A. C. L. Martin, L. M. Tonkin, E. C. Townsend, S. M. Buker, D. R. Lancia, J. A. Caravella, A. V. Toms, T. M. Charlton, J. Lahdenranta, E. Wilker, B. C. Follows, N. J. Evans, L. Stead, C. Alli, V. V. Zarayskiy, A. C. Talbot, A. J. Buckmelter, M. Wang, C. L. McKinnon, F. Saab, J. F. McGouran, H. Century, M. Gersch, M. S. Pittman, C. G. Marshall, T. M. Raynham, M. Simcox, L. M. D. Stewart, S. B. McLoughlin, J. A. Escobedo, K. W. Bair, C. J. Dinsmore, T. R. Hammonds, S. Kim, S. Urbe, M. J. Clague, B. M. Kessler, and D. Komander. 2017. 'Molecular basis of USP7 inhibition by selective small-molecule inhibitors', *Nature*, 550: 481-86.

Van Allen, E. M., N. Wagle, A. Sucker, D. J. Treacy, C. M. Johannessen, E. M. Goetz, C. S. Place, A. Taylor-Weiner, S. Whittaker, G. V. Kryukov, E. Hodis, M. Rosenberg, A. McKenna, K. Cibulskis, D. Farlow, L. Zimmer, U. Hillen, R. Gutzmer, S. M. Goldinger, S. Ugurel, H. J. Gogas, F. Egberts, C. Berking, U. Trefzer, C. Loquai, B. Weide, J. C. Hassel, S. B. Gabriel, S. L. Carter, G. Getz, L. A. Garraway, and D. Schadendorf. 2014. 'The genetic landscape of clinical resistance to RAF inhibition in metastatic melanoma', *Cancer Discov*, 4: 94-109.

van der Horst, Armando, Alida M. M. de Vries-Smits, Arjan B. Brenkman, Miranda H. van Triest, Niels van den Broek, Frédéric Colland, Madelon M. Maurice, and Boudewijn M. T. Burgering. 2006. 'FOXO4 transcriptional activity is regulated by monoubiquitination and USP7/HAUSP', *Nature Cell Biology*, 8: 1064-73.

Verfaillie, Annelien, Hana Imrichova, Zeynep Kalender Atak, Michael Dewaele, Florian Rambow, Gert Hulselmans, Valerie Christiaens, Dmitry Svetlichnyy, Flavie Luciani, Laura Van den Mooter, Sofie Claerhout, Mark Fiers, Fabrice Journe, Ghanem-Elias Ghanem, Carl Herrmann, Georg Halder, Jean-Christophe Marine, and Stein Aerts. 2015. 'Decoding the regulatory landscape of melanoma reveals TEADS as regulators of the invasive cell state', *Nat Commun*, 6: 6683.

Villanueva, J., A. Vultur, J. T. Lee, R. Somasundaram, M. Fukunaga-Kalabis, A. K. Cipolla, B. Wubbenhorst, X. Xu, P. A. Gimotty, D. Kee, A. E. Santiago-Walker, R. Letrero, K. D'Andrea, A. Pushparajan, J. E. Hayden, K. D. Brown, S. Laquerre, G. A. McArthur, J. A. Sosman, K. L. Nathanson, and M. Herlyn. 2010. 'Acquired resistance to BRAF inhibitors mediated by a RAF kinase switch in melanoma can be overcome by cotargeting MEK and IGF-1R/PI3K', *Cancer Cell*, 18: 683-95.

Vogelstein, B., D. Lane, and A. J. Levine. 2000. 'Surfing the p53 network', *Nature*, 408: 307-10.

Vredeveld, L. C., P. A. Possik, M. A. Smit, K. Meissl, C. Michaloglou, H. M. Horlings, A. Ajouaou, P. C. Kortman, D. Dankort, M. McMahon, W. J. Mooi, and D. S. Peeper. 2012. 'Abrogation of BRAFV600E-induced senescence by PI3K pathway activation contributes to melanomagenesis', *Genes Dev*, 26: 1055-69.

Wagle, N., C. Emery, M. F. Berger, M. J. Davis, A. Sawyer, P. Pochanard, S. M. Kehoe, C. M. Johannessen, L. E. Macconaill, W. C. Hahn, M. Meyerson, and L. A. Garraway. 2011. 'Dissecting therapeutic resistance to RAF inhibition in melanoma by tumor genomic profiling', *J Clin Oncol*, 29: 3085-96.

Wagle, N., E. M. Van Allen, D. J. Treacy, D. T. Frederick, Z. A. Cooper, A. Taylor-Weiner, M. Rosenberg, E. M. Goetz, R. J. Sullivan, D. N. Farlow, D. C. Friedrich, K. Anderka, D. Perrin, C. M. Johannessen, A. McKenna, K. Cibulskis, G. Kryukov, E. Hodis, D. P. Lawrence, S. Fisher, G. Getz, S. B. Gabriel, S. L. Carter, K. T. Flaherty, J. A. Wargo, and L. A. Garraway. 2014. 'MAP kinase pathway alterations in BRAF-mutant melanoma patients with acquired resistance to combined RAF/MEK inhibition', *Cancer Discov*, 4: 61-8.

Wang, L., S. Kumar, S. Dahiya, F. Wang, J. Wu, K. Newick, R. Han, A. Samanta, U. H. Beier, T. Akimova, T. R. Bhatti, B. Nicholson, M. P. Kodrasov, S. Agarwal, D. E. Sterner, W. Gu, J. Weinstock, T. R. Butt, S. M. Albelda, and W. W. Hancock. 2016. 'Ubiquitin-specific

Protease-7 Inhibition Impairs Tip60-dependent Foxp3+ T-regulatory Cell Function and Promotes Antitumor Immunity', *EBioMedicine*, 13: 99-112.

Wang, M., Y. Zhang, T. Wang, J. Zhang, Z. Zhou, Y. Sun, S. Wang, Y. Shi, X. Luan, Y. Zhang, Y. Wang, Y. Wang, Z. Zou, L. Kang, and H. Liu. 2017. 'The USP7 Inhibitor P5091 Induces Cell Death in Ovarian Cancers with Different P53 Status', *Cell Physiol Biochem*, 43: 1755-66.

Wang, N., L. Guo, B. R. Rueda, and J. L. Tilly. 2010. 'Cables1 protects p63 from proteasomal degradation to ensure deletion of cells after genotoxic stress', *EMBO Rep*, 11: 633-9.

Wang, T., K. Birsoy, N. W. Hughes, K. M. Krupczak, Y. Post, J. J. Wei, E. S. Lander, and D. M. Sabatini. 2015. 'Identification and characterization of essential genes in the human genome', *Science*, 350: 1096-101.

Wang, T., J. J. Wei, D. M. Sabatini, and E. S. Lander. 2014. 'Genetic screens in human cells using the CRISPR-Cas9 system', *Science*, 343: 80-4.

Wang, X., M. Cunningham, X. Zhang, S. Tokarz, B. Laraway, M. Troxell, and R. C. Sears. 2011. 'Phosphorylation regulates c-Myc's oncogenic activity in the mammary gland', *Cancer Res*, 71: 925-36.

Wang, X., M. Mazurkiewicz, E. K. Hillert, M. H. Olofsson, S. Pierrou, P. Hillertz, J. Gullbo, K. Selvaraju, A. Paulus, S. Akhtar, F. Bossler, A. C. Khan, S. Linder, and P. D'Arcy. 2016. 'The proteasome deubiquitinase inhibitor VLX1570 shows selectivity for ubiquitin-specific protease-14 and induces apoptosis of multiple myeloma cells', *Sci Rep*, 6: 26979.

Wang, Y., T. Zhang, N. Kwiatkowski, B. J. Abraham, T. I. Lee, S. Xie, H. Yuzugullu, T. Von, H. Li, Z. Lin, D. G. Stover, E. Lim, Z. C. Wang, J. D. Iglehart, R. A. Young, N. S. Gray, and J. J. Zhao. 2015. 'CDK7-dependent transcriptional addiction in triple-negative breast cancer', *Cell*, 163: 174-86.

Wargo, J. A., Z. A. Cooper, and K. T. Flaherty. 2014. 'Universes collide: combining immunotherapy with targeted therapy for cancer', *Cancer Discov*, 4: 1377-86.

Weinstock, J., J. Wu, P. Cao, W. D. Kingsbury, J. L. McDermott, M. P. Kodrasov, D. M. McKelvey, K. G. Suresh Kumar, S. J. Goldenberg, M. R. Mattern, and B. Nicholson. 2012. 'Selective Dual Inhibitors of the Cancer-Related Deubiquitylating Proteases USP7 and USP47', *ACS Med Chem Lett*, 3: 789-92.

Weller, M., J. Felsberg, C. Hartmann, H. Berger, J. P. Steinbach, J. Schramm, M. Westphal, G. Schackert, M. Simon, J. C. Tonn, O. Heese, D. Krex, G. Nikkhah, T. Pietsch, O. Wiestler, G. Reifenberger, A. von Deimling, and M. Loeffler. 2009. 'Molecular predictors of progression-free and overall survival in patients with newly diagnosed glioblastoma: a prospective translational study of the German Glioma Network', *J Clin Oncol*, 27: 5743-50.

West, A. C., and R. W. Johnstone. 2014. 'New and emerging HDAC inhibitors for cancer treatment', *J Clin Invest*, 124: 30-9.

Whittaker, S. R., J. P. Theurillat, E. Van Allen, N. Wagle, J. Hsiao, G. S. Cowley, D. Schadendorf, D. E. Root, and L. A. Garraway. 2013. 'A genome-scale RNA interference screen implicates NF1 loss in resistance to RAF inhibition', *Cancer Discov*, 3: 350-62.

Wood, K. C., D. J. Konieczkowski, C. M. Johannessen, J. S. Boehm, P. Tamayo, O. B. Botvinnik, J. P. Mesirov, W. C. Hahn, D. E. Root, L. A. Garraway, and D. M. Sabatini. 2012. 'MicroSCALE screening reveals genetic modifiers of therapeutic response in melanoma', *Sci Signal*, 5: rs4.

Wood, K. W., C. Sarnecki, T. M. Roberts, and J. Blenis. 1992. 'ras mediates nerve growth factor receptor modulation of three signal-transducing protein kinases: MAP kinase, Raf-1, and RSK', *Cell*, 68: 1041-50.

Wu, S. Y., and C. M. Chiang. 2007. 'The double bromodomain-containing chromatin adaptor Brd4 and transcriptional regulation', *J Biol Chem*, 282: 13141-5.

Xia, J., Y. He, B. Meng, S. Chen, J. Zhang, X. Wu, Y. Zhu, Y. Shen, X. Feng, Y. Guan, C. Kuang, J. Guo, Q. Lei, Y. Wu, G. An, G. Li, L. Qiu, F. Zhan, and W. Zhou. 2020. 'NEK2 induces autophagy-mediated bortezomib resistance by stabilizing Beclin-1 in multiple myeloma', *Mol Oncol*.

Xue, H. Y., L. J. Ji, A. M. Gao, P. Liu, J. D. He, and X. J. Lu. 2016. 'CRISPR-Cas9 for medical genetic screens: applications and future perspectives', *J Med Genet*, 53: 91-7.

Yang, Dun, Hong Liu, Andrei Goga, Suwon Kim, Mariia Yuneva, and J. Michael Bishop. 2010. 'Therapeutic potential of a synthetic lethal interaction between the MYC proto-oncogene and inhibition of aurora-B kinase', *Proceedings of the National Academy of Sciences*, 107: 13836-41.

Yang, J. Y., C. J. Chang, W. Xia, Y. Wang, K. K. Wong, J. A. Engelman, Y. Du, M. Andreeff, G. N. Hortobagyi, and M. C. Hung. 2010. 'Activation of FOXO3a is sufficient to reverse mitogen-activated protein/extracellular signal-regulated kinase kinase inhibitor chemoresistance in human cancer', *Cancer Res*, 70: 4709-18.

Yin, Hao, Wen Xue, and Daniel G. Anderson. 2019. 'CRISPR–Cas: a tool for cancer research and therapeutics', *Nature Reviews Clinical Oncology*, 16: 281-95.

Yokoyama, S., E. Feige, L. L. Poling, C. Levy, H. R. Widlund, M. Khaled, A. L. Kung, and D. E. Fisher. 2008. 'Pharmacologic suppression of MITF expression via HDAC inhibitors in the melanocyte lineage', *Pigment Cell Melanoma Res*, 21: 457-63.

Yuan, Jie, Bryson D. Bennett, and Joshua D. Rabinowitz. 2008. 'Kinetic flux profiling for quantitation of cellular metabolic fluxes', *Nature Protocols*, 3: 1328-40.

Zaika, A. I., N. Slade, S. H. Erster, C. Sansome, T. W. Joseph, M. Pearl, E. Chalas, and U. M. Moll. 2002. 'DeltaNp73, a dominant-negative inhibitor of wild-type p53 and TAp73, is up-regulated in human tumors', *J Exp Med*, 196: 765-80.

Zeller, K. I., A. G. Jegga, B. J. Aronow, K. A. O'Donnell, and C. V. Dang. 2003. 'An integrated database of genes responsive to the Myc oncogenic transcription factor: identification of direct genomic targets', *Genome Biol*, 4: R69.

Zeng, L., and M. M. Zhou. 2002. 'Bromodomain: an acetyl-lysine binding domain', *FEBS Lett*, 513: 124-8.

Zhang, W., J. Zhang, C. Xu, S. Zhang, S. Bian, F. Jiang, W. Ni, L. Qu, C. Lu, R. Ni, Y. Fan, M. Xiao, and J. Liu. 2020. 'Ubiquitin-specific protease 7 is a drug-able target that promotes hepatocellular carcinoma and chemoresistance', *Cancer Cell Int*, 20: 28.

Zhang, Wei, and Sachdev S. Sidhu. 2018. 'Allosteric inhibitors hit USP7 hard', *Nat Chem Biol*, 14: 110-11.

Zhao, X., B. Fiske, A. Kawakami, J. Li, and D. E. Fisher. 2011. 'Regulation of MITF stability by the USP13 deubiquitinase', *Nat Commun*, 2: 414.

Zhu, H., F. Bengsch, N. Svoronos, M. R. Rutkowski, B. G. Bitler, M. J. Allegrezza, Y. Yokoyama, A. V. Kossenkov, J. E. Bradner, J. R. Conejo-Garcia, and R. Zhang. 2016. 'BET Bromodomain Inhibition Promotes Anti-tumor Immunity by Suppressing PD-L1 Expression', *Cell Rep*, 16: 2829-37.

Zhu, J., J. Jiang, W. Zhou, and X. Chen. 1998. 'The potential tumor suppressor p73 differentially regulates cellular p53 target genes', *Cancer Res*, 58: 5061-5.

Zhu, S., C. J. Denman, Z. S. Cobanoglu, S. Kiany, C. C. Lau, S. M. Gottschalk, D. P. Hughes, E. S. Kleinerman, and D. A. Lee. 2015. 'The narrow-spectrum HDAC inhibitor entinostat enhances NKG2D expression without NK cell toxicity, leading to enhanced recognition of cancer cells', *Pharm Res*, 32: 779-92.

Zingg, Daniel, Julien Debbache, Simon M. Schaefer, Eylul Tuncer, Sandra C. Frommel, Phil Cheng, Natalia Arenas-Ramirez, Jessica Haeusel, Yudong Zhang, Mario Bonalli, Michael T. McCabe, Caretha L. Creasy, Mitchell P. Levesque, Onur Boyman, Raffaella Santoro, Olga Shakhova, Reinhard Dummer, and Lukas Sommer. 2015. 'The epigenetic modifier EZH2 controls melanoma growth and metastasis through silencing of distinct tumour suppressors', *Nat Commun*, 6: 6051.

Zuber, J., J. Shi, E. Wang, A. R. Rappaport, H. Herrmann, E. A. Sison, D. Magoon, J. Qi, K. Blatt, M. Wunderlich, M. J. Taylor, C. Johns, A. Chicas, J. C. Mulloy, S. C. Kogan, P. Brown, P. Valent, J. E. Bradner, S. W. Lowe, and C. R. Vakoc. 2011. 'RNAi screen identifies Brd4 as a therapeutic target in acute myeloid leukaemia', *Nature*, 478: 524-8.

Zukerberg, L. R., R. L. DeBernardo, S. D. Kirley, M. D'Apuzzo, M. P. Lynch, R. D. Littell, L. R. Duska, L. Boring, and B. R. Rueda. 2004. 'Loss of cables, a cyclin-dependent kinase regulatory protein, is associated with the development of endometrial hyperplasia and endometrial cancer', *Cancer Res*, 64: 202-8.

Appendix A: Supplementary Materials for Chapter 2

Supplementary Figure A-1. Genome-scale CRISPR screening identifies USP7 as a potential therapeutic target in NRAS-mutant melanomas

(A) Essential genes that dropped out in both MEKi arm compared to day 0 and vehicle arm compared to day 0. As expected, cell type specific essential gene NRAS dropped out in both arms. In red are genes that have been found to be common essential genes in other CRISPR screens in melanoma.
(B) GO analysis of essential genes identified pathways that are commonly essential as well.
(C) *NRAS*-mutant melanoma line SKMEL2 was infected with shRNA against control or *USP7.* After knockdown was confirmed, cells were treated with DMSO or trametinib (MEKi, 10nM) for 96 hours. Graphs represent log2 transformation of the fold change in cell number at day 4 versus day 0. Right axis shows percent change in cell number relative to day 0. Negative values represent a decrease in cell number over time and positive values represent an increase in cell number. Immunoblots show levels of USP7, phosphorylated ERK (pERK), and total ERK (ERK) after 24 hours of indicated treatment.
(D) Immunoblots demonstrating knock-down of USP7 in different *NRAS*-mutant melanoma cell lines: SKEML2, Hs936T, and WM3670.
(E) Cell counting assays with corresponding immunoblots demonstrating the effect of USP7 knock-out in the *NRAS*-mutant melanoma cell line Hs936T.

Supplementary Figure A-1 (continued)

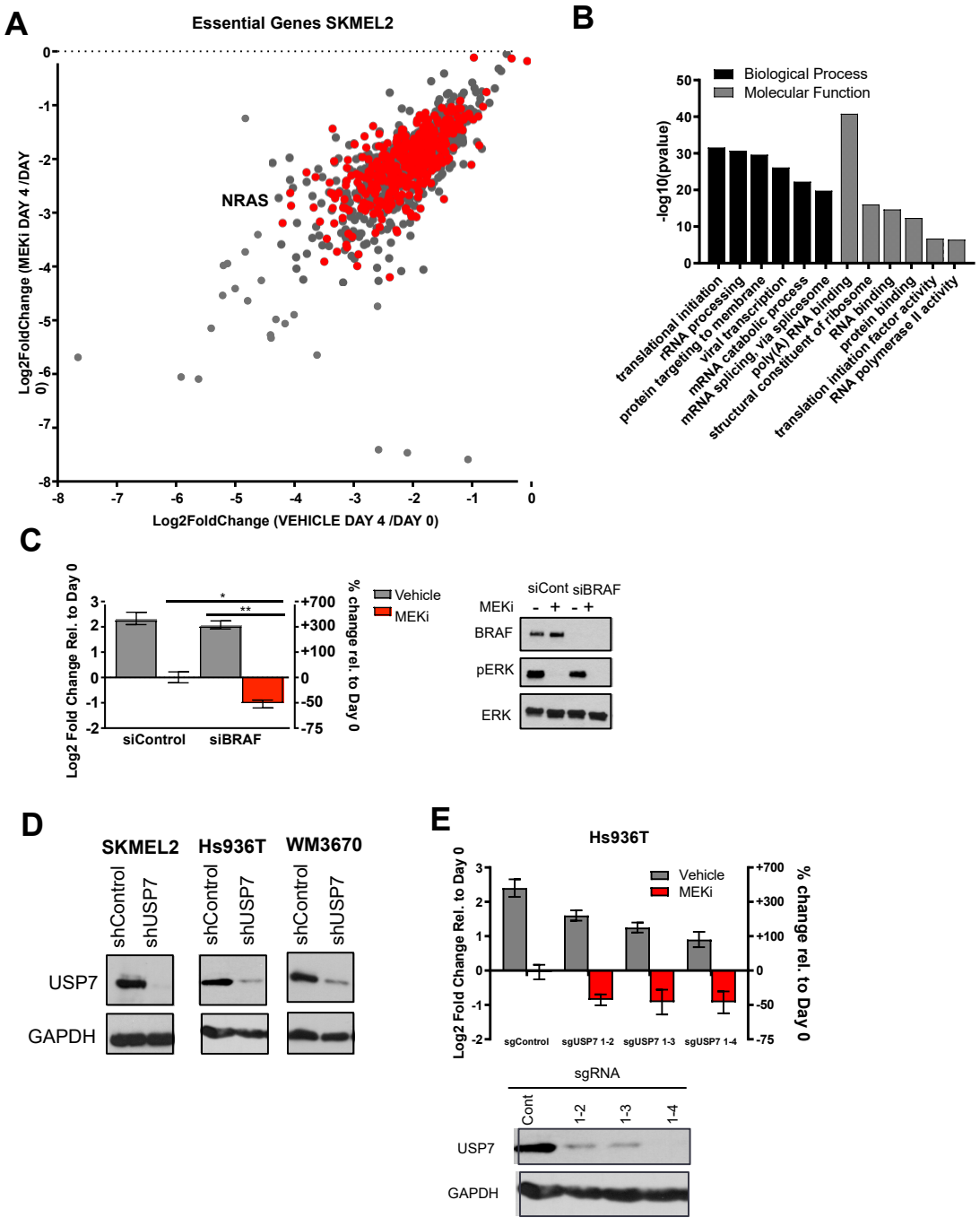

Supplementary Figure A-2. MEK and USP7 inhibitors potently synergize, trigger apoptosis, and induce the regression of NRAS-mutant melanomas in vivo

(A) Cell counting results after 4 days of treatment with USP7i P5091 and MEK inhibitor binimetinib (MEK162) in SKMEL2 *NRAS*-mutant melanoma cell line.
(B) Cell counting results after 4 days of treatment with USP7i P5091 (10uM) and MEK inhibitor trametinib (10nM) in 293T.
(C) Relative weight of YUDOSO xenograft NSG mice over time of treatment. >20% loss in weight demonstrates toxicity.
(D) Relative weight of MM415 xenograft mice over time of treatment. >20% loss in weight demonstrates toxicity.
(E) Relative weight of A375 xenograft mice over time of treatment. >20% loss in weight demonstrates toxicity.

Supplementary Figure A-. (continued)

A

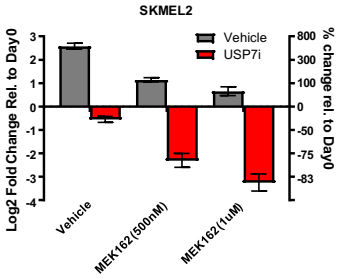

B

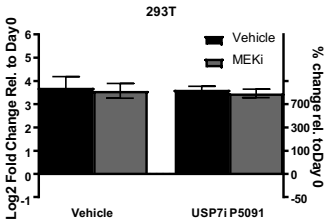

C

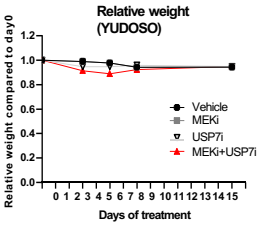

D

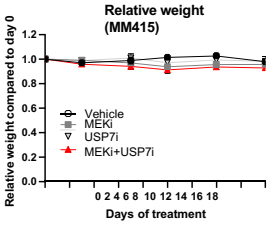

E

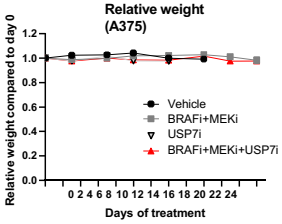

Supplementary Figure A-3. USP7 inhibitors function by suppressing the USP7-EPOP-ELOB/C complex in melanomas

(A) Cell counting assays and corresponding immunoblots for two *NRAS*-mutant melanomas (SKMEL2 and MM415) and one *BRAF*-mutant melanoma (MALME3M) with siControl or siP53 knock-down.
(B) Cell counting assay for SKMEL2 and MM415 *NRAS*-mutant melanoma cell lines treated with MEKi trametinib (10nM) and/or MDM2 inhibitor nutlin-3a (10uM) for 4 days. Dose of nutlin-3a determined by previous papers.
(C) Cell counting assays and corresponding qPCR results for two *NRAS*-mutant melanomas Hs936T and WM3629 with siEPOP and siEPOP.
(D) Cell counting assays and corresponding immunoblots for two *NRAS*-mutant melanomas (Hs936T and WM3629) with shControl and shELOB.

Supplementary Figure A-. (continued)

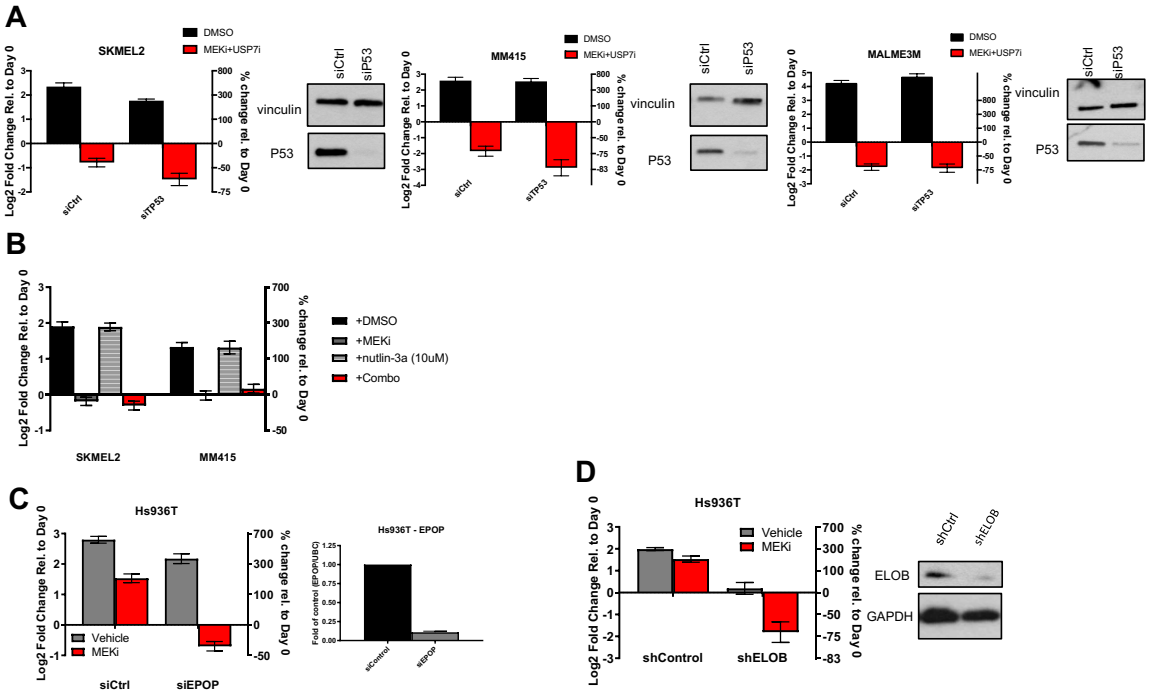

Appendix B: Supplementary Materials for Chapter 3

Figure B-1. A subset of melanoma cell lines and control cell lines do not respond to BRAF/MEK/HDAC inhibitor therapy. Therapeutic responses are unrelated to MITF status or expression changes. (A--D) melanoma cells (A2058), transformed human embryonic kidney cells (HEK293T) and fibroblasts (IMR90 and NIH3T3) were treated with DMSO, 100nM dabrafenib and 10nM trametinib (DT), 2μM vorinostat (V), 1μM entinostat (E) and the combination of MEK/BRAF and HDAC inhibitors. Cells were manually counted prior to the addition of compounds and 3 days after treatment. Graphs represent log2 transformation of the fold change in cell number at day 3 versus day 0. Right axis shows percent change in cell number relative to day 0. Immunoblots show levels of phosphorylated ERK (p--ERK), total ERK, histone H3 acetylation at lysine 9 (H3K9Ac) and total H3 after 48 hours of indicated treatment. **(E)** Real--time quantification of apoptotic cell death using the live cell imager IncuCyte Zoom. Red (nuclear restricted NucLight Red fluorescent protein for quantifiying live cells) and green (Apoptosis--3/7 Green reagent for quantifying apoptotic cells) fluorescent objects were monitored in the Incucyte ZOOM acquiring images every 2 hours (for 72 hours) following treatment with vehicle (DMSO) or drugs (MEK inhibitor, BRAF inhibitor, HDAC inhibitor) and then quantified with the IncuCyte integrated analysis software. **(F)** quantification of MITF protein levels of cell lines sensitive and resistant to MAPK/HDAC inhibition, as shown in Fig. 1A and Fig. 3D. **(G)** Western blots depicting MITF protein levels in different melanoma cell lines (high/low baseline MITF levels and sensitive/resistant to MAPK/HDAC inhibition) after 48hrs of treatment with vehicle (Veh), MEK inhibitor (MEKi) and/or HDAC inhibitors (vorinostat, VOR;; entinostat, ENT). Vinculin serves as a loading control. **(H)** Western blots depicting HDAC1, HDAC2 and HDAC3 protein levels after 48hrs of treatment with vehicle (--), HDAC inhibitor (entinostat, E) and combined MEK/BRAF/HDAC inhibitor (DTE). GAPDH serves as a loading control.

Figure B-1 (continued)

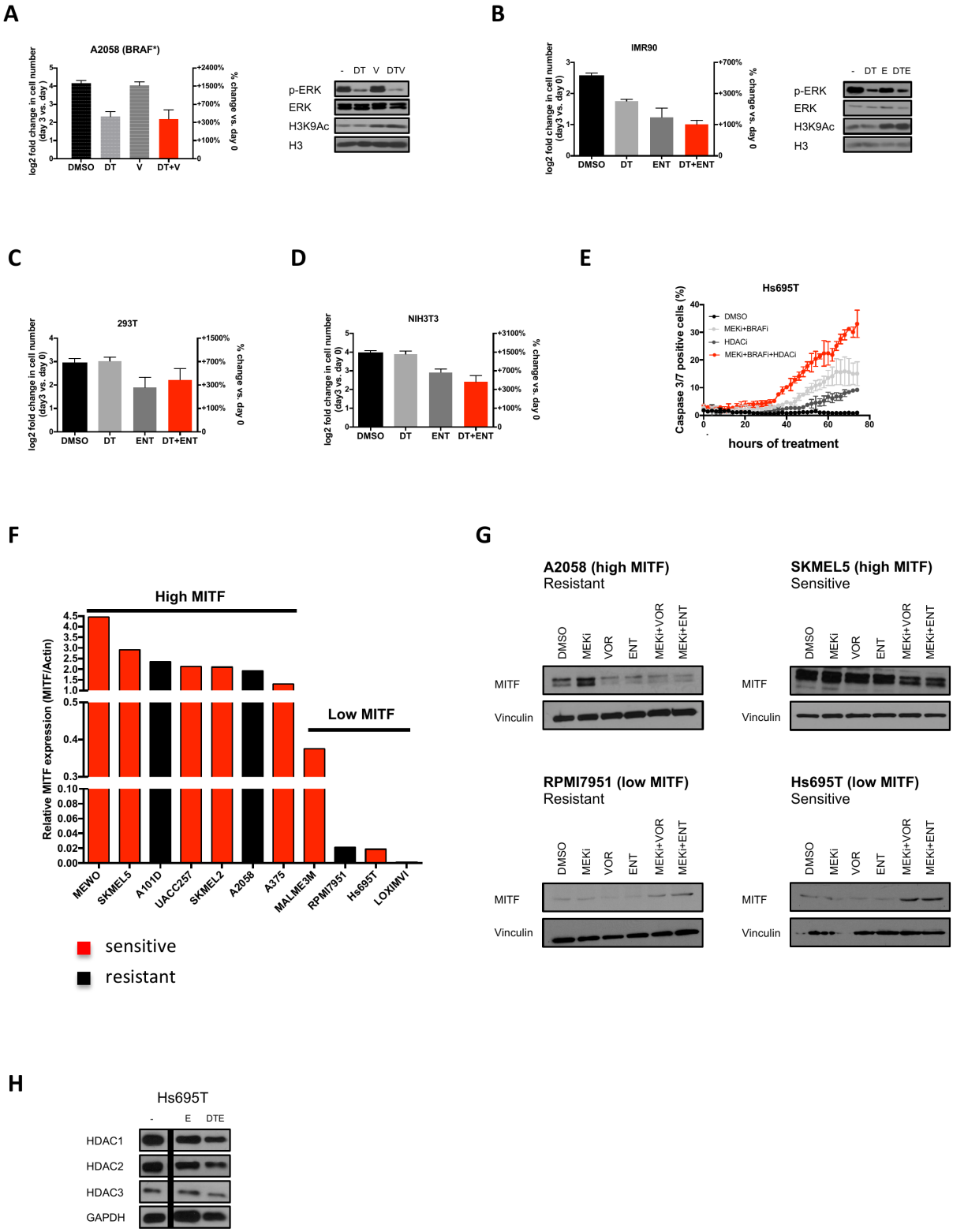

Supplementary Figure 1

A

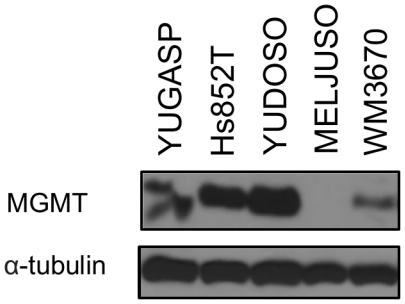

Figure B-2. Differential expression of MGMT in *NRAS*--mutant cell lines.
(A) Western blot depicting baseline MGMT protein expression levels in *NRAS*--mutant human melanoma cell lines shown in Fig. 3-2E.

Supplementary Figure B-3. Therapeutic effects are not mediated by ROS.
(A) Sensitive cell lines (Hs695T and SKMEL2) treated with DMSO, 100nM dabrafenib (D) and/or 10nM trametinib (T), 1μM entinostat (E) and the combination of MEK/BRAF and HDAC inhibitors for 24hrs (or 1mM H_2O_2 for 4hrs as a positive control) were stained with dichlorofluorescein diacetate (DCFDA), a dye that measures ROS. Graphs indicate relative mean DCFDA fluorescence intensity. ROS levels slightly decrease in Hs695T cells in response to DTE whereas they increase in SKMEL2 cells, due to the effects of T. **(B,C)** Sensitive melanoma cells (Hs695T and SKMEL2) were treated with DMSO, 100nM dabrafenib (D) and/or 10nM trametinib (T), 1μM entinostat (E) or the specified drug combinations, alone and in combination with the ROS scavenger NAC and the anti--oxidant Vitamin C. Graphs represent log2 transformation of the fold change in cell number at day 3 versus day 0. Right axis shows percent change in cell number relative to day 0. Negative values represent cell death and a decrease in cell number. NAC is toxic in Hs695T cells. Vitamin C does not suppress, but rather potentiates the therapeutic response. NAC is tolerated in SKMEL2 cells and has no effect on the therapeutic response. **(D)** Resistant melanoma cells (A2058 and RPMI7951) were treated with DMSO, 100nM dabrafenib and 10nM trametinib (DT), 1μM vorinostat (VOR) or the specified drug combinations, alone and in combination with the ROS inducer buthionine sulfoximine (BSO, 200μM). Graphs represent log2 transformation of the fold change in cell number at day 3 versus day 0. Right axis shows percent change in cell number relative to day 0. Negative values represent cell death and a decrease in cell number. BSO does not make resistant cells become sensitive to this combination. **(E)** Baseline ROS levels for 3 sensitive and 3 resistant melanoma cell lines as measured by DCFDA staining, demonstrating that ROS levels do not correlate with sensitivity.

Figure B-3 (continued)

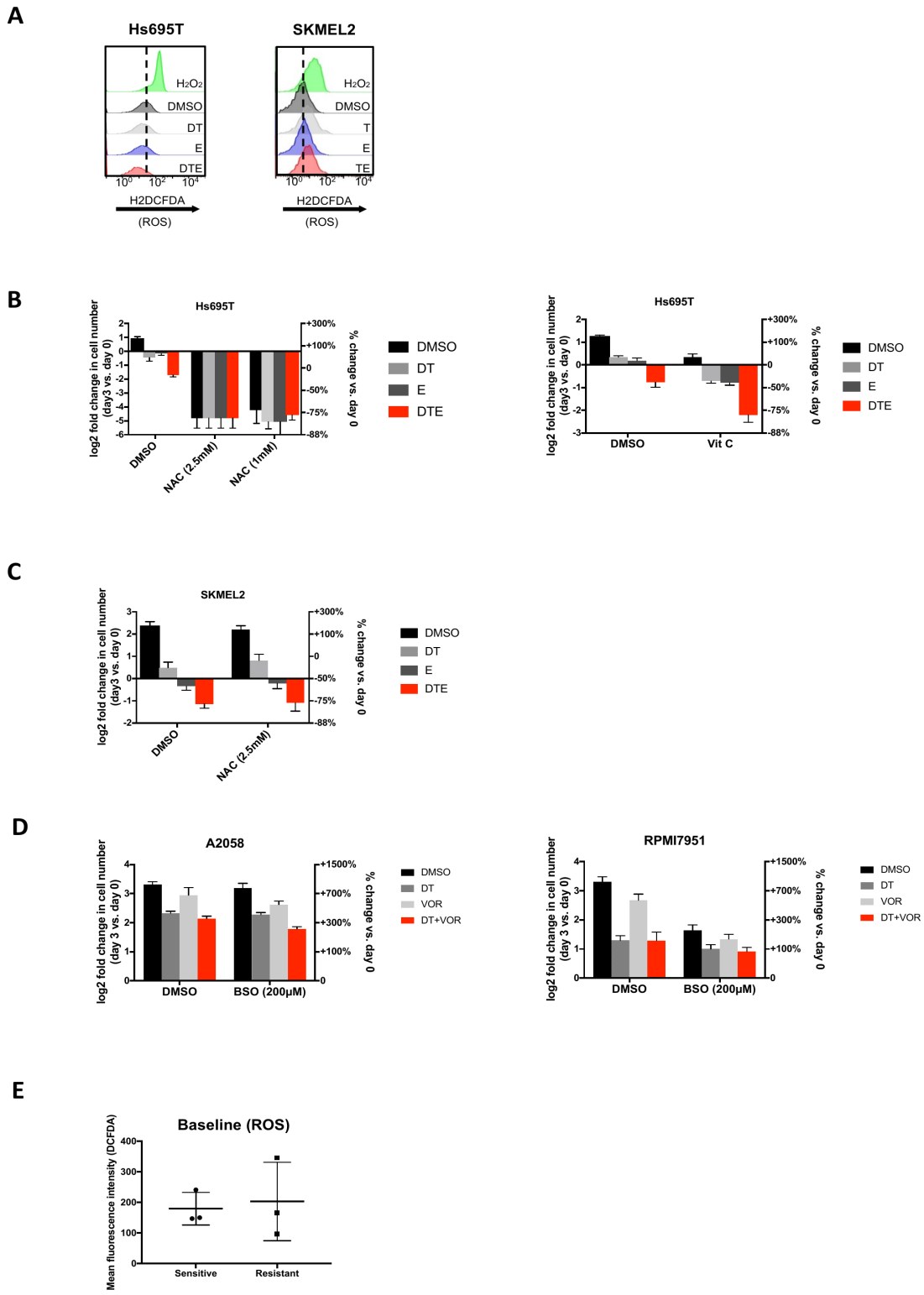

Supplementary Figure 3

Figure B-4. Induction of DNA repair genes in melanoma cells.
(A) Melanoma cells, transfected with control (siLuc) or pooled siRNAs targeting BRCA2 were irradiated with 10Gy. Cells were fixed 5 hours later and analyzed by immunofluorescence for RAD51 and gamma H2AX. Insets show magnification of merged gamma H2AX and RAD51 signals in sensitive and resistant cell lines, respectively. **(B)** Heatmap of only non--cell cycle regulated DNA repair genes in MGMT+ versus MGMT-- melanomas. Heatmap of differentially expressed DNA repair genes not regulated by the cell cycle in (MGMT+) versus (MGMT--) melanomas at significance level p=0.001. “High” expression (MGMT+) was defined as the top 10% of tumors in the TCGA SKCM provisional dataset stratified by MGMT mRNA expression, whereas “low” (MGMT--) was defined as the bottom 10%.

Figure B-4 (continued)

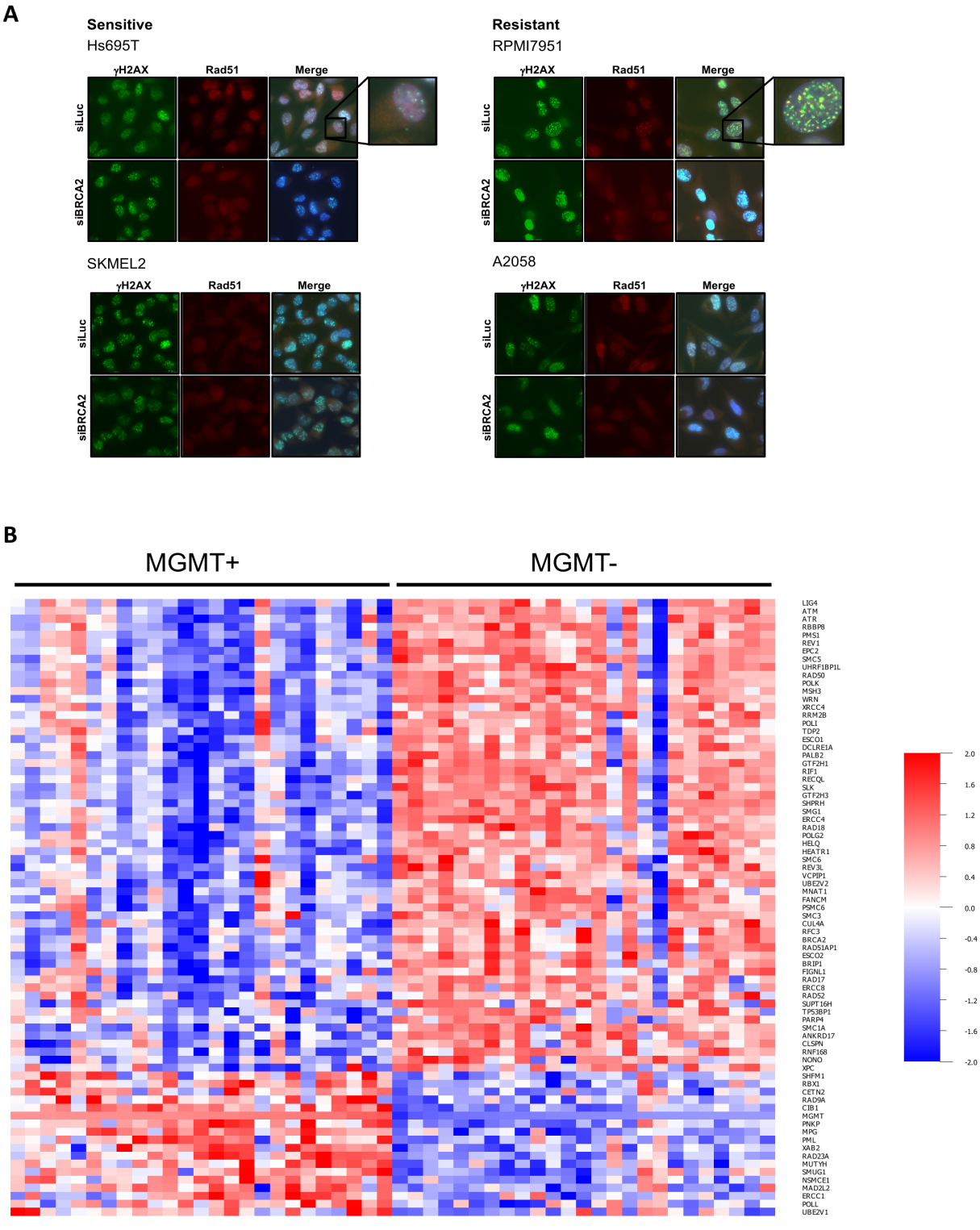

Supplementary Figure 4

A

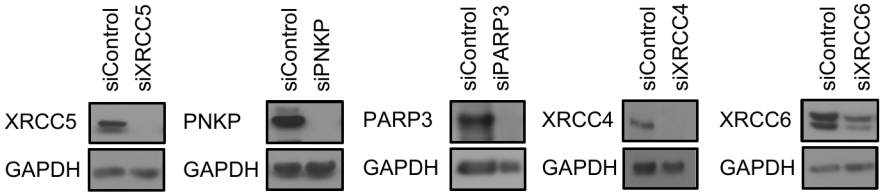

B

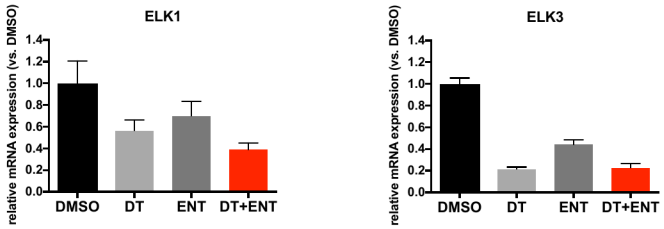

Figure B-5.
(A) Immunoblots confirming siRNA target suppression for experiment shown in Figure 6D. **(B)** mRNA levels of *ELK1* and *ELK3* in sensitive cells after 24hrs of treatment with vehicle (Veh), 100nM dabrafenib and 10nM trametinib (DT) and/or 1μM entinostat (ENT) as determined by quantitative PCR.

Appendix C: Supplementary Materials for Chapter 4

Cell Reports, Volume *21*

Supplemental Information

Melanoma Therapeutic Strategies that Select against Resistance by Exploiting MYC-Driven Evolutionary Convergence

Katherine R. Singleton, Lorin Crawford, Elizabeth Tsui, Haley E. Manchester, Ophelia Maertens, Xiaojing Liu, Maria V. Liberti, Anniefer N. Magpusao, Elizabeth M. Stein, Jennifer P. Tingley, Dennie T. Frederick, Genevieve M. Boland, Keith T. Flaherty, Shannon J. McCall, Clemens Krepler, Katrin Sproesser, Meenhard Herlyn, Drew J. Adams, Jason W. Locasale, Karen Cichowski, Sayan Mukherjee, and Kris C. Wood

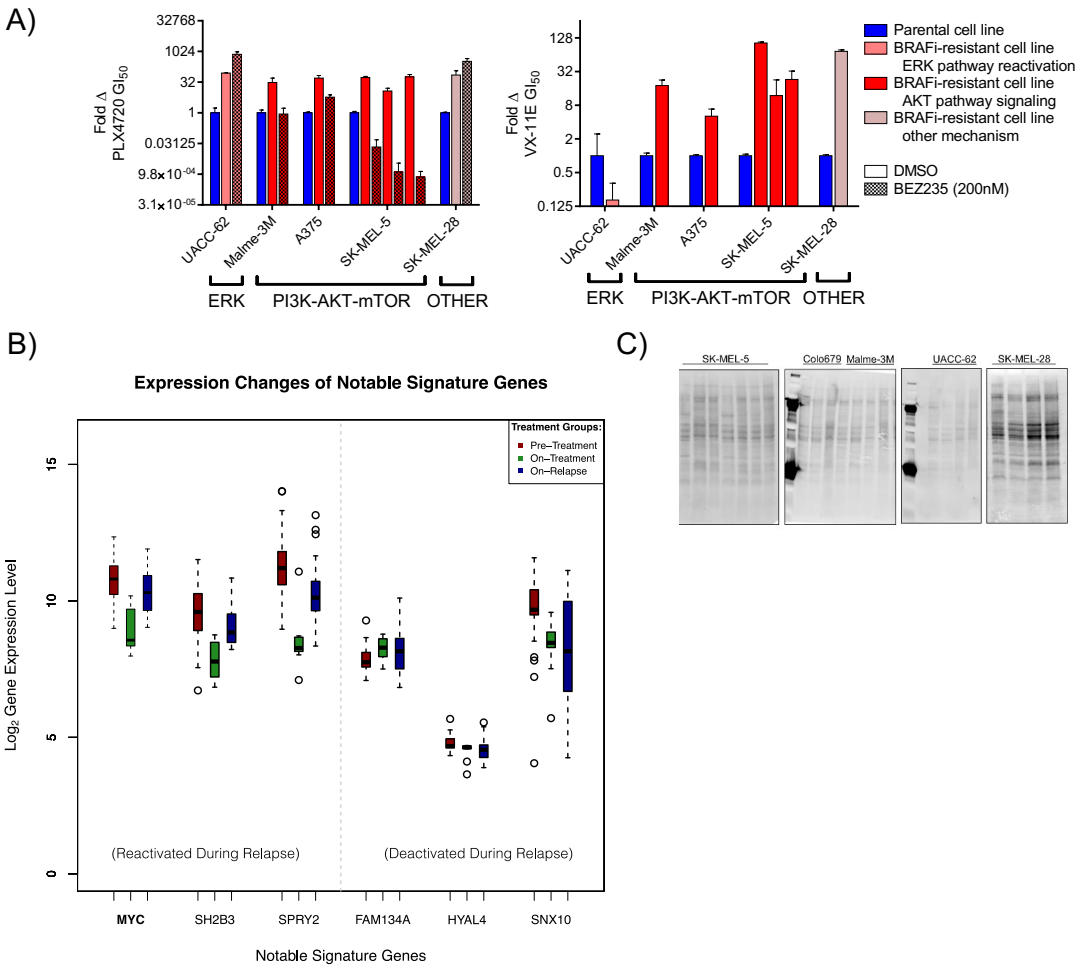

Figure S1. Characterization of MYC activation in melanomas with acquired resistance to BRAF pathway blockade, related to Figure 1. A) Evolved PLX4720 (BRAFi)-resistant cells that could be re-sensitized by the addition of the PI3K/mTOR inhibitor, BEZ235, were classified as having a functional PI3K-AKT-mTOR pathway bypass signaling resistance mechanism. Cells that were resistant to PLX4720 but not also resistant to the ERK inhibitor, VX-11E, were classified as having a functional RAF-ERK signaling re-activation resistance mechanism. Cells that could be fully re-sensitized through stable shRNA-mediated Notch1 suppression were classified as having a Notch1 pathway resistance mechanism and are described elsewhere (Martz, Ottina, Singleton *et al*., *Sci Signal* 2014, **7**, ra121). One evolved resistant cell line could not be re-sensitized by VX-11E, BEZ235, or shNotch1 and was therefore classified as other/unknown. In all cases, fold change values are relative to parental cells (blue), and data are means (+/- SD) from three experiments. **B)** Expression of indicated genes from the BRAF response signature in cell lines and primary tumors at indicated time points. Error bars indicate 90% confidence intervals and open circles are outliers. **C)** Total protein staining for immunoblots shown in Figure 1F, where for each cell line the left to right ordering of samples is the same as in Figure 1F.

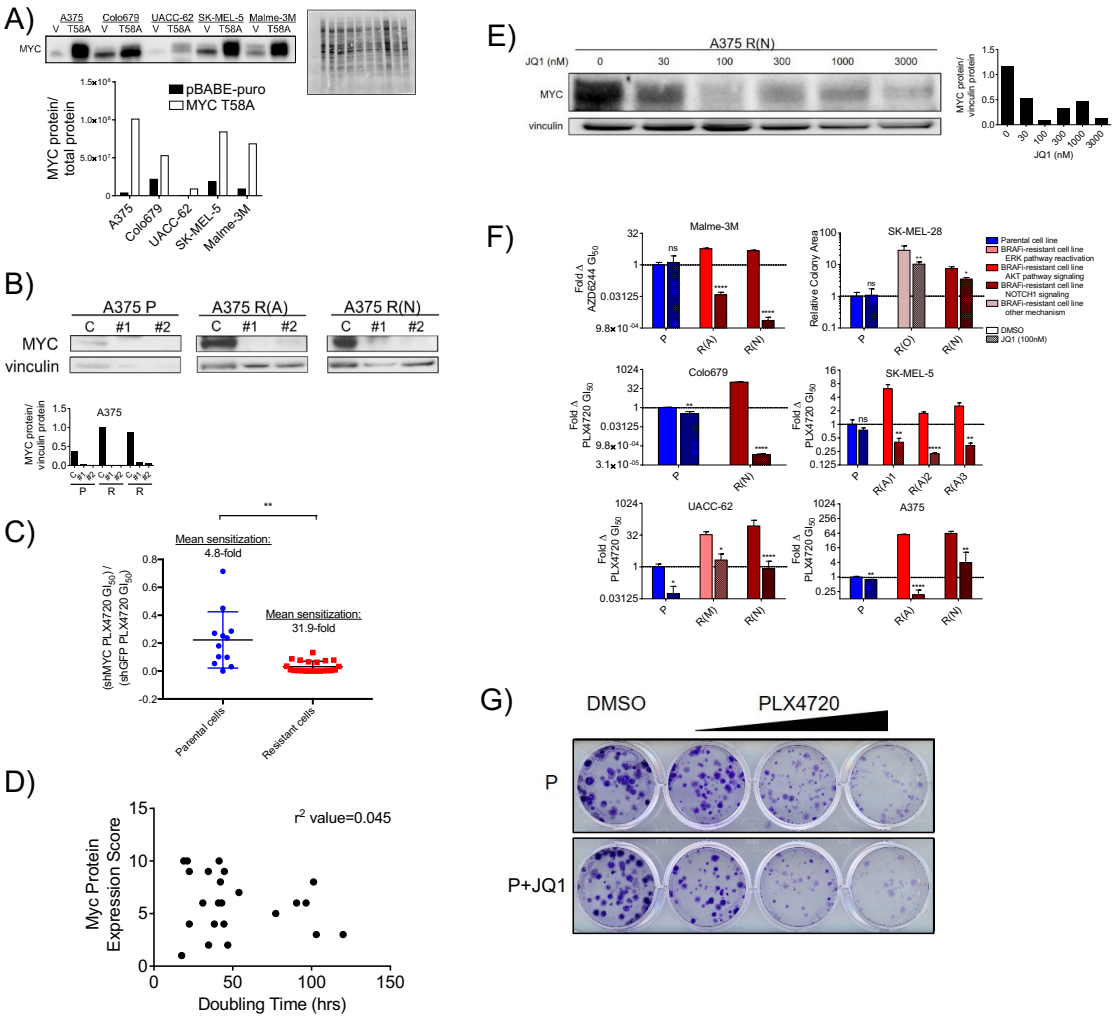

Figure S2. Functional characterization of MYC in BRAFi resistant melanomas , related to Figure 2. A) Ectopic expression of MYC^{T58A} or empty vector control in treatment-naïve, BRAFi-sensitive *BRAF* mutant melanoma cell lines, determined by immunoblotting. Quantification, bottom panel; total protein, right top panel; V, pBABE empty vector. **B)** The indicated cell lines (P, parental and R, resistant), expressing either shGFP (C) or one of two independent shRNAs targeting MYC (#1 or #2), were immunoblotted for expression of MYC and vinculin as a loading control to validate protein knockdown. Quantified, bottom panel. **C)** The ratio of GI50 values for PLX4720 in parental and resistant cell lines expressing shMYC (hairpins 1-2) and shGFP. **D)** MYC protein level was scored on a scale of 1-10, with 10 indicating highest MYC protein expression and correlated to cell line doubling time. **E)** A375 R(N) cells were treated with the indicated doses of JQ1 for 72 hours. Whole cell lysates were immunoblotted for expression of MYC and vinculin as a loading control. Quantified, right panel. **F)** Evolved PLX4720-resistant cell lines could be re-sensitized to PLX4720 or AZD6244 (Malme-3M) by the addition of JQ1 (100 nM) as determined by GI_{50} assay or clonogenic growth assay (in 3 μM PLX4720). JQ1 + BRAFi treated wells are normalized to the values of the relevant JQ1 only treated wells to account for non-specific toxicity. *P* values denote significance between DMSO and JQ1 treatment in each cell line. **G)** Effect on clonogenic growth of A375 cells (P) treated with increasing doses of PLX4720 in the presence or absence of JQ1 (100nM). Data are means (SD) from three experiments. **P* < 0.05; ***P* < 0.01; *****P* < 0.001.

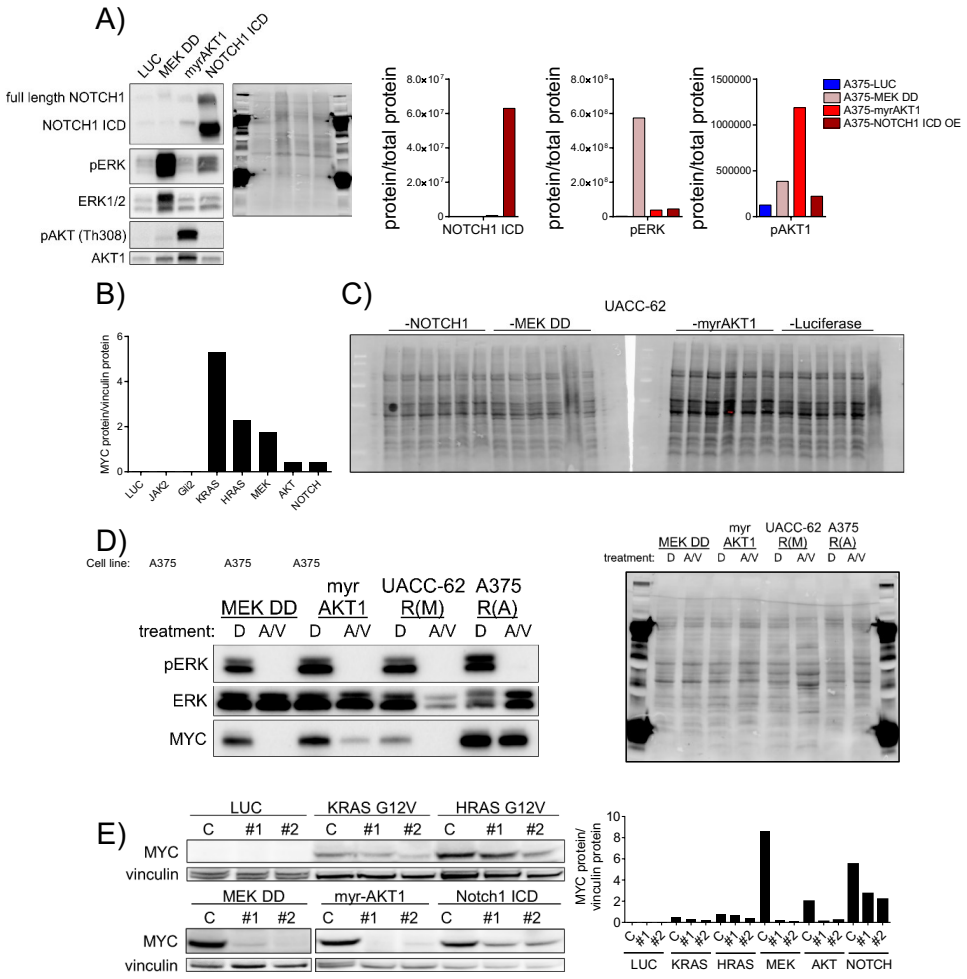

Figure S3. MYC activation and suppression in melanoma cells with engineered activation of major resistance pathways , related to Figure 3. A) A375 cells expressing the pathway activating constructs indicated were immunoblotted for Notch1, phospho-ERK and phospho-AKT1 (Th308) as evidence of activation of each pathway (left panel). Total protein is shown in the center panel and protein expression normalized to total protein is shown in the right panel. **B)** Quantification of immunoblots shown in Figure 3A. **C)** Total protein staining for immunoblots shown in Figure 3C. **D)** Immunoblot of MYC, phospho-ERK and ERK1/2 levels in the indicated cell lines treated with DMSO or 1 μM AZD6244 ("A", a MEKi) and 1 μM VX-11E ("V", an ERKi) for 24 hours. At right, total protein staining. **E)** UACC-62 cells expressing luciferase or the indicated pathway activating construct in combination with shGFP (C) or two independent shMYC constructs (#1 or #2) were immunoblotted for expression of MYC and vinculin as a loading control. Blots are quantified in the right panel.

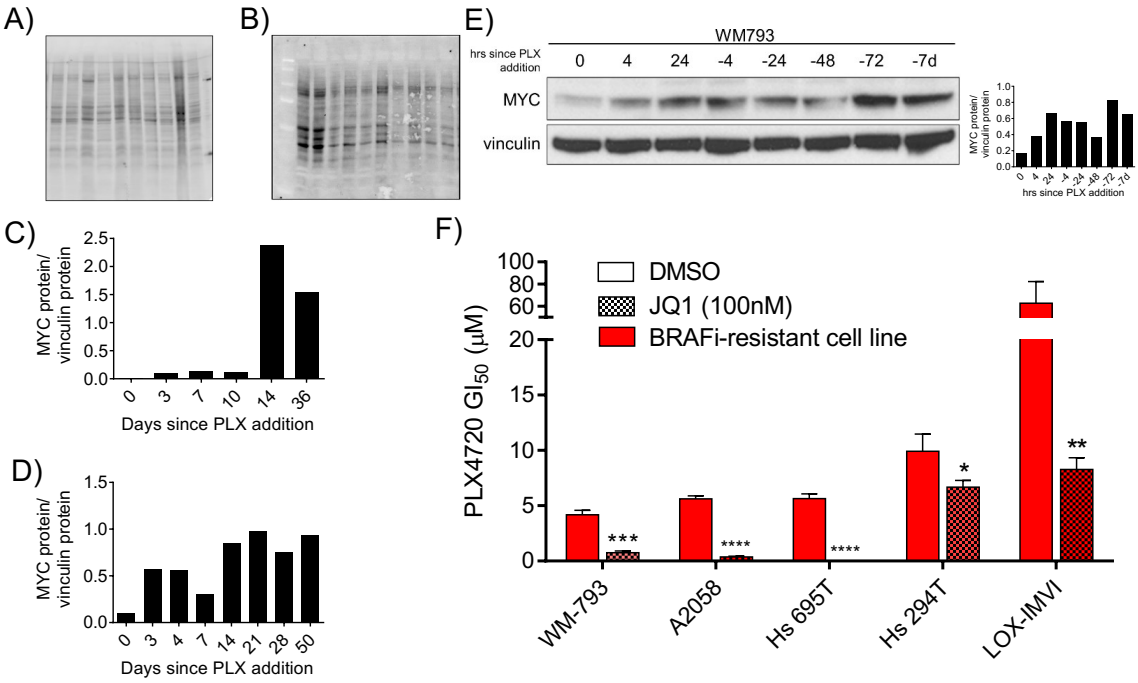

Figure S4. Characterization of the dynamics of MYC expression in intrinsically BRAFi resistant melanoma cells , related to Figure 4. A) Total protein staining for immunoblot shown in Figure 4A. Samples are ordered left to right as in Figure 4A. **B)** Total protein staining for immunoblot shown in Figure 4B. Samples are ordered left to right as in Figure 4B. **C)** Quantification of immunoblot in Figure 4F. **D)** Quantification of immunoblot in Figure 4H. **E)** WM793 cells were treated with 1 μM PLX4720 for 24 hours after which PLX4720 was withdrawn from the culture media and the cells were cultured normally for an additional 7 days. Whole cell lysates were prepared at the indicated time points and immunoblotted for expression of MYC and vinculin as a loading control. Blots are quantified in the right panel. **F)** Intrinsically BRAFi-resistant cell lines could be sensitized to PLX4720 by the addition of the indicated dose of JQ1. JQ1+PLX4720 treated cells are normalized to the viability of cells treated with JQ1 alone to account for nonspecific toxicity. *P* values denote significance between DMSO and JQ1 treatment in each cell line. Data are means (SD) from three experiments. **P* < 0.05; ***P* < 0.01; ****P* < 0.005; *****P* < 0.001.

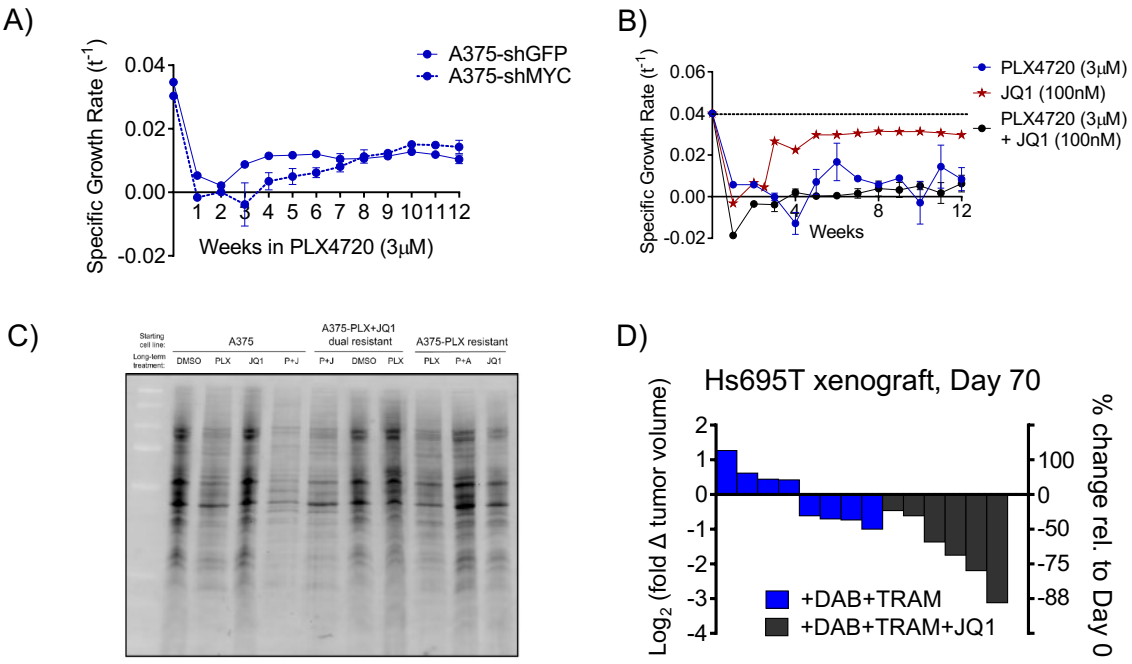

Figure S5. Evolution of resistance in treatment naïve melanoma cells with and without genetic or pharmacological MYC suppression , related to Figure 5. A) A375 cells expressing shGFP or shMYC were cultured in 3 μM PLX4720 for 12 weeks and cells were counted weekly. Growth rates were calculated from the cell counts and plotted. **B)** A375 cells were cultured in 3 μM PLX4720, 100 nM JQ1 or the combination for 12 weeks and cells were counted weekly. Growth rates were calculated from the cell counts and plotted. The growth rate of parental cells treated with DMSO is indicated with a dashed line. Data are means (SD) from three experiments. **C)** Total protein staining for the immunoblot shown in Figure 5C. **D)** Growth of Hs695T xenograft tumors treated with vehicle, JQ1 (45 mg/kg/d), dabrafenib (Dab, 30 mg/kg/d) plus trametinib (Tram, 0.6 mg/kg/d), or the combination over time. Data shown are mean tumor volume +/- SEM, with n=6-8 mice per group. Waterfall plot showing change in tumor sizes in the indicated groups on day 70 of treatment.

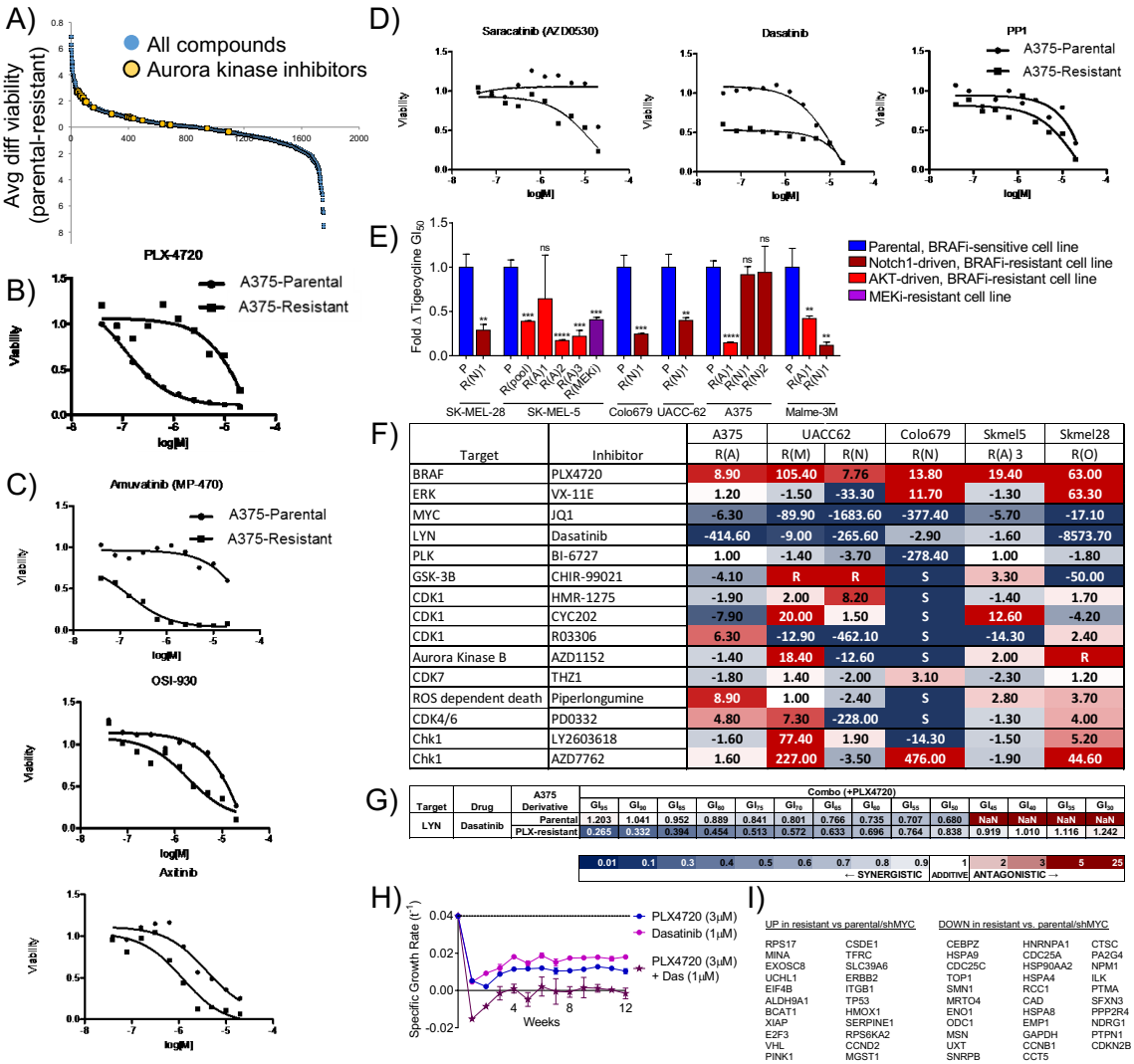

Target	Inhibitor	A375 R(A)	UACC62 R(M)	UACC62 R(N)	Colo679 R(N)	Skmel5 R(A) 3	Skmel28 R(O)
BRAF	PLX4720	8.90	105.40	7.76	13.80	19.40	63.00
ERK	VX-11E	1.20	-1.50	-33.30	11.70	-1.30	63.30
MYC	JQ1	-6.30	-89.90	-1683.60	-377.40	-5.70	-17.10
LYN	Dasatinib	-414.60	-9.00	-265.60	-2.90	-1.60	-8573.70
PLK	BI-6727	1.00	-1.40	-3.70	-278.40	1.00	-1.80
GSK-3B	CHIR-99021	-4.10	R	R	S	3.30	-50.00
CDK1	HMR-1275	-1.90	2.00	8.20	S	-1.40	1.70
CDK1	CYC202	-7.90	20.00	1.50	S	12.60	-4.20
CDK1	R03306	6.30	-12.90	-462.10	S	-14.30	2.40
Aurora Kinase B	AZD1152	-1.40	18.40	-12.60	S	2.00	R
CDK7	THZ1	-1.80	1.40	-2.00	3.10	-2.30	1.20
ROS dependent death	Piperlongumine	8.90	1.00	-2.40	S	2.80	3.70
CDK4/6	PD0332	4.80	7.30	-228.00	S	-1.30	4.00
Chk1	LY2603618	-1.60	77.40	1.90	-14.30	-1.50	5.20
Chk1	AZD7762	1.60	227.00	-3.50	476.00	-1.90	44.60

Target	Drug	A375 Derivative	Combo (+PLX4720) GI55	GI60	GI65	GI70	GI75	GI80	GI85	GI90	GI95	GI40	GI50	GI60
LYN	Dasatinib	Parental	1.203	1.041	0.952	0.889	0.841	0.801	0.766	0.735	0.707	0.680	NaN	NaN	NaN	NaN
		PLX-resistant	0.265	0.332	0.394	0.454	0.513	0.572	0.633	0.696	0.764	0.838	0.919	1.010	1.116	1.242

0.01	0.1	0.3	0.4	0.5	0.6	0.7	0.8	0.9	1	2	3	5	25
← SYNERGISTIC									ADDITIVE	ANTAGONISTIC →			

RPS17	CSDE1		CEPBZ	HNRNPA1	CTSC
MINA	TFRC		HSPA9	CDC25A	PA2G4
EXOSC8	SLC39A6		CDC25C	HSP90AA2	NPM1
UCHL1	ERBB2		TOP1	HSPA4	ILK
EIF4B	ITGB1		SMN1	RCC1	PTMA
ALDH9A1	TP53		MRTO4	CAD	SFXN3
BCAT1	HMOX1		ENO1	HSPA8	PPP2R4
XIAP	SERPINE1		ODC1	EMP1	NDRG1
E2F3	RPS6KA2		MSN	GAPDH	PTPN1
VHL	CCND2		UXT	CCNB1	CDKN2B
PINK1	MGST1		SNRPB	CCT5	

Figure S6. Identification of pharmacological strategies to target MYC activated, BRAFi-resistant melanoma cells , related to Figure 6. Analysis of compound screening data. **A)** Distribution of Aurora kinase inhibitors in the primary screen. Secondary GI50 validation assays with **B)** the RAF inhibitor PLX4720, **C)** selected c-KIT inhibitors, and **D)** selected SRC family kinase inhibitors. **E)** Fold change in tigecycline GI_{50} values of the indicated PLX-resistant lines relative to parental lines. *P* values indicate significance between parental and resistant derivatives. **F)** Fold change in GI_{50} of the indicated inhibitors in various PLX4720-resistant evolved cell lines compared to their parental counterparts. Cases where PLX-resistant cells were more resistant to the indicated inhibitor than their parental line are shaded in red and cases that the PLX-resistant lines are sensitized are shaded blue. Cases where GI_{50} was not reached are indicated with 'R' or 'S.' **G)** Combinatorial Index (CI) values for parental A375 or PLX-resistant derivatives at a range of GI_{50} values for the combination of PLX4720 and dasatinib. Synergy is indicated by CI values less than 1. **H)** A375 cells were cultured in 3 μM PLX4720, 1 μM dasatinib, or the combination for 12 weeks and cells were counted weekly. Growth rates were calculated from the cell counts and plotted. The growth rate of parental cells treated with DMSO is indicated with a dashed line. Data are means (SD) of three experiments. **I)** List of MYC target genes with differential expression in resistant compared to parental and shMYC A375 cells.

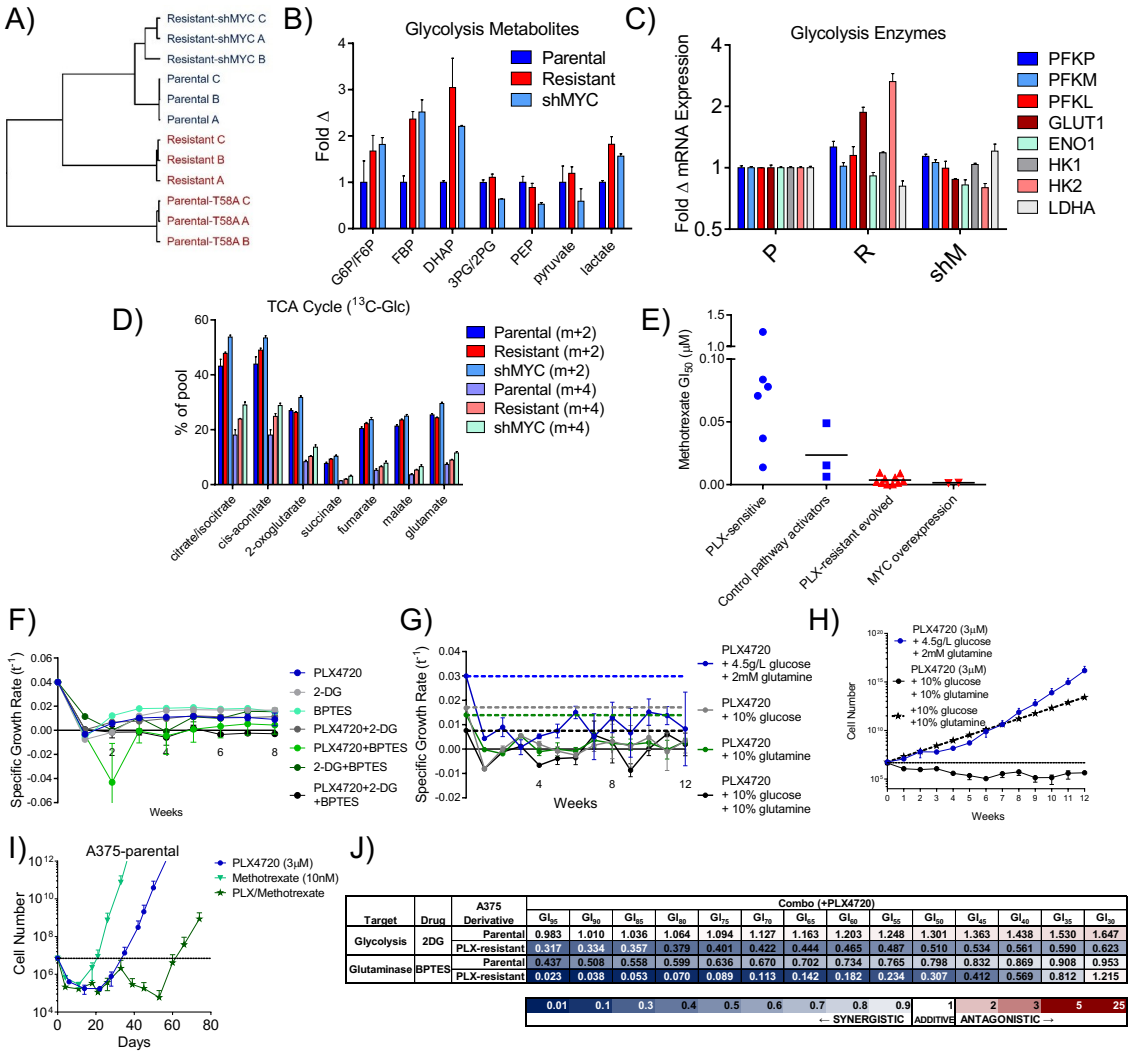

Target	Drug	A375 Derivative	Combo (+PLX4720) GI95	GI90	GI85	GI80	GI75	GI70	GI65	GI60	GI55	GI50	GI45	GI40	GI35	GI30
Glycolysis	2DG	Parental	0.983	1.010	1.036	1.064	1.094	1.127	1.163	1.203	1.248	1.301	1.363	1.438	1.530	1.647
		PLX-resistant	0.317	0.334	0.357	0.379	0.401	0.422	0.444	0.465	0.487	0.510	0.534	0.561	0.590	0.623
Glutaminase	BPTES	Parental	0.437	0.508	0.558	0.599	0.636	0.670	0.702	0.734	0.765	0.798	0.832	0.869	0.908	0.953
		PLX-resistant	0.023	0.038	0.053	0.070	0.089	0.113	0.142	0.182	0.234	0.307	0.412	0.569	0.812	1.215

0.01 0.1 0.3 0.4 0.5 0.6 0.7 0.8 0.9 | 1 | 2 3 5 25
← SYNERGISTIC | ADDITIVE | ANTAGONISTIC →

Figure S7. Metabolic dependencies in MYC activated, BRAFi-resistant melanoma cells , related to Figure 7. A) Hierarchical clustering of gene expression data (RNA-seq) from A375 parental cells (Parental), PLX4720-resistant clonal derivatives (Resistant), resistant A375 cells expressing shMYC (Resistant-shMYC), and parental A375 cells expressing MYC^{T58A} mutant (Parental-T58A). BRAFi-resistant, MYC-activated models are shown in red; BRAFi-sensitive, MYC-inactive models are shown in blue. Changes in **B)** glycolytic intermediates and **C)** expression of glycolytic enzymes among A375 (P), PLX4720-resistant A375 (R), and resistant cells expressing shMYC (shM). **D)** Changes in the incorporation of glucose into TCA cycle from labeled D-glucose. **E)** GI_{50} values of various PLX4720-sensitive (blue) and resistant (red) cell line models treated with methotrexate. **F)** A375 cells were cultured in 3 μM PLX4720, 5 mM 2-DG, 10 μM BPTES or the combinations for 12 weeks and cells were counted weekly. Growth rates were calculated from the cell counts and plotted. **G)** A375 cells were cultured in 3 μM PLX4720 and either DMEM with 4.5 g/L glucose and 2 mM glutamine, DMEM with 0.45 g/L glucose and 2 mM glutamine, DMEM with 4.5 g/L glucose and 0.2 mM glutamine, or DMEM with 0.45 g/L glucose and 0.2 mM glutamine for 12 weeks and cells were counted weekly. Growth rates were calculated from the cell counts and plotted. The growth rate of parental cells in DMEM with 4.5 g/L glucose and 2 mM glutamine is indicated with the blue dashed line. The growth rate of parental cells in DMEM with the various depleted media is indicated with the dashed lines. Growth rates in the depleted media were calculated from daily cell counts over 7 days of culture. **H)** The growth rate of A375 cells in DMEM containing 0.45 g/L glucose and 0.2 mM glutamine was measured daily over 7 days. This growth rate was used to calculate total cell numbers over 12 weeks of growth in the double depleted media and compared to cell counts with PLX4720 treatment. **I)** Projected cell numbers of A375 cultured in 3 μM PLX4720, 10 nM methotrexate or the triple combination. **J)** Combinatorial Index (CI) values for parental A375 or PLX-resistant derivatives at a range of growth inhibition (GI) values for the combination of PLX4720 and 2-DG or the combination of PLX4720 and BPTES. Synergy is indicated by CI values less than 1. Data are means (SD) from three experiments.

EXTENDED EXPERIMENTAL PROCEDURES

1 Statistical Modeling of Genomic Data

Gene Expression Data and Preprocessing Procedures

Microarray gene expression data (Rizos *et al.*, 2014) was collected that included 59 $BRAF^{V600}$-mutant melanoma metastatic samples with 38 progressing and 21 matched pretreatment samples collected from 30 patients. Only two patients, indexed as 5 and 10, were analyzed pre-treatment, on-treatment, and on-relapse (which we term as "progression"). We only utilized the samples in this dataset which had matched pre-treatment and progressed tumors (this included patients 5 and 10). To increase the sample size of the on-treatment tumors used to obtain the BRAFi/MEKi response signature, we added matched pre- and on-treatment microarray gene expression data of melanoma cell lines from two sets of data: M229, M238, and M249 (Nazarian *et al.*, 2010); and SkMel1, SkMel5, SkMel19, SkMel28, and Malme3M (Pratilas *et al.*, 2009). These data are publicly available and can be accessed in the NCBI's Gene Expression Omnibus under the GEO SuperSeries accession numbers: `GSE50509` (Rizos *et al.*, 2014), `GSE24862` (Nazarian *et al.*, 2010), and `GSE10087` (Pratilas *et al.*, 2009).

Collapsing Probes and Data Normalization

Expression data were obtained using the Illumina HumanHT-12 V4.0 Expression Beadchip (Rizos *et al.*, 2014), the Affymetrix Human Gene 1.0 ST Array (Pratilas *et al.*, 2009), and the Affymetrix Human Genome U133A 2.0 Array (Nazarian *et al.*, 2010), respectively. we took the following preprocessing and normalization steps to correct for batch effects and other possible confounders. First, using the annotations of each Affymetrix/Illumina Chip/Platform, each probe of each sample in each experiment was mapped to its corresponding HUGO gene name and symbol. Next, assuming that there is no principled way to account for "missingness", we eliminate the probes that did not match to known genes. For each sample in all three experiments, we follow previous works (Li *et al.*, 2011) and took the probes that mapped to multiple genes and averaged their expression values. Next, we identified the mapped genes that were common in all three chips/platforms and only used these genes in subsequent statistical and pathway analyses. All three datasets were RMA corrected and $\log_2$-transformed. We utilize base 2 because any transformed

2-fold ratio will be converted to an ± 1 scale. This interpretation of fold change helped with interpreting of BAKR regression coefficients and the underlying marginal covariate interactions. Lastly, we perform a final cross-platform quantile normalization (Rudy and Valafar, 2011) on the combined dataset. The goal of the cross-platform normalization was to dilute some of the random noise created by chip-to-chip batch effects and strengthen biological signal in the data. After completing these steps, we were left with a final data set consisting of $n = 68$ samples and $p = 11{,}657$ genes.

Splitting the Data: Phases I and II

The data were split into two phases: Phase I (i.e. generation of the BRAFi/MEKi response signature) corresponded to pre-treatment versus on-treatment samples ($n = 39$); Phase II (i.e. identification of genes that return to pre-treatment status) corresponded to on-treatment versus post-treatment samples ($n = 39$).

Deriving a Gene Signature

In this section, we will use the Phase I dataset to infer a BRAFi/MEKi response signature $\mathcal{G}$ of MAPK pathway addiction. In this study, we use a logistic version of the Bayesian approximate kernel regression (BAKR-logit) model (Crawford *et al.*, 2017) to derive this collection of genes. Note that this methodology is advantageous for statistically analyzing cancer genomic data such as this for a few notable reasons. One, there is no reason to assume a linear relationship between the changes in gene expression and the effect of a given therapeutic strategy. Moreover, crosstalk between signaling pathways, as well as between the genes and nodes within these pathways, has been suggested to be associated with drug response (Bostock, 2005; Bender and Nahta, 2008; Yamaguchi *et al.*, 2014).

Notation

Let $\mathbf{X}$ denote the observed $n \times p$ genotype matrix, where each element x_{ij} is the expression value of the j^{th} gene from the i^{th} sample. Next, let $\mathbf{y} = [y_1, \ldots, y_n]$ represent the following n-dimensional binary response vector with

$$y_i = \begin{cases} 1 & \text{if} \quad \text{MAPK pathway is activated (pre-treatment);} \\ 0 & \text{if} \quad \text{MAPK pathway is deactivated (on-treatment).} \end{cases}$$

Alternatively, we say that $\mathbf{y}$ is drawn as n-independent Bernoulli random variables, such that $y_i \overset{iid}{\sim} \text{Bern}(\pi_i)$.

Logistic Bayesian Approximate Kernel Regression Model

Consider the following logit link function between the gene expression and binary treatment classes:

$$\text{logit}(\mathbb{E}[y_i \mid \mathbf{x}_i]) = \text{logit}(\pi_i) = \log\left(\frac{\pi_i}{1-\pi_i}\right) = \mathbf{x}_i^\intercal \boldsymbol{\beta},$$

where $\mathbf{x}_i^\intercal$ is the i^{th} row of the $n \times p$ expression matrix $\mathbf{X}$, and $\boldsymbol{\beta} = [\beta_1, \ldots, \beta_p]$ is an unknown vector of regression coefficients for each gene $j = 1, \ldots, p$. To facilitate statistical inference and interpretation of this logistic model setup, we define a latent variable $\mathbf{z} = [z_1, \ldots, z_n]$ such that $y_i = 1$ if $z_i > 0$, and $y_i = 0$ otherwise (Kinney and Dunson, 2007). In other words, each z_i is logistically distributed with location parameter $\mathbf{x}_i^\intercal \boldsymbol{\beta}$, with a corresponding probability density function:

$$\mathcal{L}(z_i; \boldsymbol{\beta}) = \frac{\exp\{-(z_i - \mathbf{x}_i^\intercal \boldsymbol{\beta})\}}{[1 + \exp\{-(z_i - \mathbf{x}_i^\intercal \boldsymbol{\beta})\}]^2}. \tag{1}$$

It was shown that this relationship is approximately a non-central t_ν-distribution with location parameter $\mathbf{x}_i^\intercal \boldsymbol{\beta}$ and scale parameter σ_ε^2 (Kinney and Dunson, 2007). This means that we may express (1) as a scale mixture of normals, represented in matrix notation as the following:

$$\mathbf{z} = \mathbf{X}\boldsymbol{\beta} + \varepsilon, \quad \varepsilon \sim \text{MVN}(\mathbf{0}, \sigma_\varepsilon^2 \boldsymbol{\Omega}^{-1}), \tag{2}$$

where $\boldsymbol{\Omega} = \text{Diag}(\omega_1, \ldots, \omega_n)$ is an $n \times n$ diagonal matrix and $\text{MVN}(\boldsymbol{\mu}, \boldsymbol{\Sigma})$ denotes a multivariate normal distribution with mean vector $\boldsymbol{\mu}$ and covariance matrix $\boldsymbol{\Sigma}$.

As in most gene expression studies, the number of samples is far fewer than the number of genes (i.e. $p \gg n$). For this reason, low rank factorizations of the design matrix $\mathbf{X}$ are used both for numerical stability as well as for statistical efficiency (West, 2003; Liang *et al.*, 2007; Liang *et al.*, 2009; de los Campos *et al.*, 2010; Crossa *et al.*, 2014; Crawford *et al.*, 2017). In addition, there is no reason to assume a linear relationship between the latent variable $\mathbf{z}$ and the changes in gene expression as is assumed in Equation (2). To increase predictive power, we used a nonlinear regression model that can capture higher-order interactions between genes, while also providing effect size estimates for each gene. This model builds on the classical Gaussian process — or the reproducing kernel Hilbert space(RKHS) model — and is formerly

referred to as the Bayesian approximate kernel regression (BAKR) model (Crawford *et al.*, 2017). We summarize the relevant aspects of the BAKR model that we used to infer signatures.

We first specify a RKHS model — a class of models used extensively in machine learning, as well as in genetics, to improve predictive accuracy, and capture higher order nonlinear effects (Gianola *et al.*, 2006; Liang *et al.*, 2007; Liang *et al.*, 2009; de los Campos *et al.*, 2010; Crossa *et al.*, 2014; Howard *et al.*, 2014):

$$\mathbf{z} = \mathbf{K}\boldsymbol{\alpha} + \boldsymbol{\varepsilon} \quad \text{with} \quad \boldsymbol{\alpha} \sim \text{MVN}(\mathbf{0}, \sigma_{\alpha}^{2}\mathbf{K}^{-1}) \quad \text{and} \quad \boldsymbol{\varepsilon} \sim \text{MVN}(\mathbf{0}, \sigma_{\varepsilon}^{2}\boldsymbol{\Omega}^{-1}), \tag{3}$$

where $\mathbf{K}$ is an $n \times n$ kernel matrix whose entries are nonlinear functions of pairs of expression profiles, and $\boldsymbol{\alpha}$ is an n-vector of random kernel coefficients. By definition, the kernel matrix $\mathbf{K}$ is symmetric and semi-positive definite:

(1) $k(\mathbf{x}_i, \mathbf{x}_j) = k(\mathbf{x}_j, \mathbf{x}_i) \quad \forall\ i, j,$

(2) $\sum_i \sum_j k(\mathbf{x}_i, \mathbf{x}_j)\alpha_i\alpha_j \geq 0 \quad \forall\ \alpha_i, \alpha_j \in \mathbb{R}.$

The model form in Equation (3) turns a p-dimensional optimization problem into an optimization problem over just n parameters.

A key feature of the BAKR modeling framework is its ability to infer effect sizes for genes while implicitly modeling all possible higher-order interactions between them (Crawford *et al.*, 2017). In high-dimensional settings, this is something that is not feasible for linear models (Yu *et al.*, 2006; Logsdon *et al.*, 2010; Zhang *et al.*, 2010; Guan and Stephens, 2011; Lippert *et al.*, 2011; Zhou and Stephens, 2012; Zhou *et al.*, 2013) or other variable selection testing strategies (Hauck Jr and Donner, 1977; Kleinbaum and Klein, 2010; Li *et al.*, 2011; Wu *et al.*, 2011).

The advantage of BAKR over standard RKHS models is that RKHS models cannot provide estimates of effect sizes for each variable. BAKR overcomes this hurdle by using properties of shift-invariant kernel functions and employing a map between the RKHS model (i.e Equation (3)) and a linear model (i.e. Equation (2)). More specifically, shift-invariant kernel functions can be written as a weighted infinite sum of Fourier bases $\{\psi_i(x)\}_{i=1}^{\infty} = \boldsymbol{\psi}(x)$, such that $k(\|x_i - x_j\|) = \boldsymbol{\psi}(x_i)^{\intercal}\boldsymbol{\psi}(x_j)$. Though never constructed in practice, under Bochner's Theorem (Bochner, 1934), a p-dimensional approximation of these bases may be constructed using the Fourier Transform of the kernel function such that $k(\|x_i - x_j\|) \approx \sum_{j=1}^{p} \psi_j(x_i)^{\intercal}\psi_j(x_j) = \widetilde{k}(\|x_i - x_j\|)$ (Rahimi and Recht, 2007; Băzăvan *et al.*, 2012). This allows for a reformulation of Equation

(3) using an approximate kernel matrix of the form:

$$\mathbf{z} = \widetilde{\mathbf{K}}\boldsymbol{\alpha} + \boldsymbol{\varepsilon} \quad \text{with} \quad \boldsymbol{\alpha} \sim \text{MVN}(\mathbf{0}, \sigma_\alpha^2 \widetilde{\mathbf{K}}^{-1}) \quad \text{and} \quad \boldsymbol{\varepsilon} \sim \text{MVN}(\mathbf{0}, \sigma_\varepsilon^2 \boldsymbol{\Omega}^{-1}). \tag{4}$$

Going forward, we denote $\boldsymbol{\Psi}$ as the infinite Fourier basis matrix such that $\mathbf{K} = \boldsymbol{\Psi}^\intercal\boldsymbol{\Psi}$, and $\widetilde{\boldsymbol{\Psi}}$ to represent the p-term finite approximation such that $\mathbf{K} \approx \widetilde{\boldsymbol{\Psi}}^\intercal\widetilde{\boldsymbol{\Psi}} = \widetilde{\mathbf{K}}$. These approximate bases can be used in a linear mapping to relate $\boldsymbol{\alpha}$ to $\boldsymbol{\beta}$ in order to extract an effect size for each gene (Crawford *et al.*, 2017). Because of this linear mapping, BAKR can obtain posterior samples of $\boldsymbol{\beta}$ to quantify phenotype association strength and identify associated genes. This is key to defining a robust BRAFi/MEKi response signature. BAKR has the flexibility to take on the approximation of any shift-invariant kernel to model a variety of different genetic architectures; however, we detail our model strictly under the approximation of the Gaussian kernel function (Williams and Seeger, 2001; Vert *et al.*, 2004; Chang *et al.*, 2010):

$$\widetilde{k}(\|\mathbf{x}_i - \mathbf{x}_j\|) \approx k(\|\mathbf{x}_i - \mathbf{x}_j\|) = \exp\left\{-\frac{1}{p}||\mathbf{x}_i - \mathbf{x}_j||^2\right\},$$

where $||\mathbf{x}||^2 = \sum_{i=1}^n \mathrm{x}^2$ is the ℓ_2-norm.

Complete Model Specification

We now state the complete specification of BAKR-logit. Since the approximation of any shift-invariant kernel matrix is also symmetric and semi-positive definite, we took advantage of a low-rank approximation of the nonlinear kernel matrix $\widetilde{\mathbf{K}}$ to dramatically reduce computational cost (West, 2003; Liang *et al.*, 2007; Liang *et al.*, 2009; de los Campos *et al.*, 2010; Crossa *et al.*, 2014; Crawford *et al.*, 2017). This was done by using the spectral decomposition of the approximate Gaussian kernel matrix $\widetilde{\mathbf{K}}$. Specifically:

$$\mathrm{y}_i = \begin{cases} 1 & \text{if} \quad \mathrm{z}_i > 0 \\ 0 & \text{if} \quad \mathrm{z}_i \leq 0 \end{cases} \quad \text{for} \quad i = 1, \ldots, n$$

$$\mathbf{z} = \widetilde{\mathbf{U}}\boldsymbol{\theta} + \boldsymbol{\varepsilon}, \quad \boldsymbol{\varepsilon} \sim \text{MVN}(\mathbf{0}, \sigma_\varepsilon^2 \boldsymbol{\Omega}^{-1}) \tag{5}$$

$$\boldsymbol{\theta} \sim \text{MVN}_q(\mathbf{0}, \sigma_\theta^2 \widetilde{\boldsymbol{\Lambda}}) \tag{6}$$

$$\omega_i, \sigma_\theta^{-2} \sim \Gamma(\nu/2, \nu/2), \quad \sigma_\varepsilon^2 = \frac{\nu - 2}{3\nu}\pi^2 \tag{7}$$

where $\Gamma(a, b)$ is used to represent a Gamma distribution with shape a and rate b. In practice, we follow previous studies (Kinney and Dunson, 2007) and fix $\nu = 7.3$. Note that we utilize the empirical kernel factor representation where $\widetilde{\mathbf{K}} = \widetilde{\mathbf{U}}\widetilde{\mathbf{\Lambda}}\widetilde{\mathbf{U}}^{\mathsf{T}}$ and $\boldsymbol{\theta} = \widetilde{\mathbf{\Lambda}}\widetilde{\mathbf{U}}^{\mathsf{T}}\boldsymbol{\alpha}$. For numerical stability and reduction of computational complexity, eigenvectors corresponding to smaller eigenvalues were truncated (West, 2003; Lopes and West, 2004; Liang *et al.*, 2007; Pillai *et al.*, 2007; Liang *et al.*, 2009); so without loss of generality, we implement BAKR by considering $\widetilde{\mathbf{U}}$ to be an $n \times q$ matrix containing the eigenvectors of $\widetilde{\mathbf{K}}$ (i.e. $\widetilde{\mathbf{U}}\widetilde{\mathbf{U}}^{\mathsf{T}} = \mathbf{I}_n$), and $\widetilde{\mathbf{\Lambda}}$ as a $q \times q$ diagonal matrix of the top q eigenvalues of $\widetilde{\mathbf{K}}$. This consideration represented an even greater reduction in required computation since $q \leq n \ll p$. In this study, we chose q to represent the number of eigenvalues that explain 99% of cumulative variance in $\widetilde{\mathbf{K}}$.

Because $\widetilde{\mathbf{K}}$ approximates a matrix that is shift-invariant, we utilized an inverse mapping that allows for inference to be made on the p-dimensional genes $\boldsymbol{\beta}$ in the original genetic space (Crawford *et al.*, 2017):

$$\widetilde{\boldsymbol{\beta}} = \mathbf{X}^{\dagger}\widetilde{\mathbf{\Psi}}^{\mathsf{T}}(\widetilde{\mathbf{\Lambda}}\widetilde{\mathbf{U}}^{\mathsf{T}}\widetilde{\mathbf{K}}^{-1}\widetilde{\mathbf{\Psi}}^{\mathsf{T}})^{-1}\widehat{\boldsymbol{\theta}},$$

where $\widehat{\boldsymbol{\theta}}$ is an estimate of the kernel factor coefficients drawn from the posterior distribution $p(\boldsymbol{\theta} \,|\, \mathbf{y})$. Furthermore, since we were strictly concerned with a case in which $p \gg n$, the inverse of $\mathbf{X}\mathbf{X}^{\mathsf{T}}$ exists and hence we let $\mathbf{X}^{\dagger} = \mathbf{X}^{\mathsf{T}}(\mathbf{X}\mathbf{X}^{\mathsf{T}})^{-1}$. By plugging in this quantity, the linear map simplified to

$$\widetilde{\boldsymbol{\beta}} = \mathbf{X}^{\mathsf{T}}(\mathbf{X}\mathbf{X}^{\mathsf{T}})^{-1}\widetilde{\mathbf{U}}\widehat{\boldsymbol{\theta}}. \tag{8}$$

We implemented the mapping from the standard RKHS model to effect sizes as a deterministic step in an MCMC Gibbs sampler resulting in empirical draws $\widetilde{\boldsymbol{\beta}}$ from an implied posterior distribution $p(\boldsymbol{\beta} \,|\, \mathbf{y})$.

Posterior Sampling and Inference

Based on the complete BAKR-logit specification, a standard Gibbs sampler was derived from the following joint posterior distribution:

$$\begin{aligned} p(\mathbf{z}, \boldsymbol{\theta}, \sigma_{\theta}^{-2}, \boldsymbol{\Omega} \,|\, \mathbf{y}) \propto & \left[\prod_{i=1}^{n}\left(\frac{\sigma_{\varepsilon}^2}{\omega_i}\right)^{-\frac{1}{2}} \exp\left\{-\frac{\omega_i}{2\sigma_{\varepsilon}^2}(\mathsf{z}_i - \widetilde{\mathbf{u}}_i^{\mathsf{T}}\boldsymbol{\theta})^2\right\}_{1(\mathsf{A}_i)}\right] \times \prod_{i=1}^{n}\omega_i^{\frac{\nu}{2}-1}\exp\left\{-\frac{\nu}{2}\omega_i\right\} \\ & \times (\sigma_{\theta}^2)^{-\frac{q}{2}}\exp\left\{-\frac{1}{2\sigma_{\theta}^2}\boldsymbol{\theta}^{\mathsf{T}}\widetilde{\mathbf{\Lambda}}^{-1}\boldsymbol{\theta}\right\} \times (\sigma_{\theta}^{-2})^{\frac{\nu}{2}-1}\exp\left\{-\frac{\nu}{2}\sigma_{\theta}^{-2}\right\} \end{aligned} \tag{9}$$

where $\mathbf{1}(\cdot)$ is an indicator function and each member of the set $\mathbf{A} = [\mathsf{A}_1, \ldots, \mathsf{A}_n]$ is defined as

$$\mathsf{A}_i = \begin{cases} \{\mathsf{z}_i : \mathsf{z}_i > 0\} & \text{if } \mathsf{y}_i = 1, \\ \{\mathsf{z}_i : \mathsf{z}_i \leq 0\} & \text{if } \mathsf{y}_i = 0. \end{cases} \tag{10}$$

After a selection of initial values, samples of parameters and hyper-parameters were drawn sequentially from their respective complete conditional posterior distributions, which we detail below. At each algorithmic step, with all conditioning parameters fixed at their most recent values, we updated the iterates until we created a set of relevant MCMC draws. The complete posterior distributions are given:

(1) For $i = 1, .., n$

$$\mathsf{z}_i^{(t+1)} \,|\, \mathbf{z}^{(t)}, \boldsymbol{\theta}, \sigma_\theta^2, \boldsymbol{\Omega}, \mathbf{y} \sim \begin{cases} \mathsf{N}(\widetilde{\mathbf{u}}_i^\intercal \boldsymbol{\theta}, \sigma_\varepsilon^2 \omega_i^{-1}) \mathbf{1}(\mathsf{z}_i^{(t)} > 0) & \text{if} \quad \mathsf{z}_i^{(t)} > 0, \\ \mathsf{N}(\widetilde{\mathbf{u}}_i^\intercal \boldsymbol{\theta}, \sigma_\varepsilon^2 \omega_i^{-1}) \mathbf{1}(\mathsf{z}_i^{(t)} \leq 0) & \text{if} \quad \mathsf{z}_i^{(t)} \leq 0; \end{cases}$$

(2) $\boldsymbol{\theta} \,|\, \mathbf{z}, \sigma_\theta^2, \boldsymbol{\Omega}, \mathbf{y} \sim \mathsf{MVN}(\mathbf{m}_\theta^*, \mathbf{V}_\theta^*)$ where $\mathbf{V}_\theta^* = \sigma_\varepsilon^2 \sigma_\theta^2 (\sigma_\varepsilon^2 \widetilde{\boldsymbol{\Lambda}}^{-1} + \sigma_\theta^2 \widetilde{\mathbf{U}}^\intercal \boldsymbol{\Omega} \widetilde{\mathbf{U}})^{-1}$ and $\mathbf{m}_\theta^* = \frac{1}{\sigma_\varepsilon^2} \mathbf{V}_\theta^* \widetilde{\mathbf{U}}^\intercal \boldsymbol{\Omega} \mathbf{z}$;

(3) $\widetilde{\boldsymbol{\beta}} = \mathbf{X}^\intercal (\mathbf{X}\mathbf{X}^\intercal)^{-1} \widetilde{\mathbf{U}} \boldsymbol{\theta}$;

(4) $\sigma_\theta^{-2} \,|\, \mathbf{z}, \boldsymbol{\theta}, \boldsymbol{\Omega}, \mathbf{y} \sim \Gamma(a_\theta^*, b_\theta^*)$ where $a_\theta^* = \frac{1}{2}(\nu + q)$ and $b_\theta^* = \frac{1}{2}(\nu + \boldsymbol{\theta}^\intercal \widetilde{\boldsymbol{\Lambda}}^{-1} \boldsymbol{\theta})$;

(5) For $i = 1, .., n$

$\omega_i \,|\, \mathbf{z}, \boldsymbol{\theta}, \sigma_\theta, \mathbf{y} \sim \Gamma(a_\omega^*, b_\omega^*)$ where $a_\omega^* = \frac{1}{2}(\nu + 1)$ and $b_\omega^* = \frac{1}{2\sigma_\varepsilon^2}(\nu \sigma_\varepsilon^2 + \mathsf{e}_i^2)$, with $\mathsf{e}_i = \mathsf{z}_i - \widetilde{\mathbf{u}}_i^\intercal \boldsymbol{\theta}$.

In this study, we obtained over 20,000 MCMC samples from the BAKR-logit Gibbs sampler. These samples were selected from a run of a 110,000 iterations, where we keep every 5$^{\text{th}}$ sample, and then follow up with burn-in of 2,000 samples.

Variable Selection: Local False Sign Rate

We are reminded that the purpose of using the BAKR-logit in this study is to discover a set of genes $\mathcal{G}$ (i.e. a gene signature) whose expression levels robustly change following treatment with BRAFi/MEKi in *BRAF*-mutant melanomas. We used the estimate of the original effect sizes $\widetilde{\boldsymbol{\beta}}$ as a metric of the relevance for each gene. Specifically, the metric we used to determine the members of $\mathcal{G}$ is the local false sign rate (lfsr), which is analogous to the local false discovery rate (Efron, 2007). The lfsr provides a measure of

confidence in the sign of the effect rather than confidence of the effect being non-zero (Stephens, 2017). Alternatively, we say that we were more concerned with controlling the minimization of "type S errors" (i.e. the errors of sign), rather than the traditional type I errors (Gelman and Tuerlinckx, 2013). Therefore, we choose to be confident in the directional change of a gene's regulatory pattern (i.e. up-regulation or down-regulation) in the presence of drug. Given posterior samples $\widetilde{\boldsymbol{\beta}}$ for each gene j, we defined the corresponding local false sign rate as (Stephens, 2017)

$$\text{lfsr}_j = \min[p(\beta_j \geq 0 \,|\, \mathbf{y}, \widetilde{\boldsymbol{\beta}}), p(\beta_j \leq 0 \,|\, \mathbf{y}, \widetilde{\boldsymbol{\beta}})]. \tag{11}$$

This selection procedure is a post-hoc deterministic computation applied to the MCMC samples of $\boldsymbol{\beta}$. The BRAFi/MEKi response signature $\boldsymbol{\mathcal{G}}$ is then defined as the set of genes that satisfy $\boldsymbol{\mathcal{G}} = \{j : \text{lfsr}_j \leq c\}$. In this study, we subjectively choose $c = 0.01$. This resulted in a BRAFi/MEKi response signature of $p^* = 68$ genes.

Model Comparisons

To illustrate the utility of the BAKR-logit model, we compared our approach to two linear models which use t-distributed test statistics to identify differentially expressed genes. The first method is a gene-wise association analysis that uses a parametric empirical Bayes approach to borrow strength between genes in order to moderate effect sizes and residual variances (Smyth, 2004). These resulting summary statistics are used to compute Benjamini-Hochberg corrected p-values (BH q-values) for every observed gene, where those with q-values below $q \leq 0.05$ are called significantly differentially expressed. We fit this model using the publicly available `R` package `limma` (Ritchie *et al.*, 2015). The second approach that we considered identifies differentially expressed genes using the classical likelihood ratio test (LRT) (Peng *et al.*, 2002). Briefly, for each gene in turn, we computed a likelihood ratio comparing an alternative model with the gene's expression level to a null model containing just the intercept. Similarly, we then considered those genes with multiplicty corrected p-values below 0.05 as those associated with MAPK inhibition. We fit this score test for nested parametric linear models using the `lrtest` function in the publicly available `R` package `lmtest` (Zeileis and Hothorn, 2002).

Here, we evaluated the ability of the BAKR-logit model, limma, and the LRT to identify genes that fully characterize MAPK inhibition in *BRAF*-mutant melanoma. We are reminded that using the BAKR-logit

resulted in a BRAFi/MEKi response signature of $p^* = 68$ genes. Comparatively, the limma model detected 16 BRAFi/MEKi response signature genes, while the LRT BRAFi/MEKi response signature contained only 8 genes. Notedly, there was substantial overlap between the signature genes identified by the LRT, and those selected by the limma and the BAKR-logit models (see Tables S1 and S7). Again, we want to highlight that the advantage of the BAKR framework is the fact that it also implicitly considers a marginal notion of interaction effects between a given gene and all other genes (Crawford *et al.*, 2017). Hence, BAKR identifies genes as being significant that the other linear modeling approaches fail to detect. For instance, while all three methods select the proto-oncogene *MYC* as being a key downstream component in MAPK inhibition, BAKR is the only methodology to also select genes such as *ID2* and *SKI* as being potential predictors of BRAFi/MEKi response. Briefly, overexpression of the *ID2* gene has been shown to be required for *MYC* signaling (Lasorella *et al.*, 2000). Similarly, oncogenic interactions between *SKI* and *MYC*, coupled with repression of the TGF-β signaling pathway, has been suggested to be consequential to long term treatment strategies in human melanomas (Sun *et al.*, 1999). Therefore, we conclude that the BRAFi/MEKi response signature derived by the BAKR-logit model gives a more complete illustration of MAPK inhibition in *BRAF*-mutant melanoma than both the limma linear model and the LRT.

Lastly, we want to stress the one caveat that this model comparison is strictly empirical in nature. Given that our aim here is to make novel discoveries, we are not afforded any "true" answers like there would be in a typical power simulation study. Nonetheless, BAKR identified the same signature genes as the opposing methods, as well as notable others that the literature suggests to be contextually relevant. A more fundamentally comprehensive review of BAKR, its predictive accuracy, and its power to detect true causal genes and other genetic variants can be found in the original publication (Crawford *et al.*, 2017).

Software and Model Implementation

Software for implementing the BAKR modeling framework is carried out in R and Rcpp code, which is freely available at `https://github.com/lorinanthony/BAKR`.

Identifying Elements of Relapse

Inference of MAPK signaling pathway activity was just the first step in discovering the genes and/or the cellular processes that are important for therapeutic resistance and melanoma reoccurrence. To search for a potential convergent effector of resistance, we began by reasoning that such an effector should follow

two transitional rules: (1) it should be regulated downstream of the driver oncogene, and (2) it should rebound to at least pre-treatment expression or activation states at resistance, independent of the upstream mechanisms driving resistance. We considered signature genes that satisfy this criteria as a signature for patient relapse and we referred to this set as $\boldsymbol{\mathcal{R}}$. Specifically, we used Bayes factors (BF) and marginal likelihoods to determine which of the $p^* = 68$ members of $\boldsymbol{\mathcal{G}}$ belonged in $\boldsymbol{\mathcal{R}}$.

Bayes Factor Computation

In this section, we develop the methodology for identifying an expression signature for melanoma progression (i.e. the members of $\boldsymbol{\mathcal{R}}$). We begin by introducing the Bayes factor, which is the probability of observing the data under one condition relative to another (Kass and Raftery, 1995). In particular, we used the Phase II dataset to obtain $\boldsymbol{\mathcal{R}}$. We redefine the binary phenotype $\mathbf{y}^*$, where now $y_i^* = 1$ denotes a progressed (relapsed) tumor and $y_i^* = 0$ corresponds to a treated sample. Now let $p(\mathbf{y}^* \mid \mathcal{M})$ be the probability of observing the phenotype under some model $\mathcal{M}$, and $p(\boldsymbol{\Theta}^* \mid \mathcal{M})$ be a prior belief about that model's parameters (i.e. gene coefficients in our case). The Bayes factor between two models $\mathcal{M}_1$ and $\mathcal{M}_0$ is then defined as

$$\text{BF}_{10} = \frac{p(\mathbf{y}^* \mid \mathcal{M}_1)}{p(\mathbf{y}^* \mid \mathcal{M}_0)} = \frac{\int p(\mathbf{y}^* \mid \boldsymbol{\Theta}_1^*, \mathcal{M}_1) p(\boldsymbol{\Theta}_1^* \mid \mathcal{M}_1) d\boldsymbol{\Theta}_1^*}{\int p(\mathbf{y}^* \mid \boldsymbol{\Theta}_0^*, \mathcal{M}_0) p(\boldsymbol{\Theta}_0^* \mid \mathcal{M}_0) d\boldsymbol{\Theta}_0^*}. \tag{12}$$

Here, the subscript identifies which models are being compared, while the corresponding order denotes which model is in the numerator and which is in the denominator. As previously shown (Kass and Raftery, 1995; Rouder and Morey, 2012), the Bayes factor is interpretable without recourse to additional criteria or qualification. For example, $\text{BF}_{10} = 5$ means that the data are 5 times more probable under $\mathcal{M}_1$ than under $\mathcal{M}_0$.

We are particularly interested in individual members of the gene signature that track that well with progression — meaning $\boldsymbol{\mathcal{R}} \subseteq \boldsymbol{\mathcal{G}}$. In other words, we want to identify the genes that positively contribute to the explanation of melanoma reoccurrence, conditioned on none of the other genes being present. The reason for this approach is that we are strictly concerned with finding potential drivers of resistance. This is accomplished by computing Bayes factors, while comparing an intercept term (null model, $\mathcal{M}_0$) to the addition of each signature gene independently (alternative models, $\mathcal{M}_j$ for $j = 1, \ldots, p^*$). Typically, Equation (12) can be computationally expensive as one considers all possible combinations of explanatory

variables (Berger and Pericchi, 1996; Barbieri and Berger, 2004). However, given the scope of the problem in question, our logic reduces this search to just $p^* = 68$ Bayes factors that needed to be calculated. Again, we define p^* as the number of genes included in our melanoma signature, (i.e. $|\mathcal{G}| = p^* = 68$).

We used the Laplace method (Guan and Stephens, 2008) to approximate the Bayes factor for the binary responses. Assume that each phenotype is modeled by a logistic regression model,

$$\mathcal{M}_j : \quad \log\left(\frac{\Pr[y_i^* = 1]}{\Pr[y_i^* = 0]}\right) = \mu + x_{ij}^*\beta_j^* = f(\mu, \beta_j^*), \tag{13}$$

where x_{ij}^* is the j^{th} element of the i^{th} row in the $n \times g$ expression matrix $\mathbf{X}^*$ containing the treated and progressed samples from our data and the genes from our signature (i.e. a subset of the Phase II dataset). Hence, β_j^* is defined as the effect parameter for the j^{th} signature gene in $\mathcal{G}$. Lastly, we define μ as a common intercept. Then under the logistic function, Equation (13) can be stated as:

$$\mathcal{M}_j : \quad \pi_i^* = \Pr[y_i^* = 1] = \frac{\exp\{f(\mu, \beta_j^*)\}}{1 + \exp\{f(\mu, \beta_j^*)\}}. \tag{14}$$

By using Equation (14), the log-likelihood of the data is specified as

$$\begin{aligned} \ell(\mathbf{y}^*; \mu, \beta_j^*) &= \sum_i [y_i^* \log \pi_i^* + (1 - y_i^*)\log(1 - \pi_i^*)] \\ &= \sum_i y_i^* f(\mu, \beta_j^*) + \sum_i \log(1 + \exp\{f(\mu, \beta_j^*)\}). \end{aligned} \tag{15}$$

Under the null model, $\mathcal{M}_0$ with $j = 0$, we assume that $\beta_j^* = 0$ and a normal prior on μ

$$p(\mu \mid \mathcal{M}_0) \propto \exp\left\{-\frac{1}{2\sigma_\mu^2}\mu^2\right\}.$$

For the alternative models, where $j = 1, \ldots, p^*$, we put a normal prior on the gene coefficients where

$$p(\mathbf{\Theta}^* \mid \mathcal{M}_j) = p(\mu, \beta_j^* \mid \mathcal{M}_j) \propto \exp\left\{-\frac{1}{2\sigma_\mu^2}\mu^2 - \frac{1}{2\sigma_{\beta_j}^2}\beta_j^{*2}\right\},$$

with $\mathbf{\Theta}^* = (\mu, \beta^*)$. Hence for each j, Equation (12) then becomes the following:

$$\text{BF}_{j0} = \frac{p(\mathbf{y}^* \mid \mathcal{M}_j)}{p(\mathbf{y}^* \mid \mathcal{M}_0)} = \frac{\int \ell(\mathbf{\Theta}^*; \mathbf{y}^*, \mathcal{M}_j) p(\mathbf{\Theta}^* \mid \mathcal{M}_j) d\mathbf{\Theta}^*}{\int \ell(\mu; \mathbf{y}^*, \mathcal{M}_0) p(\mu \mid \mathcal{M}_0) d\mu} \tag{16}$$

Following previous studies (Guan and Stephens, 2008), we may approximate each of the integrals by the Laplace method

$$\int \exp\left\{h(\boldsymbol{\Theta}^*)\right\} d\boldsymbol{\Theta}^* \approx (2\pi)^{\frac{\mathrm{d}}{2}} |H_{\boldsymbol{\Theta}^{**}}|^{-\frac{1}{2}} \exp\left\{h(\boldsymbol{\Theta}^{**})\right\}. \tag{17}$$

where d is the dimension of the integral being approximated, $\boldsymbol{\Theta}^{**}$ is the value at which h is at its maximum, and $|H_{\boldsymbol{\Theta}^{**}}|$ is the absolute value of the determinant of the Hessian matrix of h evaluated at $\boldsymbol{\Theta}^{**}$. Under the null, $\mathcal{M}_0$, and alternative models, $\mathcal{M}_j$, respectively:

$$h(\mu) = \ell(\mu; \mathbf{y}^*) + \log p(\mu);$$
$$h(\boldsymbol{\Theta}^*) = \ell(\boldsymbol{\Theta}^*; \mathbf{y}^*) + \log p(\boldsymbol{\Theta}^*).$$

The derivation of the Hessian matrices in each model case are given in full detail in cited works (Guan and Stephens, 2008).

Bayes Factor Interpretation

We computed the Bayes factor in Equation (16) using the approximation in Equation (17) a total of p^* times — each time comparing one signature gene in $\boldsymbol{\mathcal{G}}$ to the null model containing just the intercept. Taking the log of each ratio j, we examined across results and considered genes with $\log \mathrm{BF}_{j0} > 0$ to track well with progression. Therefore, the set of signature genes satisfying this condition are called *relapse genes* and said to be members of the set $\boldsymbol{\mathcal{R}}$. Alternatively, we say that $\boldsymbol{\mathcal{R}} = \{j : \log \mathrm{BF}_{j0} > 0\}$. To further aid in this interpretation, we also implement a t-test on the relapse genes to show that the Bayes Factor results also mirror that of a standard p-value (see Table S1).

Gene Set Analysis

To investigate the biological relevance of the signature $\boldsymbol{\mathcal{G}}$ and drivers of relapse $\boldsymbol{\mathcal{R}}$, we cross referenced each member of the two sets with gene sets compiled in the molecular signature database (MSigDB) compiled at the Broad Institute (Subramanian *et al.*, 2005). We used gene set enrichment methods to identify classes of genes that are over/underrepresented given a signature, for example $\boldsymbol{\mathcal{G}}$ or $\boldsymbol{\mathcal{R}}$. In this study, we utilized the global test (Goeman *et al.*, 2004) and its corresponding R package `gloabaltest` for gene set analysis.

Briefly, this statistical approach points to whether or not significantly enriched/depleted groups have a higher association with a given phenotype than what is expected by chance. Specifically, it utilizes a logistic regression model on expression measurements to describe a binary phenotype (e.g. $1 \equiv$ treated sample; $0 \equiv$ pre-treated sample). The null hypothesis assumes that all regression coefficients for the members in a particular gene set are zero. Alternatively, we describe this procedure as a test to see if the components within a tested gene set have substantial predictive ability for classifying the targeted phenotypic response (Goeman *et al.*, 2004). This is determined by analyzing the random biological variation between subjects, rather than comparing a gene set with random counterparts. As previously shown (Goeman *et al.*, 2006; Goeman *et al.*, 2011), the global test is designed to have optimal power in the situation where a gene set has many small non-zero regression coefficients. Hence, it is directed to find gene sets for which many genes are associated with the phenotype, even if said relation is minimal. We therefore use the global test model as a way to look for "dysregulation" and differential expression among gene sets. A gene set is considered to be dysregulated if it has a Benjamini-Hochberg corrected p-value (BH q-value) below 0.05.

Determining *MYC* Reactivation on Relapse

Here, we detail the procedure used to determine the probability of *MYC* reactivation in each of the progressed tumor samples. Once again, we defined reactivation as a gene that satisfies the aforementioned *transitional requirements*. For this computation, we specifically looked at the percent change in *MYC* expression between each pre-treated tumor and its matched relapse sample(s). The intuition behind computing this change is that if *MYC* is said to be reactivated when a patient relapses, then its expression levels should be about the same or greater in the corresponding matched progressed tumors. For every patient i, we used the following to compute the percent change in *MYC* expression:

$$\%\text{change}(i) = \frac{\text{pre}(i) - \text{post}(i)}{\text{pre}(i)} \times 100\% \quad \text{for} \quad i = 1, \dots, n.$$

These percent changes were then standardized into z-scores and the probability of reactivation was computed via the transformation $1 - \Phi(z)$, where Φ is the cumulative distribution function of the standard normal distribution. Qualitatively, this value $\Phi(z)$ is similar to a lower one-tailed p-value and is interpreted as the probability of seeing something more extreme than what has already been observed in the data. In our context, this value can be defined as the probability of seeing *MYC* deactivated when a patient re-

lapses. Therefore, we took the complement of a patient relapsing, which we state as $1 - \Phi(z)$, to represent the probability of seeing *MYC* reactivated when a patient relapses. Progressed tumor samples that had probability above 0.5 (i.e. greater than random chance) were said to have *MYC* reactivated.

2 Cell Lines

A375, Colo679, UACC-62, Malme-3M, WM793 and WM1745 cells were grown in RPMI 1640 (Life Technologies Corporation, Carlsbad, CA) supplemented with 10% fetal bovine serum (Sigma-Aldrich Corporation, St. Louis, MO) and 1% penicillin/streptomycin (Life Technologies Corporation). SK-MEL-28, SK-MEL-5, A2058, RPMI-7951, Lox IMVI and Hs294T cells were cultured in Dulbecco's modified Eagle's medium (DMEM) (Life Technologies Corporation) with 10% fetal bovine serum and 1% penicillin/streptomycin.

3 Chemicals

2-DG was prepared in PBS at 1 M. VX-11E, piperlongumine and PD0332 were prepared as 20 mM stock solutions in DMSO. CHIR-99021, HMR-1275, AZD1152, LY2603618, and AZD7762 were prepared in DMSO at 10 mM. CYC202 was prepared in DMSO at 5 mM. All other inhibitors were prepared as 100 mM stock solutions in DMSO.

4 GI_{50} Assay

To measure the GI_{50} values of specific inhibitors, cells were trypsinized and seeded at 5,000 cells/well in 96-well plates. After a 24-hour incubation, diluent (typically DMSO) or concentrated 10-fold dilutions of the indicated inhibitors (at 1:1000) were added to the cells to yield the highest concentration (see Chemicals). After a 3-day incubation with the treatment, cell viability was assessed with the CellTiter-Glo luminescent viability assay (Promega Corporation, Durham, NC) according to manufacturer's instructions. Growth inhibition was calculated as a percentage of diluent-treated cells and GI_{50} values were determined.

5 Sensitization Assays

In order to quantify the effect of resistance pathway inhibition on the sensitivity of cell lines to ERK pathway inhibition, small molecule sensitization assays were performed as previously described (Martz *et al.*, 2014). The ERK pathway inhibitor GI_{50} values were determined as described in the previous section with the addition of DMSO added to the media at a 1:1000 dilution. The ERK pathway inhibitor GI_{50} values were also determined with the indicated inhibitor in the background at the indicated dose. GI_{50} values were then determined to be the dose of ERK pathway inhibitor that resulted in half-maximal growth inhibition relative to the viability of non-ERK pathway inhibitor-only wells.

6 Immunoblotting

In order to measure protein levels in whole cell lysates, aliquots of cell extracts prepared in lysis buffer (0.5% Triton X-100, 50 mM β-glycerophosphate (pH 7.2), 0.1 mM Na3VO4, 2 mM $MgCl_2$, 1 mM EGTA, 1 mM DTT, 0.3 M NaCl, 2 μg/mL leupeptin and 4 μg/mL aprotinin (Sigma-Aldrich)) were submitted to SDS-PAGE. Where indicated, proteins were run on Mini-PROTEAN TGX Stain-Free Precast Gels (Bio-Rad) and total protein was visualized on the ChemiDoc Imaging System (Biorad). After electrophoretic transfer to PDMF, filters were blocked in 5% BSA and probed overnight at 4°C with the following primary antibodies and dilutions: c-MYC (1:200; #764 Santa Cruz Biotechnology, Dallas, TX or 1:10,000 ab32072 Abcam, Cambridge, MA), phospho-ERK (1:1000; #4376 Cell Signaling Technology, Danvers, MA), ERK1/2 (1:1000; #4695 Cell Signaling Technology), Notch1 (1:1000; #3608 Cell Signaling Technology), phospho-AKT1 (1:1000; #13038 Cell Signaling Technology), AKT1 (1:1000; #4691 Cell Signaling Technology), vinculin (1:500; #4650 Cell Signaling Technology), α-tubulin (1:1000, #2125 Cell Signaling Technology), β-actin (1:1000, #4970 Cell Signaling Technology). For quantification of immunoblots, where indicated, densitometry was performed with ImageJ software, background was subtracted and band intensity was normalized to loading control intensity. Alternatively, total protein images and Image Lab software (Bio-Rad) was used to normalize band intensity to total lane protein content.

7 Lentivirus Preparation and DNA Constructs

All expression clones were prepared in lentiviral form as previously described (Martz *et al.*, 2014). In brief, vectors were packaged in 293T cells with an overnight incubation with Fugene (Promega Corporation), pΔVPR and pVSV-G. The virus-containing media was collected after 48 and 72 hours and filtered with a 0.45 μm filter and stored at -80°C until use with 16 μg/mL polybrene (Sigma-Aldrich). The shRNA constructs and other expression vectors are listed in Table S6.

8 *In vitro* Adaption of Inhibitor Resistant Cells

Parental cells were either exposed to escalating doses of inhibitor until logarithmic growth resumed or exposed to a high dose (3 μM) of inhibitor (PLX4720, AZD6244 or VX-11E) and the resultant resistant clones were expanded and cultured. Parental cell lines were cultured concurrently with DMSO. Resistant cell lines were maintained in routine culture with the addition of 3 μM inhibitor. All resistant and DMSO parental control lines were submitted to STR profiling by the Duke University DNA Analysis Facility upon the acquisition of resistance in order to confirm their authenticity.

9 Annexin V Apoptosis Assay

The induction of apoptosis was quantified as described previously (Martz *et al.*, 2014). Briefly, cells were plated in triplicate at 200,000 cells per well in six-well plates. The following day, the growth media was removed and replaced with fresh media containing the indicated dose of drug or diluent (typically DMSO). After a 72-hour incubation in drug, cells were washed in PBS twice and resuspended in a buffer composed of 10 mM HEPES, 140 mM NaCl and 2.5 mM $CaCl_2$ (BD Biosciences, San Jose, CA). Apoptosis was quantified using allophycocyanin-conjugated Annexin V and viability was assessed with 7-Amino-actinomycin D (BD Bioscience). Gating was defined using untreated/unstained cells and treatments were evaluated at 20,000 counts using BD FACSVantage SE.

10 RNA Extraction and Quantitative Real-Time PCR

PCR primers were obtained from Integrated DNA Technologies and are as follows: ACTB forward 5'-CTTCCAGCCTTCCTTCCTGG-3,' reverse 5'-AATGCCAGGGTACATGGTGG-3,' MYC forward 5'-CCACC AGCAGCGACTCTG-3,' reverse 5'-TGTGAGGAGGTTTGCTGTGG-3'. Average cycle threshold (C_t) values were determined for MYC and normalized to the reference gene, β-actin. Relative gene expression was determined using the $\Delta\Delta C_t$ method.

11 Gene Expression Analysis

A375 cells (parental and evolved PLX4720-resistant clonal derivatives) expressing shGFP (parental and resistant) or shMYC (resistant only) were grown to ~80% confluency in triplicate in normal growth media and submitted to gene expression analysis. RNA-Seq libraries were generated using I-L-070 Kapa stranded mRNA-seq kit (Kappa Biosystems (Wilmington, MA) and the final libraries checked for quality control on a Qubit Fluorometer (Thermo Fisher) and Agilent 2200 Tapestation (Agilent Technologies), which was followed by sequencing on the Illumina HiSeq2000/2500 V4 (Illumina). RNA-seq data was processed by the Duke University Genome Analysis and Bioinformatics Core Facility using the TrimGalore toolkit which employs Cutadapt to trim low quality bases and Illumina sequencing adapters from the 3' end of the reads. Only reads that were 20nt or longer after trimming were kept for further analysis. Reads were mapped to the GRCm37r75 version of the human genome and transcriptome (Kersey *et al.*, 2012) using the STAR RNA-seq alignment tool (Dobin *et al.*, 2013). Reads were kept for subsequent analysis if they mapped to a single genomic location. Gene counts were compiled using the HTSeq tool. Only genes that had at least 10 reads in any given library were used in subsequent analysis. Normalization and differential expression was carried out using the DESeq2 (Love *et al.*, 2014) Bioconductor (Huber *et al.*, 2015) package with the R statistical programming environment. The false discovery rate was calculated to control for multiple hypothesis testing. Gene set enrichment analysis (Mootha *et al.*, 2003) was performed to identify differentially regulated pathways and gene ontology terms for each of the comparisons performed.

References

Barbieri, M. M. and Berger, J. O. (2004). Optimal predictive model selection. *Annals of Statistics 32*, 870–897.

Băzăvan, E. G., Li, F. and Sminchisescu, C. (2012). *Fourier Kernel Learning* pp. 459–473. Berlin, Heidelberg: Springer Berlin Heidelberg.

Bender, L. M. and Nahta, R. (2008). HER2 Cross Talk and Therapeutic Resistance in Breast Cancer. *Frontiers in bioscience : a journal and virtual library* , *13*, 3906–3912.

Berger, J. O. and Pericchi, L. R. (1996). The Intrinsic Bayes Factor for Model Selection and Prediction. *Journal of the American Statistical Association* , *91*, 109–122.

Bochner, S. (1934). A Theorem on Fourier-Stieltjes Integrals. *Bulletin of the American Mathematical Society* , *40*, 271–276.

Bostock, R. M. (2005). Signal Crosstalk and Induced Resistance: Straddling the Line Between Cost and Benefit. *Annual Review of Phytopathology* , *43*, 545–580.

Chang, Y.-W., Hsieh, C.-J., Chang, K.-W., Ringgaard, M. and Lin, C.-J. (2010). Training and testing low-degree polynomial data mappings via linear SVM. *J. Machine Learning Research* , *11*, 1471–1490.

Crawford, L., Wood, K. C., Zhou, X. and Mukherjee, S. (2017). Bayesian approximate kernel regression with variable selection. *Journal of the American Statistical Association*.

Crossa, J., Pérez, P., Hickey, J., Burgueño, J., Ornella, L., Cerón-Rojas, J., Zhang, X., Dreisigacker, S., Babu, R., Li, Y., Bonnett, D. and Mathews, K. (2014). Genomic Prediction in CIMMYT Maize and Wheat Breeding Programs. *Heredity* , *112*, 48–60.

de los Campos, G., Gianola, D., Rosa, G. J. M., Weigel, K. A. and Crossa, J. (2010). Semi-Parametric Genomic-Enabled Prediction of Genetic Values using Reproducing Kernel Hilbert Spaces Methods. *Genetics Research (Cambridge)* , *92*, 295–308.

Dobin, A., Davis, C. A., Schlesinger, F., Drenkow, J., Zaleski, C., Jha, S., Batut, P., Chaisson, M. and Gingeras, T. R. (2013). STAR: ultrafast universal RNA-seq aligner. *Bioinformatics* , *29*, 15–21.

Efron, B. (2007). Size, power and false discovery rates. *Annals of Statistics* , *35*, 1351–1377.

Gelman, A. and Tuerlinckx, F. (2013). Type S error rates for classical and Bayesian single and multiple comparison procedures. *Computational Statistics* , *15*, 373–390.

Gianola, D., Fernando, R. L. and Stella, A. (2006). Genomic-Assisted Prediction of Genetic Value With Semiparametric Procedures. *Genetics* , *173*, 1761–1776.

Goeman, J. J., van de Geer, S. A., de Kort, F. and van Houwelingen, H. C. (2004). A global test for groups of genes: testing association with a clinical outcome. *Bioinformatics* , *20*, 93–99.

Goeman, J. J., van de Geer, S. A. and van Houwelingen, H. C. (2006). Testing against a High Dimensional Alternative. *Journal of the Royal Statistical Society. Series B (Statistical Methodology)* , *68*, 477–493.

Goeman, J. J., van Houwelingen, H. C. and Finos, L. (2011). Testing against a high-dimensional alternative in the generalized linear model: asymptotic type I error control. *Biometrika* , *98*, 381–390.

Guan, Y. and Stephens, M. (2008). Practical issues in imputation-based association mapping. *PLoS Genetics* , *4*, e1000279.

Guan, Y. and Stephens, M. (2011). Bayesian variable selection regression for genome-wide association studies and other large-scale problems. *Annals of Applied Statistics* , *5*, 1780–1815.

Hauck Jr, W. W. and Donner, A. (1977). Wald's test as applied to hypotheses in logit analysis. *Journal of the american statistical association* , *72*, 851–853.

Howard, R., Carriquiry, A. L. and Beavis, W. D. (2014). Parametric and Nonparametric Statistical Methods for Genomic Selection of Traits with Additive and Epistatic Genetic Architectures. *G3 (Bethesda)* , *4*, 1027–1046.

Huber, W., Carey, V. J., Gentleman, R., Anders, S., Carlson, M., Carvalho, B. S., Bravo, H. C., Davis, S., Gatto, L., Girke, T., Gottardo, R., Hahne, F., Hansen, K. D., Irizarry, R. A., Lawrence, M., Love, M. I., MacDonald, J., Obenchain, V., Oles, A. K., Pages, H., Reyes, A., Shannon, P., Smyth, G. K., Tenenbaum, D., Waldron, L. and Morgan, M. (2015). Orchestrating high-throughput genomic analysis with Bioconductor. *Nat Meth* , *12*, 115–121.

Kass, R. E. and Raftery, A. E. (1995). Bayes Factors. *Journal of the American Statistical Association* , *90*, 773–795.

Kersey, P. J., Staines, D. M., Lawson, D., Kulesha, E., Derwent, P., Humphrey, J. C., Hughes, D. S. T., Keenan, S., Kerhornou, A., Koscielny, G., Langridge, N., McDowall, M. D., Megy, K., Maheswari, U., Nuhn, M., Paulini, M., Pedro, H., Toneva, I., Wilson, D., Yates, A. and Birney, E. (2012). Ensembl Genomes: an integrative resource for genome-scale data from non-vertebrate species. *Nucleic Acids Research* , *40*, D91–D97.

Kinney, S. K. and Dunson, D. B. (2007). Fixed and Random Effects Selection in Linear and Logistic Models. *Biometrics* , *63*, 690–698.

Kleinbaum, D. G. and Klein, M. (2010). *Maximum Likelihood Techniques: An Overview*, pp. 103–127. Statistics for Biology and Health. New York, NY: Springer New York.

Lasorella, A., Noseda, M., Beyna, M. and Iavarone, A. (2000). Id2 is a retinoblastoma protein target and mediates signalling by Myc oncoproteins. *Nature* , *407*, 592–598.

Li, Q., Birkbak, N. J., Gyorffy, B., Szallasi, Z. and Eklund, A. C. (2011). Jetset: selecting the optimal microarray probe set to represent a gene. *BMC Bioinformatics* , *12*, 474.

Liang, F., Mao, K., Mukherjee, S. and West, M. (2009). Nonparametric Bayesian kernel models. Department of Statistical Science, Duke University, Discussion Paper.

Liang, F., Mukherjee, S. and West, M. (2007). The Use of Unlabeled Data in Predictive Modeling. *Statistical Science* , *22*, 189–205.

Lippert, C., Listgarten, J., Liu, Y., Kadie, C. M., Davidson, R. I. and Heckerman, D. (2011). FaST linear mixed models for genome-wide association studies. *Nat Meth* , *8*, 833–835.

Logsdon, B. A., Hoffman, G. E. and Mezey, J. G. (2010). A variational Bayes algorithm for fast and accurate multiple locus genome-wide association analysis. *BMC Bioinformatics* , *11*, 1–13.

Lopes, H. F. and West, M. (2004). Bayesian Model Assessment in Factor Analysis. *Statistica Sinica* , *14*, 41–67.

Love, M. I., Huber, W. and Anders, S. (2014). Moderated estimation of fold change and dispersion for RNA-seq data with DESeq2. *Genome Biology* , *15*, 1–21.

Martz, C. A., Ottina, K. A., Singleton, K. R., Jasper, J. S., Wardell, S. E., Peraza-Penton, A., Anderson, G. R., Winter, P. S., Wang, T., Alley, H. M., Kwong, L. N., Cooper, Z. A., Tetzlaff, M., Chen, P.-L., Rathmell, J. C., Flaherty, K. T., Wargo, J. A., McDonnell, D. P., Sabatini, D. M. and Wood, K. C. (2014). Systematic identification of signaling pathways with potential to confer anticancer drug resistance. *Science Signaling* , *7*, ra121–ra121.

Mootha, V. K., Lindgren, C. M., Eriksson, K.-F., Subramanian, A., Sihag, S., Lehar, J., Puigserver, P., Carlsson, E., Ridderstrale, M., Laurila, E., Houstis, N., Daly, M. J., Patterson, N., Mesirov, J. P., Golub, T. R., Tamayo, P., Spiegelman, B., Lander, E. S., Hirschhorn, J. N., Altshuler, D. and Groop, L. C. (2003). PGC-1[alpha]-responsive genes involved in oxidative phosphorylation are coordinately downregulated in human diabetes. *Nat Genet* , *34*, 267–273.

Nazarian, R., Shi, H., Wang, Q., Kong, X., Koya, R. C., Lee, H., Chen, Z., Lee, M.-K., Attar, N., Sazegar, H., Chodon, T., Nelson, S. F., McArthur, G., Sosman, J. A., Ribas, A. and Lo, R. S. (2010). Melanomas acquire resistance to BRAF(V600E) inhibition by RTK or N-RAS upregulation. *Nature* , *468*, 973–977.

Peng, C.-Y. J., Lee, K. L. and Ingersoll, G. M. (2002). An introduction to logistic regression analysis and reporting. *The journal of educational research* , *96*, 3–14.

Pillai, N. S., Wu, Q., Liang, F., Mukherjee, S. and Wolpert, R. (2007). Characterizing the Function Space for Bayesian Kernel Models. *Journal of Machine Learning Research* , *8*, 1769–1797.

Pratilas, C. A., Taylor, B. S., Ye, Q., Viale, A., Sander, C., Solit, D. B. and Rosen, N. (2009). V600EBRAF is associated with disabled feedback inhibition of RAF–MEK signaling and elevated transcriptional output of the pathway. *Proceedings of the National Academy of Sciences* , *106*, 4519–4524.

Rahimi, A. and Recht, B. (2007). Random Features for Large-Scale Kernel Machines. *NIPS* , *3*, 5.

Ritchie, M. E., Phipson, B., Wu, D., Hu, Y., Law, C. W., Shi, W. and Smyth, G. K. (2015). limma powers differential expression analyses for RNA-sequencing and microarray studies. *Nucleic Acids Research* , *43*, e47–e47.

Rizos, H., Menzies, A. M., Pupo, G. M., Carlino, M. S., Fung, C., Hyman, J., Haydu, L. E., Mijatov, B., Becker, T. M., Boyd, S. C., Howle, J., Robyn, S., Thompson, J. F., Kefford, R. F., Scolyer, R. A. and Long, G. V. (2014). BRAF inhibitor resistance mechanisms in metastatic melanoma; spectrum and clinical impact. *Clinical Cancer Research* , *20*.

Rouder, J. N. and Morey, R. D. (2012). Default Bayes factors for model selection in regression. *Multivariate Behavioral Research* , *47*, 877–903.

Rudy, J. and Valafar, F. (2011). Empirical comparison of cross-platform normalization methods for gene expression data. *BMC Bioinformatics* , *12*, 1–22.

Smyth, G. K. (2004). Linear models and empirical bayes methods for assessing differential expression in microarray experiments. *Stat Appl Genet Mol Biol* , *3*, Article3.

Stephens, M. (2017). False discovery rates: a new deal. *Biostatistics* , *18*, 275–294.

Subramanian, A., Tamayo, P., Mootha, V. K., Mukherjee, S., Ebert, B. L., Gillette, M. A., Paulovich, A., Pomeroy, S. L., Golub, T. R., Lander, E. S. and Mesirov, J. P. (2005). Gene set enrichment analysis: A knowledge-based approach for interpreting genome-wide expression profiles. *Proceedings of the National Academy of Sciences* , *102*, 15545–15550.

Sun, Y., Liu, X., Eaton, E. N., Lane, W. S., Lodish, H. F. and Weinberg, R. A. (1999). Interaction of the Ski Oncoprotein with Smad3 Regulates TGF- Signaling. *Molecular Cell* , *4*, 499–509.

Vert, J.-P., Tsuda, K. and Schölkopf, B. (2004). A primer on kernel methods. *Kernel Methods in Computational Biology* , *47*, 35–70.

West, M. (2003). Bayesian Factor Regression Models in the "Large p, Small n" Paradigm. *Bayesian Statistics* , *7*.

Williams, C. K. I. and Seeger, M. (2001). Using the Nyström Method to Speed Up Kernel Machines. In *Advances in Neural Information Processing Systems 13*, (Leen, T. K., Dietterich, T. G. and Tresp, V., eds)„ pp. 682–688. MIT Press.

Wu, M. C., Lee, S., Cai, T., Li, Y., Boehnke, M. and Lin, X. (2011). Rare-Variant Association Testing

for Sequencing Data with the Sequence Kernel Association Test. *The American Journal of Human Genetics* , *89*, 82–93.

Yamaguchi, H., Chang, S.-S., Hsu, J. and Hung, M.-C. (2014). Signaling cross-talk in the resistance to HER family receptor targeted therapy. *Oncogene* , *33*, 1073–1081.

Yu, J., Pressoir, G., Briggs, W. H., Vroh Bi, I., Yamasaki, M., Doebley, J. F., McMullen, M. D., Gaut, B. S., Nielsen, D. M., Holland, J. B., Kresovich, S. and Buckler, E. S. (2006). A unified mixed-model method for association mapping that accounts for multiple levels of relatedness. *Nat Genet* , *38*, 203–208.

Zeileis, A. and Hothorn, T. (2002). Diagnostic Checking in Regression Relationships. *R News* , *2*, 7–10.

Zhang, Z., Ersoz, E., Lai, C.-Q., Todhunter, R. J., Tiwari, H. K., Gore, M. A., Bradbury, P. J., Yu, J., Arnett, D. K., Ordovas, J. M. and Buckler, E. S. (2010). Mixed linear model approach adapted for genome-wide association studies. *Nat Genet* , *42*, 355–360.

Zhou, X., Carbonetto, P. and Stephens, M. (2013). Polygenic Modeling with Bayesian Sparse Linear Mixed Models. *PLoS Genet* , *9*, e1003264.

Zhou, X. and Stephens, M. (2012). Genome-wide Efficient Mixed Model Analysis for Association Studies. *Nat Genet* , *44*, 821–824.